NTNU

Norwegian University of
Science and Technology

The Motion of Slender, Cylindrical Bodies

An Experimental and Theoretical
Investigation

Frid Grøtterud Birkeland

Marine Technology
Submission date: June 2018
Supervisor: Trygve Kristiansen, IMT
Co-supervisor: Hagbart Alsos, SINTEF Ocean

Norwegian University of Science and Technology
Department of Marine Technology

Preface

This thesis is the finalisation of my Master of Science degree in Marine Technology from the Norwegian University of Science and Technology (NTNU). The work presented was performed in the spring of 2018 and is a continuation of the work performed in my project thesis in the autumn of 2017.

The main objective of this thesis has been to theoretically and experimentally investigate the motion of a free falling slender, symmetric body dropped above and under the water surface, with focus on the latter. The theory has been applied in a program written in MATLAB that simulates the trajectory of a cylinder under water dependent on the characteristics of the cylinder in question. Experiments have been performed where cylinders with different characteristics have been dropped under and above the water surface. Work presented has been done in collaboration with fellow M.Sc. student Helene Salte Håland.

I would like to thank my supervisor, Trygve Kristiansen, and co-supervisor, Hagbart Skage Alsos, for guidance and support during my thesis. They have helped to determine the scope of the thesis, helped plan the experiments and to understand the relevant theory. I would like to thank Torgeir Wahl for help with the set-up of the experiments, Trond Innset, Ole Erik Vinje, Marcus Johnsen Almehagen and Kristian Minde for building the drop rig and making the cylinders that were dropped in the experiments, and the people at Sintef Ocean for providing extra help during the experiments. Finally, I would like to thank my friends and family for their support and help throughout my degree.

Trondheim, 2018-06-11

Frid Grøtterud Birkeland

Summary

An accidentally dropped object in the sea can result in critical damage on pipelines, platform base structures and underwater installations. This has to be accounted for during offshore operations and installations. Earlier experimental investigations performed by Aanesland in 1987 [4], have proved that slender, cylindrical bodies in particular can experience large excursions from the drop point. The objectives of this master thesis are therefore to study the motion of slender cylinders through experimental work, compare the results with a simulation script in MATLAB based on the manoeuvring equations corrected for viscous effects, and compare the results to DNV-GL's recommended practice, DNV-GL RP F107.

Experiments were performed in the tank Dokka at Center of Marine Technology at NTNU between the 19th and 23rd of February 2018 and between the 4th and 6th of April 2018. Drops under and above the surface have been performed with capped and open, slender cylinders and cylinders where the centre of gravity has been moved 3% and 7% of the full cylinder length from the centre of volume. Drop angles were between 15° and 75°. In the experiments it was observed that the motions of symmetric cylinders can be described by a falling leaf-like, oscillatory motion where the excursions and the trajectories are dependent on the drop angle and slenderness of the body. For cylinders that are asymmetric about the centre of gravity, the motions can be described by a straight path or a flip followed by a straight path. These are dependent on the relative position of the centre of gravity.

The largest excursions were observed for cylinders where the relative position of the centre of gravity is 3% of the cylinder length in front of the centre of volume. With excursions of 4.65 m for a depth of 4 m, this greatly exceed the excursion estimated based on the relevant method presented in DNV-GL RP F107. The method is general and largely underestimates the excursion for most cylinder types for small water depths. The highest velocities are obtained early in the trajectory for symmetric cylinders and converge to a constant value for asymmetric cylinders. The highest velocities occur for cylinders where the relative position of the centre of gravity is 3% of the length from the centre of volume. The maximum velocity is 3.47 m/s.

The motion of slender cylinders can be described theoretically by the manoeuvring equations corrected for viscous effects. The values of the effective trailing edge that give results most similar to the experimental results are 0.4 for small drop angles and 0.5 for steep angles. The form drag coefficient has only a small impact on the motion. Optimal values for the cross-flow drag coefficient are mostly between 1.0 and 1.2.

Overall, the simulation program gives a good estimate of the motion of a slender cylinder and the excursion at the sea bottom. The results are most accurate for symmetric cylinders, but underestimate the excursions for open cylinders. For cylinders that are asymmetric about the centre of gravity, the program overestimates the excursions for large depths. The theory as presented by Aanesland, assumes motion limited to the XZ plane, however large spreading observed in the experiments indicate that this assumption is only valid for open cylinders. The motion for all other cylinder types must therefore be calculated in three dimensions.

Sammendrag

Fallende objekt som mistes ved et uhell i havet kan forårsake kritisk skade på rørledninger, plaformstrukturer og undervannsinnstallasjoner. Dette må det tas høyde for i offshore operasjoner og installasjoner. Tidligere eksperimenter utført av Aanesland i 1987 [4], har vist at spesielt avlange, sylindriske objekter kan bevege seg store avstander under vann fra et gitt droppunkt. Formålet med denne masteroppgaven er derfor å undersøke bevegelsen til avlange sylindere gjennom eksperimenter, og å sammenligne resultatene fra dette med et program skrevet i MATLAB som simulerer banen til sylinderen basert på manøvreringslikningene korrigert for viskøse effekter og med DNV-GLs anbefalte praksis, DNV-GL RP F107.

Eksperimentene har blitt utført i tanken Dokka på Marinteknisk Senter på NTNU, mellom 19. og 23. februar 2018 og mellom 4. og 6. april 2018. Dropp har blitt utført under og over vannoverflaten for lukkede og åpne avlange sylindere, og med sylindere hvor gravitasjonssenteret er flyttet med 3% og 7% av sylinderens fulle lengde fra volumsenteret. Droppvinklene har vært mellom 15° og 75°. I eksperimentene ble det observert at bevegelsen til symmetriske sylindere kan beskrives som en fallende, løv-liknende, svingende bevegelse, hvor utslaget og bevegelsen bestemmes av droppvinkelen og lengden av sylinderen sammenlignet med diameteren. For sylindere som er asymmetriske om gravitasjonssenteret, kan bevegelsen beskrives som en rett linje eller en bevegelse hvor sylinderen først snur seg vertikalt og så beveger seg i en rett linje. Bevegelsen er avhengig av den relative posisjonen til gravitasjonssenteret.

Det største utslaget fra droppunktet ble observert for sylindere der den relative posisjonen av gravitasjonssenteret var 3% av sylinderlengden foran volumsenteret til sylinderen. Med en lengde på 4.65 m for en dybde på 4 m, overskrider dette i stor grad utslaget estimert ved hjelp av en passende metode fra DNV-GL RP F107. Metoden som er gitt i veiledningen for anbefalt praksis, er generell og underestimerer i stor grad utslaget for de fleste sylindertypene for små vanndyp. De høyeste hastighetene for symmetriske sylindere oppnås tidlig i fallbanen. For asymmetriske sylindere konvergerer hastigheten til en konstant verdi. Den største hastigheten er funnet for sylindere hvor gravitasjonssenteret har en avstand fra volumsenteret som tilsvarer 3% av den fulle lengden. Denne hastigheten er 3.47 m/s. Bevegelsen til en avlang sylinder kan teoretisk beskrives ved hjelp av manøvrerings-likningene korrigert for viskøse krefter. Verdiene av den effektive avløsningskanten, som gir resultater som ligner mest på de eksperimentelle resultatene, er 0.4 for små droppvinkler og 0.5 for store. Den aksielle drag-koeffisienten har liten innvirkning på bevegelsen. Optimale verdier for tverrstrømningsdrag-koeffisienten er for det meste mellom 1.0 og 1.2.

Samlet sett gir manøvreringslikningene korrigert for viskøse effekter, et godt estimat for den forventede bevegelsen til en sylinder og den endelige avstanden fra droppunktet på havbunnen. Resultatene fra simuleringene og eksperimentene stemmer best overens for symmetriske sylindere, men simuleringene underestimerer utslaget for åpne sylindere. For sylindere som er asymmetriske omkring gravitasjonssenteret, overestimerer programmet utslaget for større vanndyp. Den teoretiske beskrivelsen av bevegelsen antar at bevegelsen kan beskrives in XZ-planet. Stor spredning observert i forsøkene indikerer imidlertid at

dette kun er en antagelse som kan brukes for åpne sylindere. Bevegelsen for de andre sylindertypene må derfor regnes ut i tre dimensjoner.

Contents

Chapter 1

Introduction

Accidentally dropped objects may pose great danger to pipes, platform base structures and underwater installations. The object may be dropped from the platform deck during operation, or from a supply or installation vessel during hoisting and installation. If a drop should occur, the result will be a much more expensive installation or operation than planned. In a worst case scenario, the dropped object might cause loss of human life or release of hydrocarbons to the sea. Thus, it is a key topic when planning marine operations offshore.

The most important parameters when dealing with accidentally dropped objects are the trajectory, the velocity and the final impact point, either with sea bottom or a subsea structure. These variables are dependent on the size of the body, geometry, weight distribution and the angle of which the object penetrate the water surface. As the maximum velocity can be high, the object might experience large excursion and a large impact load on an impact point. In 2009, the Dropped Object Prevention Scheme (DROPS) presented an information sheet about the danger of falling objects. By looking at the energy that the object will have at the final impact point, DROPS proposes that most drilling equipment have the potential of causing significant damage on pipeworks and systems and/or subsea equipment when the depth is 150 meter, due to an accidental drop [1].

The probability of experiencing an accidental drop during hoisting and operation can be calculated by the use of an empirical drop frequency. Based on data issued by UK Department of Energy, covering the period from 1980 to 1986, DNV-GL has estimated some drop frequencies. The frequencies depend on the type of lift and handling load. The dropped object probability is $2.2 * 10^{-5}$ per lift for lifts between vessel and platform. For lifts above 20 tonnes the frequency is estimated to be $3.0 * 10^{-5}$ per lift. For the period in question the number of lifts to or from vessel was 4,500 per year [3]. These data give a low number of drops per year. However, in 2010 the Norwegian Oil and Gas Association reported that the number of dropped objects in 2008 was 167, in 2009 is was 192 and in 2010 it was 119 dropped objects [18]. For the latter case it is not clear what type of objects have been dropped or whether it is into the ocean. However, statistics on the matter state that 70% of all accidentally dropped objects fall onto the platform deck, while 30% fall into the sea [3].

1.1 Recommended Practice for Risk Assessment of Accidentally Falling Objects

The recommended practice (RP) for risk assessment of pipeline protection, DNV-GL RP F107 [3], includes risk assessment of accidental falling objects including object excursion on the seabed, hit probability and impact energy of the objects. With regards to slender objects the recommendations are limited to risk from crane activity. Slender objects are objects with a length, L, much larger compared to the diameter, D, defined by the slenderness parameter, $\epsilon = D/L$ [17].

The object excursion is assumed to be normal distributed around the drop point and include both flat, long, box and round shaped objects. The probability of a sinking object hitting the sea bottom at a distance x from the vertical line through the drop point, $p(x)$, is given by:

$$p(x) = \frac{1}{\sqrt{2\pi}\delta} e^{-\frac{1}{2}\left(\frac{x}{\delta}\right)^2} \tag{1.1}$$

Here x is the horizontal distance from the drop point at the sea bottom, and δ is the lateral deviation. The excursion is a function of the weight and the shape of the object. For flat or long shaped bodies with weight smaller than 2 tonnes, between 2 to 8 tonnes, and larger than 8 tonnes, the angular deviation, α, is 15°, 9° and 5°, respectively [3]. The relation between the parameters is illustrated in Figure 1.1.

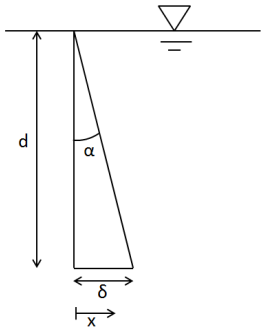

Figure 1.1: *Object excursion on the seabed, δ, dependent on the depth, d, and angular deviation, α. x is the horizontal excursion at the sea bottom for which the probability is calculated.*

Thus, from geometry the δ can be calculated from the depth, d, and α:

$$\delta = d\tan(\alpha) \tag{1.2}$$

The RP points out that slender or flat bodies may experience oscillations as presented by Aanesland's OTC paper from 1987, and this have to be accounted for. These motions are commented on more extensively in section 1.2.1. Another notion refers to a paper

by Katteland and Øygarden from 1995, where it was found that the maximum excursion was obtained at 180 m depth and it would not change significantly in deeper water [12].

In order to get a complete risk picture for marine lifting operations, RP F107 recommends to calculate the hit probability for different radii, r, from the drop point, with a constant step length. This probability, $P(x \leq r)$, is expressed as [3]:

$$P(x \leq r) = \int_{-r}^{r} p(x)\, dx \tag{1.3}$$

1.2 Literature Review

1.2.1 Experimental and Theoretical Investigation by Aanesland

One of the first attempts to theoretically study the motion of a slender cylinder freely falling in water, was presented by Aanesland in an OTC conference paper from 1987 [4]. This paper is based on a technical report from Aanesland and Huse from the year before [5]. Based on observations of the trajectory of a slender cylinder dropped under the water surface, Aanesland proposed that the motion could be described in two dimensions assuming slender body theory, by the manoeuvring equations for a ship corrected for viscous effects. Using a body-fixed coordinate system and assuming that the cylinder moves as a rigid body and is symmetric about the centre of gravity (COG), the equations of motion are described by:

$$-(M - \rho\nabla)g\sin\beta + F_{dx} = M\dot{U}_1 \tag{1.4}$$

$$-(M - \rho\nabla)g\cos\beta + F_{dz} = U_1 a_{33} U_3 - U_1(x_T + M)\Omega_2 + (A_{33} + M)\dot{U}_3 \tag{1.5}$$

$$M_{dy} = -U_1(A_{33} + x_T a_{33})U_3 + U_1 x_T^2 a_{33}\Omega_2 + (A_{55} + I_{55})\dot{\Omega}_2 \tag{1.6}$$

where U_1, U_3 and Ω_2 are velocities in surge, heave and pitch, respectively, and $\dot{U}_1$, $\dot{U}_3$ and $\dot{\Omega}_2$ are the accelerations. M is the mass of the cylinder, ρ the density of water, ∇ the displaced volume of the cylinder, and g is the gravity acceleration. β is the instantaneous angle between the cylinder axis and the free surface, x_t is the effective trailing edge, a_{33} is the two dimensional added mass in heave, and I_{55} is the mass moment of inertia in pitch. Further, A_{33} and A_{55} are the added mass in heave and pitch respectively. Finally, F_{dx} and F_{dz} are the viscous forces given by:

$$F_{dx} = -0.664\pi D\sqrt{\nu\rho^2 L}U_1\sqrt{|U_1|} - \frac{1}{8}\rho\pi C_{Dx}D^2 U_1|U_1| \tag{1.7}$$

$$F_{dz} = 0.5\int_L \rho C_{Dz} D u_z(x)|u_z(x)|dx \tag{1.8}$$

D is the diameter of the cylinder, ν the kinematic viscosity of water, and C_{Dx} and C_{Dz} are the drag coefficients in x and z direction, respectively. The viscous moment, M_{dy}, is given by:

$$M_{dy} = -0.5 \int_L \rho C_{Dz} D x u_z(x) |u_z(x)| dx \tag{1.9}$$

A program estimating the trajectory was made based on this theory. In order to verify the results from the program, drops from both above and under the water surface were performed. The paper points out that for the drops performed above the surface, the impact with the surface changed the angle of attack of the cylinder. Also, it conclude that for drops above the surface the falling height in air is of great importance to the motion itself. For drop angles of 0^o and 90^o it was observed that small disturbances in the motion of the cylinders caused a deviation in the expected straight, vertical path and thus some excursion from the drop point.

For drops under the water surface, the trajectories depending on the drop angle followed six different paths, as given in Figure 1.2. The conference paper conclude that the directional stability of the plane described by the cylinder axis have been observed to be strong, and also that the most important parameter for falling cylindrical bodies are the angle of attack immediately after submerge. [4]

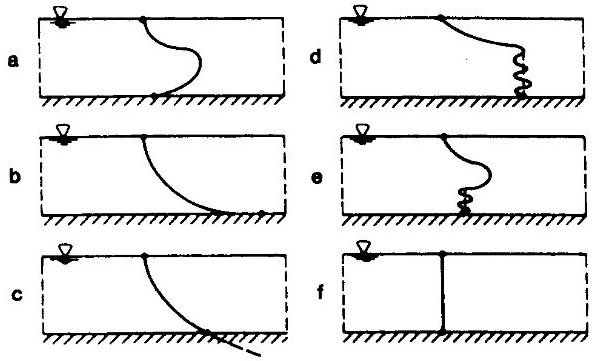

Figure 1.2: *Expected accidental drop trajectories of a slender, cylindrical bodies dropped under water, as presented by Aanesland [4].*

1.2.2 Experimental Studies on Dropped Objects

In a conference paper connected the OMAE conference (Conference on Ocean Offshore & Artic Engineering) from 1995, Katteland and Øygaarden present the results from research on the risk associated with dropped objects at depths larger than 300 m [12]. Here, accidental drops of tubular, box shaped and compact objects from crane and derrick have been considered. The investigation is mostly based on the works by Aanesland and an internal report in Dovre Safetec A/S. The paper identifies distributions on the sea floor for different object groups, evaluates the effect of environmental forces and presents a model for calculating risk for installations and pipelines on the sea floor.

In the investigation tubular objects, drill tubes and weight tubes are considered. The tubes have a length of 9.14 m and 9.95 m, outer diameter of 0.127 m and 0.2032 m, and density of 32.5 kg/m and 225 kg/m, all in respective order. Based on the internal

report the paper argues that maximum excursion occurs at depth of approximately 180 m, with an excursion of 250 m. An increased spreading had been observed down to 180 m, however at larger depths the spreading remained constant. For an accidental drop case the paper argues that two falling patterns can be expected to occur; a straight downward trajectory and a leaf-like pattern. In the first case the paper estimates a terminal velocity of 23.0 m/s for vertical falling and 10.8 m/s for horizontal falling. This will be reached after 50-100 m. For the latter case, terminal velocity will not be reached, but the velocity will be between the terminal velocities of the straight downwards trajectories. Among the assumptions made in the paper are the assumption that the majority of drops from crane will have an angle with the water surface between 45^o and 90^o, and from the derrick 75^o to 90^o. Calculated values for one side of the distribution for a water depth of 1000 m, gives for crane accidents a probability of 50% to be within 75 m from the crane, and 90% within 175 m from the crane. For drops from derrick 60% land within 75 m and 90% land within 175 m. [12]

Most research done on motion of cylinders under water are focused on mines. One study on this by Chu et al. (2005) investigated the dynamically characteristics of a falling cylinder through the water column both experimentally and theoretically [7]. The study used rigid plastic cylinders with aluminium capped ends with three different lengths. A threaded bolt of copper inside enabled changing the COG in the cylinder. The drop angles where 15°, 30°, 45°, 60° and 75°. The study observed six trajectory patterns from the experiment: straight, spiral, flip, flat, seesaw and a combination. It confirmed that the pattern was mostly dependent on the drop angle, initial speed and the characteristics of the cylinder. Further, for drops where the COG lay higher than the Centre of Volume (COV), the cylinder only flipped once in its trajectory. The distribution of mass away from the COV proved to be more important when assessing the impact force on the sea bottom. [7]

Yasseri (2014) performed an experimental study with cylindrical models with a diameter of 4 cm and lengths of 9 cm, 12 cm and 15 cm. Additionally, each lengths had three different centres of mass. All drops were performed above the water surface for drop angles of 15^o, 30^o, 45^o, 60^o and 75^o. Both trajectory and landing point were observed only by the human eye. Trajectories observed were straight, spiral, flip, flat, seesaw and combination, as presented in the paper by Chu et al. (2005). Moreover, Yasseri observed in his experiment that for objects with coinciding COG and COV, the object hit the bottom of the pool near the drop point more than 90% of the time. A small distance between the two parameters, on the other hand, caused variability. The largest excursion from the drop point occurred for objects dropped with COG behind the COV. Finally, the paper conclude that for 50%, 80%, 90%, 95% and 98% of the times, the cylinders landed respectively within lenghts that are 10%, 20%, 30%, 40% and 50% of the water depth. [24]

1.3 Objective and Limitations

The objective of this master thesis is to study the motion of a slender, symmetrical body when it is dropped under and above the water surface, with focus on the first. The term ”slender” characterise bodies that have a length significantly longer than the diameter. The cylindrical body is one of the simplest geometries to investigate for this case, and may represent simplified drill pipes or weight pipes with capped ends. In addition cylindrical bodies that are longitudinally asymmetric around COG, will also be investigated.

The focus will be on the motion of a cylinder in the XZ plane and in particular under water. It is assumed that current, waves and other environmental forces are absent. Hence the trajectory under water will only be dependent on the ratio between the mass and buoyancy forces, the hydrodynamic forces, the geometry of the cylinder and the initial drop angle between the cylinder and water surface. Above water drop height, slamming and air cavity play a part.

The motion of a cylinder can be described by the manoeuvring equations corrected for viscous effects. Dependent on the characteristics of the cylinder, small changes to these equations have to be made with regards to the effective trailing edge, added masses, viscous forces and ratio between COG and COB. This will be presented in the theory section. This theory will be used to make a program in MATLAB that can simulate the trajectory of a cylinder dropped under water, dependent on its specific geometries.

Another main part of this thesis is the experimental work that will be performed this spring. The experiments will be performed in the tank Dokka at Center of Marine Technology in Trondheim. Under water drops will be performed with slender, geometrical symmetric and capped cylinders with three different diameters, open cylinders with the largest and smallest diameter of the three, and with cylinders with a small difference between COG and COV, dropped with COG above and underneath COV. Drops above water will be performed with the three types of geometrical symmetric cylinders. The results from the experiments will be compared to the simulated results in order to verify the accuracy of the latter. In addition the results will be compared to the DNV-GL RP F107.

Chapter 2

Theory

The motion of a slender, cylindrical object can be described by the manoeuvring equations corrected for viscous effects. Thus the motion surge, heave and yaw dependent on the local coordinate system of the body can be described. For drops under water small changes in the equations dependent on the characteristics of the cylinder in question, can be made in order to calculate an approximately correct path. For drops above water, water entry effects such as slamming and air cavity have to be included. This will be presented in the following chapter.

2.1 Slender Body Theory

In slender body theory it is assumed that the length, L, of an object is much larger than the width or diameter, D. This is reflected in the slenderness parameter, ϵ, that is assumed to be small and given by:

$$\epsilon = \frac{D}{L} \tag{2.1}$$

The motion of a slender body can be described by the longitudinal and lateral motion of the body in an unbound fluid. The lateral motion is assumed to be small with the result that the two can be treated separately. Hence, the longitudinal motion is assumed to be constant and much larger than the lateral motion. Also, it is assumed that geometries are varying smoothly. [17]

2.2 Coordinate System

To describe the motion of a slender body moving in water, two coordinate systems are required: one global, space-fixed and one local, body-fixed. Both coordinate systems follow the right-hand rule and have a positive z-axis downwards. Both coordinate systems can be seen in figure 2.1.

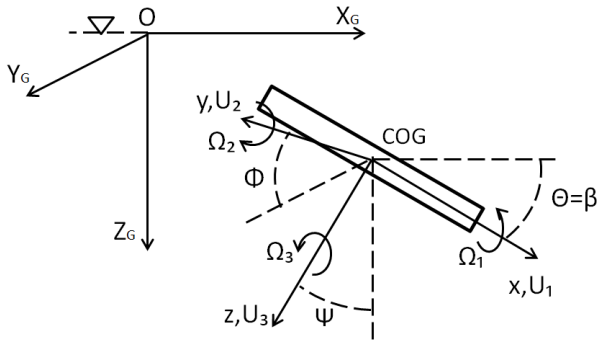

Figure 2.1: *Three-dimensional coordinate system and nomenclature for a falling cylinder in water. The upper, leftmost system is the global coordinate system ($X_GY_GZ_G$), and the rightmost is the local coordinate system of the cylinder (xyz).*

The global coordinate system has origin in the water surface with both the X-axis and Y-axis laying in this plane. These axis are denoted X_G and Y_G. The Z-axis points downwards, normal to the the water surface plane and is denoted Z_G.

The body-fixed coordinate system has origin in the centre of gravity (COG) of the body, as can be seen in figure 2.1. The X-axis, denoted x, is aligned with the axis of the body, the Y-axis, y, to the port side, and the Z-axis, z, normal to this plane. Θ, Φ and Ψ are the angles between the axes in the global and local coordinate system. When the body lay in the water surface these angles will equal zero, and the coordinate systems will coincide.

For a three-dimensional coordinate system the relation between a motion described in the local body-fixed system and the global system is expressed as [9]:

$$\frac{d}{dt}\begin{bmatrix} X_G \\ Y_G \\ Z_G \end{bmatrix} = \begin{bmatrix} \cos\Psi & -\sin\Psi & 0 \\ \sin\Psi & \cos\Psi & 0 \\ 0 & 0 & 1 \end{bmatrix} \begin{bmatrix} \cos\Theta & 0 & \sin\Theta \\ 0 & 1 & 0 \\ -\sin\Theta & 0 & \cos\Theta \end{bmatrix} \begin{bmatrix} 1 & 0 & 0 \\ 0 & \cos\Phi & -\sin\Phi \\ 0 & \sin\Phi & \cos\Phi \end{bmatrix} \begin{bmatrix} U_1 \\ U_2 \\ U_3 \end{bmatrix} \tag{2.2}$$

where U_1, U_2 and U_3 are the local velocities in surge, sway and heave, respectively. This transformation between the global and local coordinate system is obtained from a sequence of partial rotations by Euler angles, Θ, Φ and Ψ, resulting in the expression [9]:

$$\frac{d}{dt}\begin{bmatrix} \Theta \\ \Phi \\ \Psi \end{bmatrix} = \begin{bmatrix} 0 & \cos\Phi & -\sin\Phi \\ 1 & \sin\Phi\tan\Theta & \cos\Phi\tan\Theta \\ 0 & \sin\Phi\sec\Theta & \cos\Phi\sec\Theta \end{bmatrix} \begin{bmatrix} \Omega_1 \\ \Omega_2 \\ \Omega_3 \end{bmatrix} \tag{2.3}$$

In this master thesis the focus is on motion in the X_GZ_G and xz plane. Thus, $Y_G = 0$, $U_2 = 0$, $\Psi = \Phi = 0$. Also, Θ is denoted β, and equation 2.2 and equation 2.3 reduces to:

$$\frac{d}{dt}\begin{bmatrix} X_G \\ Z_G \end{bmatrix} = \begin{bmatrix} \cos\beta & \sin\beta \\ -\sin\beta & \cos\beta \end{bmatrix} \begin{bmatrix} U_1 \\ U_3 \end{bmatrix} \tag{2.4}$$

and

$$\frac{d\beta}{dt} = \Omega_2 \tag{2.5}$$

2.3 Equations of motion

For a slender object moving in water the motion is dependent on the buoyancy force, viscous forces and lifting forces. This will be described in the following section and subsections based on [9] and [11].

By applying Newton's second law and the buoyancy force to the coordinate system in figure 2.1, and by using the Euler angles, it can be shown that

$$\begin{aligned} M(\dot{U}_1 + \Omega_2 U_3 - \Omega_3 U_2) &= F_X - (Mg - \rho g \nabla)\sin\Theta \\ M(\dot{U}_2 + \Omega_3 U_1 - \Omega_1 U_3) &= F_Y + (Mg - \rho g \nabla)\cos\Theta \sin\Phi \\ M(\dot{U}_3 + \Omega_1 U_2 - \Omega_2 U_1) &= F_Z + (Mg - \rho g \nabla)\cos\Theta \cos\Phi \end{aligned} \tag{2.6}$$

where F_X, F_Y and F_Z are the hydrodynamic external forces acting on the body, ρ is the density of water and ∇ is the displaced volume of the cylinder.

The external moments about the local x, y and z axis can be derived by differentiating with respect to time the moment of momentum with the following result:

$$\begin{aligned} I_{44}\dot{\Omega}_1 - (I_{55} - I_{66})\Omega_2\Omega_3 - I_{64}(\dot{\Omega}_3 + \Omega_1\Omega_2) &= M_{dx} \\ I_{55}\dot{\Omega}_2 - (I_{66} - I_{44})\Omega_3\Omega_1 - I_{64}(\Omega_3^2 - \Omega_1^2) &= M_{dy} \\ I_{66}\dot{\Omega}_3 - (I_{44} - I_{55})\Omega_1\Omega_2 - I_{64}(\dot{\Omega}_1 - \Omega_2\Omega_3) &= M_{dz} \end{aligned} \tag{2.7}$$

Here I_{ij} is the mass moment of inertia in direction i due to motion in j. M_{dx}, M_{dy} and M_{dz} are viscous moments. Applying the simplifications corresponding limiting the domain to a plane, such that $U_2 = 0$, $\Omega_1 = \Omega_3 = 0$ and $\Phi = 0$. Moreover, denotation for Θ is β, and equation 2.6 and equation 2.7 reduce to:

$$\begin{aligned} M[\dot{U}_1 + \Omega_2 U_3] &= X - (Mg - \rho g \nabla)\sin\beta \\ M[\dot{U}_3 - \Omega_2 U_1] &= Z + (Mg - \rho g \nabla)\cos\beta \\ I_{55}\dot{\Omega}_2 &= M_y \end{aligned} \tag{2.8}$$

The boundary condition in lateral direction for a slender body is given as [17]:

$$\frac{\partial\phi}{\partial n} = n_3(U_3 - x\Omega_2) \tag{2.9}$$

where ϕ is the velocity potential, n is the unit normal and n_3 is the unit normal in z-direction.

The added mass forces, non-lifting, and non-viscous forces and moments can be calculated from:

$$\mathbf{F} = -\frac{\partial \mathbf{B}}{\partial t} - \boldsymbol{\Omega} \times \mathbf{B} \tag{2.10}$$

where $\mathbf{B}$ is a boundary vector [9]. The added mass forces on the body can be found by looking at the pressure, p, on the wetted surface of a strip of the body. This is expressed as:

$$p = -\rho \left(\frac{\partial}{\partial t} - U_1 \frac{\partial}{\partial x} \right) \phi \tag{2.11}$$

Since the surface of a cylinder is symmetric in the xz plane, the only force is acting in the x-direction. Thus, the stripwise force can be expressed as the integral over the area of each strip, $A(x)$:

$$f_3 = -\int_{A(x)} p n_3 \, ds \tag{2.12}$$

Integrating over each direction, the total forces on the body in each direction is then:

$$\begin{aligned} F_1^n &= 0 \\ F_3^n &= \int_L f_3 \, dx \\ F_5^n &= -\int_L x f_3 \, dx \end{aligned} \tag{2.13}$$

By inserting the expressions above into the set of equations in 2.8, a set expressions describing the motion in surge, heave and yaw for the cylinder:

$$\underbrace{M\dot{U}_1}_{\text{inertial force}} \underbrace{-M\Omega_2 U_3}_{\text{Coriolis force}} = \underbrace{-A_{11}\dot{U}_1 - A_{33}U_3\Omega_2 - A_{35}\Omega_2^2}_{\text{added mass force}} + \underbrace{F_{dx}}_{\text{viscous force}} \underbrace{-(Mg - \rho g \nabla)\sin\beta}_{\text{gravity and buoyancy forces}} \tag{2.14}$$

$$\begin{aligned} \underbrace{M[\dot{U}_3 - \Omega_2 U_1]}_{\text{inertial forces}} = &\underbrace{U_1 U_3 [a_{33}(x)]_{x_T}^{x_N} - U_1 \Omega_2 [x a_{33}(x)]_{x_T}^{x_N}}_{\text{lifting forces}} \underbrace{-(A_{33}\dot{U}_3 + A_{35}\dot{\Omega}_2) + A_{11}U_1\Omega_2}_{\text{added mass force}} \\ &+ \underbrace{F_{dz}}_{\text{viscous}} + \underbrace{(Mg - \rho g \nabla)\cos\beta}_{\text{gravity and buoyancy forces}} \end{aligned} \tag{2.15}$$

$$\underbrace{I_{55}\dot{\Omega}_2}_{\text{inertial moment}} = \underbrace{-U_1U_3[xa_{33}(x)]_{x_T}^{x_N} + U_1\Omega_2[x^2a_{33}(x)]_{x_T}^{x_N}}_{\text{lifting moment}} \underbrace{-(A_{53}\dot{U}_3 + A_{55}\dot{\Omega}_2) + A_{33}U_1U_3 + A_{35}U_1\Omega_2}_{\text{added mass moment}} \underbrace{+M_{dy}}_{\text{viscous force}} \tag{2.16}$$

Here A_{ij} for $i = 1, 3, 5$ and $j = 1, 3, 5$ are the added masses and a_{33} is the two-dimensional added mass in heave. For slender bodies in general A_{11} will be much smaller compared to the other forces in the equation. Therefore, it can be assumed that this added mass is without significance.

x_N and x_T are the fore and aft effective trailing edge respectively given by the percentage times the length which give the actual position of the trailing edge. It is a correction of the length due to the fact that slender body theory assume smoothly varying geometries. The end of the cylinder is abrupt and the equations of motion therefore need to be corrected for this [4]. The value of $a_{33}(x)$ in the equations are dependent on whether the fore or the aft meet the fluid first, thus whether U_1 is positive or negative:

$$U_1 > 0 \begin{cases} a_{33}(x_N) = 0 \\ a_{33}(x_T) = \dfrac{\rho\pi D^2}{4} \end{cases} \qquad U_1 < 0 \begin{cases} a_{33}(x_N) = \dfrac{\rho\pi D^2}{4} \\ a_{33}(x_T) = 0 \end{cases}$$

2.3.1 Viscous forces and moments

The longitudinal viscous force, F_{dx}, consists of a skin friction term and a form drag term, expressed as:

$$F_{dx} = -0.5\rho C_F \pi D L U_1 |U_1| - \frac{\rho}{8}\pi C_{Dx} D^2 U_1 |U_1| \tag{2.17}$$

where C_F is the friction coefficient, ν is the kinematic viscosity of water and C_{Dx} is the form drag coefficient. Here it is assumed that the cylinder is smooth and that only the outside of the cylinder is wet. For laminar flow C_F can be expressed by Blasius formula [22]:

$$C_F = \frac{1.328}{\sqrt{Re_L}} = 1.328\sqrt{\frac{\nu}{|U_1|L}} \tag{2.18}$$

as in the theory presented by Aanesland [4]. For turbulent flow C_F can be calculated from [21]:

$$C_F = 0.0015 + \left(0.30 + 0.015\left(\frac{2L}{D}\right)^{0.4}\right) Re^{-\frac{1}{3}} \tag{2.19}$$

This calculation of the friction coefficient assume that the body experience turbulent, axisymmetric flow with $10^6 < Re < 10^9$, and that the surface of the body is smooth. The Reynolds number, Re, is given by:

$$Re = \frac{U_1 D}{\nu} \tag{2.20}$$

The transverse viscous force, F_{dz}, and the viscous pitch moment, M_{dy}, can be derived from the cross-flow principle. The principle assume that the flow separates due to the cross flow past a ship, that this force is mainly the result of separated flow effects on the pressure distribution around the body, and that there are no influence of the longitudinal velocity components on the transverse forces. This gives the following expressions integrated over the length of the body:

$$F_{dz} = -0.5 \int_L \rho C_{Dz} (U_3 - \Omega_2 x) |(U_3 - \Omega_2 x)| \, dx \tag{2.21}$$

$$M_{dy} = 0.5 \int_L \rho C_{Dz} x (U_3 - \Omega_2 x) |(U_3 - \Omega_2 x)| \, dx \tag{2.22}$$

C_{Dz} is base drag. How both this coefficient and C_{Dx} can be found are described in the Section 3.1.

2.3.2 Added Mass Coefficients and Moment of Inertia

Since the body in question is a slender cylinder and it is assumed in slender body theory that the lateral and longitudinal motion can be treated separately, strip theory can be applied to calculate the added masses for the cylinder. Therefore, two dimensional added mass in heave can be expressed as:

$$a_{33} = \frac{\rho \pi D^2}{4} \tag{2.23}$$

By strip theory the added mass in heave and pitch can be defined based on a_{33}:

$$A_{33} = \int_L a_{33} \, dx \tag{2.24}$$

$$A_{55} = \int_L x^2 a_{33} \, dx \tag{2.25}$$

For added mass in heave and pitch due to motion in pitch and heave, A_{35} and A_{53}, respectively, the expressions are:

$$A_{35} = -\int_L x a_{33} \, dx = A_{53} \tag{2.26}$$

The mass moment of inertia in pitch, I_{55}, is given by:

$$I_{55} = \int_L x^2 \frac{m}{L}\, dx \tag{2.27}$$

2.3.3 Adaptation for Full Symmetry about Centre of Gravity

For the case of full symmetry it is assumed that the cylinder is symmetric about the COG. Then A_{35} and A_{53} will be equal to 0. Also, from the expressions derived by Kochin et al. (1964) [14] for acceleration dependent on force and moment components on an axisymmetric body, the term $-A_{33}U_3\Omega_2$ will be zero [6]. In addition, because of the symmetry an simplification of the lift forces and lift moment can be made. Since the cylinder is symmetric around COG $a_{33}(x_T) = a_{33}(x_N)$ and $x_T = -x_N$. With this in mind the lift force in heave, F_3^l, can be expressed as:

$$F_3^l = -|U_1|U_3 a_{33}(x_T) + U_1\Omega_2 x_T a_{33}(x_T) \tag{2.28}$$

and the lift moment in pitch, F_5^m, as:

$$F_5^m = U_1 U_3 x_T a_{33}(x_T) - |U_1|\Omega_2 x_T^2 a_{33}(x_T) \tag{2.29}$$

2.3.4 Adaptation for Asymmetry about the Centre of Gravity

For the case where the COG is not in the same place as the COV, some modifications have to be made to the equations of motion. First, all calculations of viscous forces, added masses and mass moment of inertia have to be made dependent on the new coordinate system where the origin is placed in the COG. Hence the length to the aft, L_T, and fore end, L_N, of the cylinder will not be equal, as can be seen in figure 2.2. Second, the balance between the centre of buoyancy (COB) and centre of mass (COM) of the cylinder has to be accounted for. The difference between the placement of the two forces create a moment influencing the pitch motion. The addition to the right hand side of the expression for the pitch motion (equation 2.16), is given by the buoyancy and the length from COG to COB, Δ_{CB}:

$$-\Delta_{CB} * buoyancy = \rho g \nabla \cos(\beta)\Delta_{CB} \tag{2.30}$$

A visual representation of the case can be seen in figure 2.2.

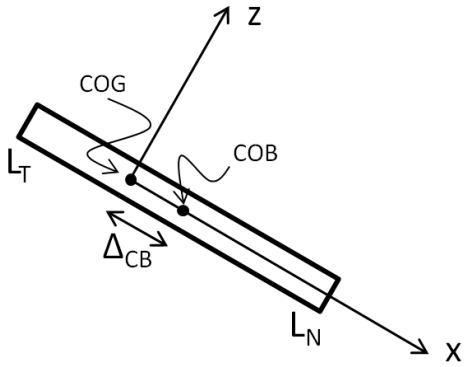

Figure 2.2: *Case where Centre of Gravity (COG) for a cylinder is positioned above the Centre of Buoyancy (COB). Δ_{CB} is the distance between COG and COB.*

Last, the fore and aft effective trailing edges have to have the same distance from their respective cylinder ends, ensuring that the assumed same flow regimes at both ends are maintained.

2.3.5 Adaptation for Open Cylinders

Open cylinders have the same geometrical properties as capped cylinders. Thus A_{35} and A_{53} will equal zero due to symmetry. The difference is the flow through the cylinder, which also has to be accounted for. The flow results in an extra component to the lift forces and moments. Thus, the lift is the sum of an outer lift component and an inner. The lift forces and moments are calculated by applying equation 2.11, and the boundary condition to equation 2.12. The boundary conditions are the same for the external and internal flow, and are given in equation 2.9. The stripwise force on the cylinder can then be expressed as:

$$f_3 = -\left(\frac{\partial}{\partial t} - u_1\frac{\partial}{\partial x}\right)(u_3 - x\Omega_2)\, a_{33} \tag{2.31}$$

Here a_{33} is slightly different for the inner and outer flow. Both can be calculated from equation 2.23, dependent on the outer and inner diameter of the cross section of the cylinder, by notation D_{out} and D_{in}, respectively. As both A_{33} and A_{55} are defined by a_{33}, a_{33} in Equation 2.24 and Equation 2.25 is the sum of the two added masses when A_{33} and A_{55} are calculated. Assuming that the open cylinder have an evenly distributed mass, the lift force, F_3^l, and moment, F_5^m, are:

$$F_3^l = -|U_1|U_3(a_{33,out}(x_T) + a_{33,in}(x_T)) + U_1\Omega_2 x_T(a_{33,out}(x_T) + a_{33,in}(x_T)) \tag{2.32}$$

$$F_5^m = U_1U_3x_T(a_{33,out}(x_T) + a_{33,in}(x_T)) - |U_1|\Omega_2x_T^2(a_{33,out}(x_T) + a_{33,in}(x_T)) \tag{2.33}$$

Last, the area over which the friction between the flow and cylinder occurs, approximately doubles, as the internal area of the cylinder has to be included. Thus, two friction coefficients are calculated, one based on D_{out} and one on D_{in}.

2.4 Additions for Motion Through the Water Surface

In a real case scenario drops of objects from some height above the surface are more likely to occur compared to drops under the surface. This adds more complexity to the fall, as motion through the surface must be accounted for. This include an initial velocity, slamming and creation of air cavity.

For an object falling in air the forces affecting the motion of the body are the gravitational force and air resistance. Assuming that the air resistance is small compared to the gravitational force the velocity of the cylinder in air v can be expressed by g and drop height, h_0:

$$v^2 = v_0^2 + 2ah_0 = 2gh_0 \tag{2.34}$$

2.4.1 Slamming

Slamming is defined as a impulse load with a high pressure peak that occur during impact between a body and water [8]. The load only occur in a very short time period and is very localised in space.

For a horizontal cylinder falling through an initially calm water surface with a constant velocity V, it is assumed that the flow is two-dimensional, irrotational and that the fluid is incompressible. The cylinder has small submerge. The parameters are shown in figure 2.3. Here Vt is the lowest point of the body relative to the water plane, t is the time variable, the wetted body is between $-c(t) \leq x \leq c(t)$, and η_b is the vertical coordinate of a point on the cylinder relative to the bottom of the cylinder.

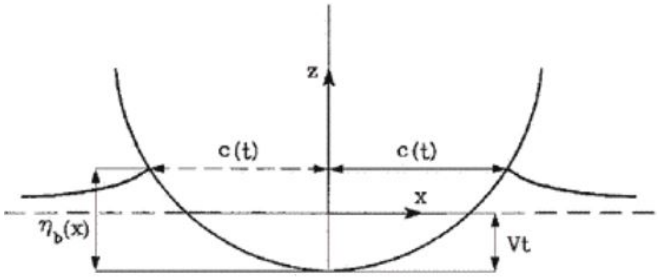

Figure 2.3: *Definition of parameters in analysis of slamming; impact forces and pressures on a cylinder [9]. Vt is the lowest point on the body relative to the water plane, t is the time, the wetted body is between $-c(t) \leq x \leq c(t)$, and η_b is the vertical coordinate of a point on the cylinder relative to the bottom of the cylinder.*

The hydrodynamic pressure, p, can be calculated from:

$$p = \rho V \frac{c}{(c^2 - x^2)^{\frac{1}{2}}} \frac{dc}{dt} \tag{2.35}$$

and the vertical force on the body by:

$$F_3 = \int_{-c}^{c} \rho \, dx = V \frac{d}{dt} \left(\rho \frac{\pi}{2} c^2 \right) \tag{2.36}$$

where ρ is the density of water. From von Karman's solution $c^2(t) = 2VtR - V^2t^2$ for a circular cylinder with radius R. From Wagner's approach $c = 2\sqrt{VtR}$. The difference between the two approaches is that Wagner's method include the local up-rise of water on the body while von Karman's do not. The result is a larger wetted length. The dynamic free surface condition hold in both instances. [8]

2.4.2 Air Cavity

Air cavity is entrained air over and behind the body as the cylinder move through the surface. As the air cavity collapses, or pinches off, an air bubble might stay connected to the fore and aft of the body dependent on the Froude number, $F_n = v/\sqrt{gD}$ [16]. For the approximate band of $4.5 \leq F_n \leq 8.5$ the flow regime is low-speed, for $8.5 \leq F_n \leq 100$ transitional and for $F_n \geq 100$ high-speed. In the low-speed and high-speed regimes closure of the cavity bubble occur relatively far down into the water. In the transitional flow regime the behaviour is complex and multiple pinch-offs may occur. [16]

In the water entry phase the air cavity affect the buoyancy force as the cylinder will not be fully enclosed by water. The resulting force direction might not be vertical and thus dependent on the angle of attack as the body pierce the surface, may alter the motion of the cylinder with the deceleration in the opposite direction of the velocity [2]. The closed cavity bubble will vibrate and collapse, and thus causing an oscillation in the acceleration of the body. [16]

Chapter 3

Numerical Work

In order to validate and compare the theory describing the trajectory of a falling cylinder a simulation script based on the theory in Chapter 2 was made in MATLAB. The script calculates the expected trajectory for drops under the surface for cases where the effect of waves and current are neglected. Effects from motion through the water surface will therefore not be included. The results from this script will be compared to the results from the experiments. The script can simulate the trajectory of a cylinder with capped ends, open ends, and with longitudinal asymmetry about COG. The classical Runge-Kutta method of 4th order, as given in [15], were used to solve the equations of motion for a time step, dt, of $dt = 0.01$ s, and the trapezoidal method were used for all integrations over the length of the body. The scripts in itself and the simulated results have been cross-checked with a similar script made by another student, as mentioned in the Preface.

3.1 Coefficients and Constants

The coefficients and constants in the script can be divided into two categories: constants independent of the characteristics of the body to be dropped, and constants and coefficients dependent on the characteristics. g, ν and ρ belong to the first group. Assuming the water in the calculations is fresh water, these are set to $g = 9.8085$ m/s^2, $\nu = 1.14{*}10^{-6}$ m^2/s and $\rho = 1000$ kg/m^3.

The other group consist of the constant defining the trailing edge x_T/L and the drag coefficients C_{Dx} and C_{Dz}. Aanesland proposed an upper and lower limit of the effective trailing edge, given by x_T/L. The geometric trailing edge was used as an upper limit, with the value 0.5, and the value used for ships with blunt after bodies, 0.3, were used as the lower limit [4]. As the local coordinate system is centred in COG, the upper limit represent the coordinate of the aft of the body.

The form drag, C_{Dx}, is caused by pressure due to boundary layer separation. The coefficient can be found in Hoerner (1965) for cylindrical bodies in axial flow, and is set to 0.65 [10]. The coefficient for the cross-flow drag, C_{Dz}, is very much dependent on Re of the flow. This is illustrated in Figure 3.1 for a circular cylinder in an incompressible flow

regime. Here area A cover the subcritical flow regime with a laminar boundary layer, area B the critical flow regime with transitional boundary layer, C the supercritical flow regime and D the post-supercritical flow regime, both with a turbulent boundary layer. For an approximate heave velocity of 1 m/s and $D = 0.01$ m, $Re \approx 9{*}10^3$. This is clearly in the subcritical area and give C_{Dz} equal to 1.0.

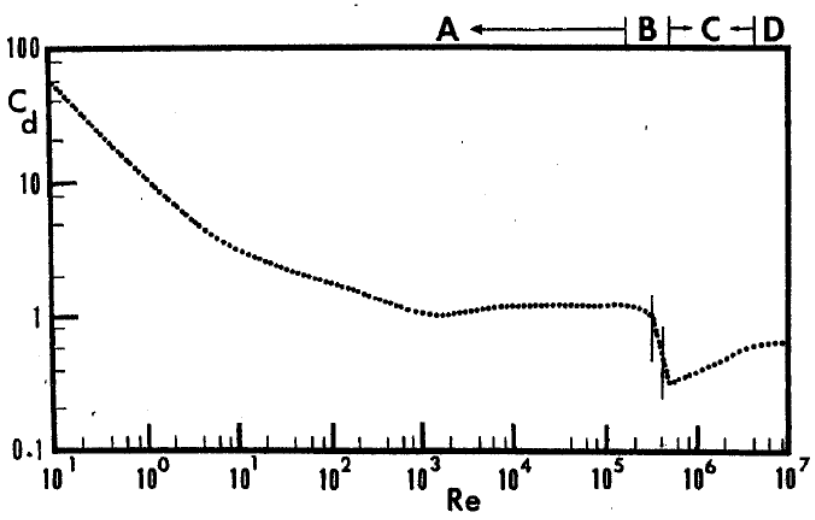

Figure 3.1: *Cross flow drag coefficient, C_{Dz}, for circular cylinder in steady incident flow. Area A cover subcritical flow, area B critical flow, area C supercritical flow and area D post-supercritical flow. [20]*

Chapter 4

Experimental Work

Drop experiments were performed in the tank, Dokka, at the Centre of Marine Technology between 19.02.2018 and 23.02.2018, and 04.04.2018 and 06.04.2018. The first time period marks the first round of experiments and the latter the second. The experiments consisted of drops under and above the surface with drop angles from 15° to 75°. The drops where performed with symmetric cylinders with varying diameter, with cylinders with asymmetry around centre of gravity, and with open cylinders. The characteristics of the cylinders where scaled with respect to the the depth of the tank to represent full size drill pipes.

4.1 Scaling

In order to achieve similarity between the forces in model and full scale the following conditions must be satisfied [20]:

- Geometrical similarity
- Kinematic similarity
- Dynamic similarity

With geometrical similarity the model and full scale geometry must be the same. This also applies to the environment. This is given by a constant ratio between the dimensions of the two:

$$\lambda = \frac{L_F}{L_M} \tag{4.1}$$

where L_F and L_M are any dimensions of the full scale and model scale structure.

For kinematic similarity to be satisfied between model and full scale, the ratio between the velocities in one scale has to be equal to the ratio of the other. This ensures that the flow will undergoes similar geometrical motion in both scales.

Finally, dynamic similarity requires that the ratios for the different force contributions present in the problem are the same for model and full scale. These force contributions may be inertia forces, viscous forces, gravitational forces, pressure forces, elastic forces in the fluid or surface forces.

4.1.1 Reynolds scaling

The Reynolds number expresses the ratio between the inertia and viscous forces, given by

$$\frac{F_i}{F_v} \propto \frac{\rho U^2 L^2}{\mu U L} = \frac{\rho U L}{\mu} = \frac{U L}{\nu} = Re \tag{4.2}$$

where ρ is the density of the water, U the velocity and L the length. $\nu = \mu/\rho$ is the kinematic viscosity. This way it is ensured that the viscous forces are correctly scaled. As the dominating force for the case of a falling cylinder in water is the drag force, and thus the viscous forces, the Reynolds number will be used in the scaling of the experiments. The scaling factors are given in the table 4.1 underneath.

Table 4.1: *Scaling Factors by Reynolds number [13]*

Parameter	Expression	Reynolds Scaling
Length, width, height	L_F/L_M	λ
Volume	V_F/V_M	λ^3
Velocity	U_F/U_M	λ
Kinematic viscosity	ν_F/ν_M	1
Mass	m_F/m_M	λ^3
Force	F_F/F_M	1

.

Generally it is not possible to achieve equality in Reynolds scaling, even though it should in principle be satisfied. The viscous effect will not be correctly scaled and in the scaling process from model to full scale, this effect has to be evaluated.

4.2 Set-up of the Experiments

The first round of drop experiments was performed between 19th and 23rd of February 2018 and consisted of drops under and above water with closed cylinders with varying diameter and asymmetric cylinders. A drawing of the tank with the set-up is presented in Figure 4.1, underneath. The cylinders were dropped from the middle of the tank, parallel to the right and left wall. As the basin has a supporting wall to a basin beside Dokka, and an open, deeper hole on the right hand side of the tank, the drop point was moved 90 cm towards the left wall. This can be seen in figure 4.1.

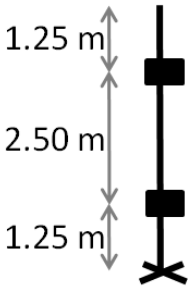

(a) The vertical position of the Oqus cameras on each camera rig.

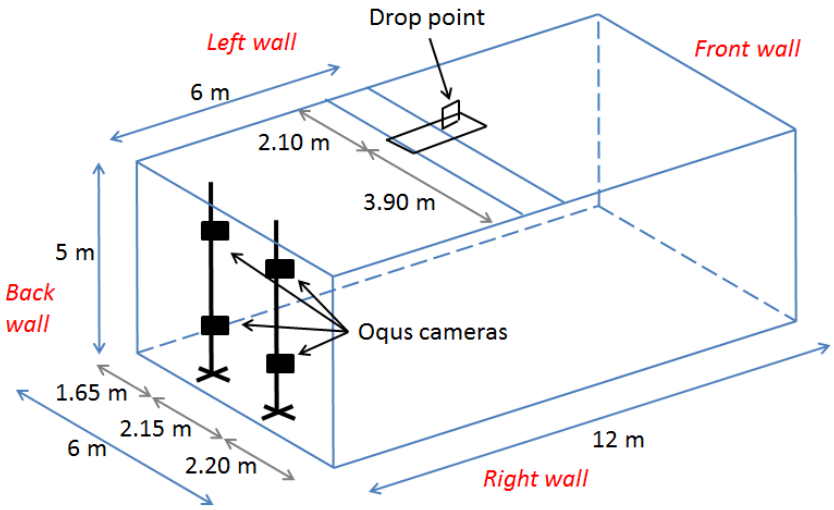

(b) Overview of the set-up in the tank, Dokka.

Figure 4.1: *Overview of the set-up for the first round of experiments, including positions of cameras and drop rig in the tank (grey arrows). Please notice that the drop rig is placed such that the cylinders will be dropped parallel to the left and right wall.*

The second round of drop experiments was performed between the 4th and 6th of April 2018. In this round drops where performed with open cylinders with variation in diameter. A drawing of the set-up in the tank can be seen in Figure 4.2. The cylinders were dropped along the back side of the tank. This was done in order to properly trace the markers on the pipes as it was not possible to attach the marker to the back end of the pipe. The drop point was 33 cm from the wall and 92 cm from the back wall and the drop rig was the same as in round 1. This can be seen in figure 4.2 and figure 4.4. Four Oqus 5+ cameras were used and the placement can also be seen in the figure 4.2. The position of the cameras on each camera rig is the same as in the first round of experiments.

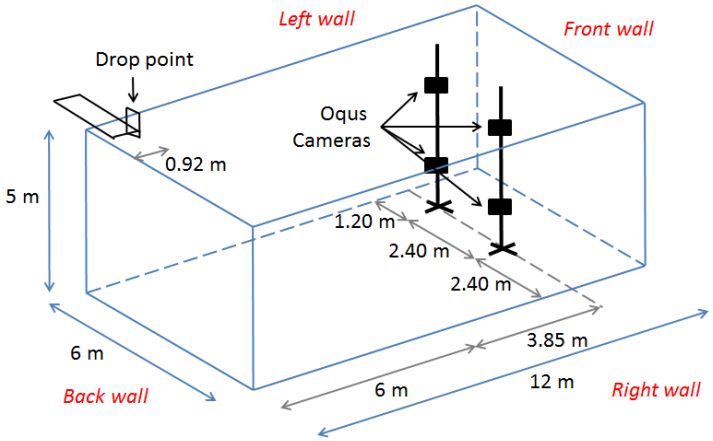

Figure 4.2: *Overview of the set-up for the second round of experiments, including positions of cameras and drop rig in the tank (grey arrows). Please notice that the drop rig is placed such that the cylinders will be dropped parallel to the back wall.*

4.2.1 Measurement Equipment

The trajectories of the dropped cylinders in the experiments, were captured by an Oqus Underwater System. For the first round of experiments three Oqus 5+ camaeras and one Oqus 7+ camera, all with waterproof housing, were used. In the second round four Oqus 5+ cameras were used. For both rounds the frame rate was 179 frames per second. The cameras are able to capture motion in three dimensions as long as at least two cameras are able to identify the object in the water. As the cylinders in the experiments could land in a range from 0 to 6 m from the drop point, the cameras were placed in the back end of the tank in order to capture an area as large as possible in the first round. This can be seen in figure 4.1, above. In the second round the cameras were placed with the distance to the back wall where they were able to capture as much of the tank as possible and still close enough to actually capture the motion.

The cameras capture the motion of an object by logging the position of a marker or markers over time. The markers in the experiments in this thesis, were a reflex tape with a thickness of 5 cm, glued on to one end and back of the cylinders. This can be seen in figure 4.6. The Oqus cameras have a set of lights around the lens of each camera that transmit light out into the water. The light is reflected in the markers and picked up by the cameras.

Before the experiment different alternatives of marking the cylinders were tried out. It was found, that with the set-up as given in the first round, the best and most even capture of the position would occur for the cylinders were only one of the ends was marked with reflex tape. The results from these experiments are therefore only the motion of the back end of the cylinder. This is true for all drop cases except for drops with cylinders with COG 1.4 cm above COV. For this instance the cylinders had to be dropped in the opposite direction in order to prevent the cylinders from crashing into the cameras. Therefore, the markers were placed in the front of the cylinder as this would be closest to the cameras. The markers can be seen in figure 4.6.

4.2.2 Drop Rig

The drops in the experiments were executed by the help of the rig that can be seen in figure 4.3. The construction is made out of wood plates and is painted to prevent the wood from expanding or moving when subjected to water.

For drops above the water surface in round 1, two aluminium constructions were used to give a drop height above the surface of 63 cm for a drop angle of 0^o. Scaled to full scale this gives a drop height of 13 m over the surface. The set-up was secured by weights and vises, as can be seen in figure 4.3a. For drops 8.5 cm underneath the surface for a drop angle of 0^o, the rig lay on the cement covers over the tank, secured by two weights. This can be seen in figure 4.3b For both cases the set-ups have been checked to be horizontal with a leveler. This was also the case for drops in the second round of experiments, as can be sin in Figure 4.4.

(a) *Above surface drop* ***(b)*** *Under surface drop*

Figure 4.3: *Setup of the rig in the first round of experiments.*

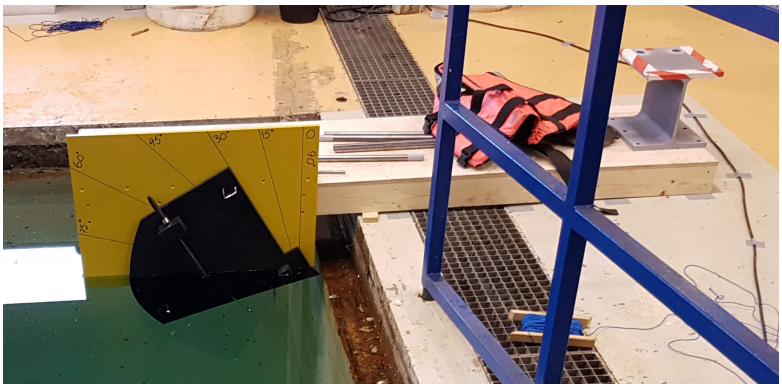

Figure 4.4: *Set-up of the rig for drops under the surface for the second round of experiments.*

As the experiment includes drops with initial drop angles of 15°, 30°, 45°, 60° and 75°, the rig had to be built for this. The design of the drop section of the rig can be seen in figure 4.5. The angle for which one drop is to be performed, is adjusted by moving the black plate such that the side with the incision follows the line of the given angle. The setting is secured by a metal stick through both plates. In the experiments it was measured that the angles given on the drop section had an error of maximum $\pm\ 1^o$.

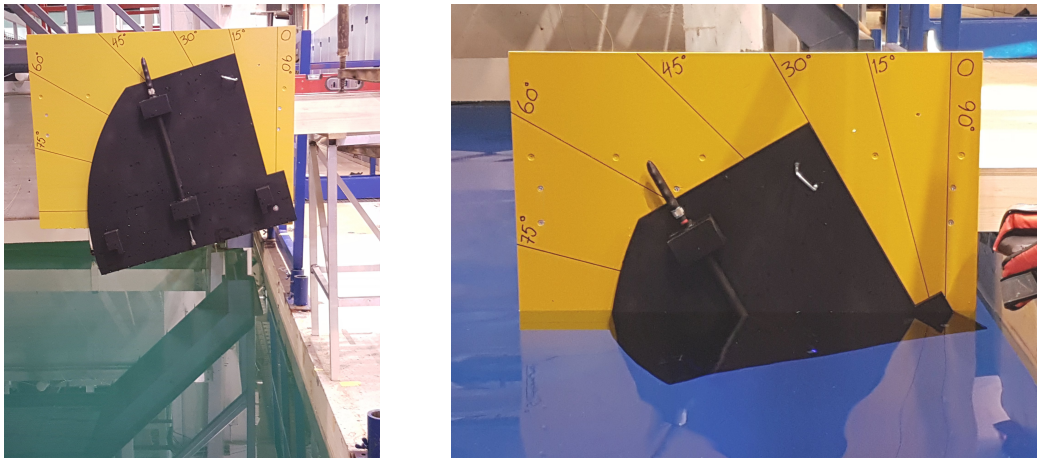

(a) Above surface drop *(b) Under surface drop*

Figure 4.5: *Drop section of the rig. The cylinders are dropped by the help of a magnetic telescope arm. The drop angle are set by aligning the right side of the plate with the indicated angles on the yellow back plate.*

The drop mechanism consist of a magnet attached to a telescope arm and a steel pipe holding the arm into place. During a drop the magnet is attached to the centre of the cylinder such that the cylinder is normal to the steel pipe. Two wooden blocks on each side of the end of the steel pipe support the cylinder in the right position. The cylinder is released by pulling the telescope arm away from the cylinder.

4.2.3 Pipe Characteristics

As the theory in this thesis are based on the equations of motion presented by Aanesland in 1987 [4], the scale and dimensions of the cylinders used in the experiments should be as close as possible to what was used in his experiments. For a scale of 1:20.32, Aanesland used tubes with $L = 0.45$ m, $D_{out} = 0.01$ m and sectional weight of 0.548 kg/m [4]. Using a model scale of 1:20 and the same D_{out} and L as Aanesland, it is possible to model a drill pipe of a full size length of 9 m. The depth of Dokka is 5 m hence giving a real depth of 100 m.

In the experiments, the dependence of the theory on the slenderness of the body will be checked. Therefore, while keeping the length the same, cylinders with three different diameters will be tested. For ϵ equal to 1/45, 1/28 and 1/24 give approximately diameters, D, of 0.010 m, 0.016 m and 0.019 m respectively. The dimensions in model and full size are listed for type 1, 2 and 3 in Table 4.2.

In addition, the effect of a slightly displaced COG compared to COV will be investigated. In particular a shift of 3% and 7% of the length will be used, that give a distance of COV from COG, Δ_{CB}, of 0.014 m and 0.030 m respectively. As the trajectory is expected to be different for cases where COG is above COV in the drop and opposite, both will be tested. As illustrated in Figure 2.2 in Section 2.3.4 Δ_{CB} will be positive for drops where COG is behind COV, and negative for the opposite case. The model size and full size

characteristics of the cylinders used in the experiments are listed for type 4 to 7 in Table 4.2.

Table 4.2: *Cylinder characteristics in full scale and model scale (1:20) as used in the first round of experiments. M/L is the sectional mass and W is the weight of the cylinder.*

Type	**Model scale (1:20)**					**Full scale**				
	D_{out} [m]	L [m]	M/L [kg/m]	W [kg]	Δ_{CB} [m]	D_{out} [m]	L [m]	M/L [kg/m]	W [kg]	Δ_{CB} [m]
1	0.010	0.45	0.215	0.097	0	0.20	9	86.22	776	0
2	0.016	0.45	0.451	0.203	0	0.32	9	180.44	1624	0
3	0.019	0.45	0.533	0.240	0	0.38	9	213.33	1920	0
4	0.010	0.45	0.233	0.105	0.014	0.20	9	93.33	840	0.28
5	0.010	0.45	0.233	0.105	-0.014	0.20	9	93.33	840	-0.28
6	0.010	0.45	0.253	0.144	0.030	0.20	9	128.00	1152	0.60
7	0.010	0.45	0.253	0.144	-0.030	0.20	9	128.00	1152	-0.60

From the set-up of the experiment it is required that the cylinders are made out of steel. For the closed cylinders the ends were capped by gluing turned plugs of equal size to each end. The ends were also covered by a sealing compound afterwards. The same method was applied to cylinder types 4 to 7, but with plugs of different sizes dependent on Δ_{CB}. The cylinders used can be seen in Figure 4.6.

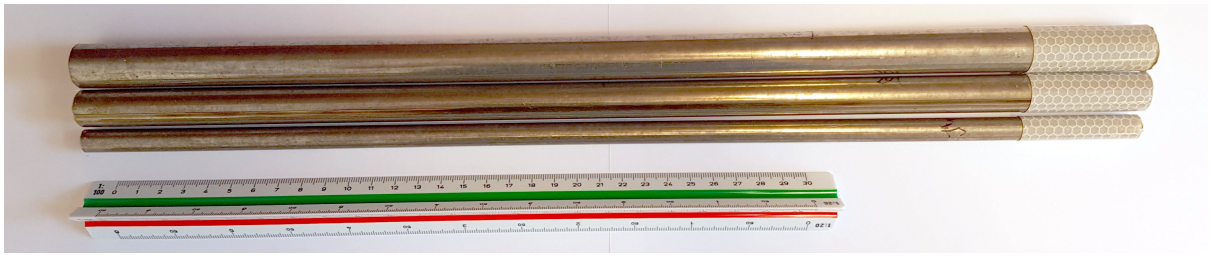

Figure 4.6: *The cylinders used in the experiment, with D equal to 0.019 m, 0.016 m and 0.010 m, from top to bottom.*

The open cylinders dropped in the second round of experiments, have the same dimensions as cylinder type 1 and 3, given above. The characteristics of the open cylinders are listed in Table 4.3.

Table 4.3: *Characteristics of the test pipes in model scale (1:20) and full scale used in the second round of experiments. M/L is the sectional mass and W is the weight of the cylinder.*

Type	**Model scale (1:20)**					**Full scale**				
	D_{out} [m]	D_{in} [m]	L [m]	M/L [kg/m]	W [m]	D_{out} [m]	D_{in} [m]	L [m]	M/L [kg/m]	W [m]
8	0.01	0.008	0.45	0.209	0.094	0.20	0.16	9	83.56	752
9	0.019	0.0165	0.45	0.513	0.231	0.38	0.33	9	205.33	1848

4.2.4 Test Matrices

The test matrix from the first round of experiments can be seen in Table 4.4. Initially all drops were performed 8 times for all types under water and for type 1 to 3 above the water. Additional drops were performed for the drop angles where the result showed a large spread. The weight of each cylinder was checked between each drop in order to determine whether the cylinder was still watertight.

Table 4.4: *Test matrix for the first round of experiments. The numbers listed in the table, are the number of drops performed for each drop angle and cylinder type.*

Type	**Underneath the surface**					**Above the surface**				
	15^o	**30^o**	**45^o**	**60^o**	**75^o**	**15^o**	**30^o**	**45^o**	**60^o**	**75^o**
1	8	8	8	8	8	8	8	8	8	8
2	8	8	8	16	8	8	8	8	8	16
3	8	8	8	16	8	8	8	8	16	15
4	8	8	8	8	8					
5	8	16	13	8	8					
6	8	8	8	8	8					
7	8	8	8	8	8					

For open cylinders only drops underneath the surface were performed. The reason is that the objective of the thesis does not include comparison of capped and open cylinders dropped above the surface as the effects and forces altering the trajectory will be very different for the two cylinders. Thus, the test matrix has been as listed in Table 4.5. Initially 9 drops were performed for each drop angle, but for the drops where the measurements were not detailed enough, additional drops were performed.

Table 4.5: *Test matrix for the second round of tests with drops under the surface. The numbers listed in the table, are the number of drops performed for each drop angle and cylinder type.*

Type	15°	30°	45°	60°	75°
8	9	11	11	11	11
9		10	9	9	9

4.3 Post-processing

The measured position in time of each dropped cylinder in the water column, was automatically saved in structure arrays in MATLAB file format by the Oqus System. The analysis and plotting of the measurement data has consequently been performed in MATLAB.

The results from the experiments include position plots and velocity plots. For the first the trajectory have been plotted in the XYZ plane, the XY plane and XZ plane. For

the latter the X coordinates have been found by projecting the coordinates in the XY plane unto the X axis. This has been done in order to make it easier to compare the experimental results to the simulations, as the theory behind assume a two-dimensional motion.

Some of the drop data included have sudden indents in the trajectories in the transitional area between the cameras. This might have been caused by the cameras not being perfectly calibrated. For these cases the position plot have been smoothed by the *smooth*-function in MATLAB where the effect of the smoothing did not significantly alter the trajectory itself.

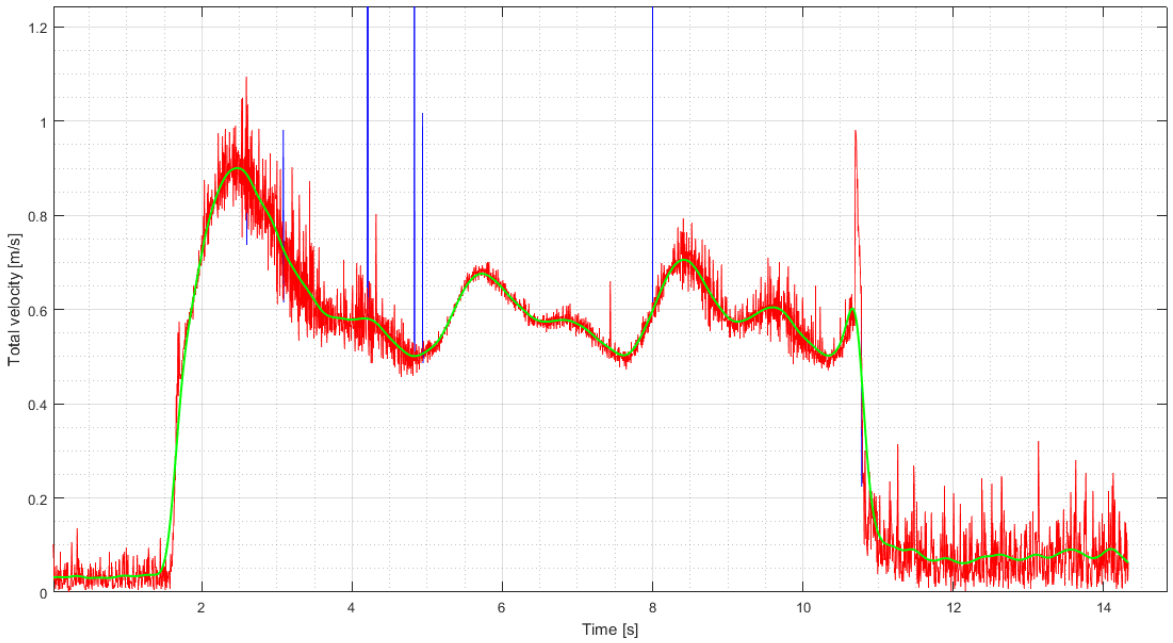

Figure 4.7: *Illustration of the post-processing performed on the plotted total velocity calculated from the position data. Blue plot line is the total velocity calculated from the raw position data in time, red line the total velocity when peaks are removed and green line the final velocity plot. Data before the cylinder has begun to move and after the bottom has been reached, are not removed.*

The velocities have been calculated from the change of position in time. As the position data contain some noise and this noise will be amplified for the calculated velocity, some processing of the data have to be performed in order to get proper velocity plots. Figure 4.7 illustrates the effect of this process. First, peaks where removed by checking whether the difference between the velocities in two time steps was larger than half of the standard deviation of the difference between each time step. For each time step where this occurred, the total velocity was set to the mean of the the two neighbouring points in time. The effect of this procedure can be seen in Figure 4.7 as a red plot line. Second, the plot where smoothed by the same function in MATLAB as described above. This can be seen as a green plot line in the Figure 4.7. In the final results calculated velocities for time

instances where the cylinder had not been dropped and after the bottom was reached, have been removed before the processing.

Chapter 5

Results and Discussion

The following chapter present the most important results and the discussion of these. This include the results from the experiments, the results from the theoretical simulations, comparison of these and comparison with RP F107. The results from the experiments are in their entirety, listed in the Appendix, and the different cylinder types are referred to as the numbered type given in Table 4.2 and 4.3 in Chapter 4.

5.1 Results from the Experiments

The following section presents and discuss the most important results from the experiments. This include drops under and above water for cylinders with variation in diameter, open cylinders dropped under water and cylinders with longitudinal asymmetry about the centre of gravity (COG). In the position plots of the XZ plane, the coordinates on the X-axis are coordinates in the XY plane transposed to the X axis. In order to prevent confusion this will be referred to as *the transformed XZ plane* in the following text and as X_{tr} for X coordinates for this plane.

5.1.1 Drops Under the Surface with Capped Cylinders

The results from the experiments for drops under the surface for closed cylinders, are presented as trajectory plots in Appendices A.1 to A.3, and plots of the velocity development in Appendices B.1 to B.3. Tables with positions of the first and second turn, and maximum velocities are given in Appendices C.1 and D.1. The cylinders in question are listed as cylinders of type 1 to 3 in Table 4.2 in the Section 4.2.

The motion of a capped cylinder falling through the water column can be described by a slightly curved outwards motion in the transformed XZ plane, where the steepness of the curve is dependent on the initial angle with the surface. After a certain depth, dependent on the initial drop angle, the motion of the cylinder slow down and an oscillatory, leaf-like motion starts. This can be seen for a drop angle of 30° for type 1 and 3 cylinders in Figure 5.1 and Figure 5.2. The height in the water for which the pendulum motion

start, is listed as the first turn in Table 5.1 dependent on the drop angle and cylinder type. As can be observed from the table the oscillatory motion begins in general higher up in the water for smaller drop angles. For symmetric cylinders, the lift force created by the axial motion of the cylinder, is concentrated at the leading edge, and thus the front of the cylinder [17]. This will create a moment in the positive pitch direction of the cylinder. Since the angle of the cylinder with the horizontal plane for small drop angles is small, the required moment before the oscillatory motion start, is relatively small.

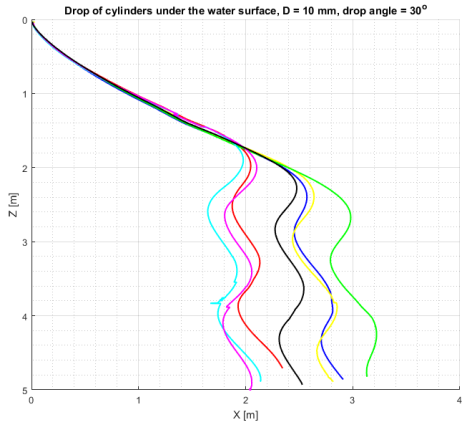

Figure 5.1: *Trajectory for a capped cylinder of type 1 dropped under water with drop angle 30°. Each coloured line represent a drop performed in the experiments.*

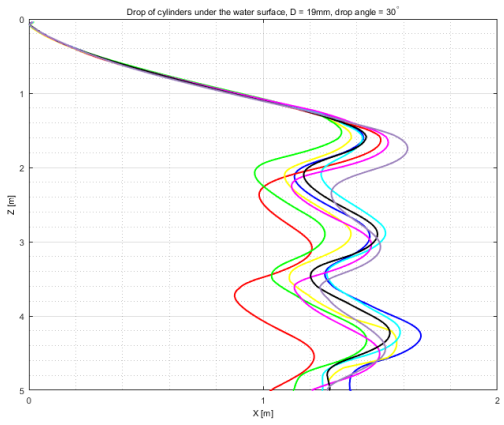

Figure 5.2: *Trajectory for a capped cylinder of type 3 dropped under water with drop angle 30°. Each coloured line represent a drop performed in the experiments.*

Table 5.1: *Mean position of the first turn dependent on cylinder geometry and drop angle, measured as the maximal horizontal excursion of the first turn. The cylinders are of type 1, 2 and 3. X_{tr} is the transposed coordinate from the XY plane to the X axis and σ_{tr} and σ_Y are the standard deviations from the mean coordinates. Drop angles not included have few or no turns compared to the number of drops.*

Type:	**1**				**2**				**3**			
Drop angle	X_{tr} [m]	σ_{tr} [m]	Z [m]	σ_Z [m]	X_{tr} [m]	σ_{tr} [m]	Z [m]	σ_Z [m]	X_{tr} [m]	σ_{tr} [m]	Z [m]	σ_Z [m]
15°	0.73	0.08	1.13	0.06	0.49	0.05	0.98	0.04	0.40	0.07	0.88	0.06
30°	2.37	0.35	2.20	0.27	1.61	0.23	1.72	0.18	1.47	0.09	1.60	0.07
45°	3.79	0.53	3.63	0.56	2.89	0.11	2.93	0.10	2.76	0.16	2.84	0.14

From Table 5.1 one can also observe that the oscillatory motion starts higher up in the water and closer to the origin for larger diameters. This is the case for all drop angels in the experiment where the oscillatory motion has been observed. For a larger diameter the axial and cross sectional flow have to separate over a larger body, thus resulting in larger negative viscous forces that will decrease the velocity of the cylinder. In addition, the larger area of the surface of the body increases the lift and thus a larger momentum about the COG.

The final excursion of the cylinder from the drop point, is very much dependent on the drop angle and the geometric properties of the cylinder. From the plots in the appendices it is possible to observe that the falling leaf-motion oscillate around an approximate X_{tr} position. Some of the drops experience a small drift skewing this oscillation line a little. As a result the steepest drop angle has the largest excursion and the smallest the shortest excursion, and the cylinders with the largest diameter have the shortest excursion compared to cylinders with a larger one. This can also be observed in excursion at a depth of 4 m for drop angles from 15° to 45°, as is presented in Table 5.2. For drop angles of 60° to 75° few of the cylinders have begun their oscillatory motion before a depth of 4 m, and the excursion for these can therefore be expected to be larger at an increased depth.

Table 5.2: *Mean position of a cylinder dropped under water at a depth of 4 m for each drop angle for cylinder type 1, 2 and 3. X_{tr} is the transposed coordinate from the XY plane to the X axis and σ_{tr} and σ_Y are the standard deviations from the mean coordinates.*

Type:	**1**				**2**				**3**			
Drop angle	X_{tr} [m]	σ_{tr} [m]	Y [m]	σ_Y [m]	X_{tr} [m]	σ_{tr} [m]	Y [m]	σ_Y [m]	X_{tr} [m]	σ_{tr} [m]	Y [m]	σ_Y [m]
15°	0.89	0.19	-0.01	0.05	0.79	0.17	-0.05	0.04	0.35	0.18	-0.02	0.06
30°	2.32	0.56	-0.10	0.36	1.51	0.35	0.07	0.27	1.35	0.19	-0.10	0.14
45°	3.67	0.51	-0.04	0.81	2.79	0.12	-0.05	0.27	2.58	0.13	-0.21	0.29
60°	2.79	0.39	0.06	0.50	2.94	0.45	-0.73	0.59	2.48	0.67	-0.73	1.08
75°	1.49	0.18	0.02	0.18	1.68	0.04	0.16	0.26	1.81	0.17	-0.11	0.46

The spread in the results in the transformed XZ plane is also indicated in Table 5.2. It is in general very varying independent geometry and drop angle. As can be seen in Figure 5.1 and Figure 5.2 there are small differences in the trajectory before the oscillatory motion starts, indicating that the difference might be caused by mass and small differences in viscous forces.

The highest velocities occur for the steepest drop angle independent on cylinder type. This can be read from Table 5.3 where the mean maximum velocity, $\bar{V}_{max}$, is listed with the standard deviation, $\sigma_{\bar{V}_{max}}$, for each cylinder type and drop angle. For steeper drop angles the mass force have a larger impact on the motion compared to the lift and viscous forces, resulting in a higher velocity. As the highest velocity for each drop angle are obtained for cylinder type 1 and cylinder type 3 is more than twice as heavy as type 1, it is possible to conclude that the effect of the size of the viscous forces acting on the cylinder, influence the velocity and the trajectory to a larger extent than the mass.

Table 5.3: *The average maximal total velocity, $\bar{V}_{max}$, and standard deviation, $\sigma_{\bar{V}_{max}}$, dependent on cylinder type and drop angle in the experiments. The cylinders are of type 1, 2 and 3.*

Type:	**1**		**2**		**3**	
Drop angle:	$\bar{V}_{max}$ [m/s]	$\sigma_{\bar{V}_{max}}$ [m/s]	$\bar{V}_{max}$ [m/s]	$\sigma_{\bar{V}_{max}}$ [m/s]	$\bar{V}_{max}$ [m/s]	$\sigma_{\bar{V}_{max}}$ [m/s]
15°	0.85	0.02	0.85	0.03	0.79	0.02
30°	1.53	0.09	1.33	0.09	1.17	0.03
45°	2.17	0.09	1.92	0.07	1.70	0.03
60°	2.68	0.07	2.43	0.10	2.43	0.10
75°	2.96	0.05	2.60	0.02	2.33	0.03

In general, the total velocity peaks in value before the first turn, and then the size of the velocity decreases and increases with a small difference corresponding to the oscillatory motion afterwards. This can be seen Figure 5.3 for cylinder type 1 and 3. An approximate minimum is 0.5 m/s for cylinder type 1 and 0.4 m/s from cylinder type 3. The approximate maxima in the oscillations are 0.8 m/s for both type 1 and 3. The fact that the minima are not zero are caused by a vertical motion in the water even when the horizontal motion is zero and the cylinder shift direction. However, these results are not very exact and more experiments on a larger water depths are required to give a good result.

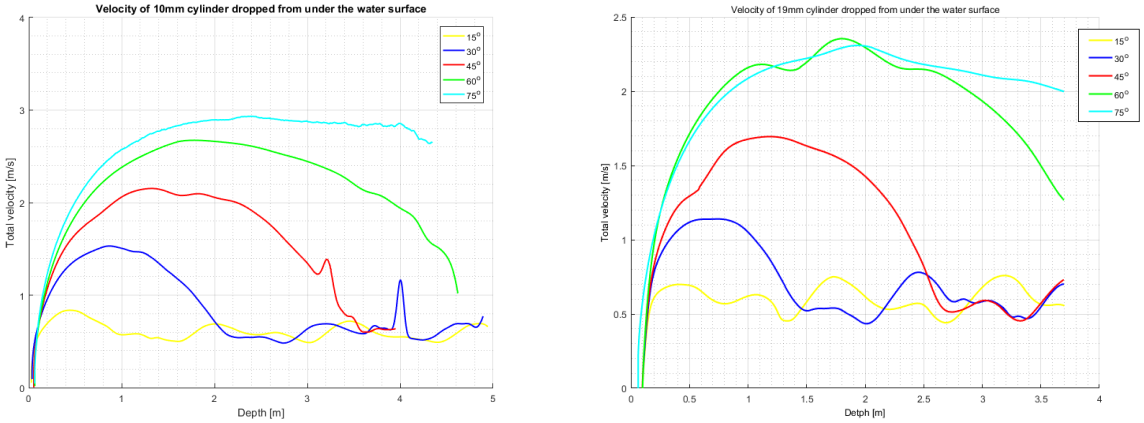

(a) *Type 1.* ***(b)*** *Type 3.*

Figure 5.3: *Total velocity compared to depth for closed cylinders. The cylinders are dropped under the surface with initial drop angles* 15°, 30°, 45°, 60° *and* 75°. *Each plot line represents an example of the total velocity development. The sudden jumps in the graphs are caused by a jump in the position measurement, resulting in a jump in the velocity graphs as the velocity is calculated from the position.*

5.1.2 Drops of Open Cylinders

The results from the experiments for drops under the surface for closed cylinders, are presented as trajectory plots in Appendices A.7 and A.8, and as velocity plots in Appendices B.7 and B.8. Tables with positions of the first and second turn, and maximum velocities are given in Appendices C.3 and D.3. The cylinders in question are listed as cylinders of type 8 and 9 in Table 4.3 in Section 4.2.

The trajectory of open cylinders falling in the water column can be described in similar terms to the motion of capped cylinders in the transformed XZ plane. As with capped cylinders, the oscillatory motion begin higher up in the water column for cylinders with a larger diameter compared to those with a smaller one, resulting in a smaller excursion from the drop point. The difference in the excursion can be seen in Table 5.4, listing the excursions, X_{tr}, Y coordinates and their respective standard deviations at a depth of 4 m.

Table 5.4: *Mean position of an open cylinder dropped under the water at a depth of 4 m for each drop angle for cylinder type 8 and 9. X_{tr} is the transposed position from the XY plane onto the X axis, and σ_{tr} and σ_Y are the standard deviations from the mean coordinates.*

Type:	**8**				**9**			
Drop angle	X_{tr} [m]	σ_{tr} [m]	Y [m]	σ_Y [m]	X_{tr} [m]	σ_{tr} [m]	Y [m]	σ_Y [m]
15°	0.85	0.13	-0.15	0.08				
30°	1.91	0.14	-0.19	0.18	1.20	0.37	-0.06	0.09
45°	2.57	0.17	-0.22	0.28	1.38	0.10	-0.07	0.14
60°	3.12	0.12	-0.10	0.25	2.09	0.10	-0.10	0.19
75°	2.62	0.26	-0.20	0.24	1.79	0.09	-0.14	0.24

In general, the excursions for open cylinders are significantly shorter compared to cylinders with capped ends. This can be deduced by comparing the excursions from the drop point for the open and closed cylinders that have turned. The difference is caused by the fact that the open cylinders turn higher in up in the water column and closer to the drop point, as can be observed for a drop angle of 60° in Figure 5.4. For the open cylinder the axial drag is reduced as the flow does not meet a blunt front end of the cylinder, but only have to separate around the edges. Thus, there will be flow through and around the body, reducing the pressure on the cylinder itself. The result is a higher axial velocity and consequently an increased lift on the cylinder. The effect of this on the motion can be seen in Figure 5.5 where the motion of a cylinder with capped ends and one with open ends with the same dimensions and the same drop angle, are plotted. By studying the two plots it can be observed that the angle with the horizontal plane as the cylinder turn, are steeper for the open cylinder compared to the closed one. This is also caused by the size of the velocity and the lift force.

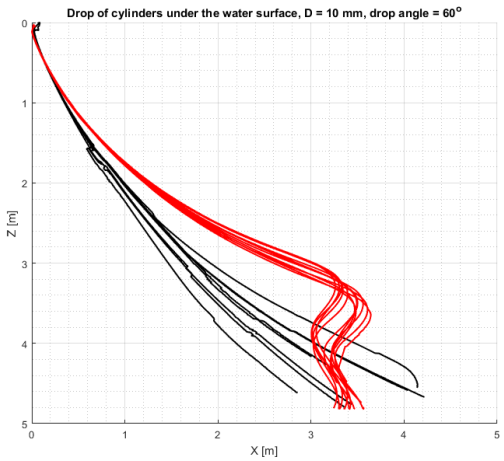

(a) Type 8.

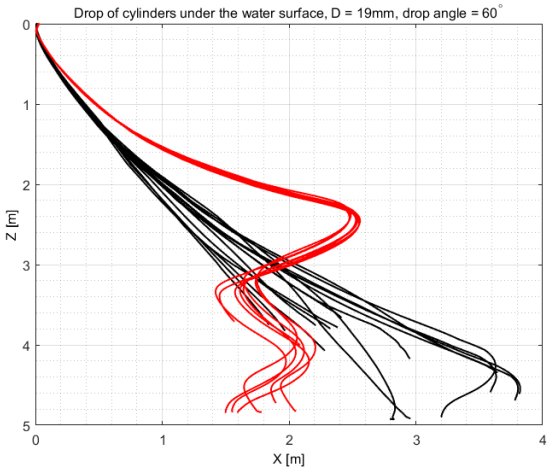

(b) Type 9.

Figure 5.4: *Comparison between the trajectory in the XZ plane for open (red lines) and closed cylinders (black lines) dropped under water with a drop angle of* 60°.

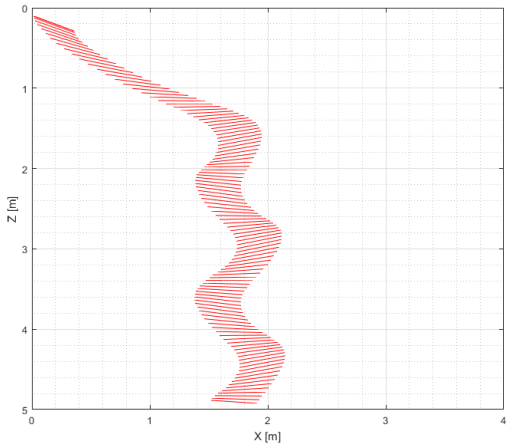

(a) Type 3.

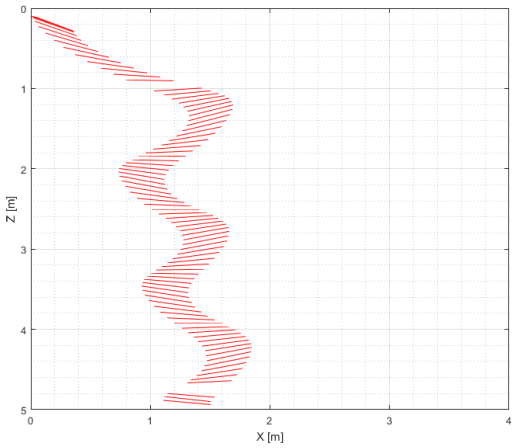

(b) Type 9.

Figure 5.5: *Orientation in water for capped and open cylinder at an drop angle of* 30° *as measured in the experiments.*

In Figure 5.4 it is possible to observe that for cylinders of type 9 have a larger first turn as part of the oscillatory motion compared to the turns further down into the water. As this is not the case for capped cylinders, this indicate that this might be caused by the internal flow. However, this pattern are not observed for type 8 cylinders. Type 9 cylinders have a double internal diameter compared to cylinder type 8. The internal flow regime might therefore be slightly different in the two cylinders. Also, the fact that this occur for the first turn, indicate that this is linked to the velocity of the cylinder. The velocities further down in the oscillatory motion are much smaller.

For open cylinders the maximum velocities are approximately the same for both cylinder types, as listed in Table 5.5, thus indicating that the value of the slenderness parameter is of less significance when considering the velocity. As the flow separation in the direction of motion is limited to the separation around the edges of the cylinder the velocity is less reduced for larger diameters. This is also the reason why $\bar{V}_{max}$ is in general larger for all drop angles compared to capped cylinders. However, as with cylinders with end caps, $\bar{V}_{max}$ is obtained relatively early in the trajectory and before the oscillatory motion begins, as can be seen in Figure 5.6.

Table 5.5: *The average maximal total velocity, $\bar{V}_{max}$, and standard deviation, $\sigma_{\bar{V}_{max}}$, dependent on cylinder type and drop angle in the experiments. The cylinders are open and dropped under the water surface.*

Type:	**8**		**9**	
Drop angle:	$\bar{V}_{max}$ [m/s]	$\sigma_{\bar{V}_{max}}$ [m/s]	$\bar{V}_{max}$ [m/s]	$\sigma_{\bar{V}_{max}}$ [m/s]
15°	1.05	0.05		
30°	1.68	0.05	1.66	0.03
45°	2.35	0.07	2.32	0.04
60°	2.87	0.06	2.89	0.02
75°	3.29	0.05	3.30	0.02

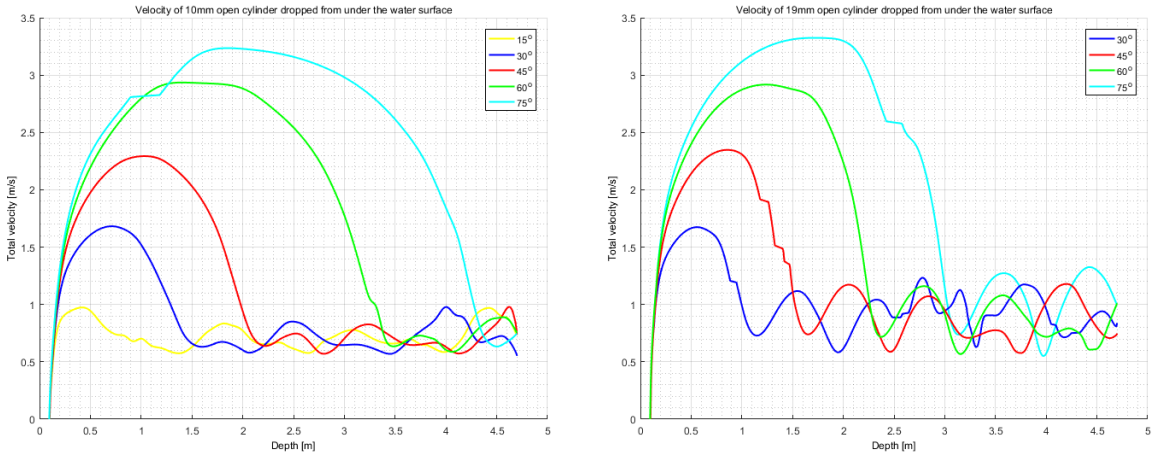

(a) *Type 8.* ***(b)*** *Type 9.*

Figure 5.6: *Total velocity compared to depth for open cylinders. The cylinders are dropped under the surface for drop angels 15° (only type 8), 30°, 45°, 60° and 75°. Each plot line represent an example of the total velocity development.*

5.1.3 Cylinders Asymmetric about the Centre of Gravity

The drops performed for cylinders with a COG different from the centre of volume (COV) have been executed for COG above the COV, and COG in front of the COG, as described in Section 4.2. The results are presented as position plots in Appendices A.9 to A.12, and as velocity plots in Appendices B.9 to B.12. Position and velocity tables are presented in Appendices C.4 and C.5, and Appendices D.4 and D.5, respectively. The characteristics of the cylinders are listed in Table 4.2 in Section 4.2.

For all drops except drops with cylinders of type 4 with initial drop angle of 15°, 30° and 45°, the motion of the aft of the cylinder has been tracked. For the excepted cases the fore part has been tracked. As a result of measuring the front end instead of the back, the cylinder will start slightly deeper in the water dependent on the drop angle, the excursion of the first turn will be larger and the measurements of the trajectory will stop before the bottom. However, the motion of the cylinder before and after the area where the turn occur, will be very similar to the motion of a cylinder with the same characteristics where the aft is measured.

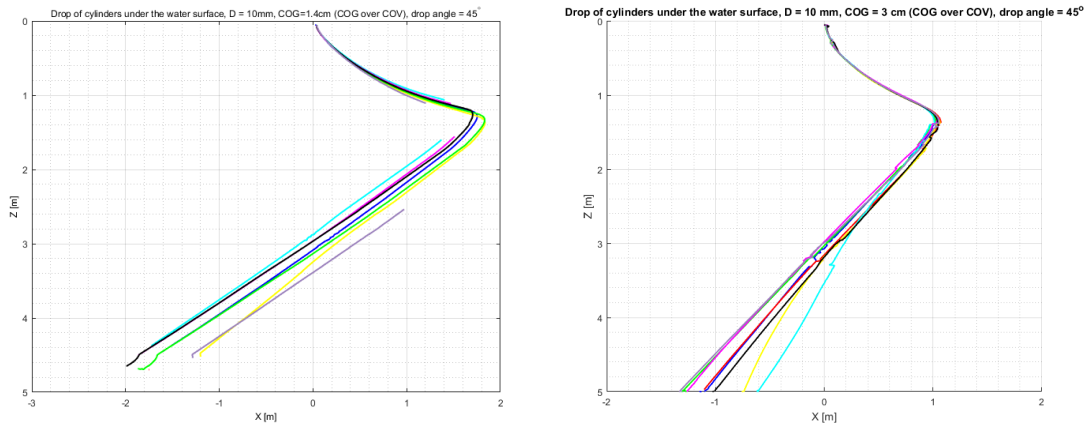

(a) Type 4. *(b) Type 6.*

Figure 5.7: *Trajectory for cylinders dropped under water with COG above COV for an drop angle of* 45°*. Each coloured line represent a drop.*

For all performed drops where the COG is above the COV, the general motion can be described by a slight curved motion before the cylinder flips, followed by a straight, very stable motion in the opposite direction thereafter. This can be seen in Figure 5.7. The height in the water column for which the turn occur, is dependent on the drop angle and the relative position of the COG in the cylinder. This can be read from Table 5.6, listing the positions of the flip in the water column for each cylinder type dependent on the drop angle.

Table 5.6: *Mean position of the flip for cylinders dropped with COG above COV. The positions are dependent on the relative position of COG and the drop angle. The cylinders are of type 4 and 6. Drops where the front of the cylinder are measured is marked with F and cases where the back are measured is marked A. Z corr. give an estimate of where the aft would have been in the turns, as the origin mark the beginning of the tracked motion. Z corr. has been calculated basted on the initial drop angle and length of the cylinders.*

Type:	**4**						**6**				
Drop angle	Fore(F)/ Aft (A)	X_{tr} [m]	σ_{tr} [m]	Z [m]	Z corr. [m]	σ_Z [m]	Fore(F)/ Aft (A)	X_{tr} [m]	σ_{tr} [m]	Z [m]	σ_Z [m]
15°	F	0.21	0.10	0.36	0.47	0.15	A	0.07	0.01	0.45	0.01
30°	F	0.65	0.05	0.57	0.8	0.03	A	0.41	0.01	0.84	0.01
45°	F	1.74	0.09	1.29	1.61	0.08	A	1.04	0.02	1.35	0.02
60°	A	2.62	0.21	2.97		0.21	A	1.66	0.03	2.15	0.05
75°	A	3.04	0.03	4.31		0.05	A	2.14	0.00	3.17	0.07

For small drop angles there are little difference between the two types of cylinders for the height of which the flip occur. For small angles the required moment necessary for this to happen is small and thus less dependent on the relative position of COG. For drop angles from 45° there is a clear dependence on the relative position of COG as cylinder type 4 with only a small Δ_{CB} flip increasingly deeper compared to type 6, dependent on the drop angle.

In general for cylinders dropped with COG above COV, the cylinders with the smallest shift in COG have the largest excursion from the drop point. As the length of Δ_{CB} the moment created by the relative position of COG is small and hydrodynamic forces will affect the motion to a larger extent, compared to higher values of Δ_{CB}.

Table 5.7: *Mean position at a depth of 4 m for a cylinder dropped under water with COG above COV, for each drop angle for cylinder type 4 and 6. X_{tr} is the radial coordinate from the XY plane, and σ_{tr} and σ_Y are the standard deviations from the mean coordinates.*

Type:	**4**					**6**				
Drop angle	Fore(F)/ Aft (A)	X_{tr} [m]	σ_{tr} [m]	Y [m]	σ_Y [m]	Fore(F)/ Aft (A)	X_{tr} [m]	σ_{tr} [m]	Y [m]	σ_Y [m]
15°	F	-4.35	0.41	-0.27	0.94	A	-2.49	0.19	0.07	0.45
30°	F	-3.43	0.20	-0.57	0.80	A	-1.66	0.14	0.04	0.50
45°	F	-1.04	0.24	0.01	0.54	A	-0.71	0.15	0.41	0.29
60°	A	1.72	0.46	-0.13	0.14	A	0.65	0.15	-0.12	0.30
75°	A	2.73	0.06	-0.31	0.15	A	1.80	0.14	-0.03	0.19

For drops where the cylinder has been dropped with COG under COV, the trajectory can simply be described as a straight path from the drop point to the bottom. This can be seen in Figure 5.8. The steepness of the path depends on the initial drop point. The trajectory is most linear for type 5 cylinders where the COG are only displaced with a few percentage of the length. For type 7 cylinders the trajectory is slightly curved inwards. This very stable, linear motion, which also occur for cases where cylinders are

dropped with COG above COV, can be explained from the dynamic stability of a ship as described in [17]. The stability is dependent on the length from the COG to the trailing edge, x_T. For sufficiently large values of x_T the ship will be stable and thus by moving the COG towards the fore part of the ship, the directional stability will increase [17]. However, as the cylinder is falling in the water column, which is not the case for a ship, and thus affected by the moment created by the buoyancy and mass force, moving COG too far towards the front will affect the trajectory. This is the case of the slightly curved trajectory of cylinder type 7.

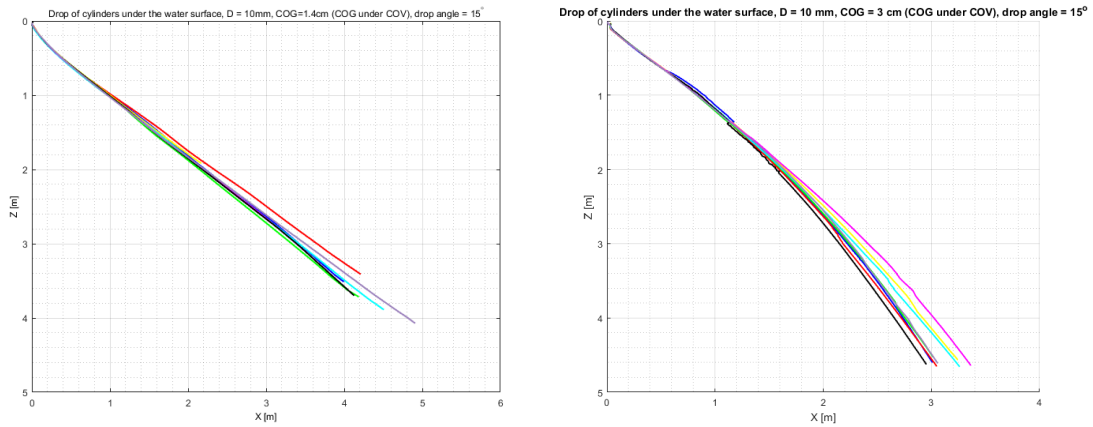

(a) *Type 5.* ***(b)*** *Type 7.*

Figure 5.8: *Trajectory for cylinders dropped under water with COG under COV for an drop angle of* 45°. *Each coloured line represent a drop.*

As for cases where the cylinder has been dropped with COG above COV, the maximum excursion for cylinders dropped with COG under COV from the drop point, is also largest for the cylinder with the smallest shift in the relative position of COG. This can be found by comparing the excursions in Table 5.8 for a depth of 4 m. Compared to the other drop experiments performed in this thesis, the excursion for cylinder type 5 for an drop angle of 15° is the absolute largest.

Table 5.8: *Mean position of a cylinder dropped under water with COG under COV at a depth of 4 m for each drop angle for cylinder type 5 and 7.* X_{rad} *is the radial coordinate from the XY plane and* σ_{rad} *and* σ_Y *are the standard deviations from the mean coordinates.*

Type:	**5**				**7**			
Drop angle	X_{rad} [m]	σ_{rad} [m]	Y [m]	σ_Y [m]	X_{rad} [m]	σ_{rad} [m]	Y [m]	σ_Y [m]
15°	4.65	0.22	0.20	1.28	2.81	0.12	0.33	0.33
30°	3.79	0.27	-0.43	1.08	2.34	0.07	0.24	0.34
45°	2.59	0.17	-0.16	0.57	1.73	0.12	-0.05	0.36
60°	1.70	0.16	-0.22	0.38	1.14	0.12	0.10	0.17
75°	0.98	0.04	-0.09	0.09	0.52	0.10	0.02	0.10

The cylinders dropped with COG above COV have velocities that peak before they decrease and the cylinders turn. Afterwards the velocity increases. For the cylinder with the largest shift in COG the velocity is larger after the flip. The maximum velocities are listed in Table 5.9. As can be read from the table there is a large difference in $\bar{V}_{max}$ for type 4 and type 6 cylinders.

Table 5.9: *The average maximal total velocity, $\bar{V}_{max}$, and standard deviation, $\sigma_{\bar{V}_{max}}$, dependent on cylinder type and drop angle in the experiments. The cylinders have COG behind COV and are dropped under water. The cylinders are of type 4 and 6.*

Type:	**4**		**6**	
Drop angle:	$\bar{V}_{max}$ [m/s]	$\sigma_{\bar{V}_{max}}$ [m/s]	$\bar{V}_{max}$ [m/s]	$\sigma_{\bar{V}_{max}}$ [m/s]
15°	1.88	0.20	2.94	0.18
30°	1.94	0.11	3.04	0.12
45°	2.11	0.05	3.03	0.07
60°	2.39	0.04	3.06	0.13
75°	2.88	0.03	2.82	0.09

For cylinders dropped with COG under and in front of COV, the velocity increases from the drop point before it converges to a constant velocity. The converged velocity is nearly independent of the drop angle for the cylinder where the COG is closest to the front end. This might be because the angle of attack of cylinder type 7 is much steeper compared to type 5. This may indicate that the mass forces are affecting the motion to larger degree compared to the hydrodynamic forces. This may also explained the difference observed for cylinders of type 4 and 6.

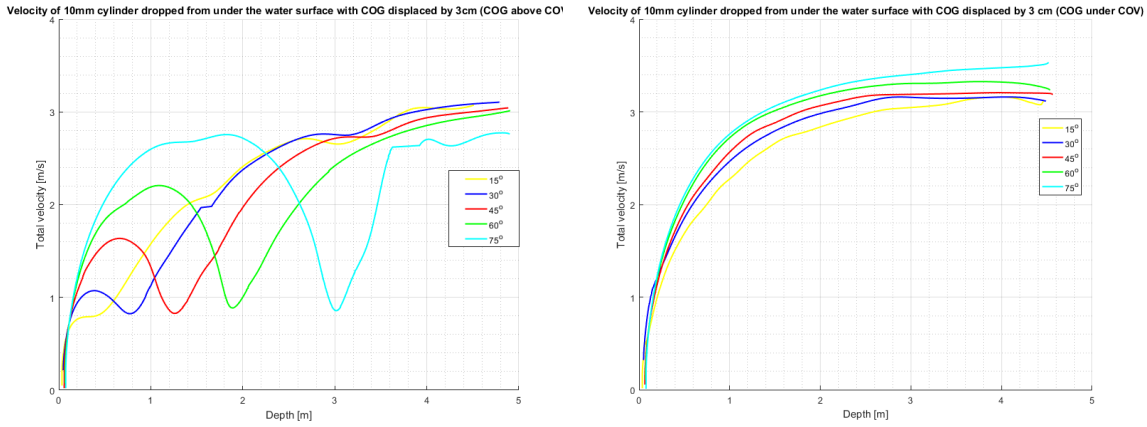

(a) *Type 5.* ***(b)*** *Type 7.*

Figure 5.9: *Total velocity compared to depth for cylinders with asymmetry about COG. The cylinders are dropped under the surface for drop angles* 15°, 30°, 45°, 60° *and* 75°. *Each plot line represent an example of the total velocity development.*

$\bar{V}_{max}$ are listed for cylinder type 5 and 7 in Table 5.10. Cylinder type 7 has, as mentioned, the highest $\bar{V}_{max}$. Compared to closed and open, geometrical symmetric cylinders the

maximum velocities for cylinder type 7 are higher. More importantly the velocity converge and consequently the probability of causing critical damage on equipment and structures in the water column, is much higher.

Table 5.10: *The average maximal total velocity, $\bar{V}_{max}$, and standard deviation, $\sigma_{\bar{V}_{max}}$, dependent on cylinder type and drop angle in the experiments. The cylinders have COG in front of COV and are dropped under water. The cylinders are of type 5 and 7.*

Type:	**5**		**7**	
Drop angle:	$\bar{V}_{max}$ [m/s]	$\sigma_{\bar{V}_{max}}$ [m/s]	$\bar{V}_{max}$ [m/s]	$\sigma_{\bar{V}_{max}}$ [m/s]
15°	2.03	0.10	3.20	0.09
30°	2.33	0.15	3.22	0.05
45°	2.75	0.13	3.27	0.11
60°	2.98	0.04	3.33	0.10
75°	3.08	0.05	3.47	0.09

5.1.4 Drops from Above the Surface

The results from drops of cylinders of type 1, 2 and 3 dropped above the water surface are presented as position plots in Appendices A.4 to A.6, as velocity plots in Appendices B.4 to B.6, and as position and velocity tables in Appendix C.2 and Appendix D.2.

The motion of a slender, cylindrical object dropped above the surface, is to a large degree altered by the motion through the surface itself. This can clearly by observed by studying the figures of the cylinder trajectories in the transformed XZ plane in the appendices. By comparing the experimental results for drops above water with the results for drops underneath the surface, one can roughly observe that the angle of attack is in general altered with $-15°$ to $-30°$. This is caused by the impact force between the cylinder and the water surface, described as slamming, and the occurrence of air cavity.

Air cavity was observed for all cylinders dropped from air, and air bubbles at the upper front and the aft of the cylinder were observed for drop angles from 30° to 75°. For cylinder type 3 this can be seen in Figure 5.10 that show the development in the water entry phase, and in Figure 5.11 and Figure 5.12 that show attached air bubbles at the upper front and at the back of the cylinder. As described in Chapter 2, the creation of bubbles and time until pinch-off are dependent on the Froude number, F_n. By applying Equation 2.34 in Chapter 2 the velocity of a cylinder falling in air from a height of 0.65 m is estimated to be 3.57 m/s. This give a F_n between 8.3 and 11.4 which correspond to a low-speed and transitional flow regime. Thus one could expect pinch-off to occur relatively deep into the water for the first, while for the second there could be several pinch-offs and a more complex cavity behaviour.

The effect of the presence of air cavity contribute to the difference observed for drops under and above water. Only the position of the cylinder in the water have been measured, and it is therefore hard to determine the exact impact of the vibrating air bubbles. The

change of buoyancy as the cylinder move through the surface might explain why the first turn for drop angles of 15° has a small radii compared to the following oscillatory motion.

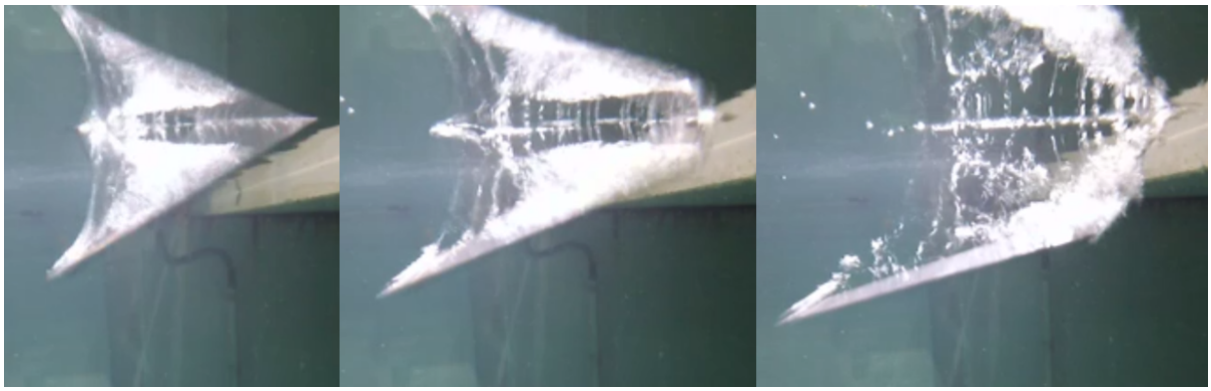

Figure 5.10: *Water entry of a cylinder of type 3 dropped with COG 63 cm above the surface with a drop angle of* 45°. *The upper part of the picture is the mirrored reflection from the free surface.*

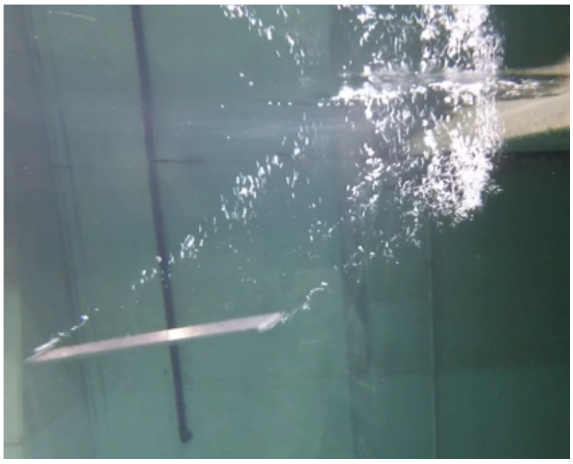

Figure 5.11: *Drop angle:* 45°. *Cavitation bubbles on the upper front and the back end of a type 3, dropped with COG 63 cm above the water surface with a drop angle of* 45°.

Figure 5.12: *Drop angle* 60°. *Cavitation bubbles on the upper front and the back end of a type 3 cylinder, dropped with COG 63 cm above the water surface with a drop angle of* 60°.

The motion through the surface has a great impact on the motion of the cylinders. This can also be observed in the maximum radial excursion and the excursion at a depth of 4 m. The latter are listed in Table 5.11. Compared to the results for the cylinders dropped under the surface the excursion of the drop cases where the cylinder has started its oscillatory motion, the drops above the surface have a smaller excursion. The pattern that the most slender cylinder have the largest excursion, is also the case when dropped above water.

Table 5.11: *Mean position of a cylinder dropped above the water at a depth of 4 m for each drop angle for cylinder type 1, 2 and 3. X_{tr} is the transposed coordinate from the XY plane to the X axis, and σ_{tr} and σ_Y are the standard deviations from the mean coordinates.*

Type:	**1**				**2**				**3**			
Drop angle	X_{tr} [m]	σ_{tr} [m]	Y [m]	σ_Y [m]	X_{tr} [m]	σ_{tr} [m]	Y [m]	σ_Y [m]	X_{tr} [m]	σ_{tr} [m]	Y [m]	σ_Y [m]
15°	0.22	0.12	-0.02	0.03	0.16	0.29	0.05	0.11	0.04	0.15	-0.03	0.03
30°	0.70	0.25	0.01	0.10	0.34	0.26	0.04	0.05	0.05	0.20	-0.08	0.13
45°	1.47	0.28	-0.04	0.15	0.90	0.22	0.03	0.08	0.64	0.17	-0.12	0.16
60°	2.64	0.57	0.20	0.31	1.66	0.14	-0.15	0.18	1.54	0.54	-0.36	0.72
75°	3.21	0.24	-0.28	0.71	3.40	0.49	0.39	1.16	2.83	0.47	-0.43	1.50

In the experiments the velocity of the dropped cylinder is first captured by the cameras after the cylinder has pierced the surface. For drop angles from 15° to 45° the cylinder will gain the maximum velocity as it falls through the air. In the velocity plots in in Figure 5.13 it can clearly be seen that the total velocity of the cylinder decreases rapidly after the object pierce the surface for drop angles 15° to 60°. By applying Equation 2.34 in Chapter 2 the velocity of a cylinder falling in air from a height of 0.65 m is estimated to be 3.57 m/s.

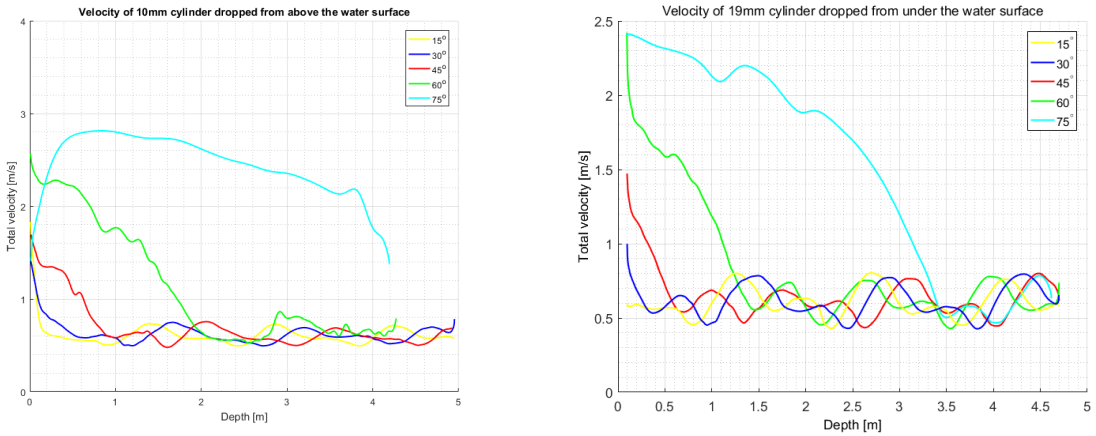

(a) *Type 1.* ***(b)*** *Type 3.*

Figure 5.13: *Total velocity compared to depth for cylinders with dropped above the surface. The cylinders are dropped under the surface for drop angles* 15°, 30°, 45°, 60° *and* 75°. *Each plot line represent an example of the total velocity development.*

As the cylinder lose a large part of its energy gained from falling in the air, $\bar{V}_{max}$ is smaller for all drop angles and cylinder types tested in the water column. This can be read from Table 5.12 listing $\bar{V}_{max}$ dependent on cylinder type and drop angle. As with closed cylinders dropped under water, the maximum velocities are highest for the cylinder with the smallest diameter. In general the velocities are higher compared to the velocities

for drops under water, but this is mainly a result of the velocity achieved as the cylinder fall through air.

Table 5.12: *The average maximal total velocity, $\bar{V}_{max}$, and standard deviation, $\sigma_{\bar{V}_{max}}$, dependent on cylinder type and drop angle in the experiments for drops above the water surface. The cylinders are of type 1, 2 and 3.*

Type:	**1**		**2**		**3**	
Drop angle:	$\bar{V}_{max}$ [m/s]	$\sigma_{\bar{V}_{max}}$ [m/s]	$\bar{V}_{max}$ [m/s]	$\sigma_{\bar{V}_{max}}$ [m/s]	$\bar{V}_{max}$ [m/s]	$\sigma_{\bar{V}_{max}}$ [m/s]
15°	1.91	0.50	1.56	0.19	0.78	0.03
30°	1.51	0.15	1.74	0.35	0.81	0.04
45°	1.76	0.30	1.66	0.20	1.22	0.04
60°	2.13	0.19	2.09	0.20	1.79	0.07
75°	2.88	0.14	2.65	0.09	2.39	0.05

5.1.5 Spreading in the XY Plane

The largest spreading in the XY plane can be observed for drops of closed cylinders that are symmetric about the COG. In general the degree of spreading for all drop cases are dependent on the cylinder diameter and the initial drop angle. For cylinders of type 1 to 3 an increase in diameter result in a larger deviation from the X-axis in the XY plane. This can be read from σ_Y in Table 5.2 and Table 5.11. For both cases the spreading increase up until a drop angle of 45° for type 1 cylinders dropped under water, 60° for type 2 and 3 dropped under water, and 75° for type 2 and 3 dropped above the water surface. The most extreme excursions occur for type 3 cylinders under water, as can be seen in Figure 5.14, and for both type 2 and 3 above water. The excursion of the latter can be seen in Figure 5.15. For these drops some of the cylinders turn up to 180° and land parallel to the drop rig. Some of the cylinders turned up to 90° and then hit the wall either on the left or right side, indicating that for a larger tank the excursion could have been even larger.

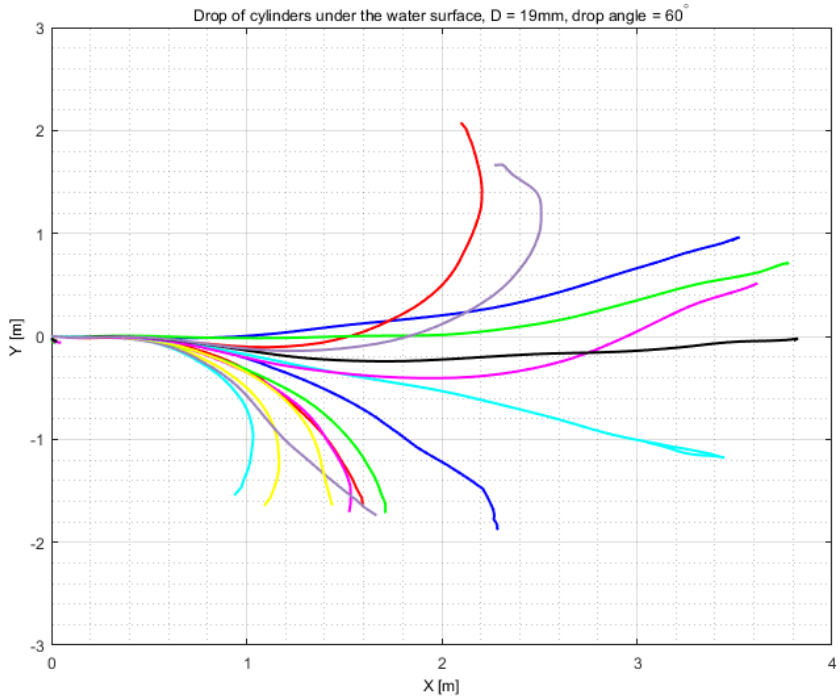

Figure 5.14: *XY plot for drop under the surface for closed cylinders of type 3, at a drop angle of 60°. This is the maximum excursion from the X axis for all capped cylinders dropped under water. The cameras have not managed to capture the full width of the tank and the actual excursion observed in the experiments are wider.*

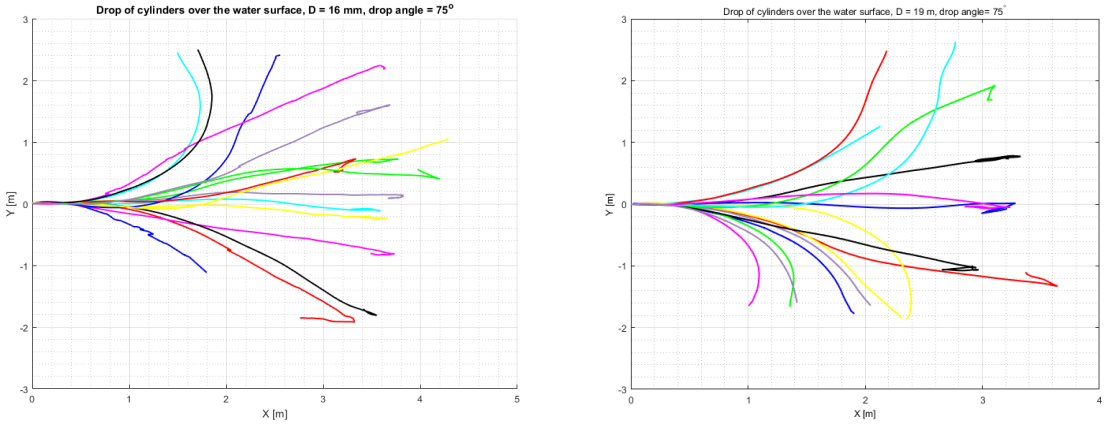

(a) *Type 2.* ***(b)*** *Type 3.*

Figure 5.15: *XY plot for closed cylinders dropped 0.63 m above the surface at a drop angle of 75°. These are the instances where the maximum excursion occur as observed in the experiments. The cameras have not managed to capture the full width of the tank and the actual excursion observed in the experiments are larger.*

The deviation from the X-axis might be caused by asymmetric cross-flow separation.

The asymmetry will cause a side force on the cylinder resulting in a curved motion in in the XY plane [6]. In general the vortex shedding around a cylindrical object develop over time. The boundary layer of a cylinder in an impulsively started flow will after a certain time lapse, separate from the surface of the cylinder [19]. The time is dependent on the Reynolds number, Re, and the diameter of the cylinders. The distance covered until boundary layer separation begin, s', for a cylinder with constant acceleration from rest, is $s' = 0.293 * d = 5.567$ mm for a cylinder with a diameter of 19 mm. The vortex shedding is expressed in the theory as the cross-flow coefficient, C_{Dz}. The development of C_{Dz} over time can be seen in Figure 5.16, where the data is based on experiments performed by Sarpkaya [19]. Based on Figure 5.16 one can roughly estimate that the first asymmetry will occur for $s = 76$ mm after boundary layer separation, and the first vortex at $s = 162$ mm. Comparing this to Figure 5.14 and results in the appendices, this correspond with the development of the motion, and could therefore be the cause of the large spread. Further work on the subject is required to determine this properly.

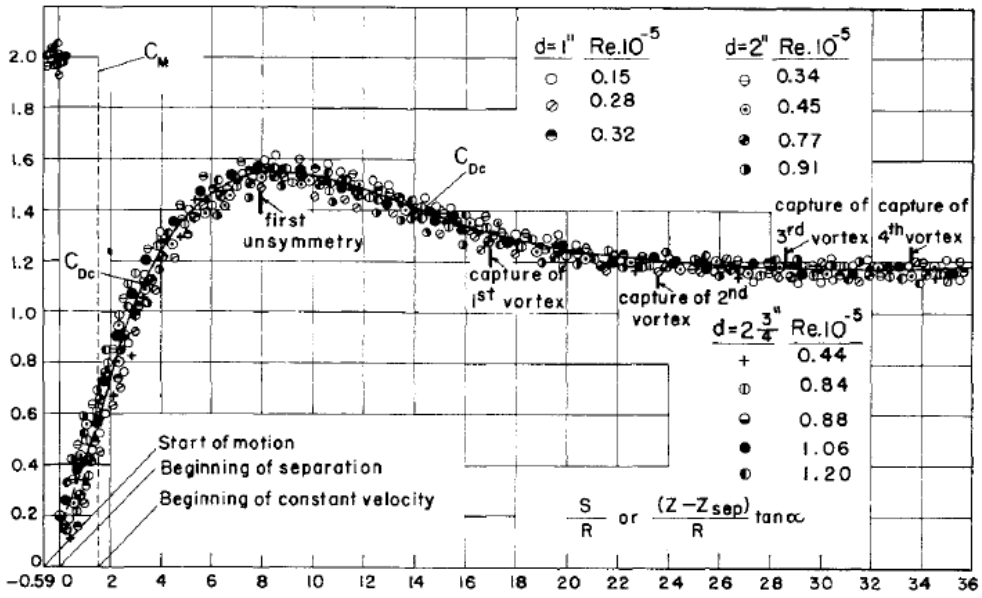

Figure 5.16: *Drag coefficient, C_{Dz}, noted as C_{Dc} in the figure, for a circular cylinder in impulsively started laminar flow. $\frac{s}{R}$ is the relative displacement where s is the displacement of the cross flow and R is the radius or the half width of the body. For circular cylinders $\frac{s}{R} \approx \frac{Vt}{R}$ for all practical purposes.[19]*

The fact that the largest excursion occur for a drop angle of 60° for cylinders dropped under water and for 75° for cylinders dropped above, indicate that there might be a certain angle of attack where a large directional instability occur. From the position plots in the appendices the angle of attack of the cylinder around the point where the excursions begin, can roughly be calculated to be around 60°.

The spread in the XY plane for open cylinders are small. σ_Y as given in Table 5.4 have small values with a maximum deviation from the X axis of ± 0.8 m. The flow through the cylinders work as a stabilizing steering effect along the X-axis. This is especially clear for cylinder type 3. Moreover, because of the small area over which the flow have

to separate, the separation around the edges is less likely to cause a complex flow over the cylinder.

For cylinders that are asymmetric around the COG, the largest excursion in the XY plane occur for small drop angles, independent on whether the COG or COV are above the other. For cylinders with a small shift in COG from COV, as are the case for type 4 and 5, there is a clear reduction in the excursions for higher drop angles, as can be concluded from Table 5.7 and Table 5.8. This is not as evident for cylinder type 6 and 7 as the COG is moved further towards the front of the cylinder, thus resulting in a more stable motion in the XY plane. For small drop angles the velocities are small in the beginning, and thus small disturbances can affect the direction of motion. As with closed cylinders the cylinders with COG different from COV experience a slightly curved motion that might be caused by asymmetric vortex shedding along the cylinder.

In conclusion, the largest spreading occur for closed, symmetric cylinders for steep drop angles. For these cases, the assumption presented by Aanesland that the motion can be assumed to have small deviations in the XY plane such that the trajectory can be described in the 2D plane [4], is not correct. This is also the case for asymmetric cylinders around the COG. However, for open cylinders the deviation from the X-axis is in general small enough to assume two dimensional motion.

5.1.6 Risk Assessment and Evaluation of the Results

For all drop cases performed in the experiments, the highest velocities occurred for open cylinders for drops under water with a mean maximum velocity at 3.3 m/s for a drop angle of 75° for cylinder type 9. Scaled to full size this give a velocity of 66.0 m/s. This velocity is reached early in the trajectory and before the maximum horizontal excursion of the first turn. The maximum velocity in the oscillatory motion, however, is less than 1.4 m/s, i.e. 28.0 m/s in full size. Therefore, the most critical risk for symmetric cylinders will be to hit an object high up in the water as this is where the highest velocity and thus the highest impact, force will occur.

For cylinders that are asymmetric around the COG the velocities converge towards a maximum velocity for cylinders dropped with COG under COV. From the velocity plots it looks like this would also be the case for drops with COG above COV, but this require experiments at larger depths to determine. Compared to symmetric cylinders this constant final velocity is quite high. Maximum velocity occur for cylinder type 7 for a drop angle of 75°, with $\bar{V}_{max}$ equal to 3.47 m/s, i.e. 69.4 m/s in full scale. Thus, the impact risk is quite high for all depths where the maximum velocity has been reached.

As accidental drops from under the water surface will only have the possibility to occur for an installation process occurring under water, effects from entering the water surface have to be considered. In the few drops performed above the surface in this thesis, the water surface has been completely still. This is rarely the case offshore. The presence of waves will alter the angle of attack of the dropped cylindrical object, and dependent on the velocity of the wave it might act on the cylinder as a sideways force, altering the trajectory. Thus, the possibility that the cylinder will enter the surface with a completely

vertical orientation is small. Katteland and Øygarden (1995) argue that the majority of drops from crane accidents will hit the surface with an angle of attack between 45° and 90°. For drop of pipes from the derrick, the angle of attack is between 75° and 90° [12]. Even with water entry effects the cylinders will still have an angle of attack after entering the surface, that can result in high velocities and a large spread.

Overall, the maximum velocities obtained in the experiments could indicate critical damage on installations and equipment in the sea. However, it should be noted that it is not possible to scale the results to full a full size environment, as the geometrical similarity will not be obtained both for the Reynolds number and Froude number. In addition, in full scale there will be a larger presence of turbulent flow and the boundary layer will be larger and might be slightly different. Nevertheless, the scaling of the results from the experiments can give an estimate of what one can expected.

5.2 Comparison Between Experimental Results and DNV-GL RP F107

In RP F107 it is assumed that the excursion under the drop point for accidentally dropped objects will be normal distributed. The width of the distribution used to calculate the expected excursion of a accidentally dropped object, is dependent on the object in question. Figure 5.17 show the distribution at a depth of 4 m for the the aft end of the cylinders obtained in the experiments. This include all the drops performed in the experiments. Since the distribution is based on radial excursion, it is assumed that the cylinders dropped with COG behind COV are dropped in the opposite direction of the rest.

Even though the distribution presented in Figure 5.17 might be hard to fit to a distribution in particular, mirroring the distribution around origin will not give a normal distribution. However, including bulkier and less slender objects might give a result closer to the distribution assumed in RP F107. One should bare in mind that the distribution in Figure 5.17 does not include drops with initial angles of 0^o and 90^o. These would, for ideal conditions, land straight underneath the drop point. Though, as also Aanesland remarked, for 90° small disturbances the symmetry about the cylinder axis will be destroyed and thus the cylinder will deviate from its straight trajectory and there would be a larger excursion [4]. Also some of the capped cylinders dropped with initial angels of 60° and 75° had not yet started their oscillatory motion. Therefore, one can expect that the the distribution at a larger depth will be wider and rightmost part elongated.

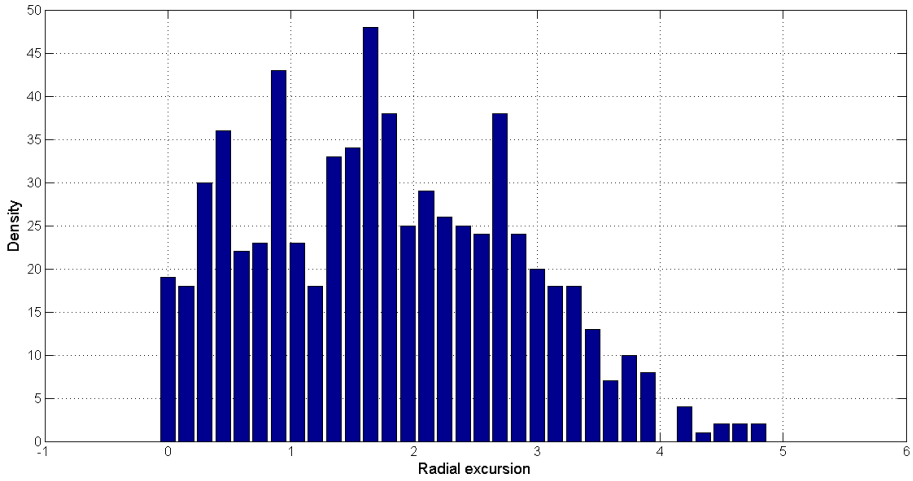

Figure 5.17: *Statistical distribution of the radial excursion at a depth of 4 m based on the experiments performed in this master thesis. This include drops of cylinders with length 0.45 m and diameter of 0.01 m, 0.016 m and 0.019 m under and above the surface, open cylinders with the same length and diameter of 0.01 m and 0.019 m, and cylinders with length 0.45 m and diameter of 0.01 m with COG 1.4 cm and 3 cm from COV. The drops have been performed with initial drop angles of* 15°, 30°, 45°, 60° *and* 75° *and the positions refere to the aft end of the cylinders.*

The recommended practice provide a method to roughly estimate the excursion from the drop point, δ, at the sea floor. The method have been described in Section 1.1. As full scale excursion is most relevant the results from the experiments are scaled to represent full scale cylinders. The full scale characteristics of the dropped cylinders are presented in Table 4.2 and Table 4.3 in Section 4.2. As the full size weight of the largest cylinder is less than 2 tonnes, the objects in question can be categorised as flat or long shaped cylinders with a weight less than 2 tonnes, giving an angular deviation, α, of 15° from RP F107 for all cylinders. The estimated excursion based on and the scaled results from drops with cylinder type 1, 5 and 9 in the experiments, are presented in Table 5.13. Cylinder type 1 and 5 have the largest excursions found in the experiments, while type 9 have the shortest. For type 1 cylinders few of the dropped cylinders have started their oscillatory motion for drop angles of 60° and 75°, and these excursions are therefore expected to be larger. This will be included in the following comparison.

Table 5.13: *Comparison with estimated excursion from DNV-GL RP F107 and excursion from the experimental results scaled to full size drilling pipes by a factor of 20.*

Type	**1**		**5**		**9**		**DNV-GL RP F107**		
Drop angle	δ [m], 80 m	σ [m]	δ [m], 80 m	σ [m]	δ [m], 80 m	σ [m]	δ [m], 80 m	δ [m], 180 m	δ [m], 400 m
15°	17.80	3.80	93.00	4.40			21.44	48.23	107.18
30°	46.40	11.20	75.80	5.40	24.00	7.40	21.44	48.23	107.18
45°	73.40	10.20	51.80	3.40	27.60	2.00	21.44	48.23	107.18
60°	55.80	7.80	34.00	3.20	41.80	2.00	21.44	48.23	107.18
75°	29.80	3.60	19.60	0.80	35.80	1.80	21.44	48.23	107.18

For a depth of 80 m the method provided in RP F107 largely underestimate the expected excursion for most drop angles. This is the full scale depth for the experiments executed in this thesis. It is however able to cover the excursion for a few of the drop angles.

At 180 m RP F107 argue that the increase in the spreading due to increased depth, will stop and the spreading will be constant and independent on depth. For perfectly symmetric cylinders this might be true because of the oscillatory motion, however as the experiments in this thesis have proved, only a small change in the relative position of COG might alter the trajectory of a slender body in the water column a lot. Either way, as can be read from the Table 5.13, the estimated excursions do not cover the full possible length from the drop point on the sea bottom for cylinders of type 1 and 5. The estimated excursions first cover the experimental excursions calculated at 80 m, for a depth of 400 m.

Overall, the method provided in RP F107 underestimate the excursion of the dropped cylinders. The difference between the excursions estimated and the excursions found in the experiments, are smallest for cylinder type 9 in general, but also here the excursions are larger. If a worst case scenario is considered the method is not sufficient at all. Even though proper scaling to full size application cannot be achieved, the difference between the experimental excursions and the estimated excursions are too large. The method given in RP F107 in itself, is very general in the treatment in body types and weights, where the categories used to estimate the excursion could cover bodies with very different slenderness parameters. This might explain the difference between the estimated and actual results.

5.3 Results from the Calculated Trajectories

The theory presented by Aanesland in 1987 [4], to describe the motion of a falling cylinder in the water column, assume that the motion will have negligible excursion from the XZ plane. This is not the case for capped cylinders dropped above and under the surface for large drop angles. For open cylinders the assumption can be valid, while for cylinders with a small shift in COG it could be valid for large drop angles, as discussed in Section 5.1.5. In order to be able to compare the simulated results with the actual experimental results, the coordinates in the XY plane have been transformed to the X axis. In addition, in the following results of the simulations the position of the aft and fore part of the cylinder has been calculated and plotted dependent on which end has been measured in the experiments.

5.3.1 Capped cylinders

In the theory presented in Chapter 2, the coefficients and constants not absolutely determined are the axial drag coefficient, C_{Dx}, the cross-flow drag coefficient, C_{Dz}, and the effective trailing edge, x_T. Underneath in Figure 5.18 and 5.19 the effect of varying C_{Dx} for cylinders of type 1 and 3 are presented. As can be seen in the figures, only values half as big and a half value larger as 0.65 of C_{Dx} give a noticeable change in the trajectory. Therefore it is reasonable to keep the value of $C_{Dx} = 0.65$ as given in Hoerner [10].

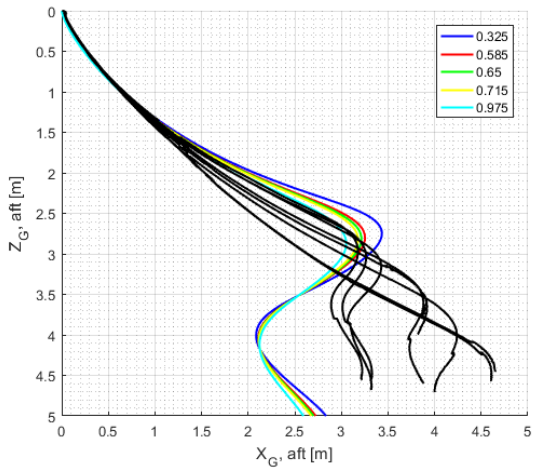

Figure 5.18: *Simulated results for variations in C_{Dx} with ± 50% (0.975 and 0.325) and ± 10% (0.715 and 0.585) from $C_{Dx} = 0.65$ for a drop angle of 45° for cylinder type 1. The calculated results are represented as coloured lines and the experimental results in black. As can be observed the variation in C_{Dx} have a relatively small impact on the trajectory.*

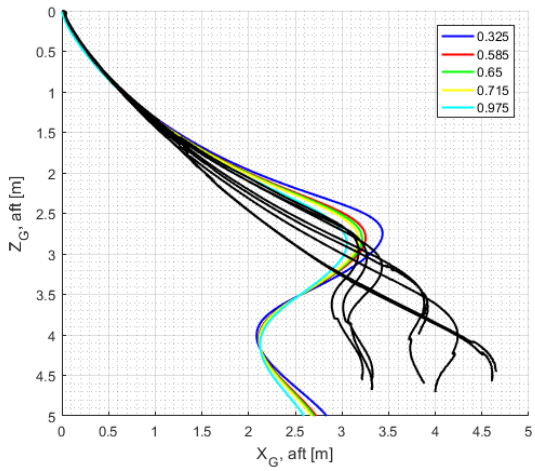

Figure 5.19: *Simulated results for variations in C_{Dx} with ± 50% (0.975 and 0.325) and ± 10% (0.715 and 0.585) from $C_{Dx} = 0.65$ for a drop angle of 45° for cylinder type 3. The calculated results are represented as coloured lines and the experimental results in black. As can be observed the variation in C_{Dx} have a relatively small impact on the trajectory.*

Variations in x_T and C_{Dz} however, give a variation in the result of significance. Figure 5.26 to Figure 5.31 show the results of variation in these coefficients compared to the experimental results. As can be observed from the figures x_T influence the size of the oscillatory motion, while C_{Dz} mainly has an impact on the excursion from the drop point. When considering the value of x_T for each drop angle the best fit for small drop angels is a value of x_T/L from 0.3 to 0.4. For steep drop angles a value of x_T/L of 0.5 gives the best fit. This correspond well to the results found by Aanesland. He suggest to use a small value of x_T/L for small drop angle and values corresponding to x_T/L close to the trailing edge for steeper drop angles [4].

In general the effect of varying C_{Dz} has more impact on the motion for type 1 cylinder compared to type 3 cylinder. For type 1 cylinder the best value of C_{Dz} is 1.0 for most drop angles. For type 3 cylinders the most similar results compared to the experimental results occur when the value of C_{Dz} varies between 0.8 and 1.0 for drop angles from 15° to 30°, and 1.2 for 45° to 75°. Xiang et al. (2017), however, found that a value C_{Dz} equal to 1.0 gives the overall best fit to the experimental data from Aanesland [23].

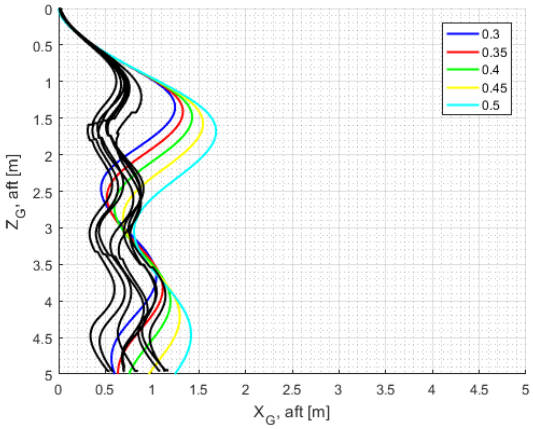

Figure 5.20: *Simulated results for variations in x_T from 0.3 to 0.5 for a drop angle of 15° for cylinders of type 1. Here C_{Dx} = 0.65 and C_{Dz} = 1.0. The simulated results are presented as coloured lines and the experimental results in black.*

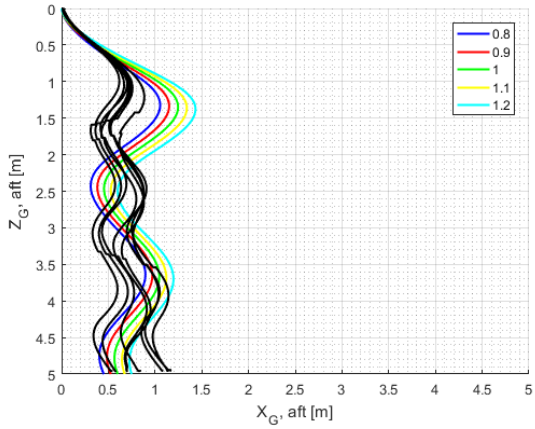

Figure 5.21: *Simulated results for variations in C_{Dz} from 0.8 to 1.2 for a drop angle of 15° for cylinders of type 1. Here C_{Dx} = 0.65 and x_T = 0.3. The simulated results are presented as coloured lines and the experimental results in black.*

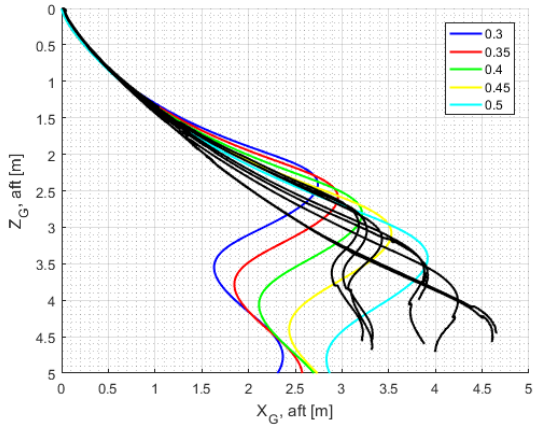

Figure 5.22: *Simulated results for variations in x_T from 0.3 to 0.5 for a drop angle of 45° for cylinders of type 1. Here $C_{Dx} = 0.65$ and $C_{Dz} = 1.0$. The simulated results are presented as coloured lines and the experimental results in black.*

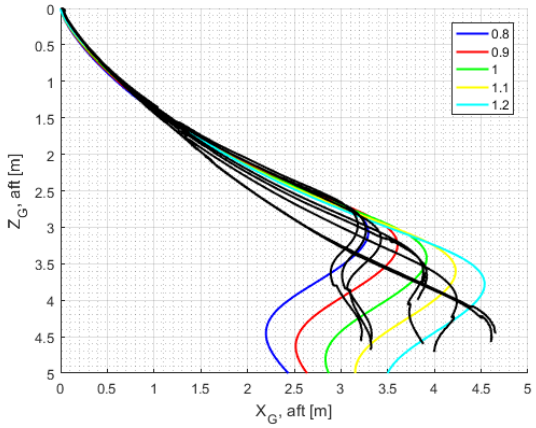

Figure 5.23: *Simulated results for variations in C_{Dz} from 0.8 to 1.2 for a drop angle of 45° for cylinders of type 1. Here $C_{Dx} = 0.65$ and $x_T = 0.5$. The simulated results are presented as coloured lines and the experimental results in black.*

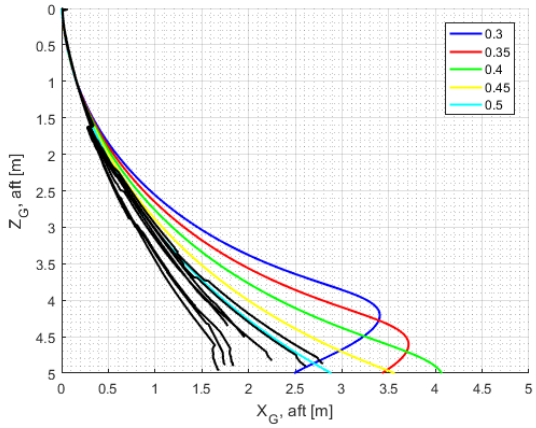

Figure 5.24: *Simulated results for variations in x_T from 0.3 to 0.5 for a drop angle of 75° for cylinders of type 1. Here $C_{Dx} = 0.65$ and $C_{Dz} = 1.0$. The simulated results are presented as coloured lines and the experimental results in black.*

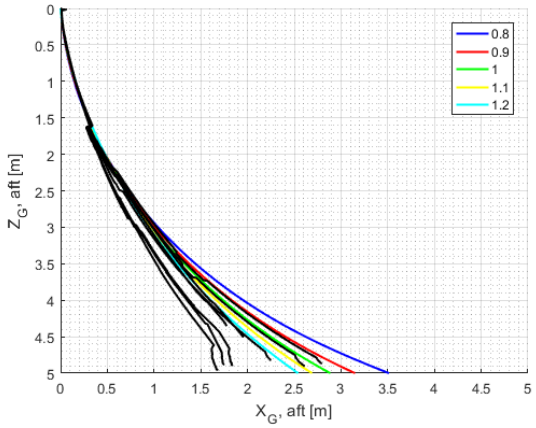

Figure 5.25: *Simulated results for variations in C_{Dz} from 0.8 to 1.2 for a drop angle of 75° for cylinders of type 1. Here $C_{Dx} = 0.65$ and $x_T = 0.5$. The simulated results are presented as coloured lines and the experimental results in black.*

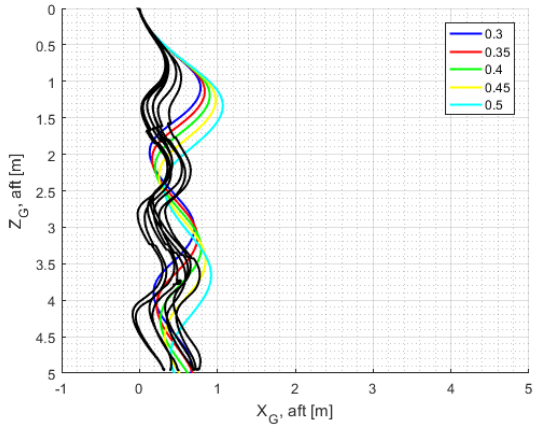

Figure 5.26: *Simulated results for variations in x_T from 0.3 to 0.5 for a drop angle of 15° for cylinders of type 3. Here $C_{Dx} = 0.65$ and $C_{Dz} = 1.0$. The simulated results are presented as coloured lines and the experimental results in black.*

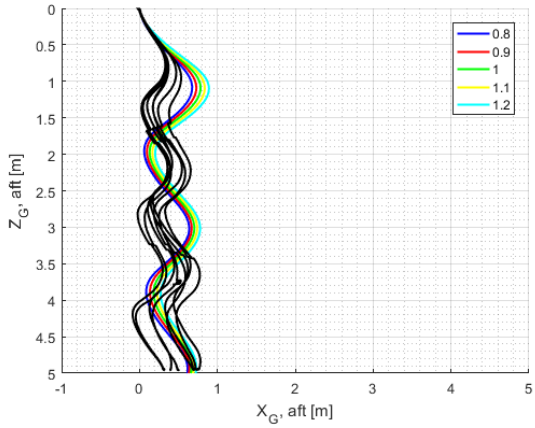

Figure 5.27: *Simulated results for variations in C_{Dz} from 0.8 to 1.2 for a drop angle of 15° for cylinders of type 3. Here $C_{Dx} = 0.65$ and $x_T = 0.3$. The simulated results are presented as coloured lines and the experimental results in black.*

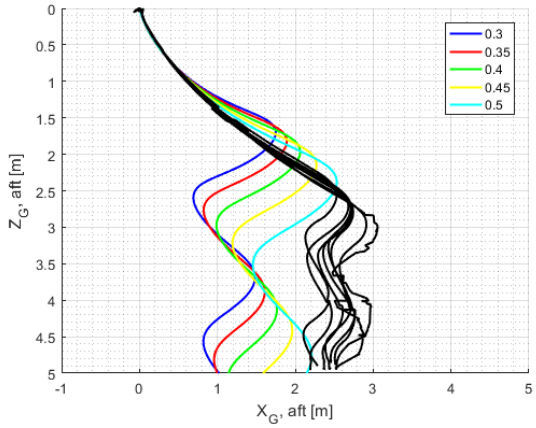

Figure 5.28: *Simulated results for variations in x_T from 0.3 to 0.5 for a drop angle of 45° for cylinders of type 3. Here $C_{Dx} = 0.65$ and $C_{Dz} = 1.0$. The simulated results are presented as coloured lines and the experimental results in black.*

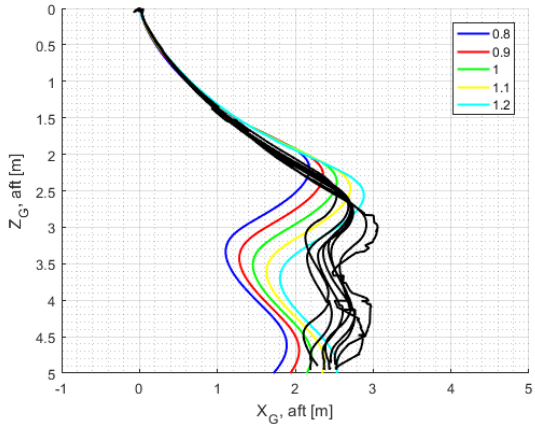

Figure 5.29: *Simulated results for variations in C_{Dz} from 0.8 to 1.2 for a drop angle of 45° for cylinders of type 3. Here $C_{Dx} = 0.65$ and $x_T = 0.5$. The simulated results are presented as coloured lines and the experimental results in black.*

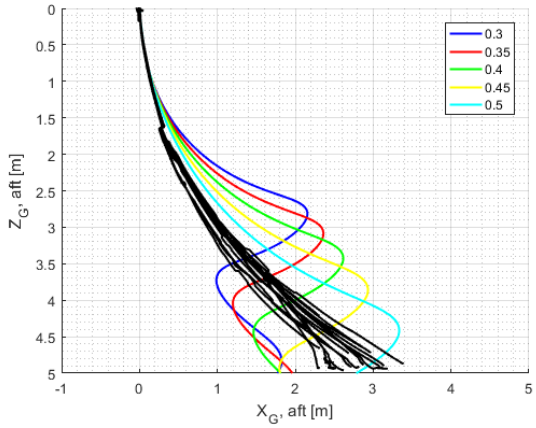

Figure 5.30: *Simulated results for variations in x_T from 0.3 to 0.5 for a drop angle of 75° for cylinders of type 3. Here C_{Dx} = 0.65 and C_{Dz} = 1.0. The simulated results are presented as coloured lines and the experimental results in black.*

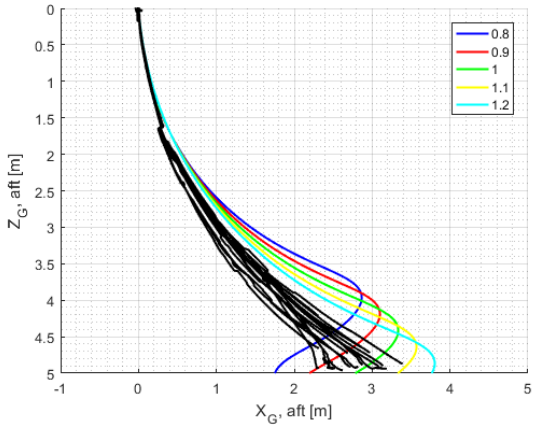

Figure 5.31: *Simulated results for variations in C_{Dz} from 0.8 to 1.2 for a drop angle of 75° for cylinders of type 3. Here C_{Dx} = 0.65 and x_T = 0.5. The simulated results are presented as coloured lines and the experimental results in black.*

Overall, the simulation program gives a good approximate estimate on the excursion from the drop point. It is however not able to capture the oscillatory behaviour correct as it simulate too wide and large turns. Dependent on the chosen values for C_{Dz} and x_T/L the calculated excursions are approximately the same for cylinder type 1. For cylinder type 3 the program deliver good results with respect to estimated excursions for drop angles from 15° to 45°. For higher drop angles it overestimate the lift force on the body.

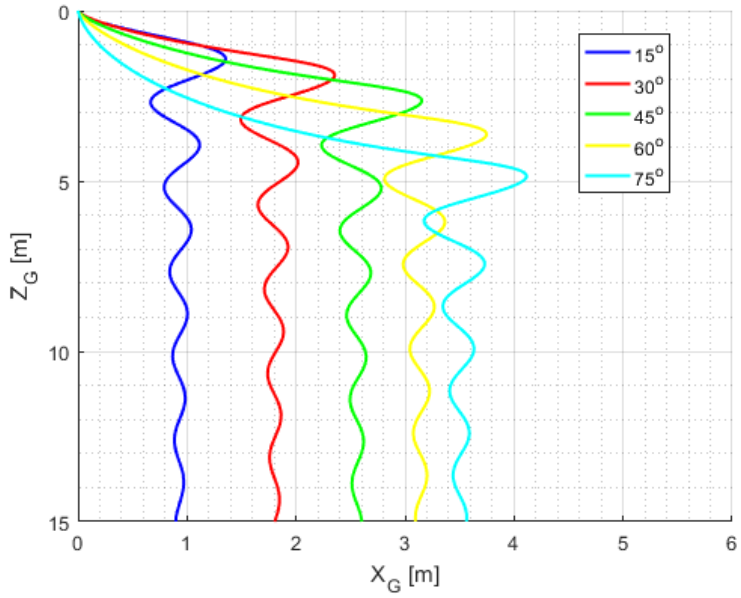

Figure 5.32: *Simulated trajectories for a cylinder of type 1 for a depth of 15 m for drop angles from 15° to 75°. x_T = 0.4, C_{Dz} = 1.0, C_{Dx} =0.65.*

Figure 5.32 show the simulated results for each drop angle for a depth of 15 m and cylinder type 1. As can be observed in the figure the theory predict the oscillatory motion to decrease in width as the cylinder moves further down in the water column. This in particular was not observed in the experiments for capped cylinders, but it is in general hard to determine as the depth of the tank is limited. However, it is an expected pattern in RP F107 for depths above 180 m [3], based on [12].

5.3.2 Cylinders with Open Ends

Equal to capped cylinders a variation in C_{Dx} have a small impact on the whole motion of the cylinder. Figure 5.33 to Figure 5.36 show the calculated trajectories for 45° and 75° for open cylinders with variations in C_{Dz}. The figures have a fixed value of x_T dependent which value have been found to give the best fit. For open cylinders as for closed the calculations correspond best to the experiments for values of x_T/L equal to 0.4 for drop angles of 15° to 30° and 0.5 for drop angles of 45° to 75°. In the following figures a value of C_{Dz} equal to 1.2 give approximately the same landing point at 5 m.

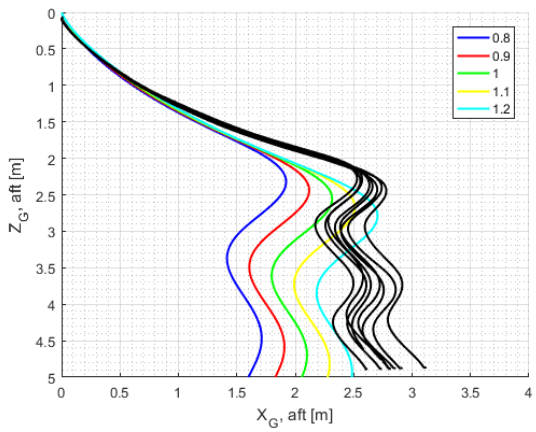

Figure 5.33: *Simulated results for variations in C_{Dz} from 0.8 to 1.2 for a drop angle of 45° for cylinders of type 8. Here C_{Dx} = 0.65 and x_T = 0.5. The simulated results are presented as coloured lines and the experimental results in black.*

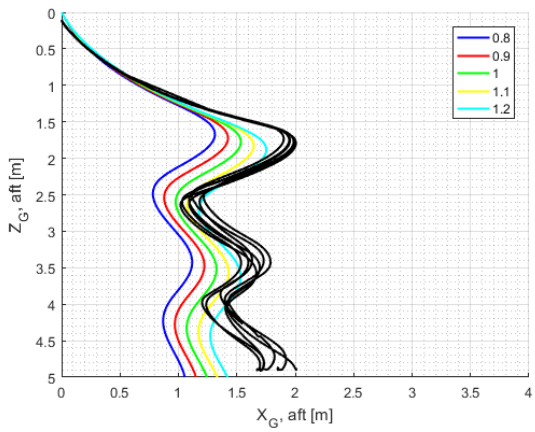

Figure 5.34: *Simulated results for variations in C_{Dz} from 0.8 to 1.2 for a drop angle of 45° for cylinders of type 9. Here C_{Dx} = 0.65 and x_T = 0.5. The simulated results are presented as coloured lines and the experimental results in black.*

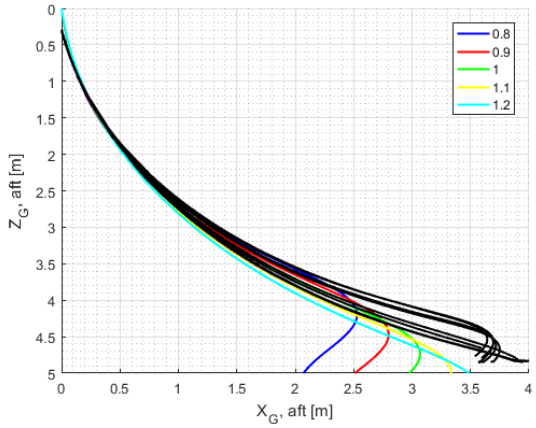

Figure 5.35: *Simulated results for variations in C_{Dz} from 0.8 to 1.2 for a drop angle of 75° for cylinders of type 8. Here $C_{Dx} = 0.65$ and $x_T = 0.5$. The simulated results are presented as coloured lines and the experimental results in black.*

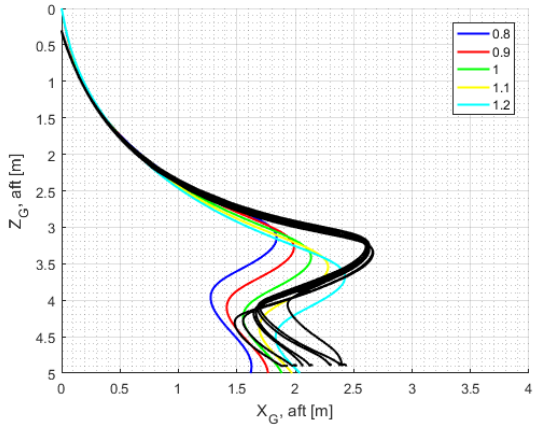

Figure 5.36: *Simulated results for variations in C_{Dz} from 0.8 to 1.2 for a drop angle of 75° for cylinders of type 9. Here $C_{Dx} = 0.65$ and $x_T = 0.5$. The simulated results are presented as coloured lines and the experimental results in black.*

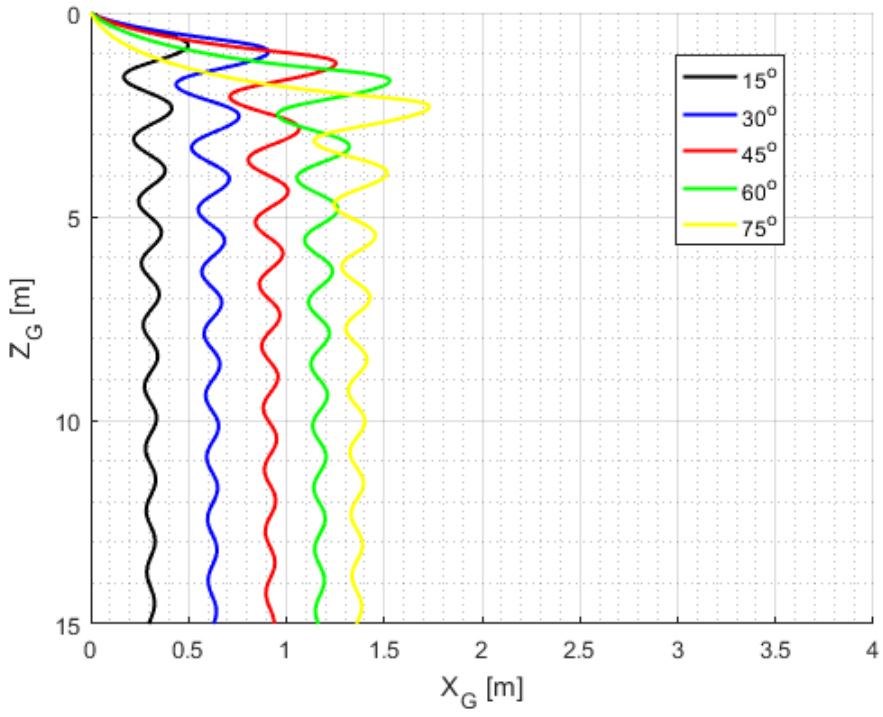

Figure 5.37: *Simulated trajectories for a cylinder of type 9 for a depth of 15 m for drop angles from 15° to 75°. $x_T = 0.4$, $C_{Dz} = 1.0$, $C_{Dx} = 0.65$.*

The estimated trajectories calculated in the program can give an approximate estimation of the maximum excursion of the cylinder and the approximate point at which it will land

on the sea floor. However, for most drop angles the program slightly underestimates the excursion from the drop point. In addition, similar to the closed cylinders, the simulation program is not able to capture the oscillatory behaviour in a right manner and calculate a slightly smaller lift force as the cylinder approaches the leaf-like part of its motion. In addition, similar to closed cylinders, the script calculates trajectories with a decreasing width of the oscillatory motion, as can be seen in Figure 5.51. For type 9 cylinders the results from the experiments might indicate that this is the actual case, as can be seen in Figure 5.34, but further drop experiments in a deeper tank is required in order to get a proper result.

5.3.3 Cylinders Asymmetric about the Centre of Gravity

As with fully symmetric cylinders C_{Dx} only has a minor influence on the calculated trajectory for cylinders with a slightly shifted COG. As can be seen in Figure 5.38 and Figure 5.39, a difference of significance is first reach when the value of C_{Dx} of 0.65 as given in Hoerner [10] is changed with ± 50%. C_{Dx} has some influence on the straightness of the of the calculated path. A larger axial drag coefficient will contribute to a deceleration of the axial velocity. As the destabilising hydrodynamic forces depend on this velocity, a larger C_{Dx} results in a straighter path. As can be observed at a depth of 4.5 m to 5 m in Figure 5.39, C_{Dx} might have a larger influence for an increased depth.

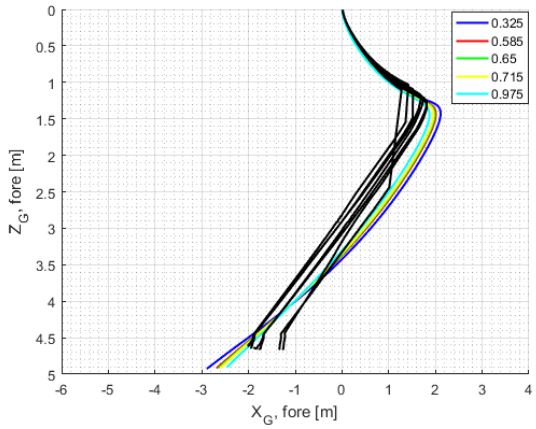

Figure 5.38: *Calculated trajectories for variations in C_{Dx} with ± 50% (0.975 and 0.325) and ± 10% (0.715 and 0.585) from C_{Dx} = 0.65 for a drop angle of 45° for a cylinder of type 4. The calculations are for a cylinder dropped with COG 1.4 cm in front of COV, $x_T = 0.4$ and $C_{Dz} = 0.1$. The calculated results are represented as coloured lines and the experimental results as black.*

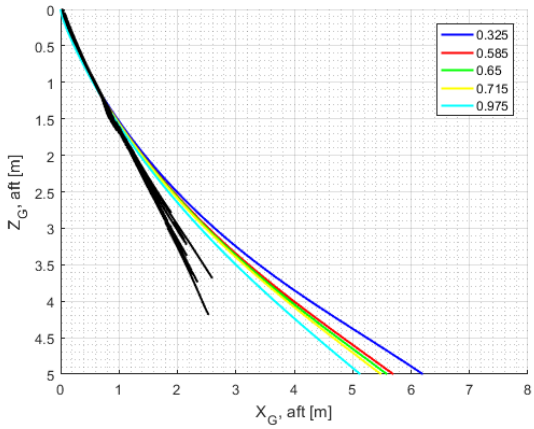

Figure 5.39: *Calculated trajectories for variations in C_{Dx} with ± 50% (0.975 and 0.325) and ± 10% (0.715 and 0.585) from C_{Dx} = 0.65 for a drop angle of 45° for a cylinder of type 5. The calculations are for a cylinder dropped with COG 1.4 cm in front of COV, $x_T = 0.4$ and $C_{Dz} = 0.1$. The calculated results are represented as coloured lines and the experimental results as black.*

Results for COG above COV

The most optimal values of x_T/L compared to the experimental results for type 4 cylinders, are for $x_T/L = 0.4$ for drop angles from 15° to 45° and $x_T/L = 0.5$ for drop angles from 60° to 75°. For type 6 cylinders the calculated trajectories have straight path after the first turn, while the experimental results curve slightly inward. For that reason, one either have to prioritise whether the path should most closely resemble the area around the first turn or the point at which the cylinder hit the bottom. For increased depths the simulation program will therefore not be able to estimate the excursion. This is especially true for small drop angles, as can be seen in Figure 5.41. As it was found in the experiments that the velocity might converge to a constant velocity and thus have a large impact force on the sea bottom, the final excursion will be prioritised. The best fit for drop angles from 45° to 60° is $x_T/L = 0.4$, and $x_T/L = 0.5$ for the rest. This can be seen in Figure 5.40 to Figure 5.45.

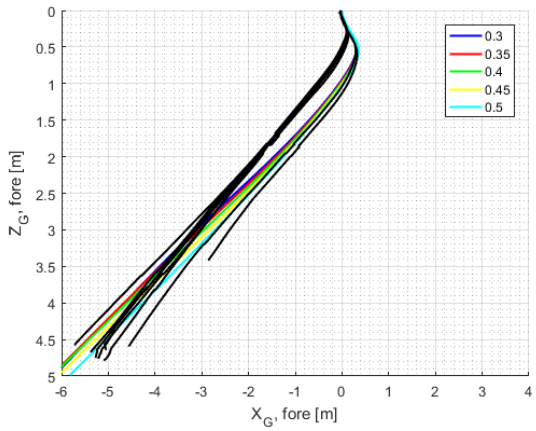

Figure 5.40: *Calculated trajectories (coloured lines) for variations in x_T/L from 0.3 to 0.5 for a drop angle of 15° compared to experimental results (black lines). Here C_{Dx} = 0.65, C_{Dz} = 1.0 and the cylinder is of type 4.*

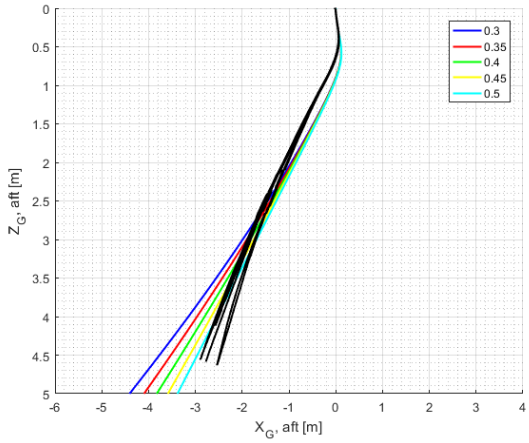

Figure 5.41: *Calculated trajectories (coloured lines) for variations in x_T/L from 0.3 to 0.5 for a drop angle of 15° compared to experimental results (black lines). Here C_{Dx} = 0.65, C_{Dz} = 1.0 and the cylinder is of type 6.*

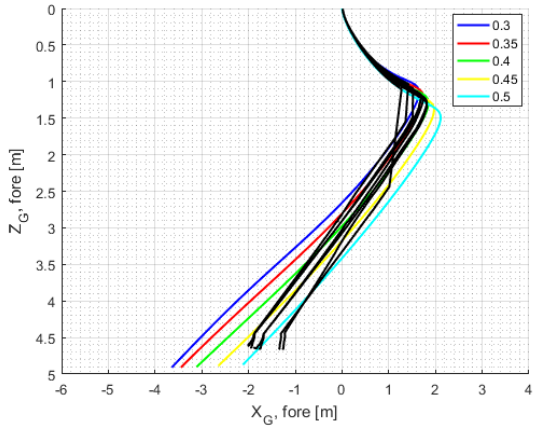

Figure 5.42: *Calculated trajectories (coloured lines) for variations in x_T/L from 0.3 to 0.5 for a drop angle of 45° compared to experimental results (black lines). Here C_{Dx} = 0.65, C_{Dz} = 1.0 and the cylinder is of type 4.*

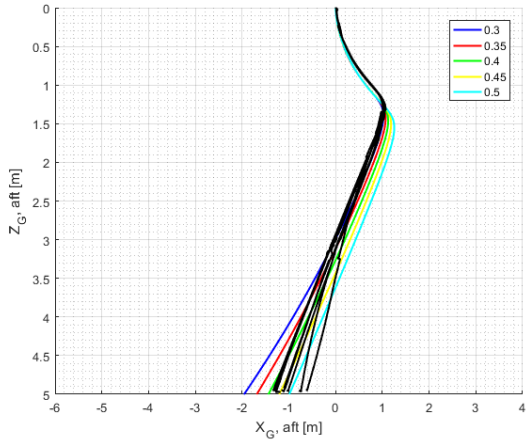

Figure 5.43: *Calculated trajectories (coloured lines) for variations in x_T/L from 0.3 to 0.5 for a drop angle of 45° compared to experimental results (black lines). Here C_{Dx} = 0.65, C_{Dz} = 1.0 and the cylinder is of type 6.*

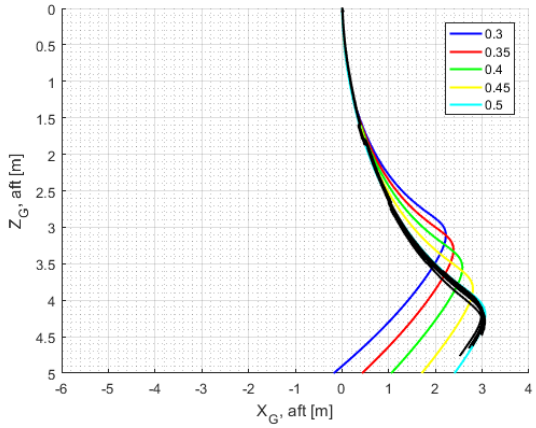

Figure 5.44: *Calculated trajectories (coloured lines) for variations in x_T/L from 0.3 to 0.5 for a drop angle of 75° compared to experimental results (black lines). Here C_{Dx} = 0.65, C_{Dz} = 1.0 and the cylinder is of type 4.*

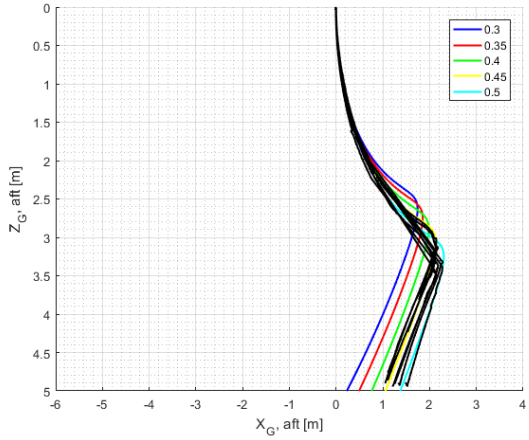

Figure 5.45: *Calculated trajectories (coloured lines) for variations in x_T/L from 0.3 to 0.5 for a drop angle of 75° compared to experimental results (black lines). Here C_{Dx} = 0.65, C_{Dz} = 1.0 and the cylinder is of type 6.*

The effect of varying C_{Dz} is quite small. It has some influence on the radial excursion from the drop point, but a relatively little effect on the landing point. For drop angles of 15° and 30° a C_{Dz} around 0.8 will give the most similar calculated trajectory, while for drop angles of 45° to 75° a value of C_{Dz} of 1.0 gives a better result.

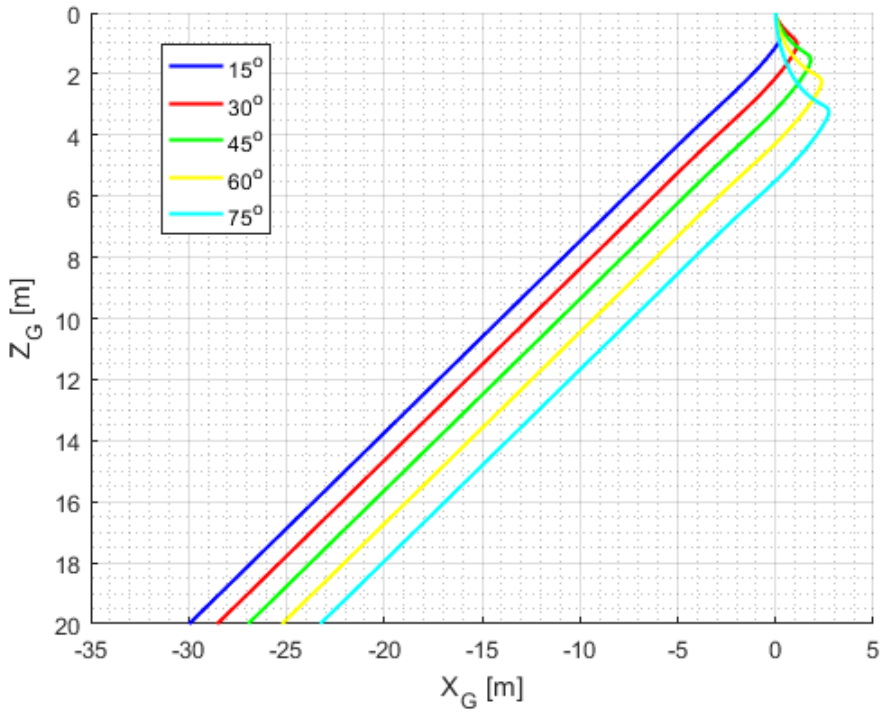

Figure 5.46: *Simulated trajectories for a cylinder of type 4 for a depth of 20 m for drop angles from* 15° *to* 75°. $x_T = 0.4$, $C_{Dz} = 1.0$, $C_{Dx} = 0.65$.

Overall, the calculated results that correspond best with the experimental results occur for a drop angle of 75°. As can be observed in the results for the cylinder of type 6, the experimental results slightly curve inwards with depth, while the calculated trajectory do not. The curving of the arc is increased with an increasing Δ_{CB}. The result is an overestimation of the radial excursion. The calculated excursion can therefore only give an indication of the excursion at small depths and for small values of Δ_{CB}. As can be seen in Figure 5.51 the simulated results have a very straight path after the flip independent on depth. The value of the drag coefficients and effective trailing edge must be chosen dependent on depth.

Results for COG Underneath COV

The results from the experiments show that for cases where the cylinders are dropped with COG in front of COV, the trajectory of the cylinder will be a very straight path. Thus, variations in C_{Dz} have very little impact on the trajectory. Compared to the experimental results the optimal value of C_{Dz} is 1.2 as this will give the most similar calculated trajectories.

The stabilizing effect of the trailing edge dependent on the value chosen for this parameter, can clearly be observed in Figure 5.47 to Figure 5.50. For small values of x_T/L the calculated trajectory either has a slight wave-like motion or quite a curved path. The first is the case in Figure 5.47 and the latter in Figure 5.49. For calculation of the

trajectory of cylinders dropped with COG in front of COV, a value of x_T/L equal to 0.5 gives the most similar results for all drop angles, as can be observed in the figures.

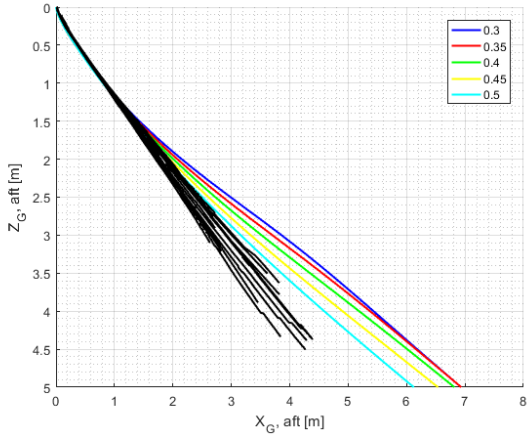

Figure 5.47: *Calculated trajectories (coloured lines) for variations in x_T/L from 0.3 to 0.5 for a drop angle of* 30° *compared to experimental results (black lines). Here C_{Dx} = 0.65, C_{Dz} = 1.0 and the cylinder is of type 5.*

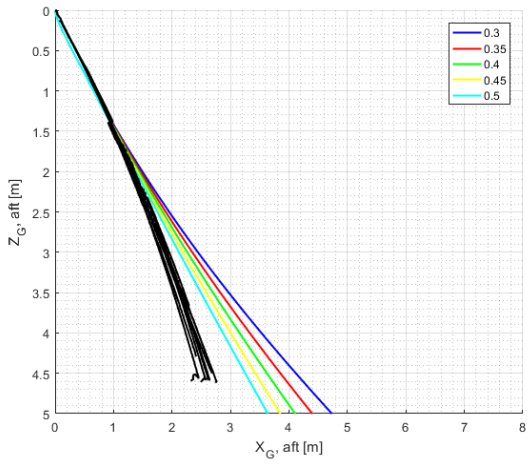

Figure 5.48: *Calculated trajectories (coloured lines) for variations in x_T/L from 0.3 to 0.5 for a drop angle of* 30° *compared to experimental results (black lines). Here C_{Dx} = 0.65, C_{Dz} = 1.0 and the cylinder is of type 7.*

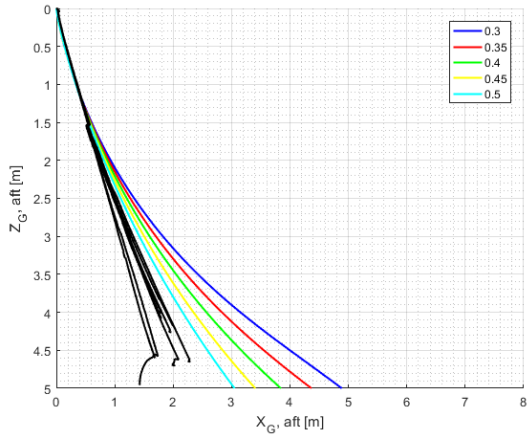

Figure 5.49: *Calculated trajectories (coloured lines) for variations in x_T/L from 0.3 to 0.5 for a drop angle of* 60° *compared to experimental results (black lines). Here C_{Dx} = 0.65, C_{Dz} = 1.0 and the cylinder is of type 5.*

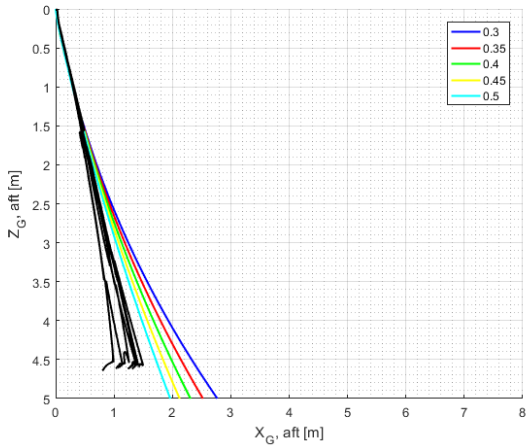

Figure 5.50: *Calculated trajectories (coloured lines) for variations in x_T/L from 0.3 to 0.5 for a drop angle of* 60° *compared to experimental results (black lines). Here C_{Dx} = 0.65, C_{Dz} = 1.0 and the cylinder is of type 7.*

Comparing the calculated trajectories with the experimental results, the estimated paths are closest to the experimental results for steep drop angels for a depth of 5 m. In

general, the calculated trajectories curve outward, while the results from the experiments do not, as is the case for cylinder type 5, or curve slightly inwards, as is the case for cylinder type 7. The theory applied to calculate the trajectories gives an indication of the final excursion for small water depths. For increasingly larger depths the theory would overestimate the excursion with a corresponding increasingly factor. As can be seen in Figure 5.51 this overestimation is largest for steep drop angles as the curve flatten out over time.

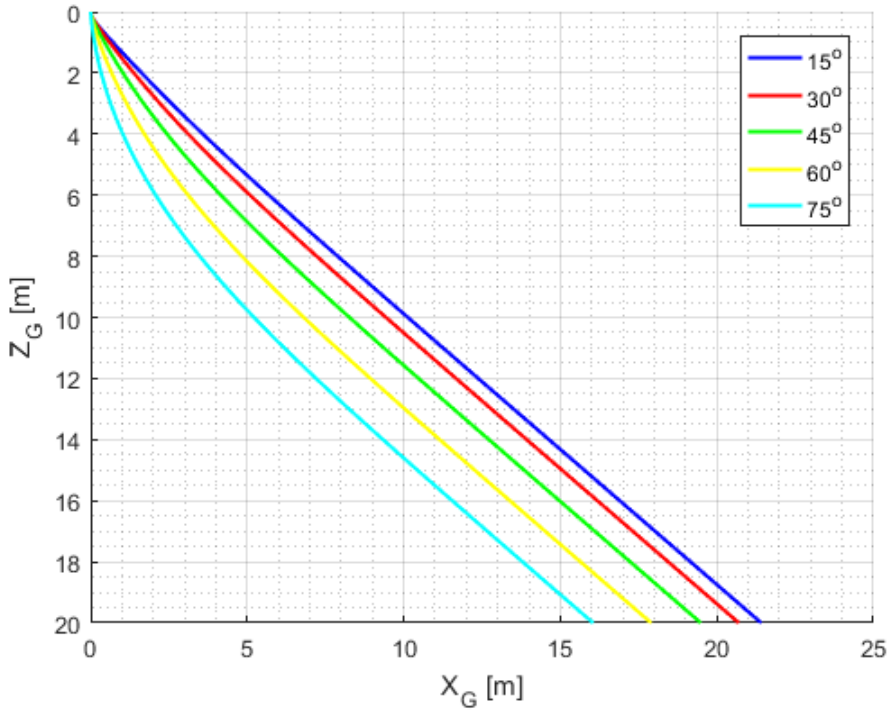

Figure 5.51: *Simulated trajectories for a cylinder of type 7 for a depth of 20 m for drop angles from* 15° *to* 75°. $x_T = 0.4$, $C_{Dz} = 1.0$, $C_{Dx} = 0.65$.

5.3.4 Comment on the Friction Coefficient

As described in the theory section, the value of the friction coefficient, C_F, depend on whether the boundary layer can be assumed to be laminar or turbulent. As can be seen in Figure 5.52 the difference between the two assumptions greatly affect the result. In general, C_F for laminar flow give larger excursions compared to C_F for turbulent flow. This is especially evident for open cylinders, as can be seen in Figure 5.52a.

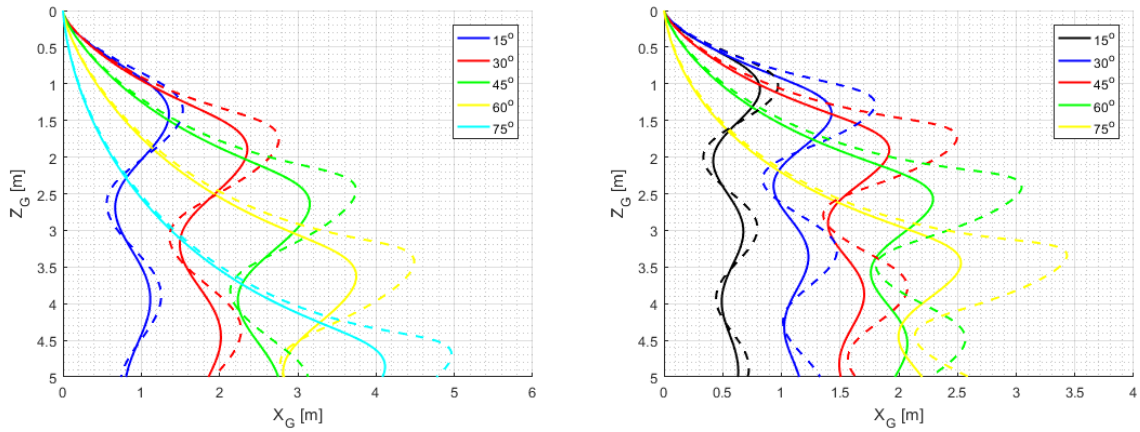

(a) *Type 1: capped cylinder.* ***(b)*** *Type 8: open cylinder.*

Figure 5.52: *Comparison of the difference with applying a laminar (dotted lines) and turbulent (whole lines) in the simulations. The drop angles are* 15°, 30°, 45°, 60° *and* 75°.

In general, the use of a turbulent C_F has given simulated results most similar to the experimental results. This might be caused by how the abrupt edge of the front of the cylinder causing a flow around the front that is not entirely laminar. For open cylinders the simulation program underestimate the maximum excursion. A laminar assumption might therefore be more proper for this instance. There is also a good probability that the flow inside the open cylinders is laminar while the flow outside is turbulent. Further investigations are required to determine this properly.

5.4 Errors and Uncertainties

The errors and uncertainties in the experiments are mostly limited to the characteristics of the cylinders, the measurement equipment and the basin where the experiments were performed. In the case of the cylinders, there was a large problem of keeping the cylinders watertight for a repeated number of drops. For steep drop angles the impact force on the cylinder from the tank bottom could be significant and the sealing of the cylinder would break along the edge. It was discovered that only small amounts of water inside the cylinder would give an observable change in trajectory as the COG would shift to one side or the other of COV dependent on the orientation of the cylinder. Therefore the weight of the cylinder where checked between each drop. The weight used had an uncertainty of $\pm$ 1 g. Smaller differences in weight could therefore not be observed.

The second factor that could have affected the measured trajectory of the cylinders were the measurement tape. The tape itself has a thickness of 0.25 mm and a width of 5 cm. It could therefore have contributed to a slightly increased drag on the cylinder in the negative longitudinal direction or contributed to a changed flow regime at the back end of the cylinder. In addition, disturbances in the flow could have been made in the area where the tape ends meet around the cylinder. Tests performed with asymmetric

appendices attached to the back of the cylinder body, showed that a small asymmetry of 2 mm would significantly affect the motion of the cylinder. The motion would swerve to one side independent on drop angle. This was not observed for all drop angles in the experiments, which indicate that the influence of the tape have been little.

With regards to the measurement equipment, the result would have been even more accurate if a larger tank was used where the cameras could capture the motion from two different sides. This could have allowed for tracking of both ends and would eliminate the problem encountered when the cylinder turned to one side or flipped. Furthermore, the calibration of the cameras became less accurate during the experiments resulting in the sudden jumps in some of the measurement data. The calibration procedure should therefore have been repeated more times than it was.

Last, experiments with waves were performed in the tank against Dokka. As the two tanks are connected by a steel wall vibrations from the wave generation could have created small vibrations in the water or a small current. This was not possible to observe by the naked eye, but could have affected the trajectory of the dropped cylinders to a small degree.

5.5 Further work

One of the surprising effects observed in the experiments, was how for certain drop angles and diameters the cylinder would have a large spreading where some of the cylinders swerved out to one side. This greatly contradicted the assumption that the motion of the cylinder would be limited to the XZ plane. Experiments investigating exactly at what angles and which geometries this occur, and the hydrodynamic behaviour causing and affecting this, would be of great interest. Other experimental work contributing to the knowledge of the cylinder trajectory, would be to study the effect of air cavity and slamming as the cylinder enter the water, the effect of attaching small appendices to the cylinders, and to investigate the trajectory where waves and currents are present. In addition, drops at a greater water depths should be performed in order to obtain some knowledge of how the oscillatory motion changes over a larger depth. This would help determine the accuracy of the theory presented in this thesis.

With regards to the simulation program it remains to develop the program to include drops above the water surface with inclusion of drop height and water entry effects. In order to make a program that could give an accurate estimate of the excursion and velocity both high up in the water and at the sea bottom, the effect of waves and currents also need to be included. Finally, in the program presented in this thesis, the cross-flow is assumed to be constant over the cylinder. However, it is most likely to develop over time and over the length of the cylinder affecting the trajectory, as found by Sarpkaya [19]. In order to get a more accurate simulation this also needs to be included.

Chapter 6

Conclusion

The motion of a slender, symmetric cylinder dropped under water can be described as a slightly curved motion that after a certain depth begins an oscillatory, leaf-like motion. The point at which the oscillatory motion starts is dependent on the drop angle and diameter of the cylinder; a decrease in the steepness of the drop angle and an increase in diameter both give oscillatory motion higher up in the water column. The maximum excursion is directly linked to where the oscillatory motion starts, and thus the closed cylinder with the smallest diameter has the largest excursion. Open cylinders have in general a smaller excursion compared to capped. For drops above the surface the trajectory is similar to that of capped cylinders, but the angle of attack is altered by water entry effects.

For cylinders with asymmetry, the motion is a straight path through the water with an angle of attack dependent on the drop angle. For cases where the cylinder has been dropped with COG above COV, the cylinder flips once before it follows this path. The depth at which the flip occurs is dependent on the drop angle, similar to symmetric cylinders, and the distance between COG and COV, Δ_{CB}. Steeper drop angles and decrease in Δ_{CB} results in a flip deeper in the water. The angle of attack is also dependent on Δ_{CB}, where a smaller Δ_{CB} gives a smaller angle of attack with the surface, and thus a larger excursion. Cylinders with $\Delta_{CB} = 1.4$ cm that are dropped with COG under COV have the largest excursions out of all the drops performed, with an excursion of 4.65 m for a depth of 4 m.

The highest velocity occurs for drops with COG under COV and $\Delta_{CB} = 1.4$ cm. The velocity increases from the drop point and converges to a value of 3.47 m/s. Because of the convergence, this cylinder type provides a great risk as the possible impact force will be high independent on what water depth the impact should occur. In order to give a realistic picture of the accuracy of the DNV-GL RP F107, the experimental results have been scaled up to represent 9 m long drill pipes. This gives a depth of 80 m. Comparing the results with the estimated excursions for a depth of 80 m, the conclusion is that the method largely underestimate the final excursion. It is closest for open cylinders, but estimated excursions do not cover the excursions for all drop angles. The difference in the estimated excursion and the excursions found in the experiments, are largest for cylinders with a slight shift in COG of 1.4 cm with a difference of 72 m.

The theory presented in this thesis assume that the trajectory of a slender, cylindrical body is limited to the XZ plane. For open cylinders this is approximately true, but for capped cylinders with a large diameter the spreading is large for steep drop angles. For angles of attack just under the surface of 60° a certain number of cylinders swerve to one side creating a large spreading. The assumption is therefore not valid and may be a reason for deviations between the experimental and simulated results.

A simulation script has been made based on earlier known theory describing the motion of the cylinders by the manoeuvring equations corrected for viscous forces. In the equations the effective trailing edge, x_T, the form drag, C_{Dx}, and the cross-flow drag, C_{Dz}, can be varied dependent on the drop case. x_T affects the stability of the oscillatory motion, C_{Dz} affects the horizontal excursion and C_{Dx} have in general little effect on the motion. The latter has to be increased or decreased by more than 50% in order to gain an observable result. The values of x_T that give the most similar results to the experimental results, are for symmetric cylinders $x_T/L = 0.4$ for small drop angles and $x_T/L = 0.5$ for steep drop angles. With regards to C_{Dz}, values between 1.0 and 1.2 give the most similar results compared to the experimental results. For cylinders that are asymmetric about the COG these values varies between $x_T/L = 0.4$ and $x_T = 0.5$ dependent on Δ_{CB} for cases where the cylinders are dropped with COG above COV. For small drop angles $C_{Dz} = 0.8$ and for large $C_{Dz} = 1.0$. For cases where the cylinder has been dropped with COG under COV the most similar results occur for $x_T = 0.5$ and $C_{Dz} = 1.2$. These parameters also have to be changed dependent on the depth for cylinders with a shifted position of COG.

Overall, the simulation program is able to give an estimate of the motion of the cylinder and the excursion at the bottom for symmetric cylinders. It gives most accurate results for capped cylinders while slightly underestimating the excursion for open cylinders. However, the program fails to predict the behaviour of the oscillatory motion properly. In both cases the trajectories for larger depths indicate an assumption of decreasing oscillatory motion for increased depth. This has not been observed in the experiments, but experiments at larger depths are required to determine this properly. For cylinders with a position of COG different from COV, the program is able to give a good estimate of the excursion for small depths. For larger depths the program overestimates the excursion with an increasing factor for an increasing depth.

In conclusion, the use of the manoeuvring equations corrected for viscous forces could be used for pipes, while the spreading for all other cylinder types indicate the motion have to be calculated for a three dimensional plane.

Bibliography

[1] Subsea dropped objects. Technical report, DROPS (Dropped Objects Prevention Scheme), August 2010. `http://www.dropsonline.org/assets/documents/DROPS-SubseaDROPS.pdf` [2017-12-09].

[2] DNV-GL ST E406 - design of free-fall lifeboats. Standard, January 2016.

[3] Recommended practice: DNVGL RP F107 - risk assessment of pipeline protection, May 2017.

[4] V. Aanesland and Marintek A/S. Numerical and experimental investigation of accidentally falling drilling pipes. In *OTC 5497*, pages 117 – 125. Offshore Technology Conference, January 1987.

[5] V. Aanesland and E. Huse. Experimental and numerical investigations of accidental drops of drilling tubes. Technical Report 86-0139 520075, Norwegian Marine Technology Research Institute A/S, 1986.

[6] H. S. Alsos and O. M. Faltinsen. 3D motion dynamics of axisymmetric bodies falling through water. Revised revision submitted to Ocean Engineering.

[7] P. C. Chu, A. Gilles, and C. Fan. Experiment of falling cylinder through the water column. *Experimental Thermal and Fluid Science*, Vol.29(5):555–568, 2005.

[8] O. Faltinsen. *Sea Loads on Ships and Offshore Structures (Cambridge Ocean Technology Series)*. Cambridge University Press, 1993.

[9] O. Faltinsen. *Hydrodynamics of High-Speed Marine Vehicles*. Cambridge University Press, first paperback edition edition, 2010.

[10] S. F. Hoerner. *Fluid-dynamic drag : practical information on aerodynamic drag and hydrodynamic resistance*. S.F. Hoerner, Midland Park, N.J, [3rd ed.] edition, 1965.

[11] S. Hui and O. Faltinsen. Accidentally dropped pipe. Exercise 10.10.5 in Faltinsen, O., 2005, Hydrodynamics of high-speed marine vehicles, Cambridge University Press. Exercise solution, November 2013.

[12] L. H. Katteland and B. Øygarden. Risk analysis of dropped objects for deep water development. In *OMAE*, volume ll of *Safety and Reliability*, pages 443–450, 1995.

[13] J. Kirkegaard, G. Wolters, J. Sutherland, R. Soulsby, L. Frostick, S. McLelland, T. Mercer, and H. Gerritsen. *Users Guide to Physical Modelling and Experimenta-*

tion: Experience of the HYDRALAB Network (IAHR Design Manual). IAHR. CRC Press, 2011.

[14] N. E. Kochin, I. A. Kibel, and N. V. Roze. *Theoretical Hydromechanics*. Interscience Publishers, 1964.

[15] E. Kreyszig. *Advanced Engineering Mathematics*. John Wiley & Sons, 9th edition, 2006.

[16] J. Mann, Y. Liu, Y. Kim, and D. K. P. Yue. Deterministic and stochastic predictions of motion dynamics of cylindrical mines falling through water. *IEEE Journal of Oceanic Engineering*, 32(1):21–33, January 2007.

[17] J. N. Newmann. *Marine Hydrodynamics*. MIT University Press Group Ltd, Cambridge, Masschusetts, second printing edition, 1978.

[18] Norwegian Oil and Gas Association. Dropped objects project - background and purpose, 12 2010. `https://www.norskoljeoggass.no/en/Activities/HSE-and-operation/Dropped-objects/Dropped-objects-project/` [2017-12-09].

[19] T. Sarpkaya. Separated flow about lifting bodies and impulsive flow about cylinders. *AIAA Journal*, 4:414–420, March 1966.

[20] Sverre Steen. Tmr7: Experimental methods in marine hydrodynamics. Lecture Notes, August 2014.

[21] F. M. White. An analysis of axisymmetric turbulent flow past a long cylinder. *Journal of Basic Engineering*, Vol. 94(1):200–2014, 1972.

[22] F. M. White. *Viscous Fluid Flow*. McGraw-Hill Mechanical Engineering. McGraw-Hill, Croydon, UK, 3rd edition edition, 2006.

[23] G. Xiang, L. Birk, X. Yu, and H. Lu. Numerical study on the trajectory of dropped cylindrical objects. *Ocean Engineering*, 130:1–9, January 2017.

[24] S. Yasseri. Experiment of free-falling cylinders in water. *Underwater Technology*, 32(3):177–191, 2014.

APPENDIX

Complete Results from Experiments Performed as
a Part of the Master Thesis

June 2018

Contents

A Position plots

A.1 Drop of 10 mm diameter cylinders under the water surface

A.1.1 15° initial drop angle

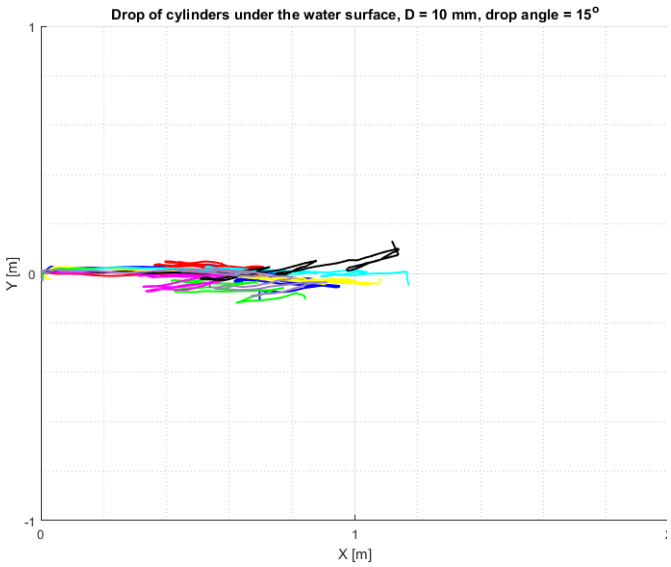

Figure 1: X-Y view: Drop of 10 mm diameter cylinders under the water surface at 15° initial drop angle. Each coloured line represents a drop.

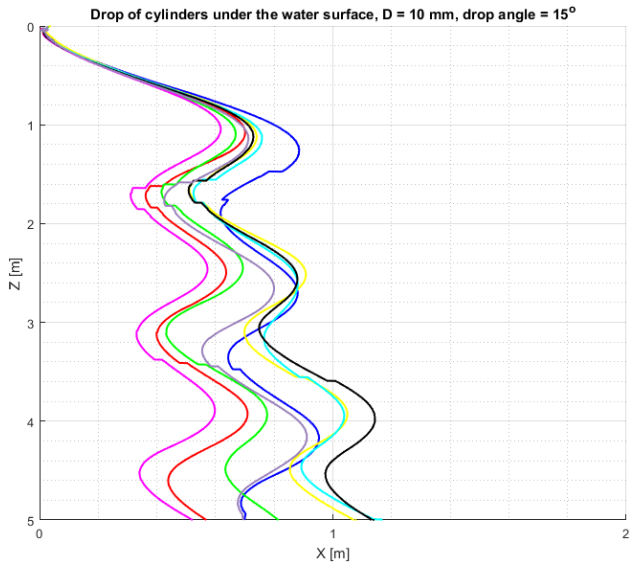

Figure 2: X-Z view: Drop of 10 mm diameter cylinders under the water surface at 15° initial drop angle. The X-coordinates are radial coordinates from the X-Y plane and each coloured line represents a drop.

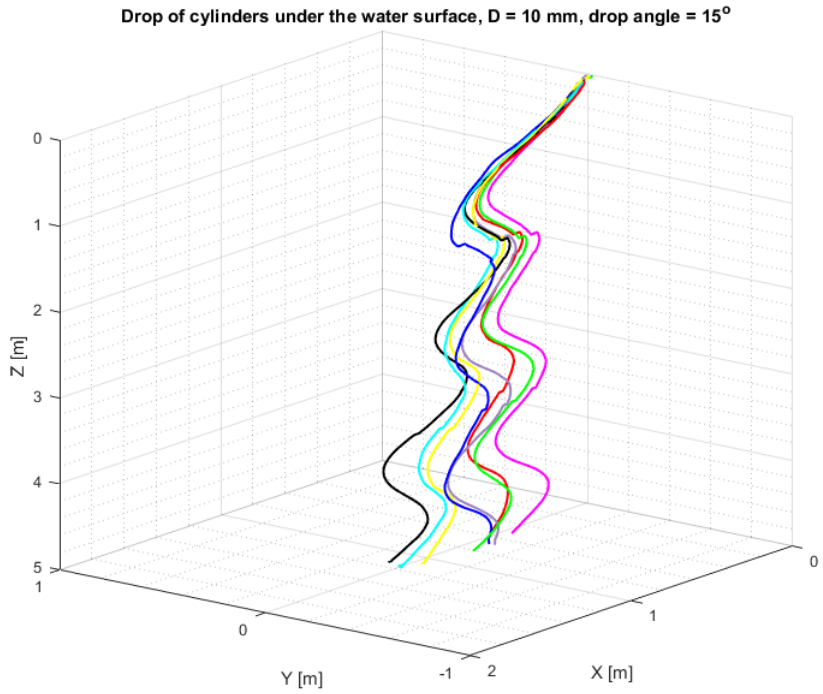

Figure 3: X-Y-Z view: Drop of 10 mm diameter cylinders under the water surface at 15° initial drop angle. Each coloured line represents a drop.

A.1.2 30° initial drop angle

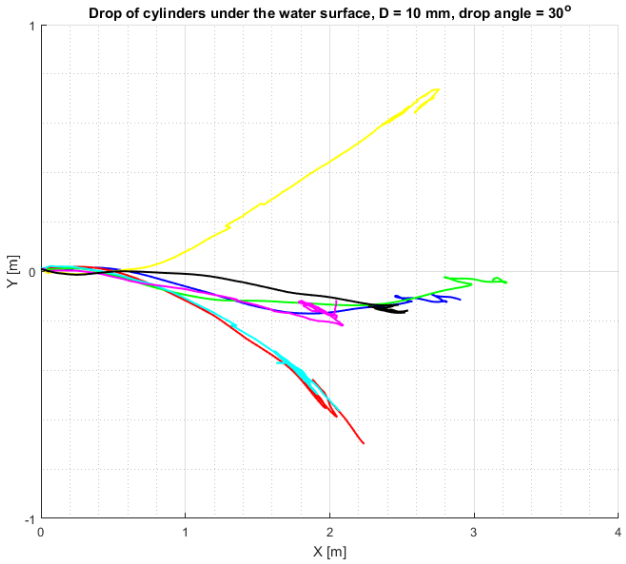

Figure 4: X-Y view: Drop of 10 mm diameter cylinders under the water surface at 30° initial drop angle. Each coloured line represent a drop in order.

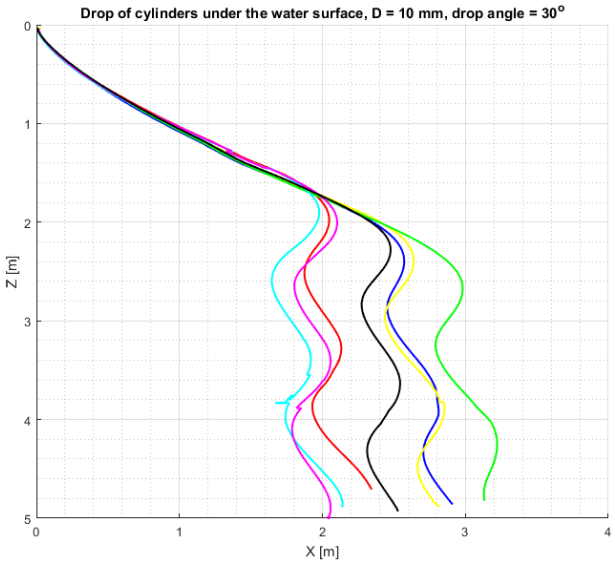

Figure 5: X-Z view: Drop of 10 mm diameter cylinders under the water surface at 30° initial drop angle. The X-coordinates are radial coordinates from the XY plane and each coloured line represents a drop.

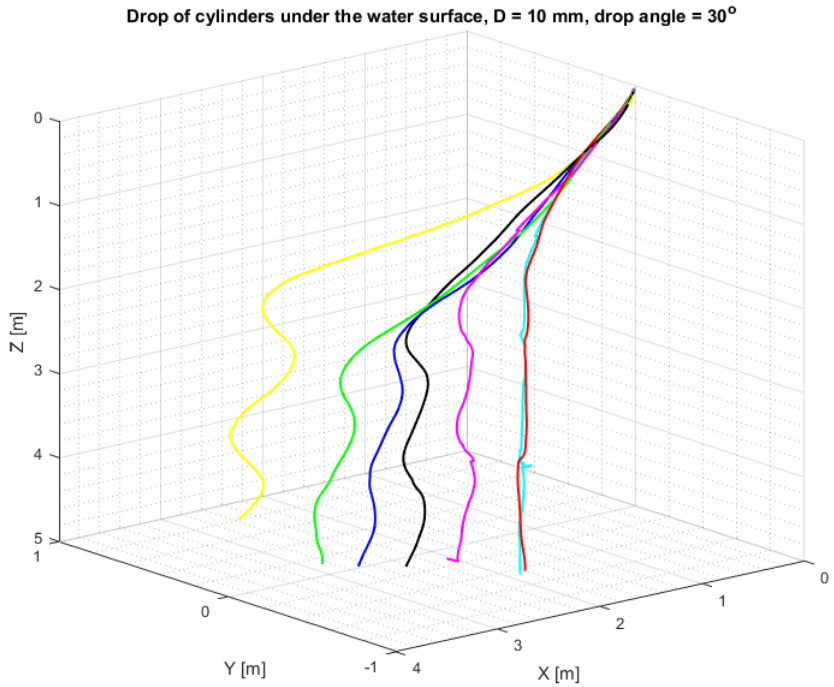

Figure 6: X-Y-Z view: Drop of 10 mm diameter cylinders under the water surface at 30° initial drop angle. Each coloured line represents a drop.

A.1.3 45° initial drop angle

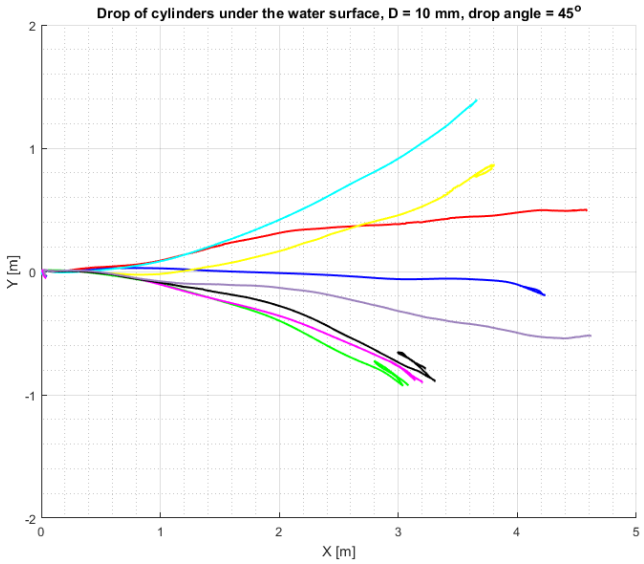

Figure 7: X-Y view: Drop of 10 mm diameter cylinders under the water surface at 45° initial drop angle. Each coloured line represent a drop in order.

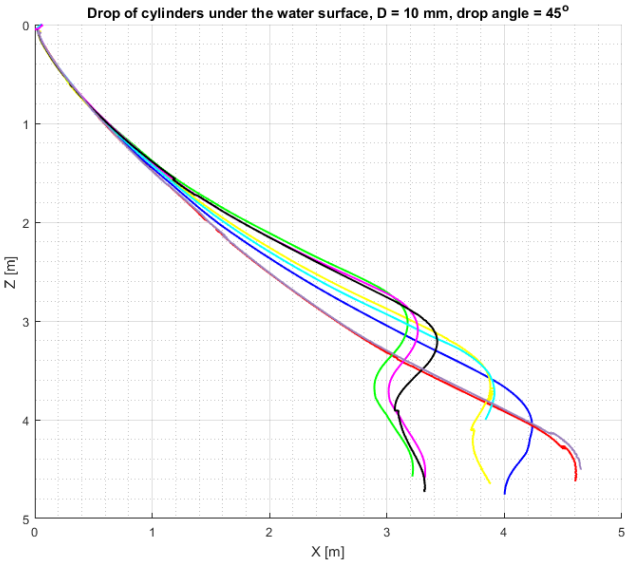

Figure 8: X-Z view: Drop of 10 mm diameter cylinders under the water surface at 45° initial drop angle. The X-coordinates are radial coordinates from the XY plane and each coloured line represents a drop.

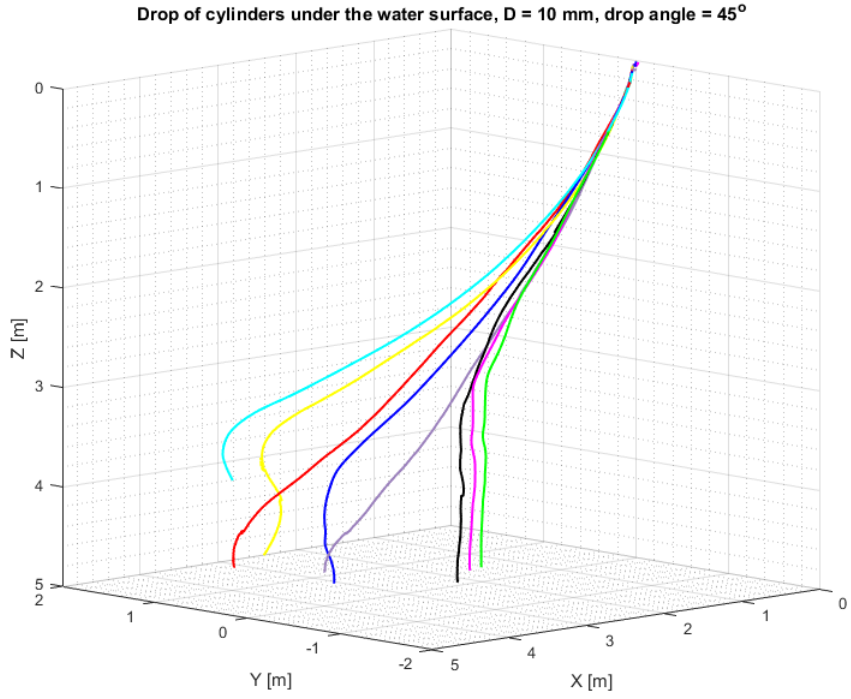

Figure 9: X-Y-Z view: Drop of 10 mm diameter cylinders under the water surface at 45° initial drop angle. Each coloured line represents a drop.

A.1.4 60° initial drop angle

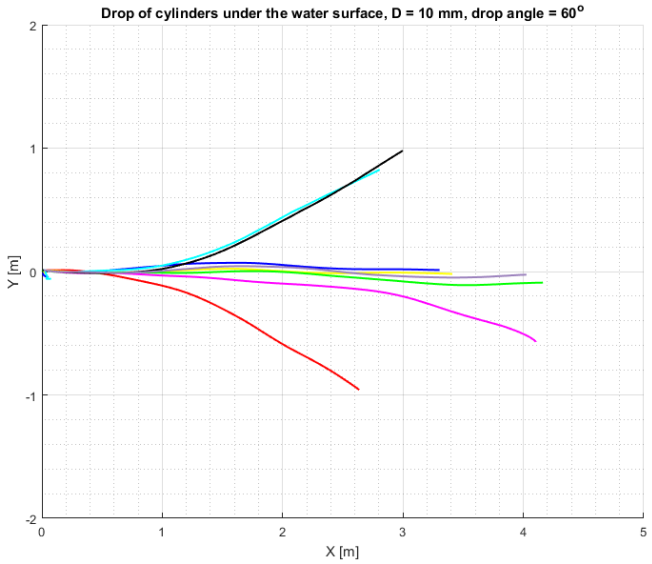

Figure 10: X-Y view: Drop of 10 mm diameter cylinders under the water surface at 60° initial drop angle. Each coloured line represent a drop in order.

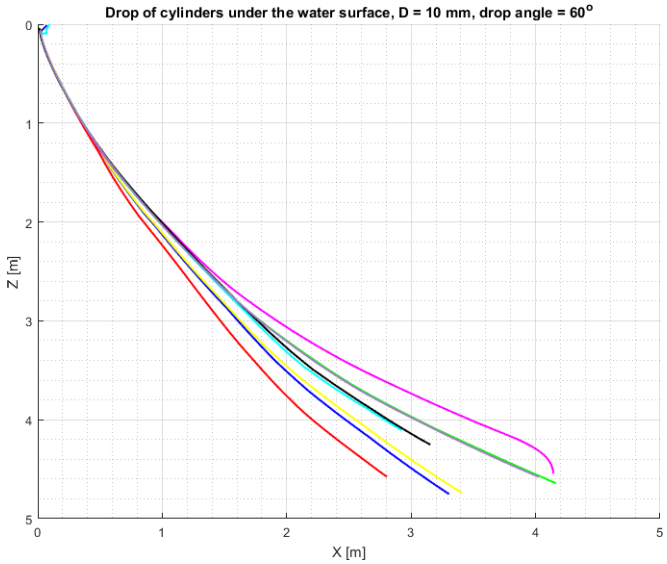

Figure 11: X-Z view: Drop of 10 mm diameter cylinders under the water surface at 60° initial drop angle. The X-coordinates are radial coordinates from the XY plane and each coloured line represents a drop.

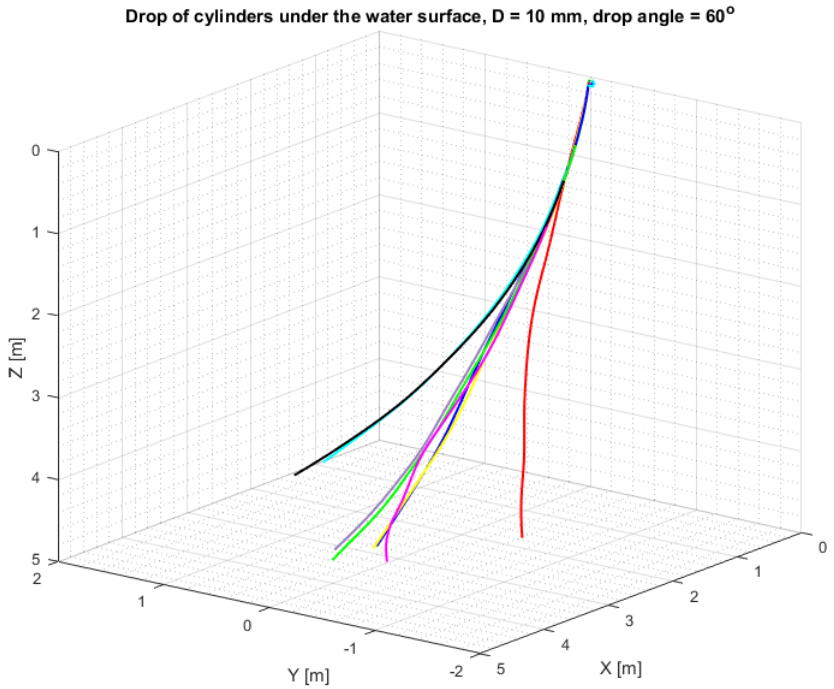

Figure 12: X-Y-Z view: Drop of 10 mm diameter cylinders under the water surface at 60° initial drop angle. Each coloured line represents a drop.

A.1.5 75° initial drop angle

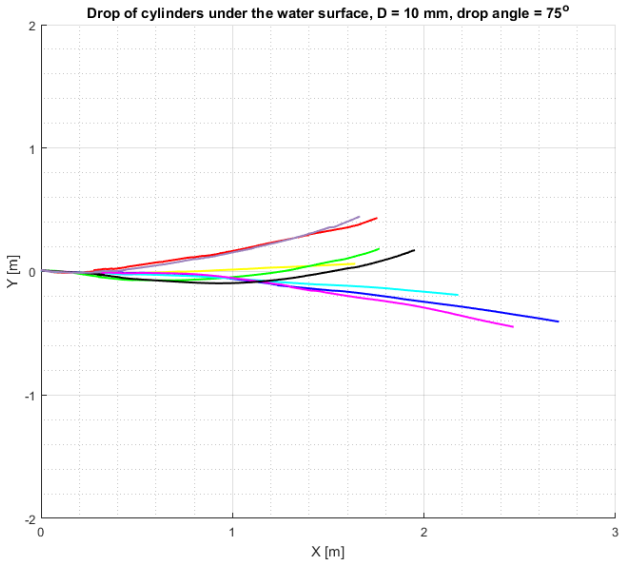

Figure 13: X-Y view: Drop of 10 mm diameter cylinders under the water surface at 75° initial drop angle. Each coloured line represent a drop in order.

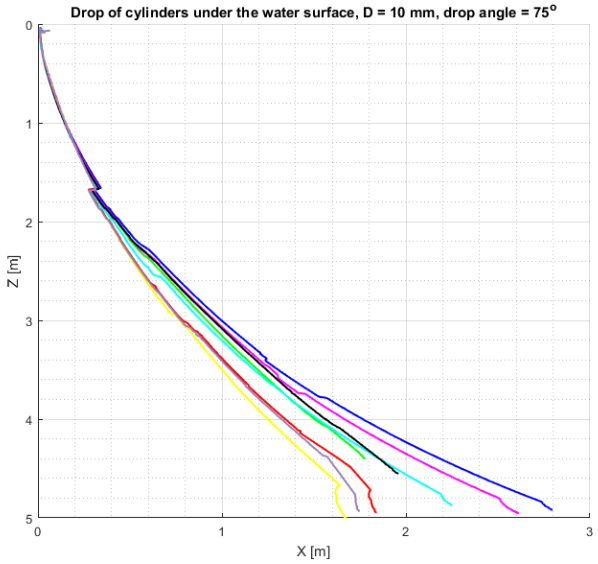

Figure 14: X-Z view: Drop of 10 mm diameter cylinders under the water surface at 75° initial drop angle. The X-coordinates are radial coordinates from the XY plane and each coloured line represents a drop.

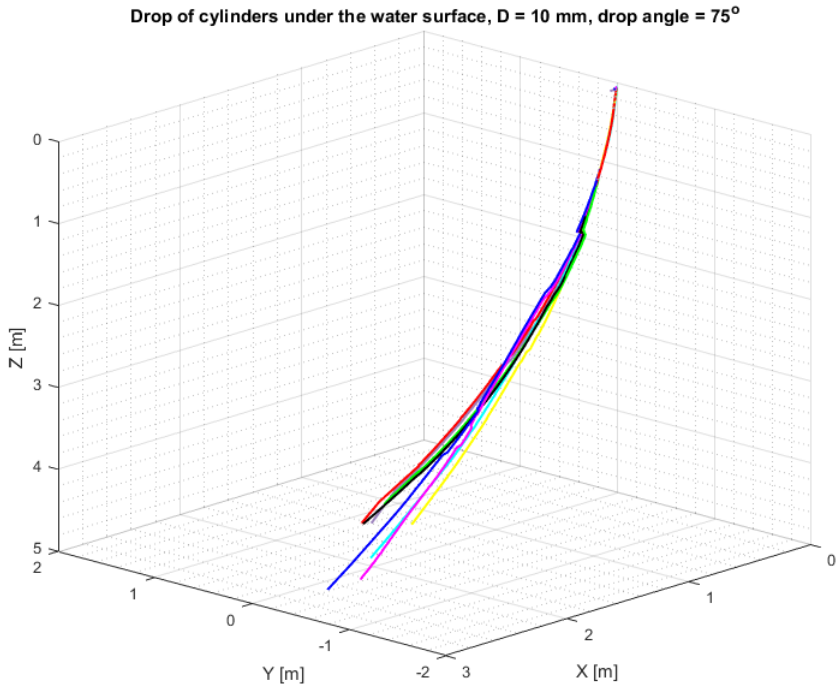

Figure 15: X-Y-Z view: Drop of 10 mm diameter cylinders under the water surface at 75° initial drop angle. Each coloured line represents a drop.

A.2 Drop of 16 mm diameter cylinders under the water surface

A.2.1 15° initial drop angle

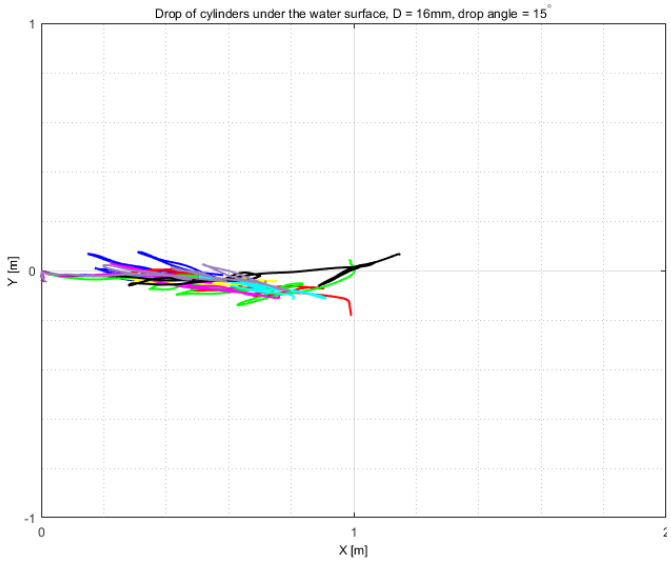

Figure 16: X-Y view: Drop of 16 mm diameter cylinders under the water surface at 15° initial drop angle. Each coloured line represent a drop in order.

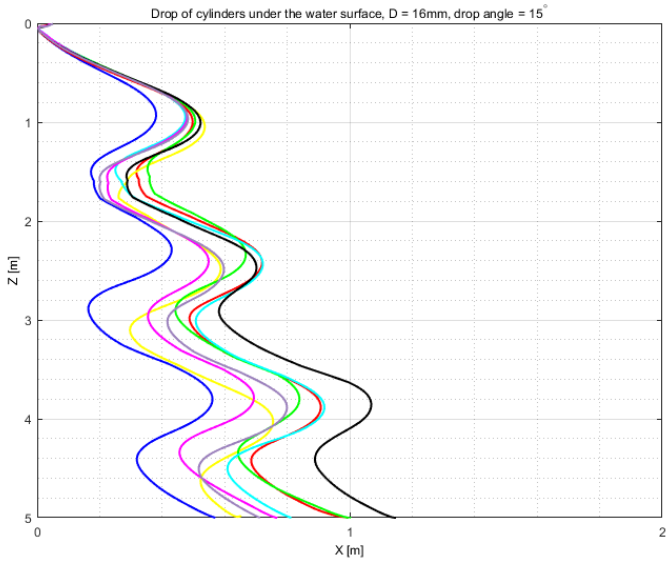

Figure 17: X-Z view: Drop of 16 mm diameter cylinders under the water surface at 15° initial drop angle. The X-coordinates are radial coordinates from the XY plane and each coloured line represents a drop.

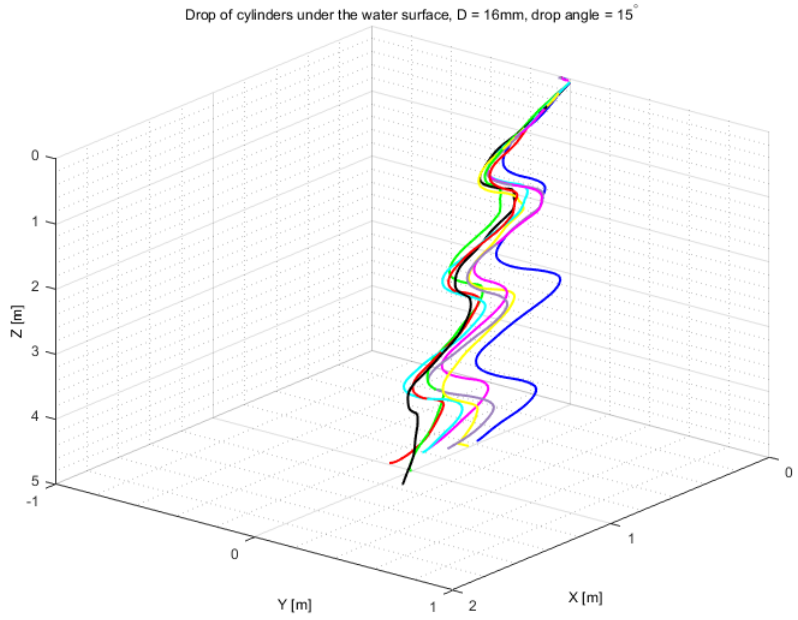

Figure 18: X-Y-Z view: Drop of 16 mm diameter cylinders under the water surface at 15° initial drop angle. Each coloured line represents a drop.

A.2.2 30° initial drop angle

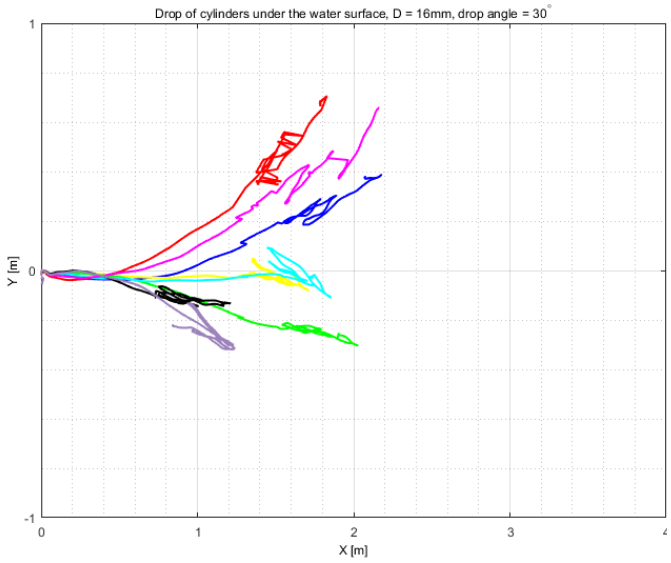

Figure 19: X-Y view: Drop of 16 mm diameter cylinders under the water surface at 30° initial drop angle. Each coloured line represent a drop in order.

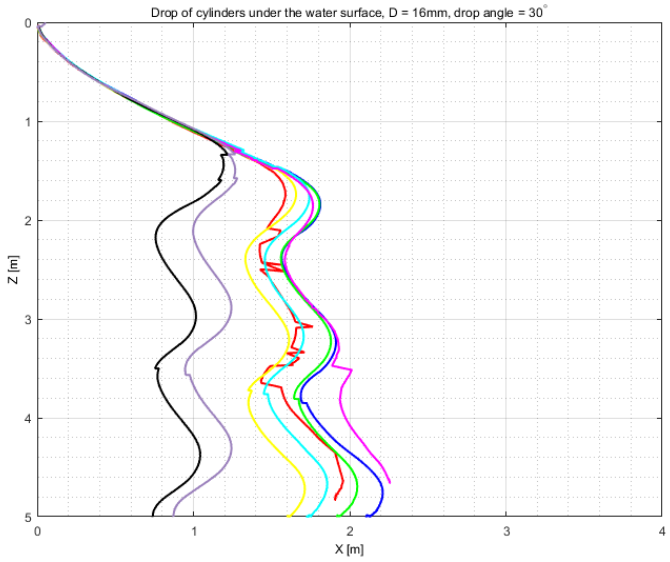

Figure 20: X-Z view: Drop of 16 mm diameter cylinders under the water surface at 30° initial drop angle. The X-coordinates are radial coordinates from the XY plane and each coloured line represents a drop.

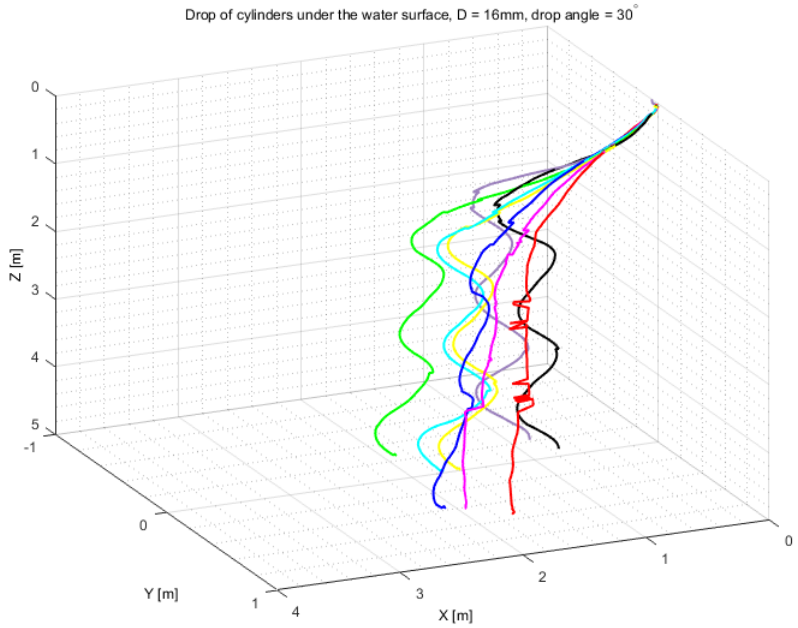

Figure 21: X-Y-Z view: Drop of 16 mm diameter cylinders under the water surface at 30° initial drop angle. Each coloured line represents a drop.

A.2.3 45° initial drop angle

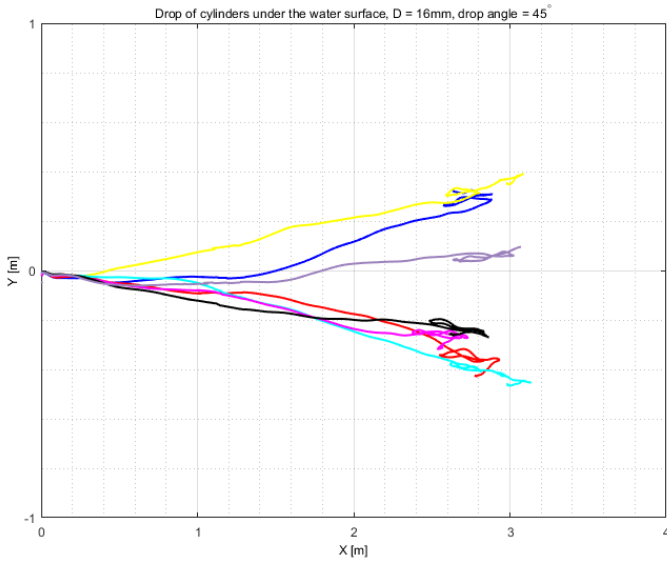

Figure 22: X-Y view: Drop of 16 mm diameter cylinders under the water surface at 45° initial drop angle. Each coloured line represent a drop in order.

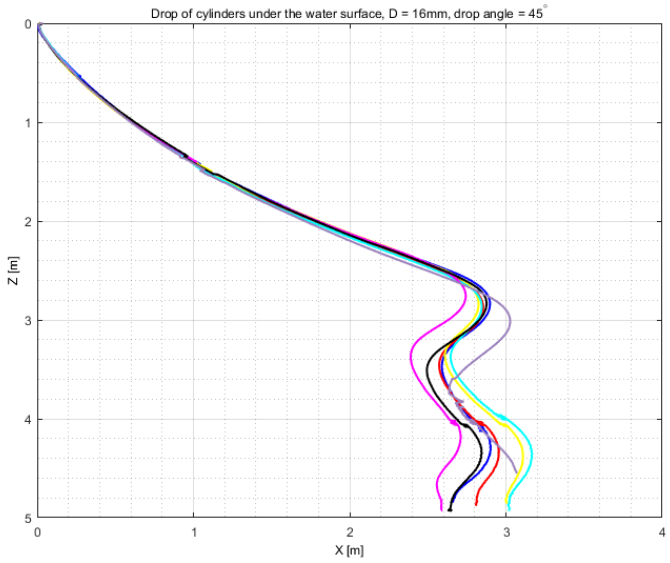

Figure 23: X-Z view: Drop of 16 mm diameter cylinders under the water surface at 45° initial drop angle. The X-coordinates are radial coordinates from the XY plane and each coloured line represents a drop.

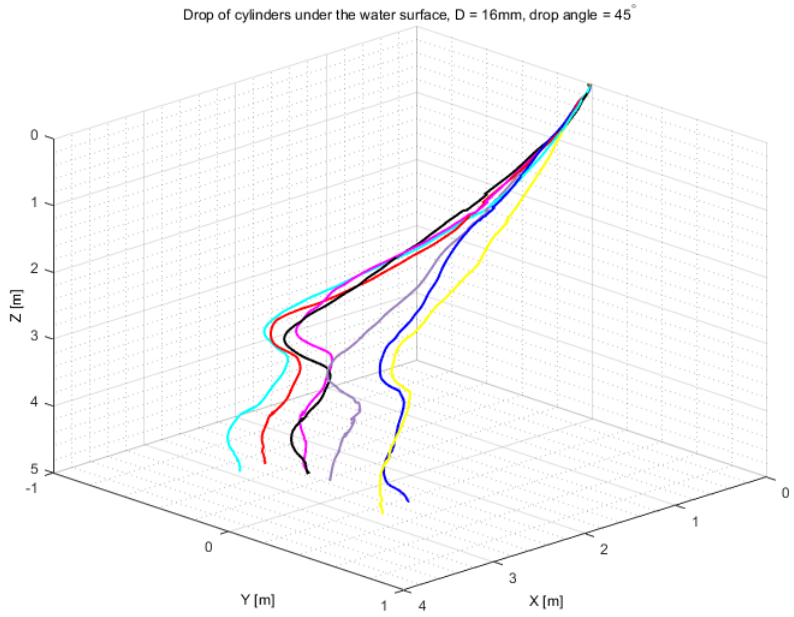

Figure 24: X-Y-Z view: Drop of 16 mm diameter cylinders under the water surface at 45° initial drop angle. Each coloured line represents a drop.

A.2.4 60° initial drop angle

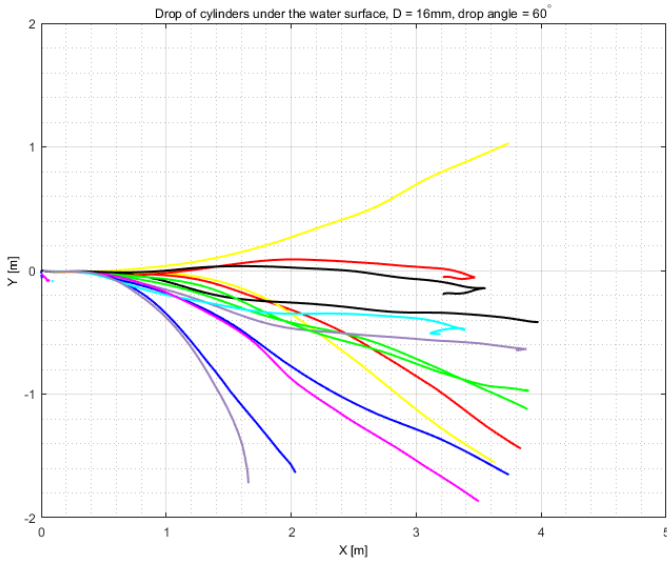

Figure 25: X-Y view: Drop of 16 mm diameter cylinders under the water surface at 60° initial drop angle. Each coloured line represent a drop in order.

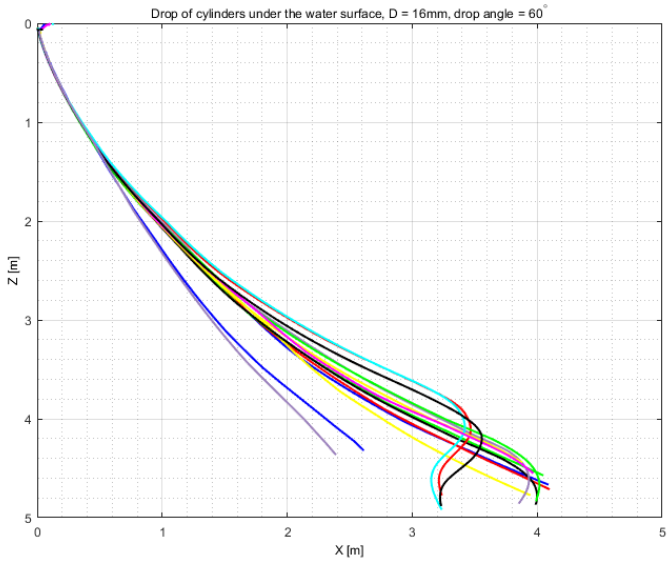

Figure 26: X-Z view: Drop of 16 mm diameter cylinders under the water surface at 60° initial drop angle. The X-coordinates are radial coordinates from the XY plane and each coloured line represents a drop.

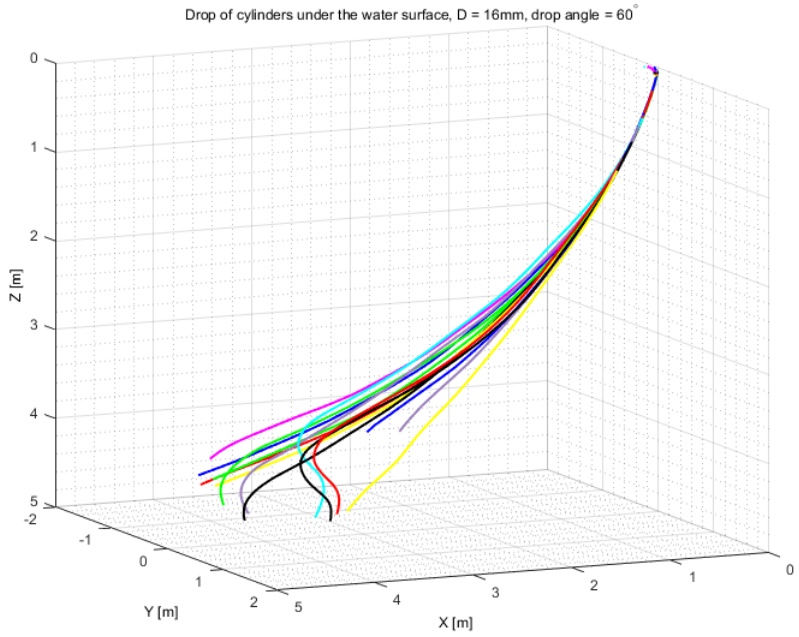

Figure 27: X-Y-Z view: Drop of 16 mm diameter cylinders under the water surface at 60° initial drop angle. Each coloured line represents a drop.

A.2.5 75° initial drop angle

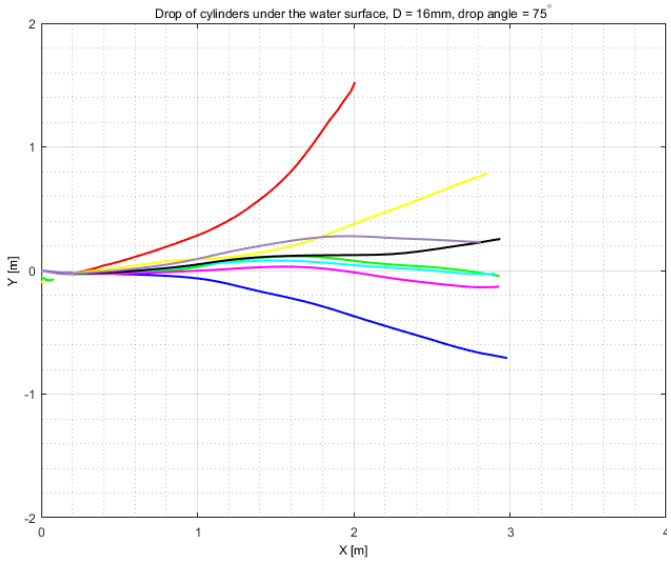

Figure 28: X-Y view: Drop of 16 mm diameter cylinders under the water surface at 75° initial drop angle. Each coloured line represent a drop in order.

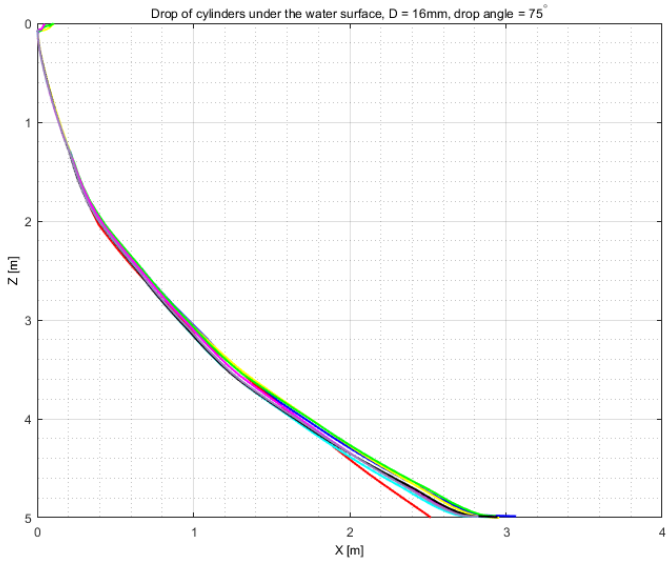

Figure 29: X-Z view: Drop of 16 mm diameter cylinders under the water surface at 75° initial drop angle. The X-coordinates are radial coordinates from the XY plane and each coloured line represents a drop.

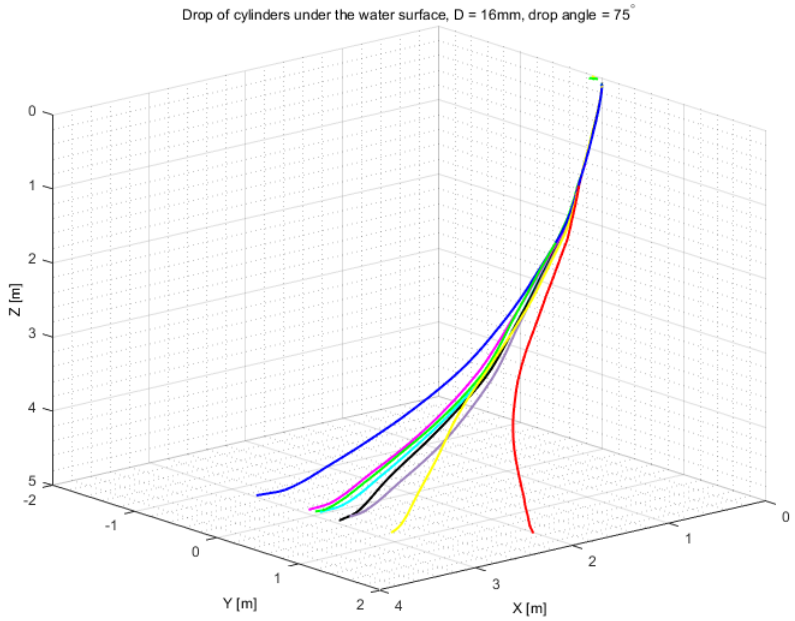

Figure 30: X-Y-Z view: Drop of 16 mm diameter cylinders under the water surface at 75° initial drop angle. Each coloured line represents a drop.

A.3 Drop of 19mm diameter cylinders under the water surface

A.3.1 15° initial drop angle

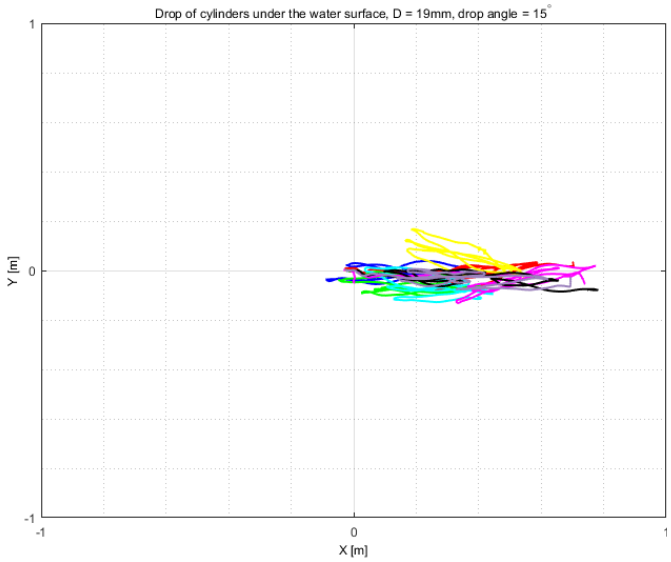

Figure 31: X-Y view: Drop of 19 mm diameter cylinders under the water surface at 15° initial drop angle. Each coloured line represent a drop in order.

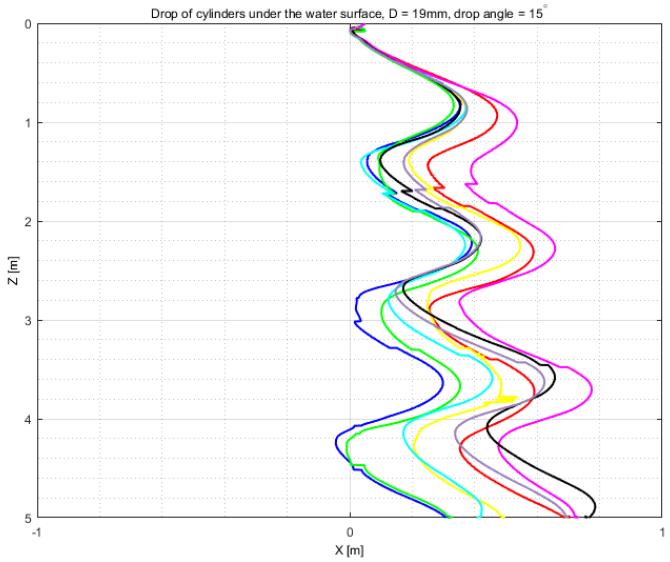

Figure 32: X-Z view: Drop of 19 mm diameter cylinders under the water surface at 15° initial drop angle. The X-coordinates are radial coordinates from the XY plane and each coloured line represents a drop.

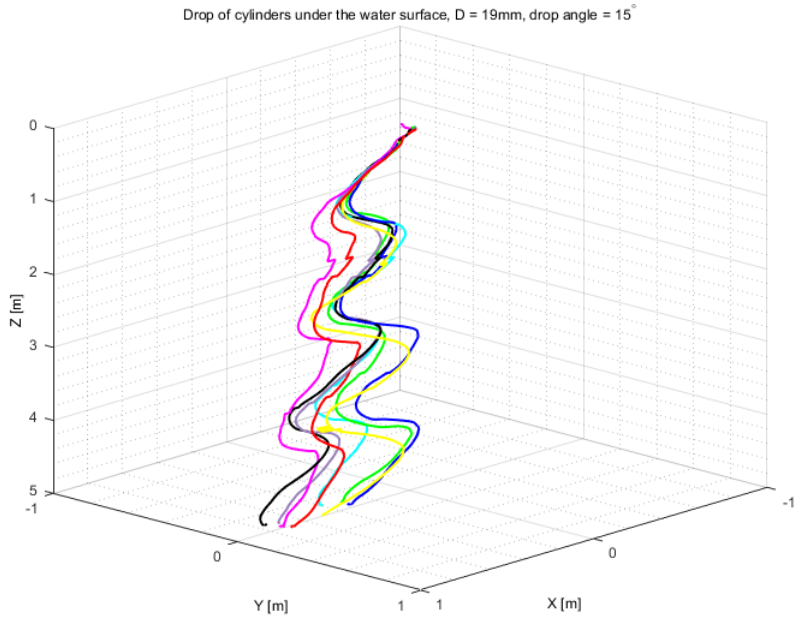

Figure 33: X-Y-Z view: Drop of 19 mm diameter cylinders under the water surface at 15° initial drop angle. Each coloured line represents a drop.

A.3.2 30° initial drop angle

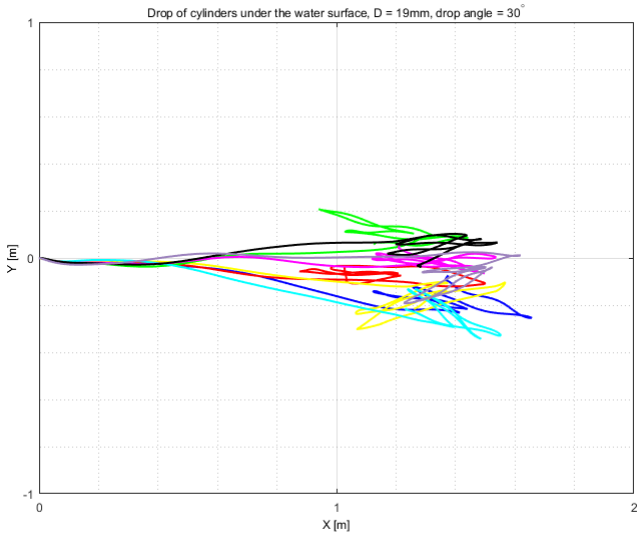

Figure 34: X-Y view: Drop of 19 mm diameter cylinders under the water surface at 30° initial drop angle. Each coloured line represent a drop in order.

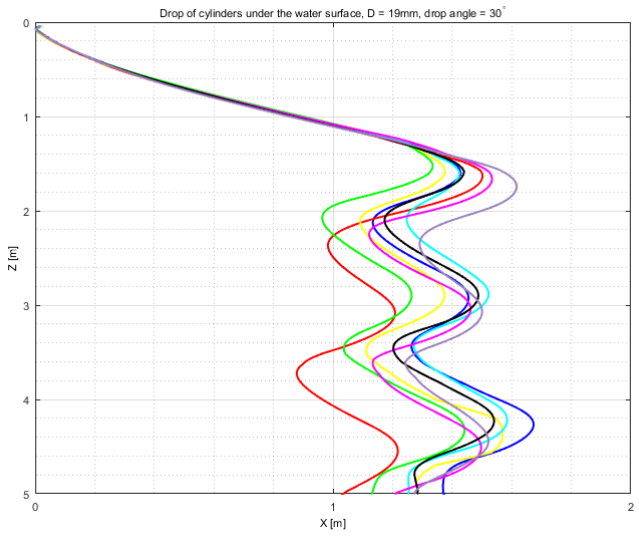

Figure 35: X-Z view: Drop of 19 mm diameter cylinders under the water surface at 30° initial drop angle. The X-coordinates are radial coordinates from the XY plane and each coloured line represents a drop.

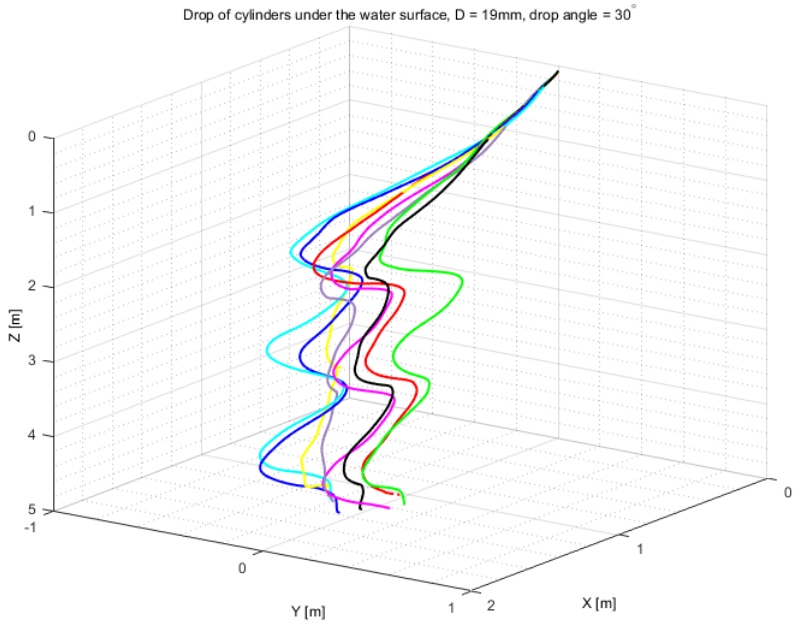

Figure 36: X-Y-Z view: Drop of 19 mm diameter cylinders under the water surface at 30° initial drop angle. Each coloured line represents a drop.

A.3.3 45° initial drop angle

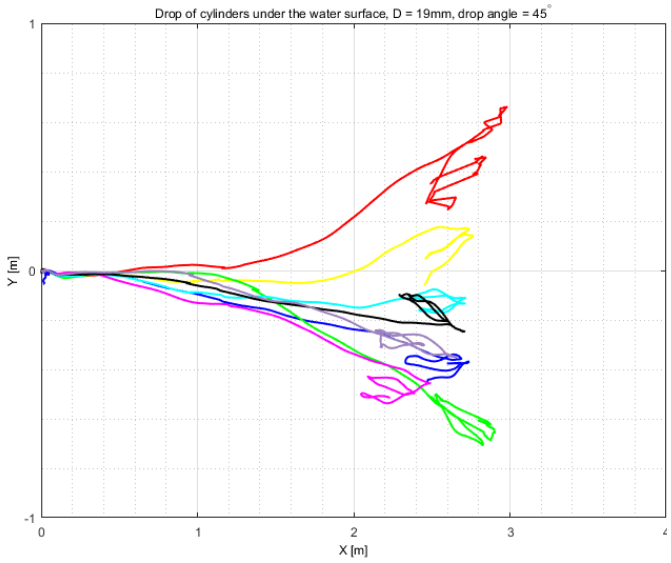

Figure 37: X-Y view: Drop of 19 mm diameter cylinders under the water surface at 45° initial drop angle. Each coloured line represent a drop in order.

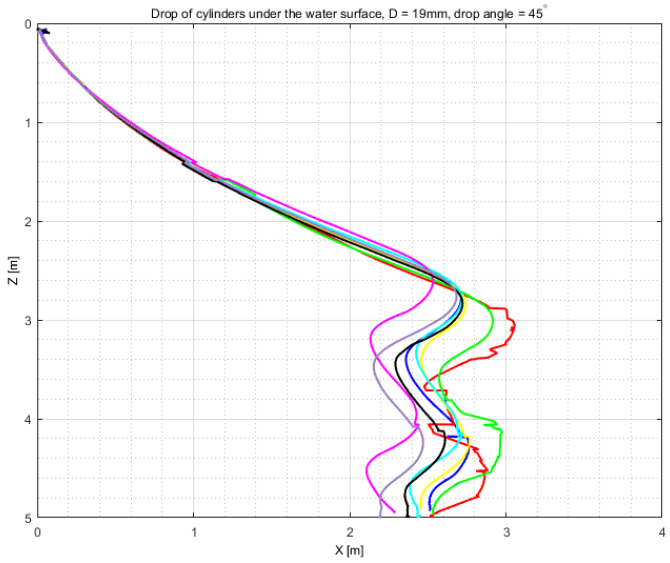

Figure 38: X-Z view: Drop of 19 mm diameter cylinders under the water surface at 45° initial drop angle. The X-coordinates are radial coordinates from the XY plane and each coloured line represents a drop.

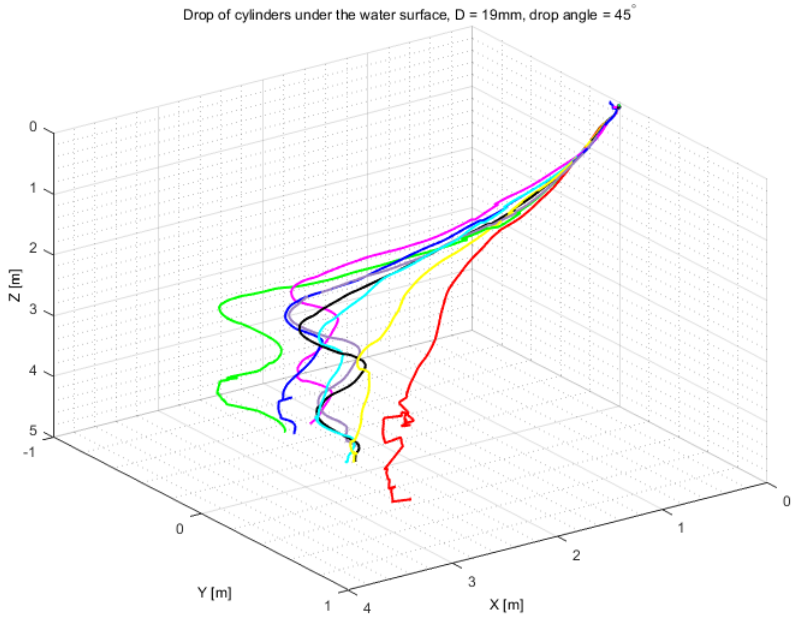

Figure 39: X-Y-Z view: Drop of 19 mm diameter cylinders under the water surface at 45° initial drop angle. Each coloured line represents a drop.

A.3.4 60° initial drop angle

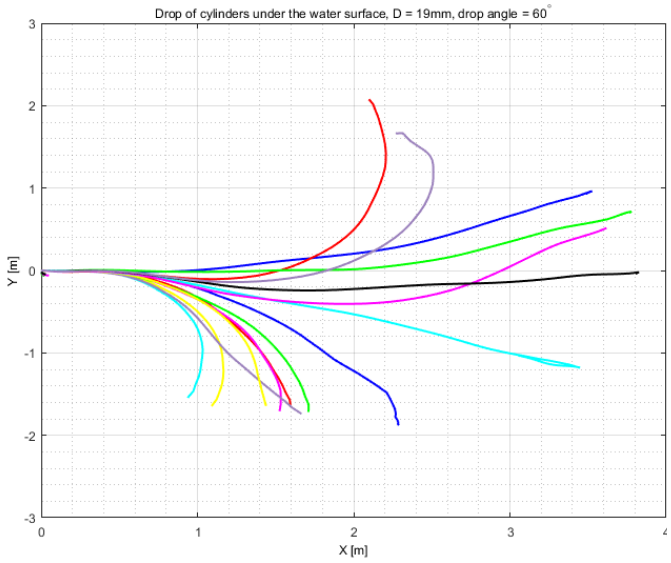

Figure 40: X-Y view: Drop of 19 mm diameter cylinders under the water surface at 60° initial drop angle. Each coloured line represent a drop in order.

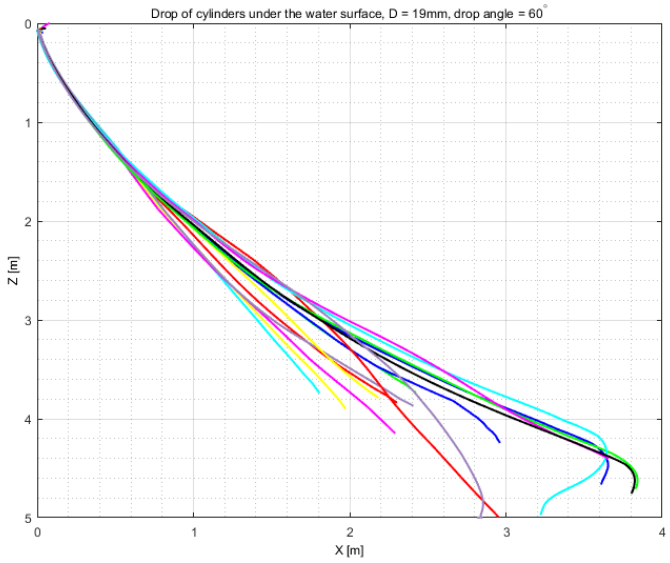

Figure 41: X-Z view: Drop of 19 mm diameter cylinders under the water surface at 60° initial drop angle. The X-coordinates are radial coordinates from the XY plane and each coloured line represents a drop.

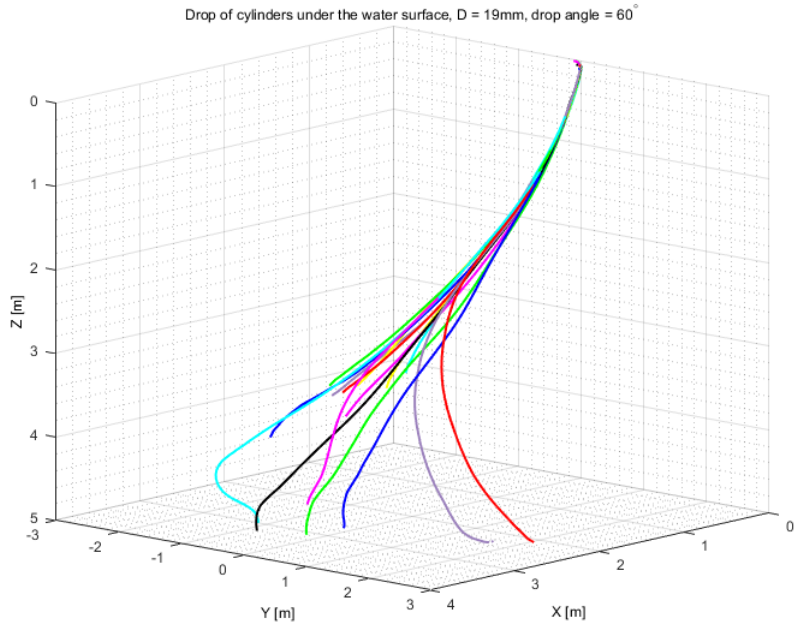

Figure 42: X-Y-Z view: Drop of 10mm diameter cylinders under the water surface at 60° initial drop angle. Each coloured line represents a drop.

A.3.5 75° initial drop angle

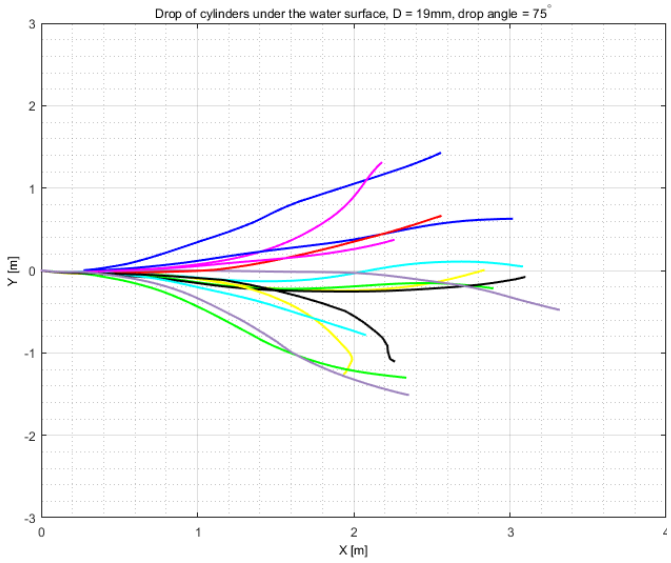

Figure 43: X-Y view: Drop of 19 mm diameter cylinders under the water surface at 75° initial drop angle. Each coloured line represent a drop in order.

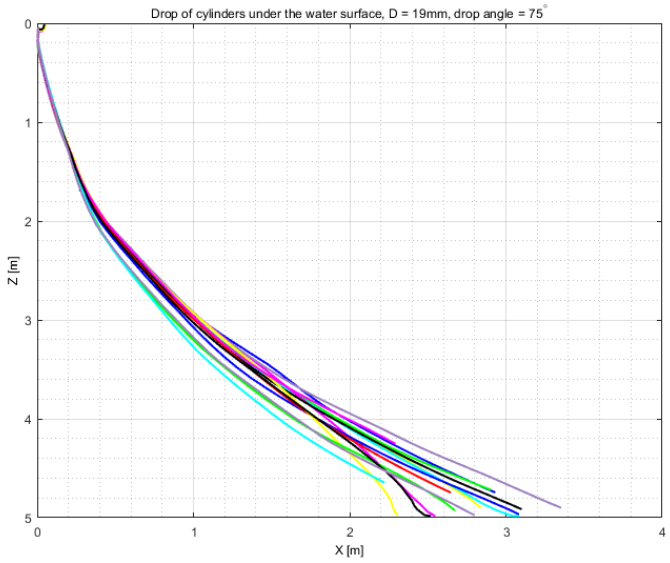

Figure 44: X-Z view: Drop of 19 mm diameter cylinders under the water surface at 75° initial drop angle. The X-coordinates are radial coordinates from the XY plane and each coloured line represents a drop.

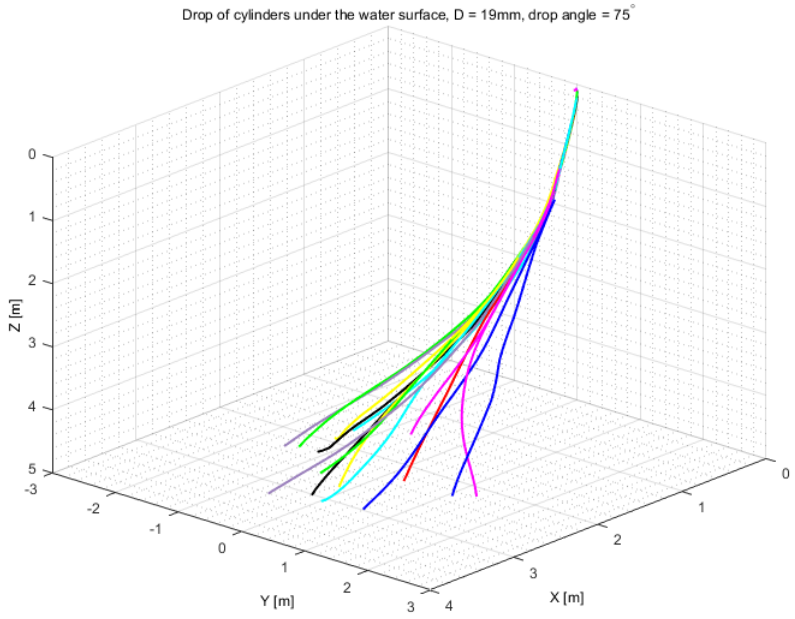

Figure 45: X-Y-Z view: Drop of 19 mm diameter cylinders under the water surface at 75° initial drop angle. Each coloured line represents a drop.

A.4 Drop of 10mm diameter cylinders over the water surface

A.4.1 15° initial drop angle

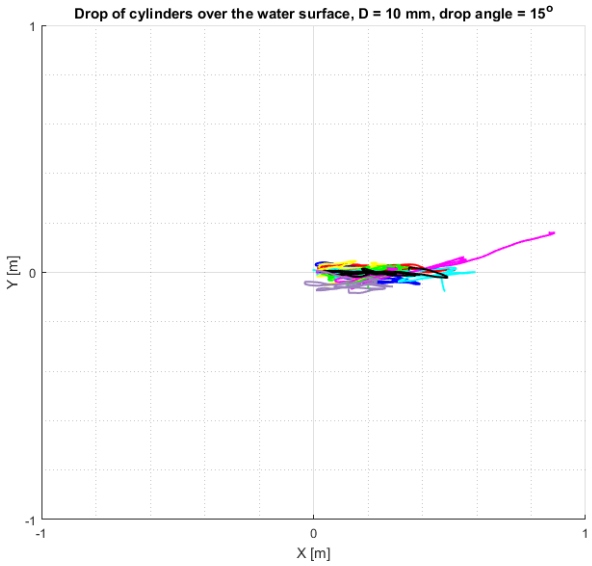

Figure 46: X-Y view: Drop of 10mm diameter cylinders over the water surface at 15° initial angle. Each coloured line represents a drop.

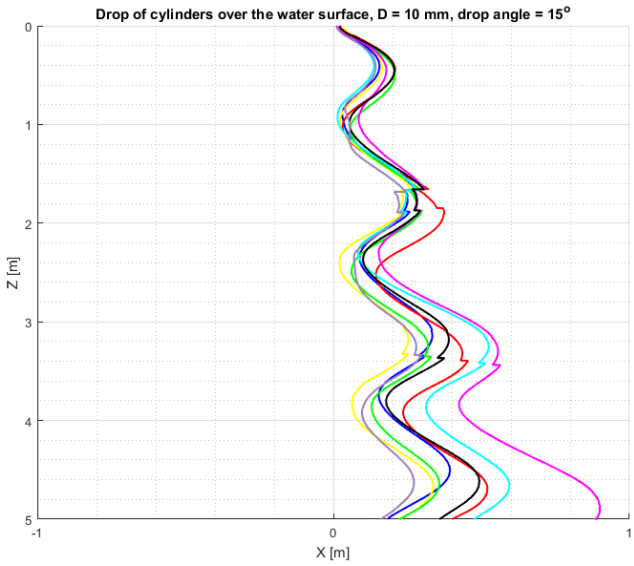

Figure 47: X-Z view: Drop of 10mm diameter cylinders over the water surface at 15° initial angle. The X-coordinates are radial coordinates from the XY plane and each coloured line represents a drop.

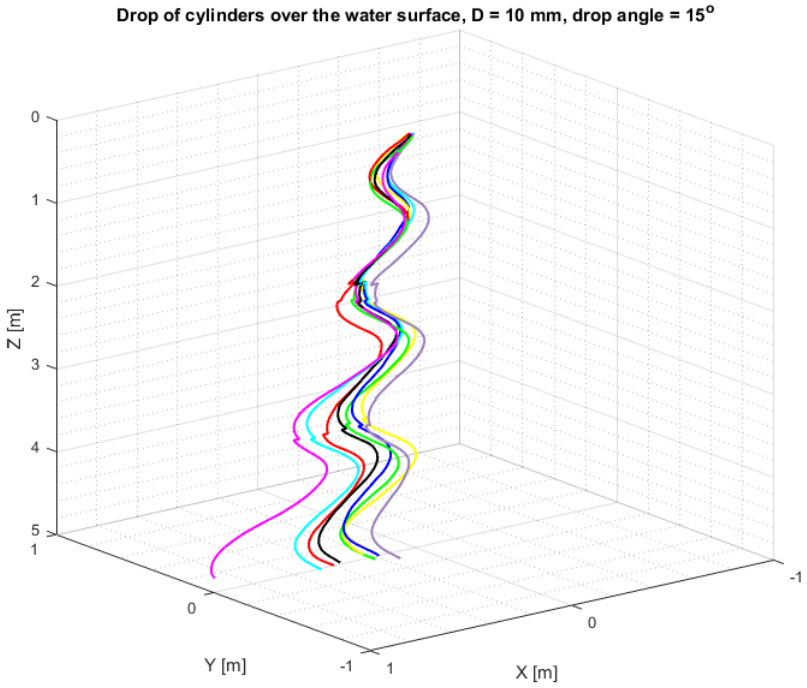

Figure 48: X-Y-Z view: Drop of 10mm diameter cylinders over the water surface at 15° initial angle. Each coloured line represents a drop.

A.4.2 30° initial drop angle

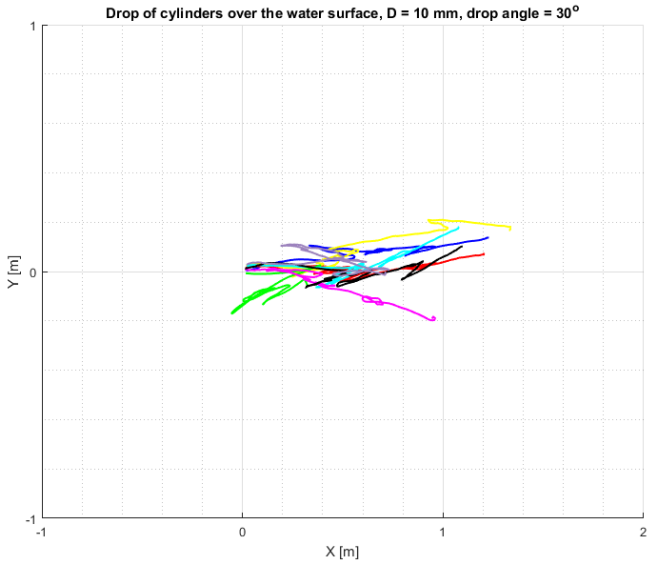

Figure 49: X-Y view: Drop of 10mm diameter cylinders over the water surface at 30° initial angle. Each coloured line represents a drop.

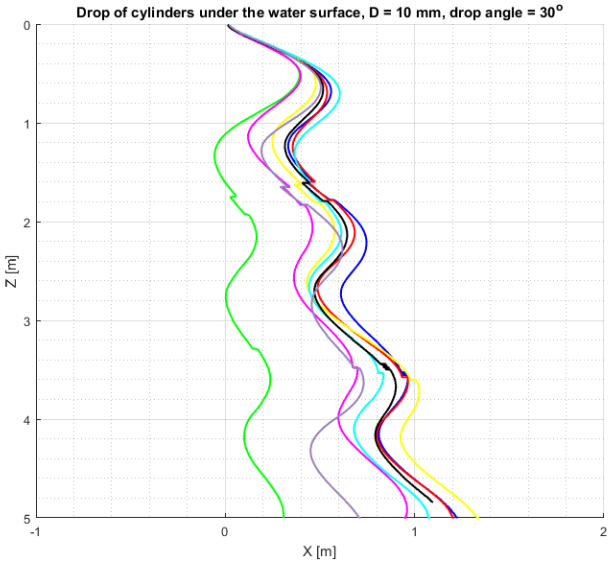

Figure 50: X-Z view: Drop of 10mm diameter cylinders over the water surface at 30° initial angle. The X-coordinates are radial coordinates from the XY plane and each coloured line represents a drop.

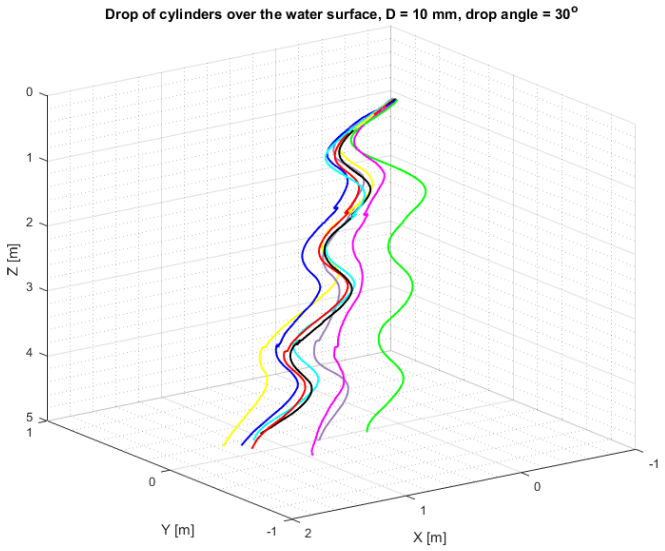

Figure 51: X-Y-Z view: Drop of 10mm diameter cylinders over the water surface at 30° initial angle. Each coloured line represents a drop.

A.4.3 45° initial drop angle

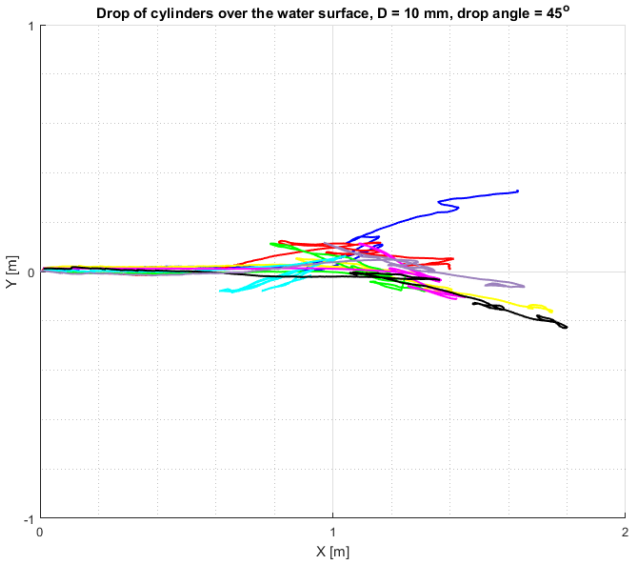

Figure 52: X-Y view: Drop of 10mm diameter cylinders over the water surface at 45° initial angle. Each coloured line represents a drop.

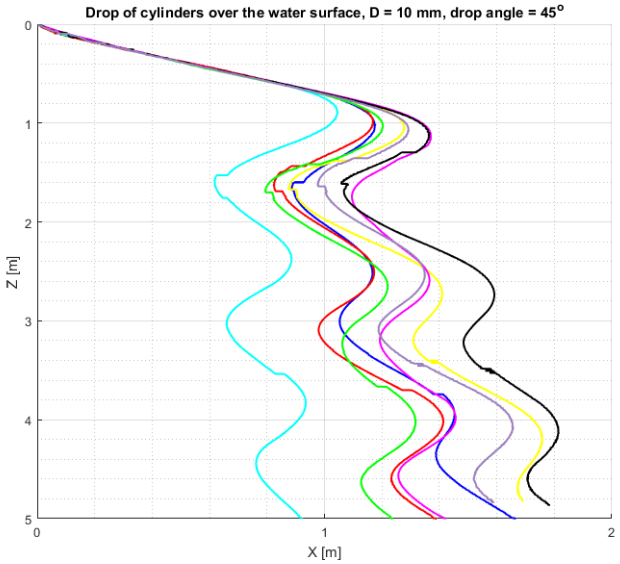

Figure 53: X-Z view: Drop of 10mm diameter cylinders over the water surface at 45° initial angle. The X-coordinates are radial coordinates from the XY plane and each coloured line represents a drop.

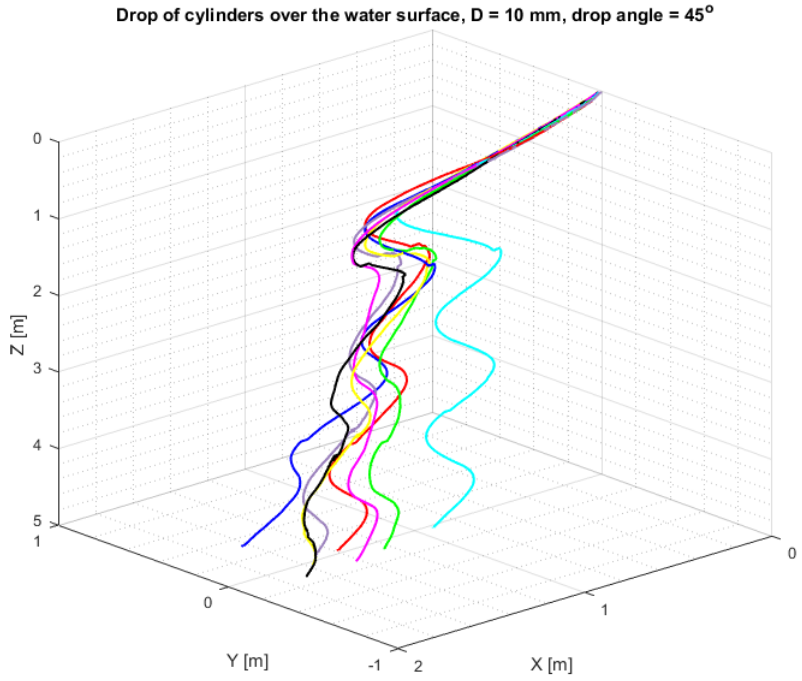

Figure 54: X-Y-Z view: Drop of 10mm diameter cylinders over the water surface at 45° initial angle. Each coloured line represents a drop.

A.4.4 60° initial drop angle

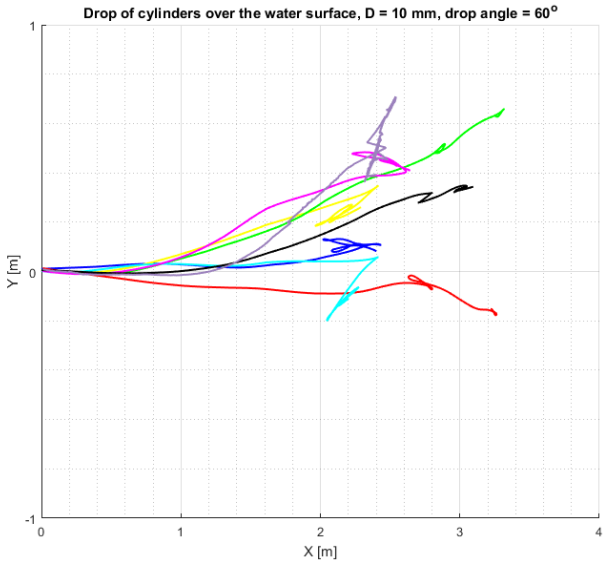

Figure 55: X-Y view: Drop of 10mm diameter cylinders over the water surface at 60° initial angle. Each coloured line represents a drop.

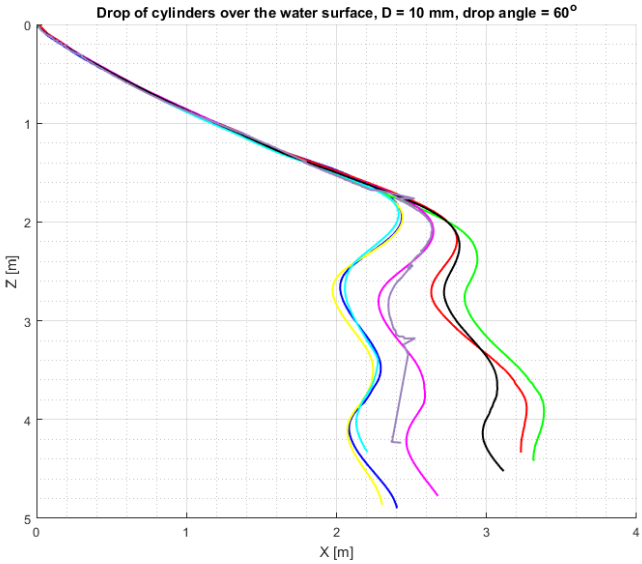

Figure 56: X-Z view: Drop of 10mm diameter cylinders over the water surface at 60° initial angle. The X-coordinates are radial coordinates from the XY plane and each coloured line represents a drop.

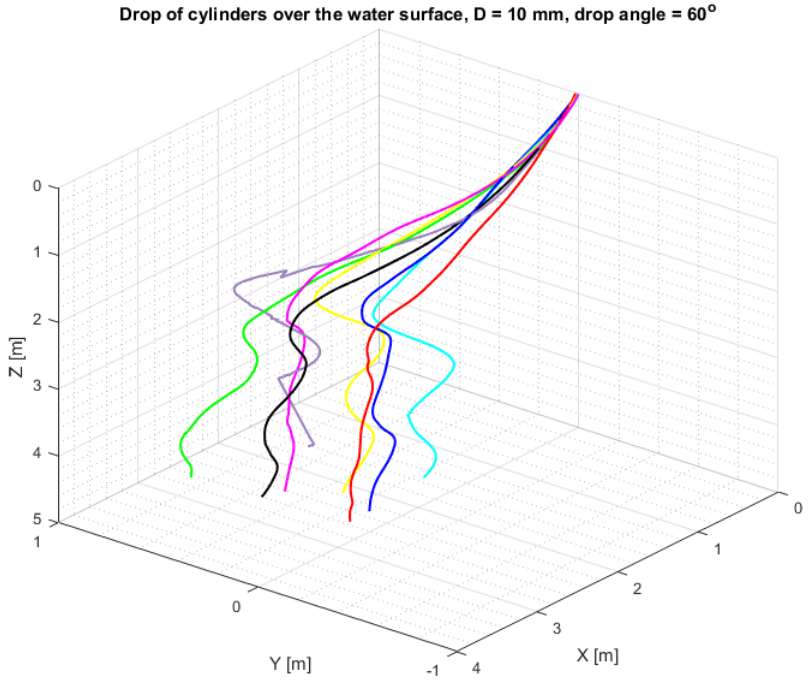

Figure 57: X-Y-Z view: Drop of 10mm diameter cylinders over the water surface at 60° initial angle. Each coloured line represents a drop.

A.4.5 75° initial drop angle

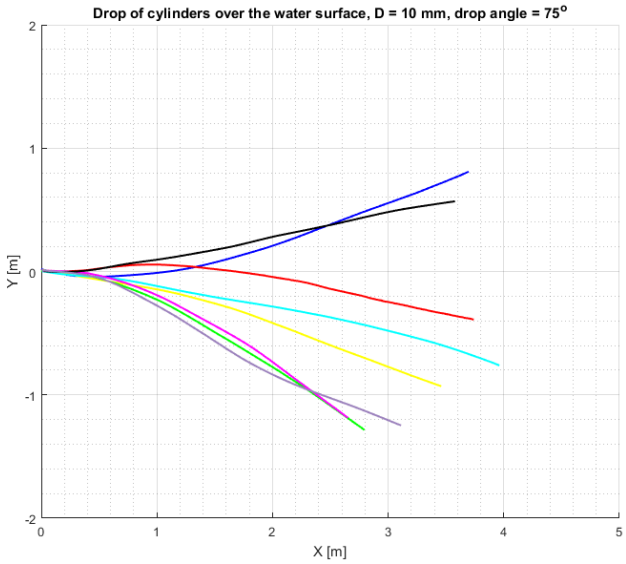

Figure 58: X-Y view: Drop of 10mm diameter cylinders over the water surface at 75° initial angle. Each coloured line represents a drop.

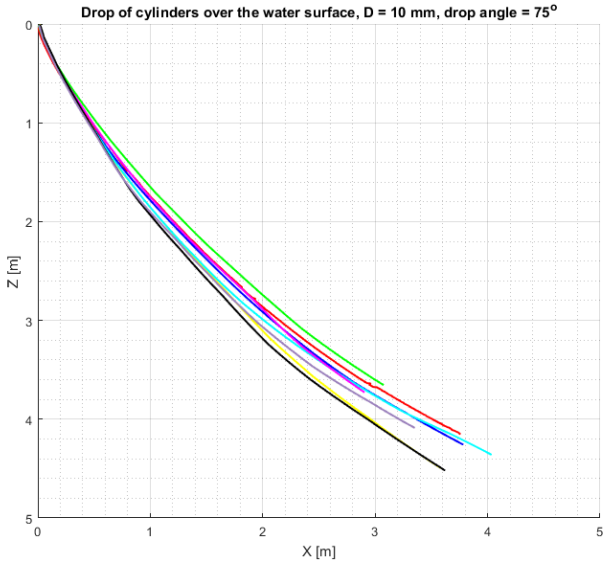

Figure 59: X-Z view: Drop of 10mm diameter cylinders over the water surface at 75° initial angle. The X-coordinates are radial coordinates from the XY plane and each coloured line represents a drop.

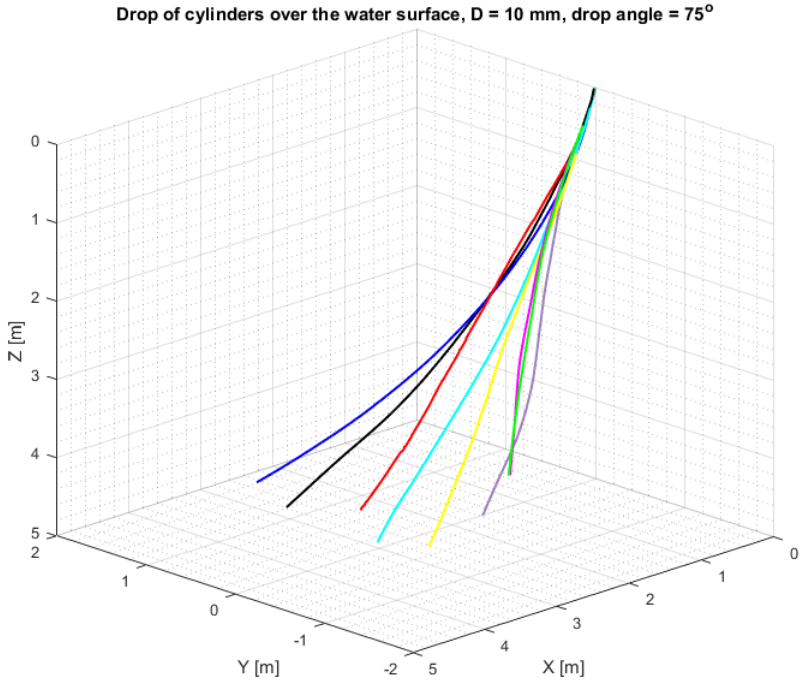

Figure 60: X-Y-Z view: Drop of 10mm diameter cylinders over the water surface at 75° initial angle. Each coloured line represents a drop.

A.5 Drop of 16 mm diameter cylinders over the water surface

A.5.1 15° initial drop angle

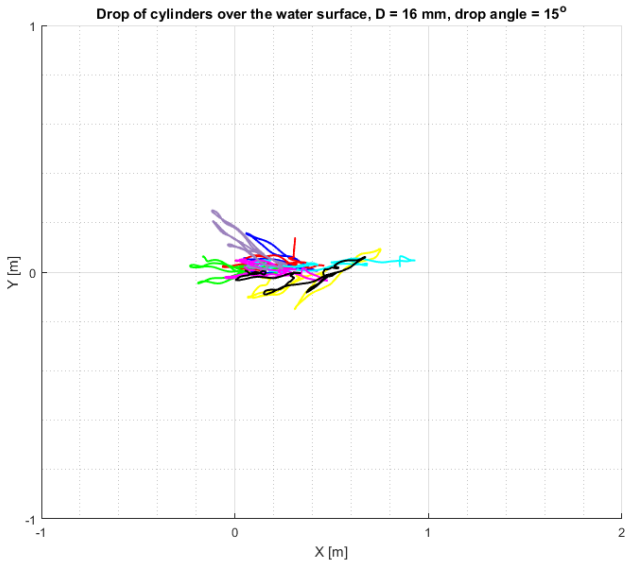

Figure 61: X-Y view: Drop of 16 mm diameter cylinders over the water surface at 15° initial angle. Each coloured line represents a drop.

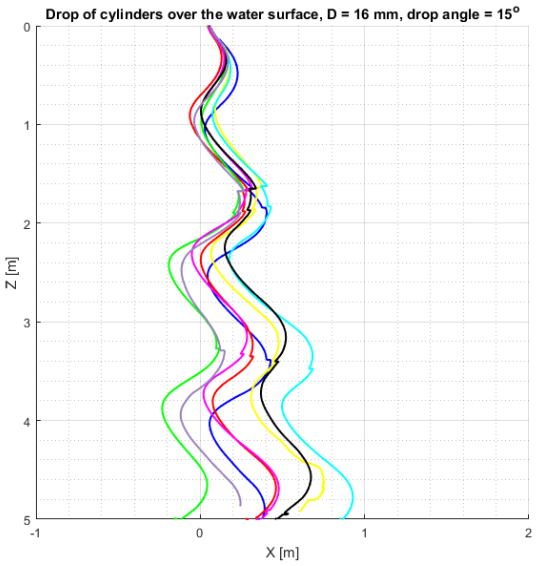

Figure 62: X-Z view: Drop of 16 mm diameter cylinders over the water surface at 15° initial angle. The X-coordinates are radial coordinates from the XY plane and each coloured line represents a drop.

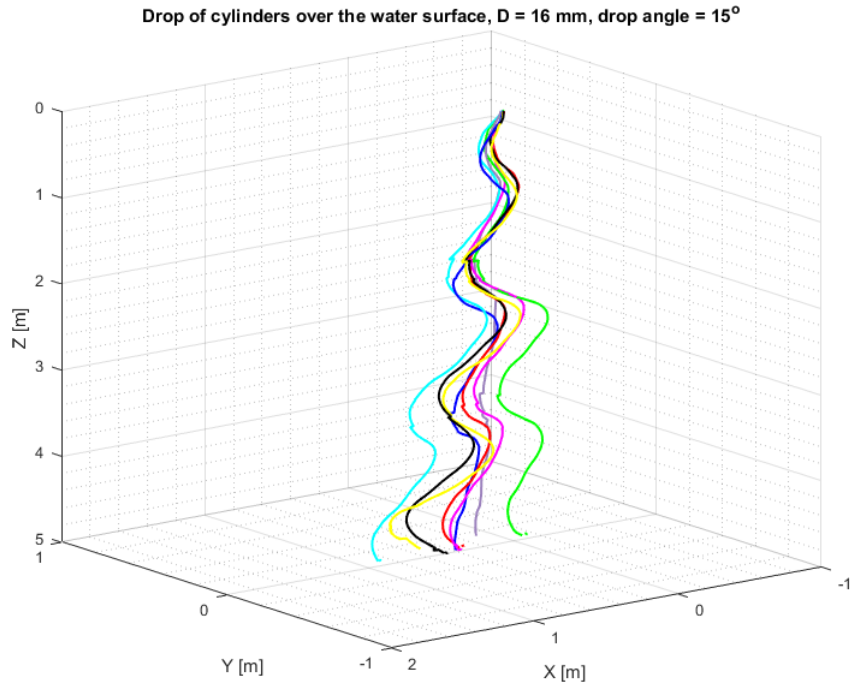

Figure 63: X-Y-Z view: Drop of 16 mm diameter cylinders over the water surface at 15° initial angle. Each coloured line represents a drop.

A.5.2 30° initial drop angle

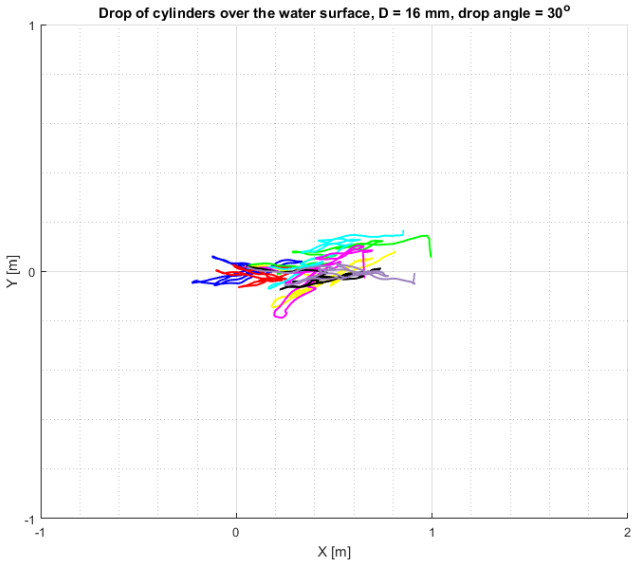

Figure 64: X-Y view: Drop of 16 mm diameter cylinders over the water surface at 30° initial angle. Each coloured line represents a drop.

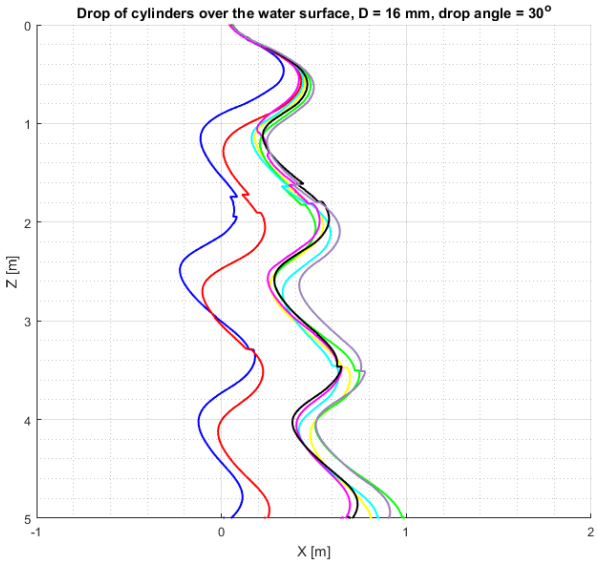

Figure 65: X-Z view: Drop of 16 mm diameter cylinders over the water surface at 30° initial angle. The X-coordinates are radial coordinates from the XY plane and each coloured line represents a drop.

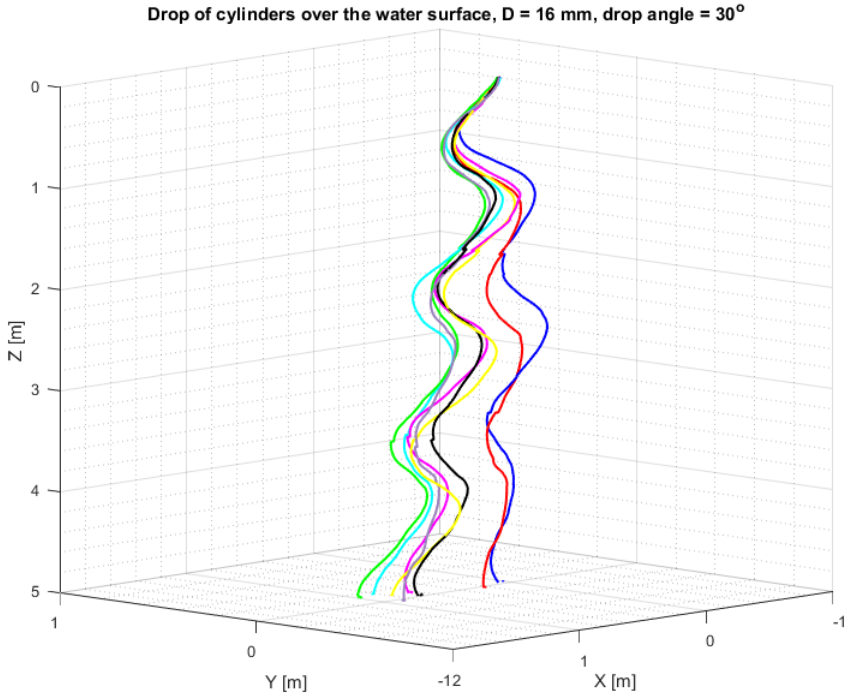

Figure 66: X-Y-Z view: Drop of 16 mm diameter cylinders over the water surface at 30° initial angle. Each coloured line represents a drop.

A.5.3 45° initial drop angle

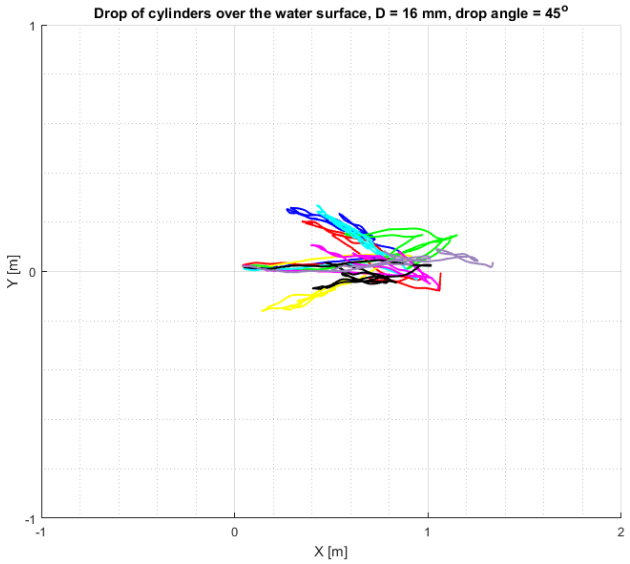

Figure 67: X-Y view: Drop of 16 mm diameter cylinders over the water surface at 45° initial angle. Each coloured line represents a drop.

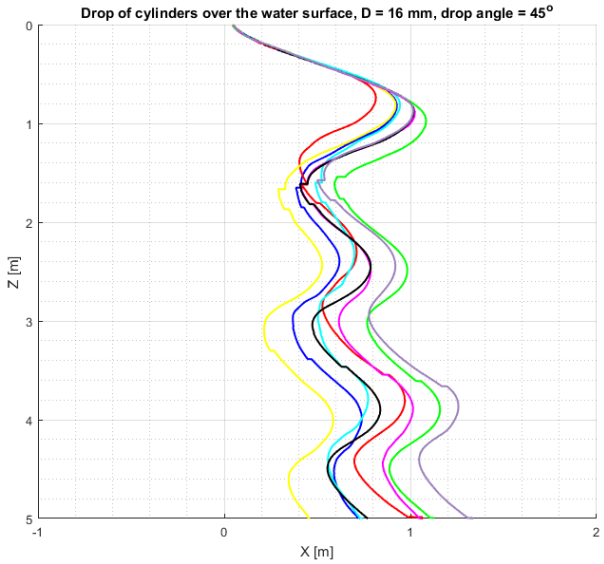

Figure 68: X-Z view: Drop of 16 mm diameter cylinders over the water surface at 45° initial angle. The X-coordinates are radial coordinates from the XY plane and each coloured line represents a drop.

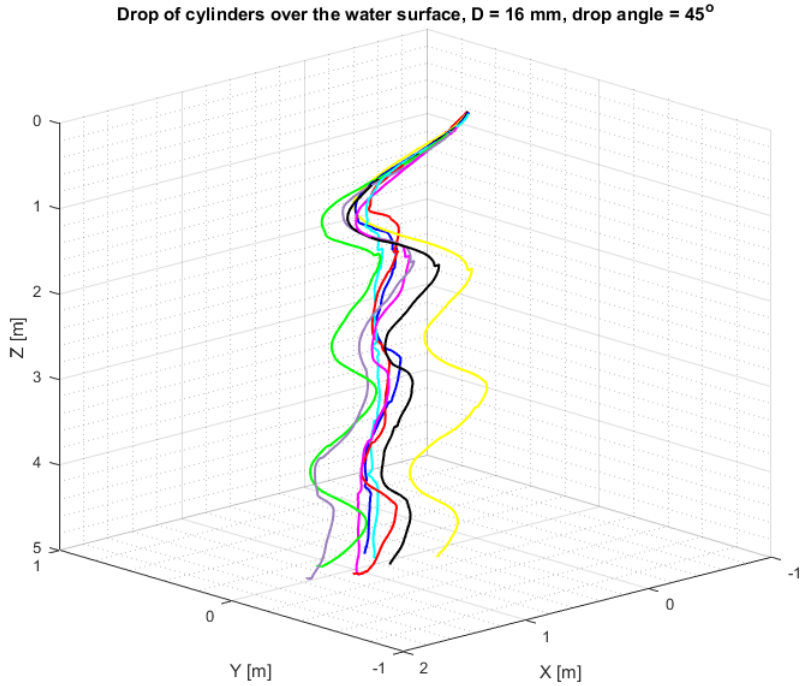

Figure 69: X-Y-Z view: Drop of 16 mm diameter cylinders over the water surface at 45° initial angle. Each coloured line represents a drop.

A.5.4 60° initial drop angle

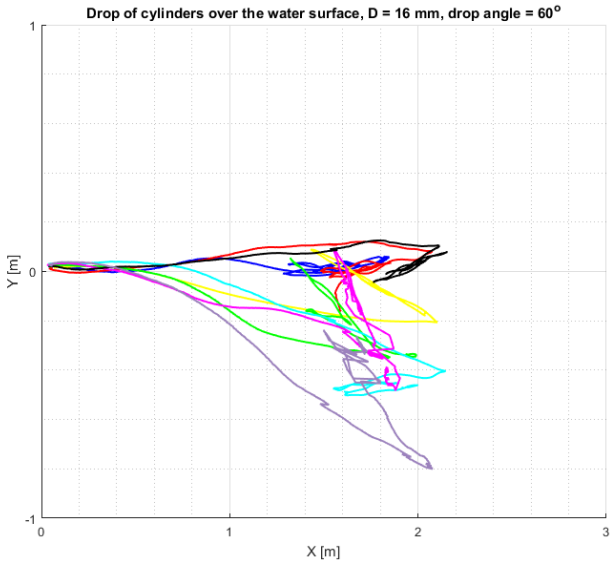

Figure 70: X-Y view: Drop of 16 mm diameter cylinders over the water surface at 60° initial angle. Each coloured line represents a drop.

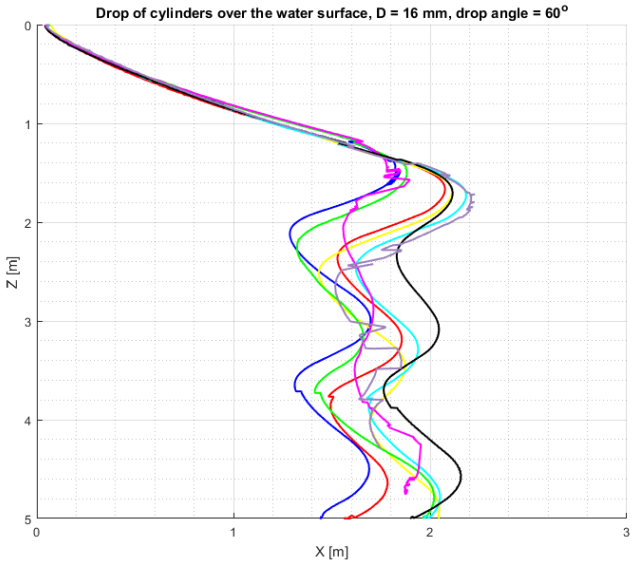

Figure 71: X-Z view: Drop of 16 mm diameter cylinders over the water surface at 60° initial angle. The X-coordinates are radial coordinates from the XY plane and each coloured line represents a drop.

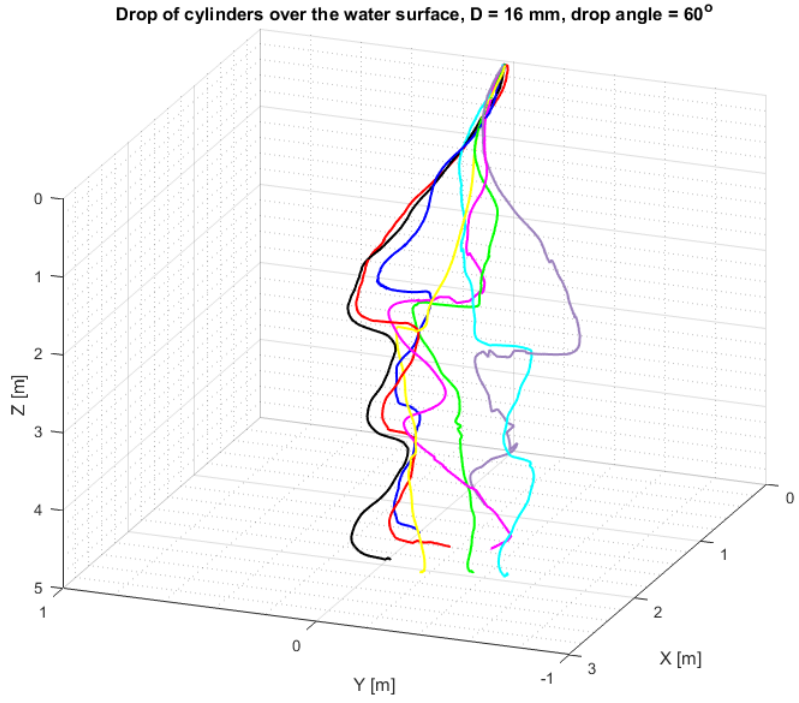

Figure 72: X-Y-Z view: Drop of 16 mm diameter cylinders over the water surface at 60° initial angle. Each coloured line represents a drop.

A.5.5 75° initial drop angle

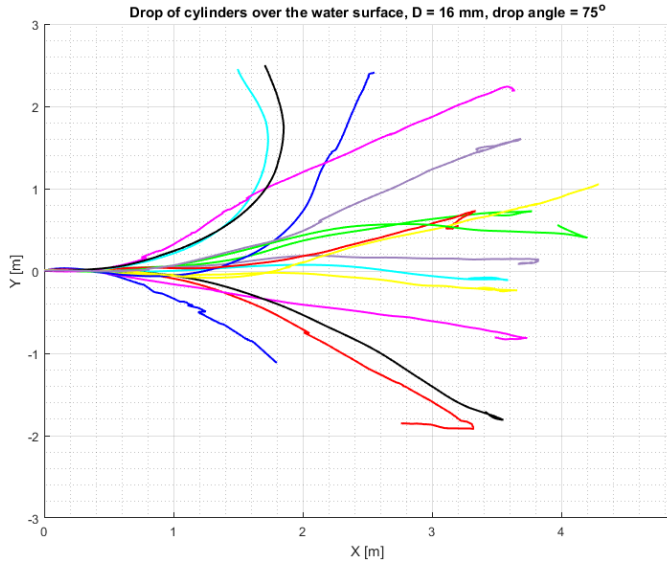

Figure 73: X-Y view: Drop of 16 mm diameter cylinders over the water surface at 75° initial angle. Each coloured line represents a drop.

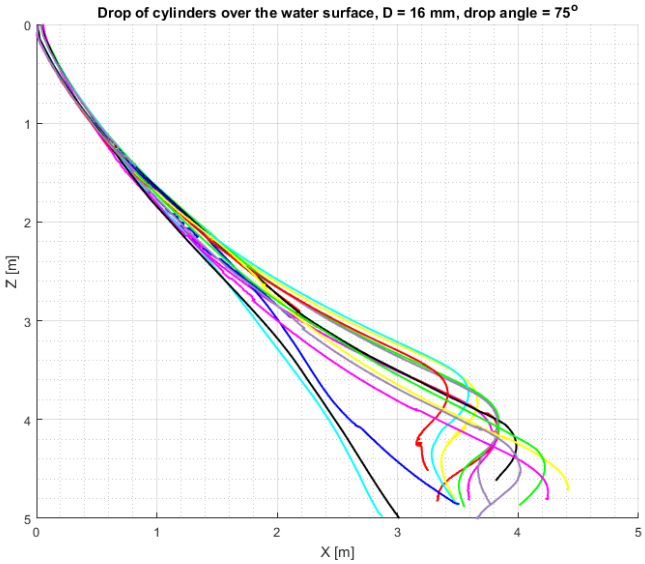

Figure 74: X-Z view: Drop of 16 mm diameter cylinders over the water surface at 75° initial angle. The X-coordinates are radial coordinates from the XY plane and each coloured line represents a drop.

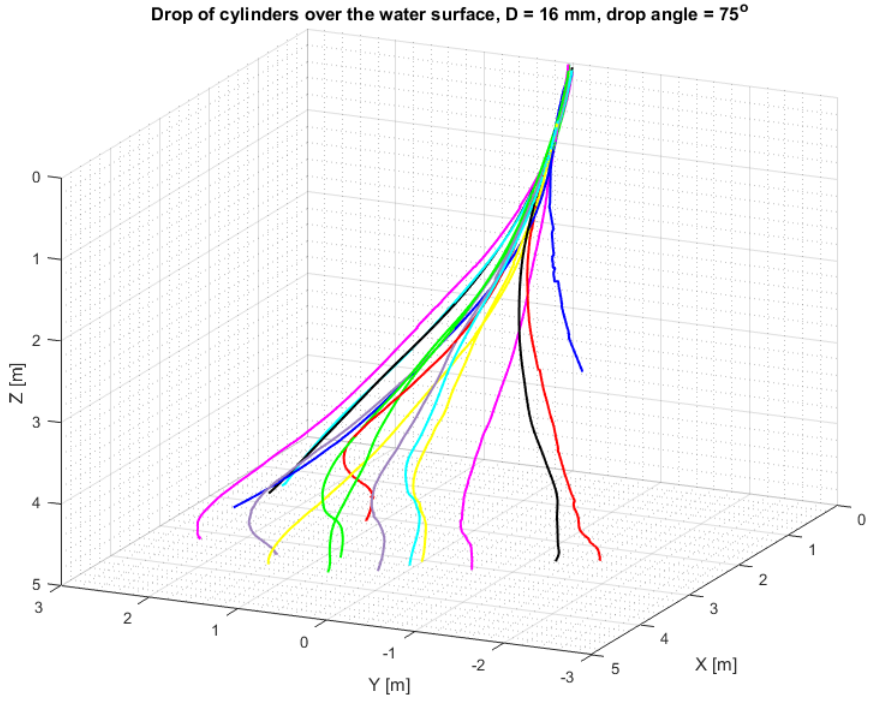

Figure 75: X-Y-Z view: Drop of 16 mm diameter cylinders over the water surface at 75° initial angle. Each coloured line represents a drop.

A.6 Drop of 19mm diameter cylinders over the water surface

A.6.1 15° initial drop angle

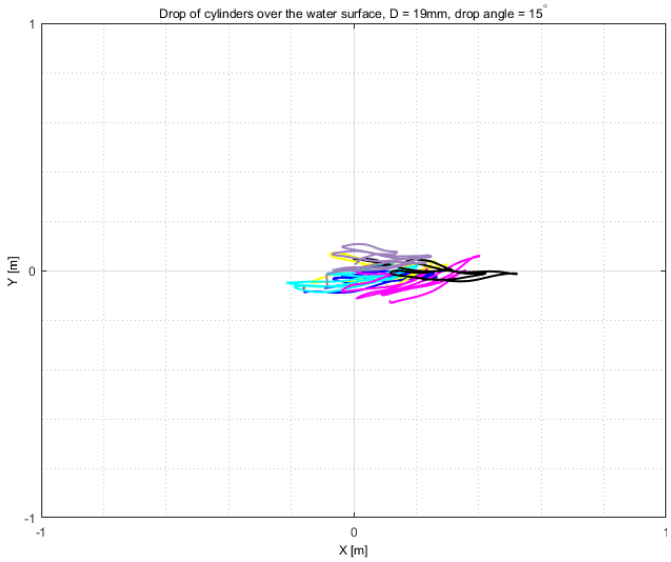

Figure 76: X-Y view: Drop of 19mm diameter cylinders over the water surface at 15° initial angle. Each coloured line represents a drop.

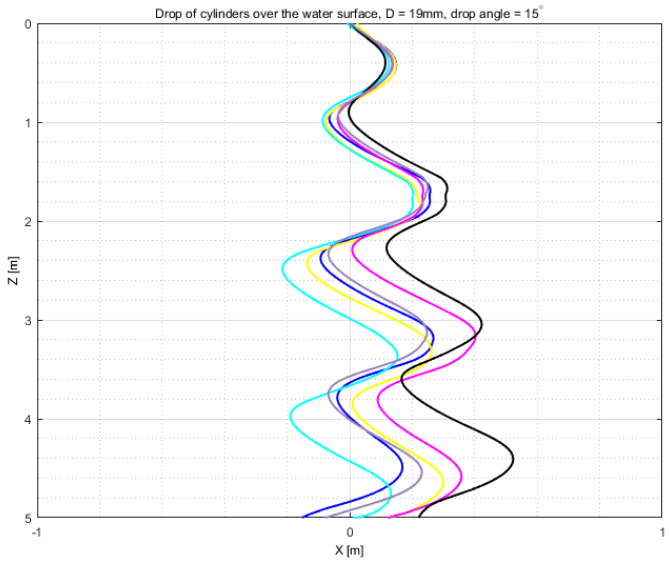

Figure 77: X-Z view: Drop of 19mm diameter cylinders over the water surface at 15° initial angle. The X-coordinates are radial coordinates from the XY plane and each coloured line represents a drop.

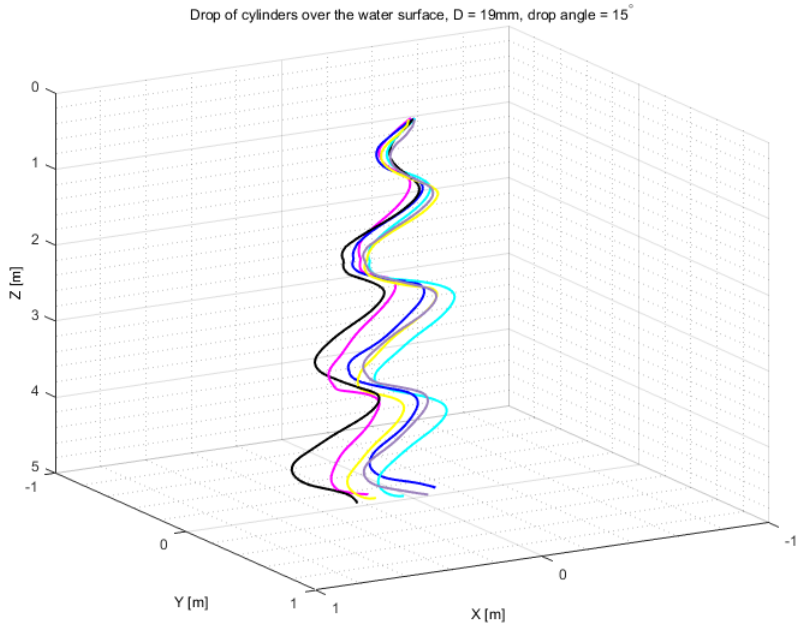

Figure 78: X-Y-Z view: Drop of 19mm diameter cylinders over the water surface at 15° initial angle. Each coloured line represents a drop.

A.6.2 30° initial drop angle

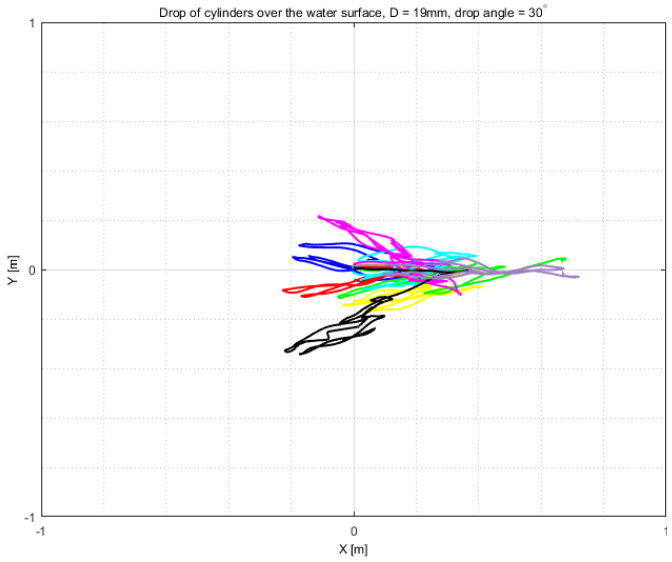

Figure 79: X-Y view: Drop of 19mm diameter cylinders over the water surface at 30° initial angle. Each coloured line represents a drop.

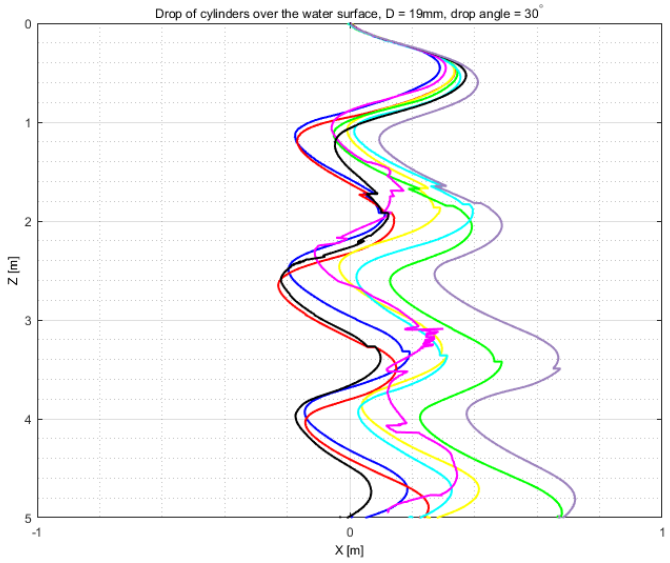

Figure 80: X-Z view: Drop of 19mm diameter cylinders over the water surface at 30° initial angle. The X-coordinates are radial coordinates from the XY plane and each coloured line represents a drop.

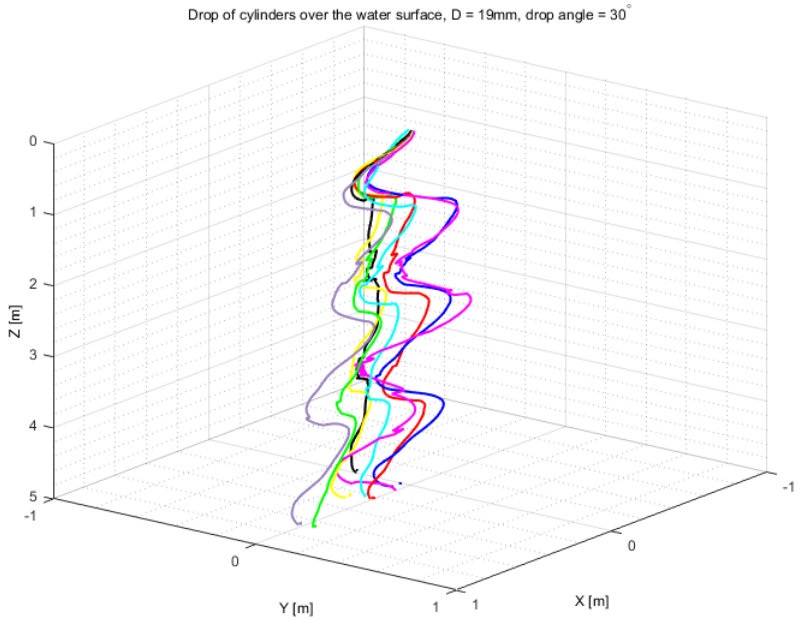

Figure 81: X-Y-Z view: Drop of 19mm diameter cylinders over the water surface at 30° initial angle. Each coloured line represents a drop.

A.6.3 45° initial drop angle

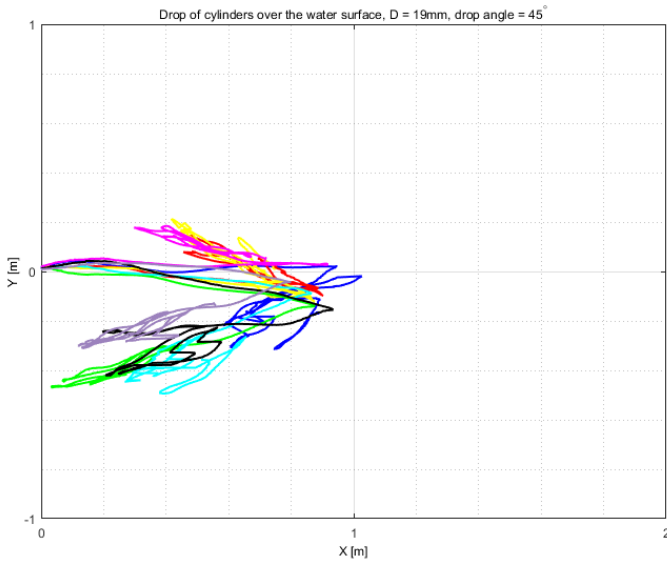

Figure 82: X-Y view: Drop of 19mm diameter cylinders over the water surface at 45° initial angle. Each coloured line represents a drop.

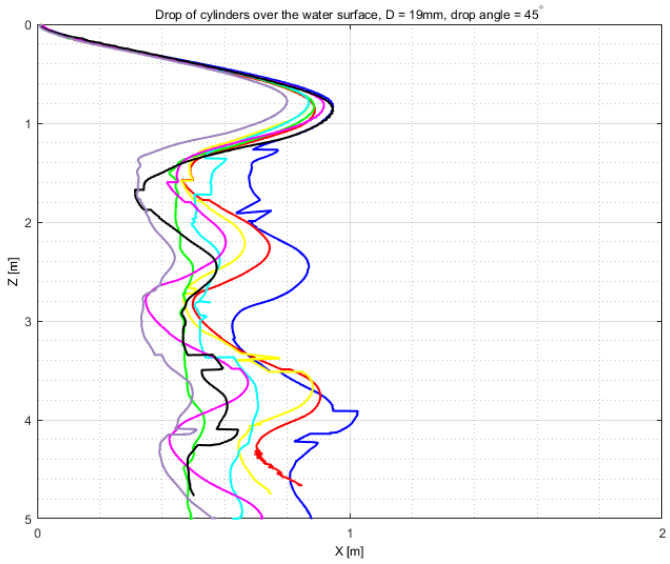

Figure 83: X-Z view: Drop of 19mm diameter cylinders over the water surface at 45° initial angle. The X-coordinates are radial coordinates from the XY plane and each coloured line represents a drop.

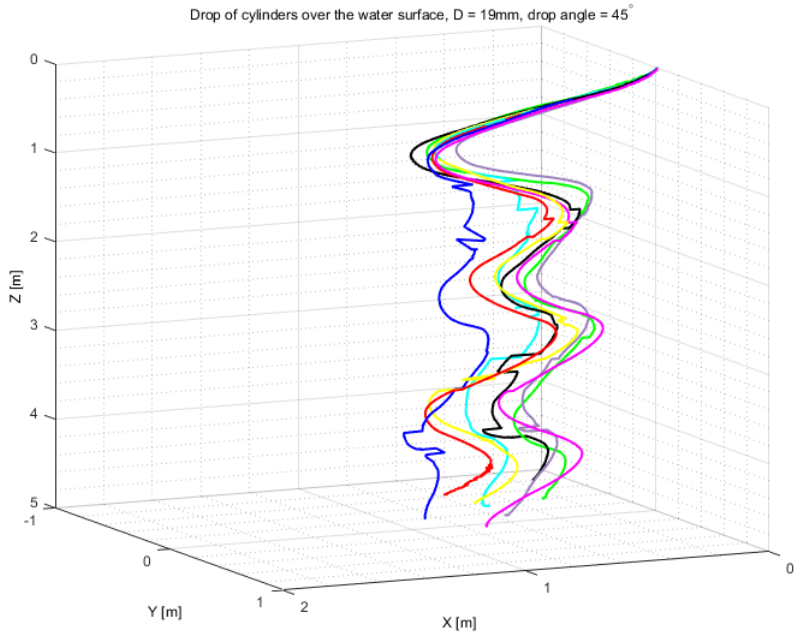

Figure 84: X-Y-Z view: Drop of 19mm diameter cylinders over the water surface at 45° initial angle. Each coloured line represents a drop.

A.6.4 60° initial drop angle

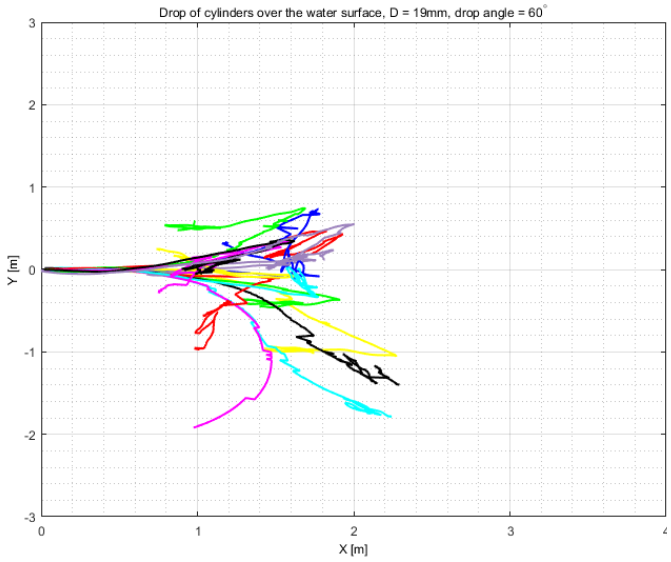

Figure 85: X-Y view: Drop of 19mm diameter cylinders over the water surface at 60° initial angle. Each coloured line represents a drop.

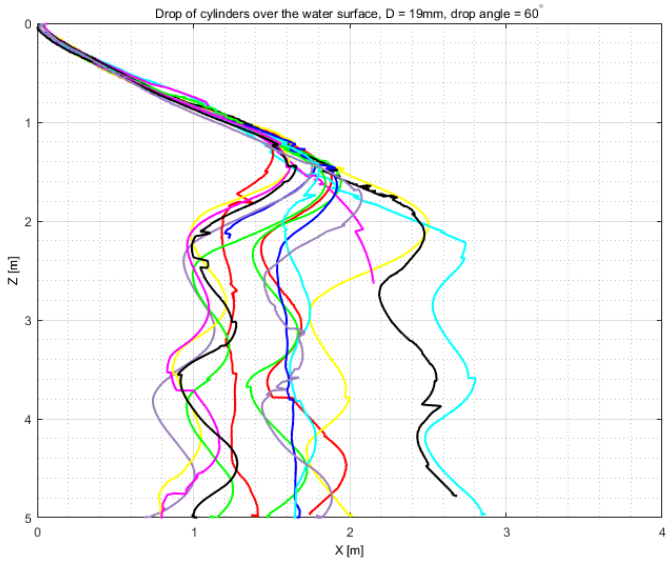

Figure 86: X-Z view: Drop of 19mm diameter cylinders over the water surface at 60° initial angle. The X-coordinates are radial coordinates from the XY plane and each coloured line represents a drop.

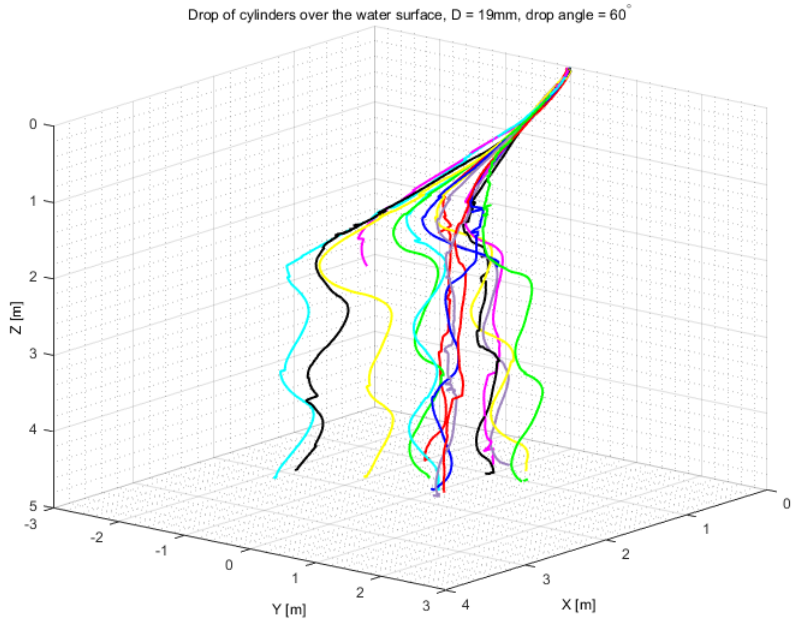

Figure 87: X-Y-Z view: Drop of 19mm diameter cylinders over the water surface at 60° initial angle. Each coloured line represents a drop.

A.6.5 75° initial drop angle

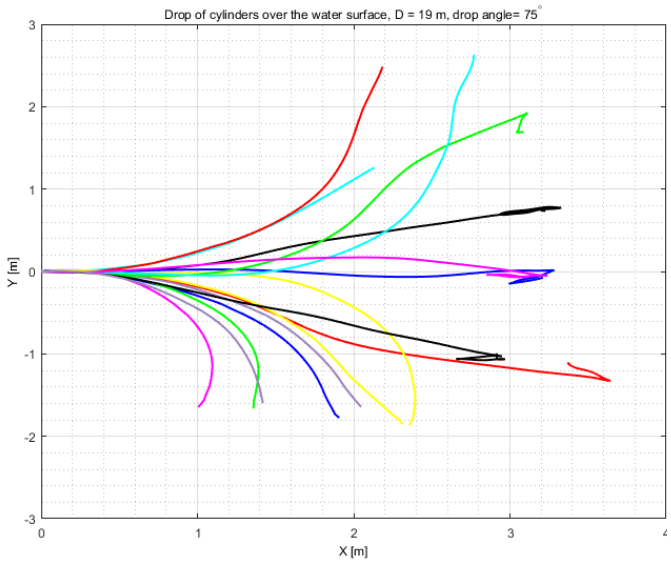

Figure 88: X-Y view: Drop of 19mm diameter cylinders over the water surface at 75° initial angle. Each coloured line represents a drop.

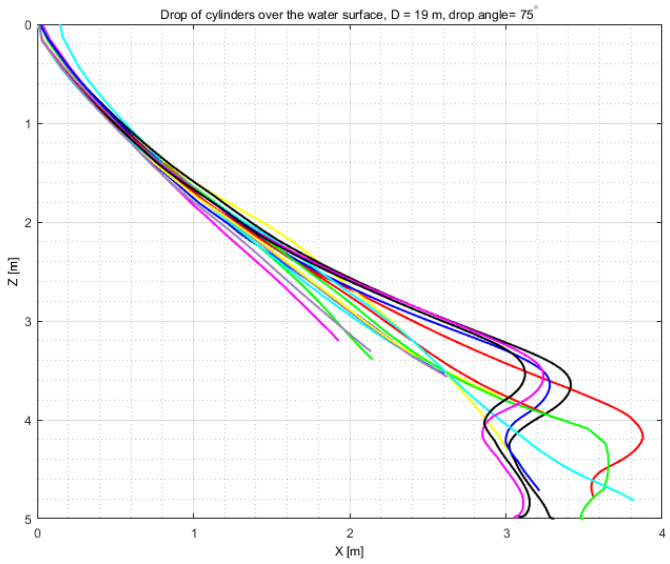

Figure 89: X-Z view: Drop of 19mm diameter cylinders over the water surface at 75° initial angle. The X-coordinates are radial coordinates from the XY plane and each coloured line represents a drop.

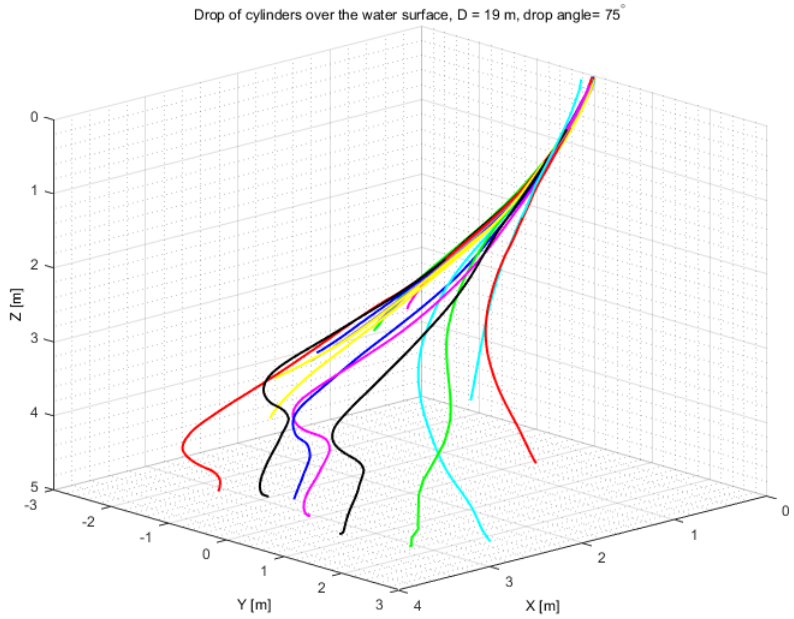

Figure 90: X-Y-Z view: Drop of 19mm diameter cylinders over the water surface at 75° initial angle. Each coloured line represents a drop.

A.7 Drop of open 10 mm cylinders under the water surface

A.7.1 15° initial drop angle

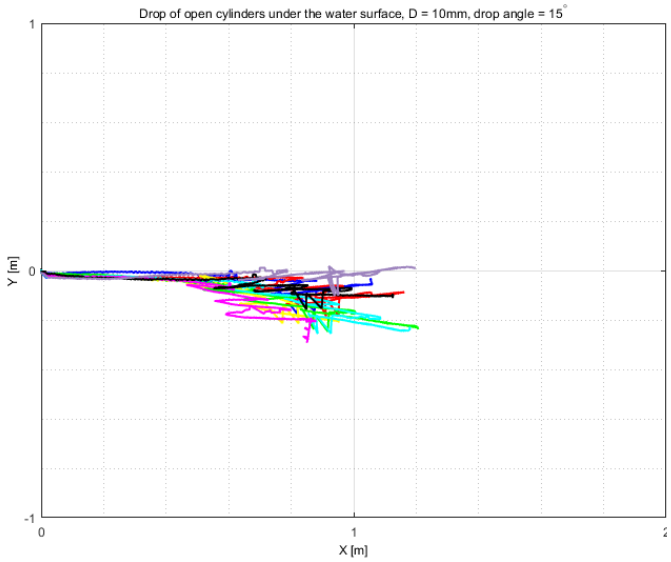

Figure 91: X-Y view: Drop of open 10mm diameter cylinders under the water surface at 15° initial drop angle. Each coloured line represents a drop.

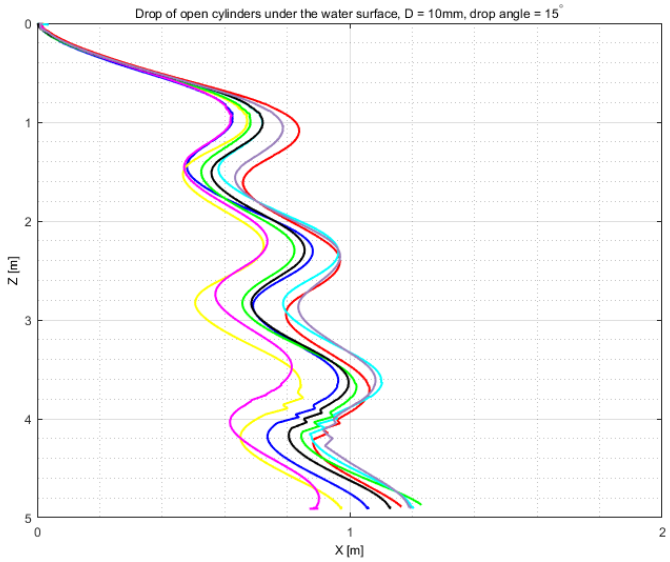

Figure 92: X-Z view: Drop of open 10mm diameter cylinders under the water surface at 15° initial drop angle. The X-coordinates are radial coordinates from the XY plane and each coloured line represents a drop.

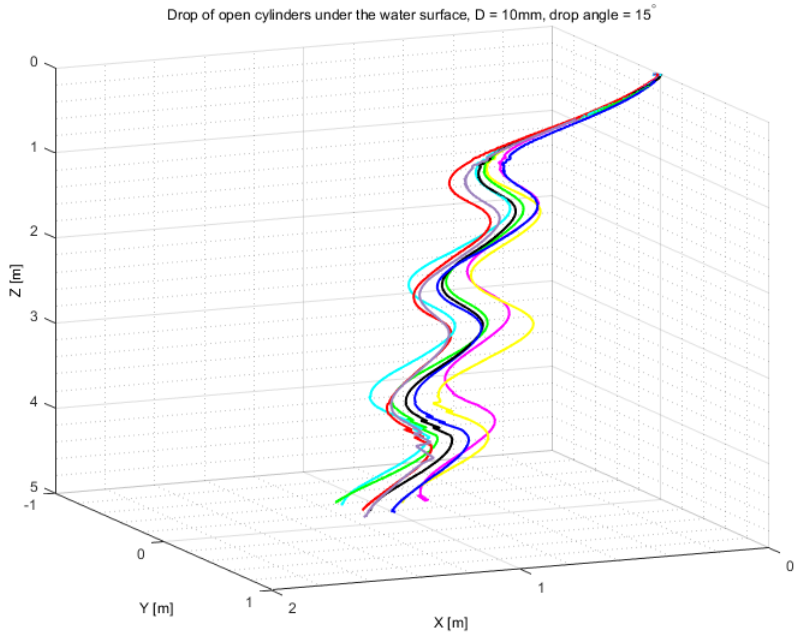

Figure 93: X-Y-Z view: Drop of open 10mm diameter cylinders under the water surface at 15° initial drop angle. Each coloured line represents a drop.

A.7.2 30° initial drop angle

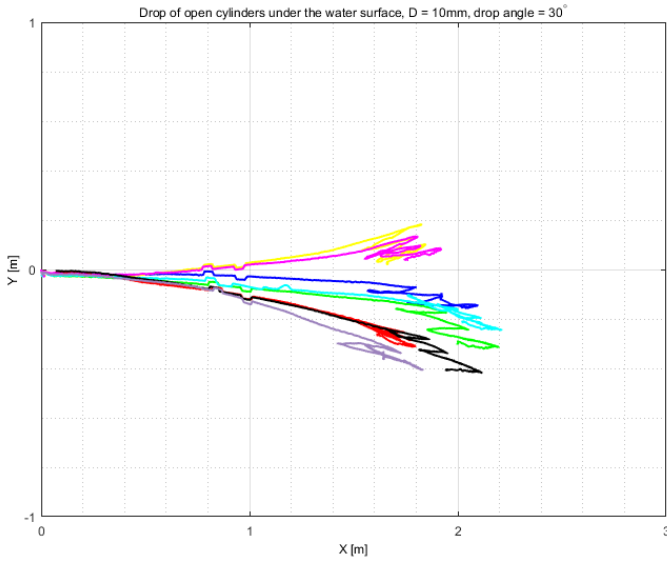

Figure 94: X-Y view: Drop of open 10mm diameter cylinders under the water surface at 30° initial drop angle. Each coloured line represents a drop.

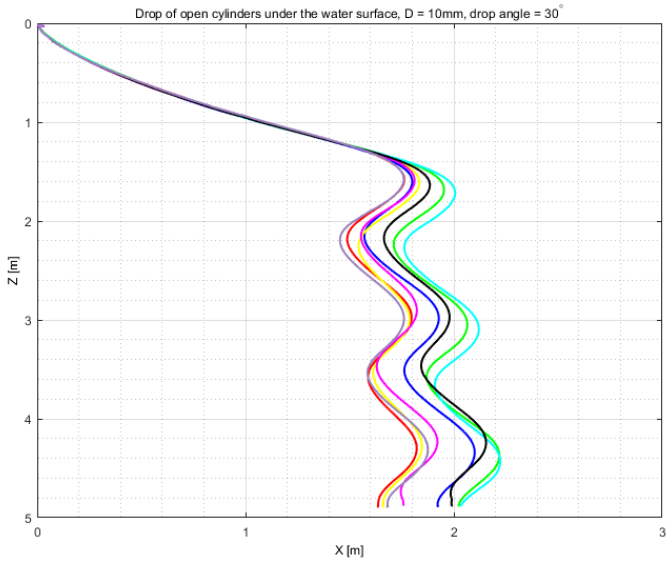

Figure 95: X-Z view: Drop of open 10mm diameter cylinders under the water surface at 30° initial drop angle. The X-coordinates are radial coordinates from the XY plane and each coloured line represents a drop.

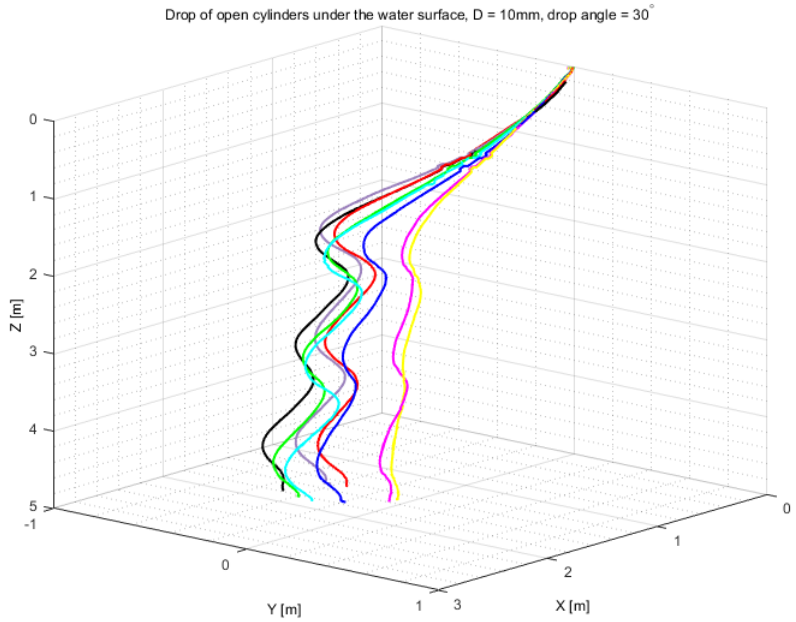

Figure 96: X-Y-Z view: Drop of open 10mm diameter cylinders under the water surface at 30° initial drop angle. Each coloured line represents a drop.

A.7.3 45° initial drop angle

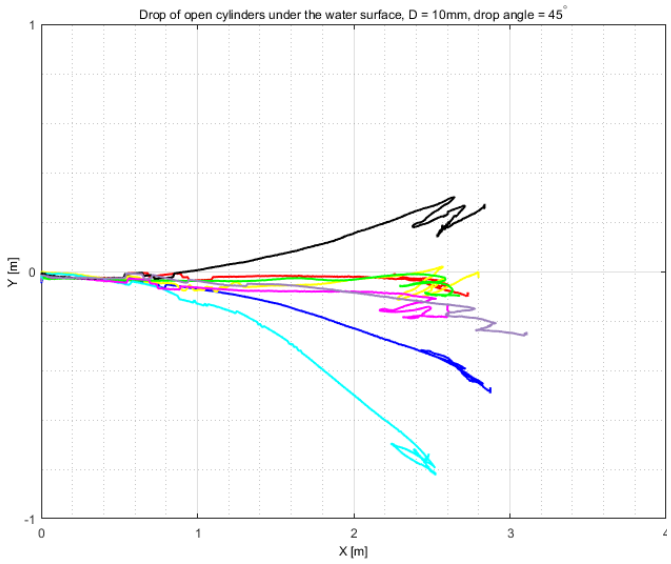

Figure 97: X-Y view: Drop of open 10mm diameter cylinders under the water surface at 45° initial drop angle. Each coloured line represents a drop.

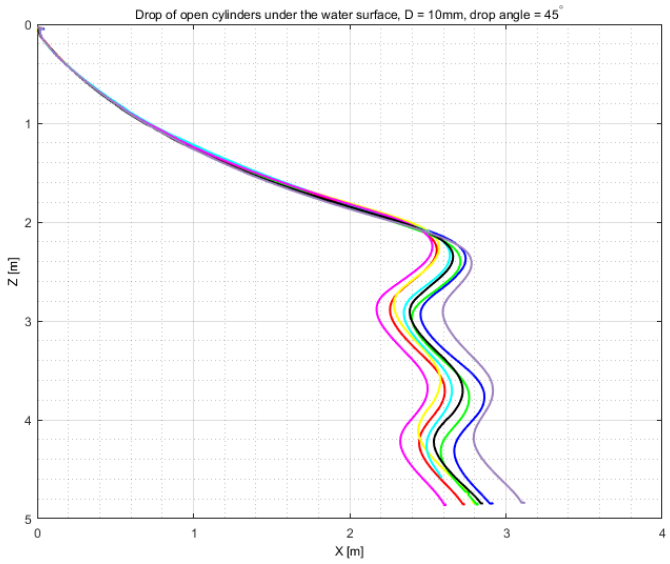

Figure 98: X-Z view: Drop of open 10mm diameter cylinders under the water surface at 45° initial drop angle. The X-coordinates are radial coordinates from the XY plane and each coloured line represents a drop.

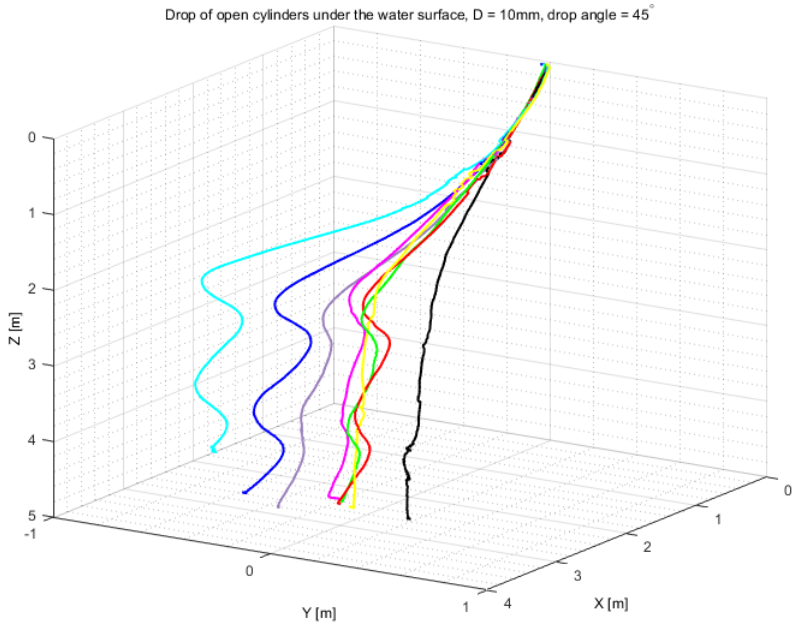

Figure 99: X-Y-Z view: Drop of open 10mm diameter cylinders under the water surface at 45° initial drop angle. Each coloured line represents a drop.

A.7.4 60° initial drop angle

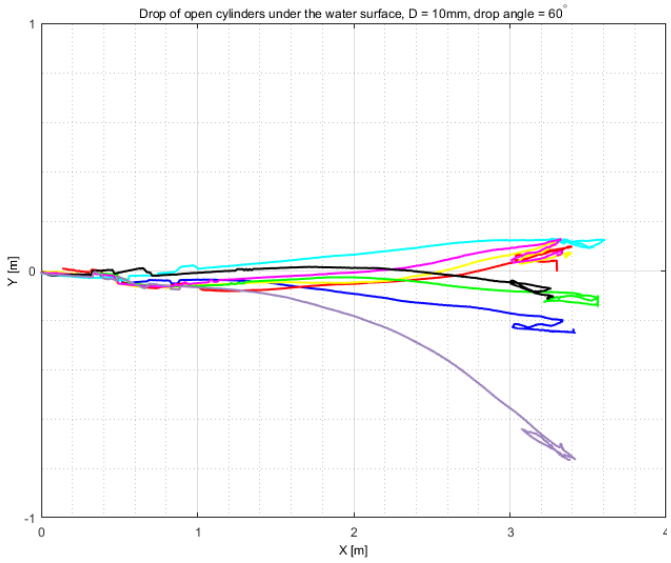

Figure 100: X-Y view: Drop of open 10mm diameter cylinders under the water surface at 60° initial drop angle. Each coloured line represents a drop.

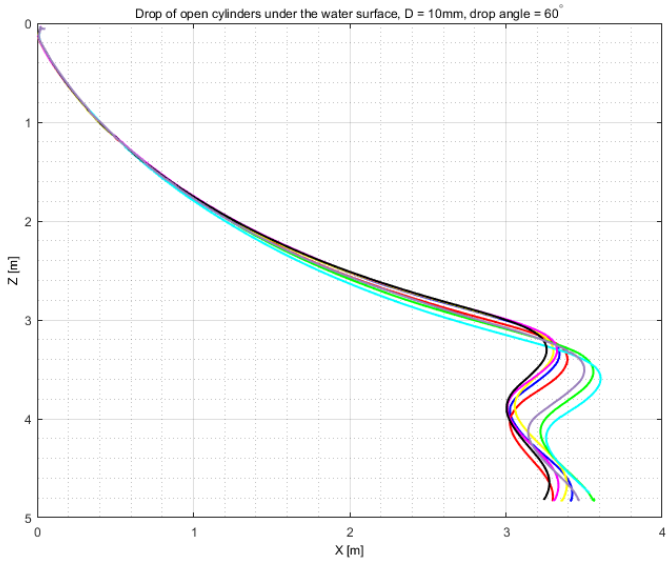

Figure 101: X-Z view: Drop of open 10mm diameter cylinders under the water surface at 60° initial drop angle. The X-coordinates are radial coordinates from the XY plane and each coloured line represents a drop.

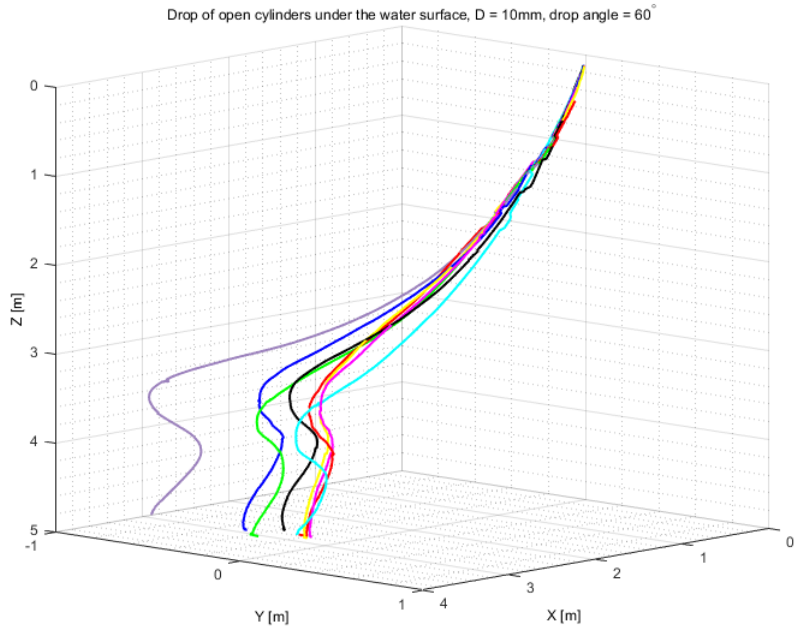

Figure 102: X-Y-Z view: Drop of open 10mm diameter cylinders under the water surface at 60° initial drop angle. Each coloured line represents a drop.

A.7.5 75° initial drop angle

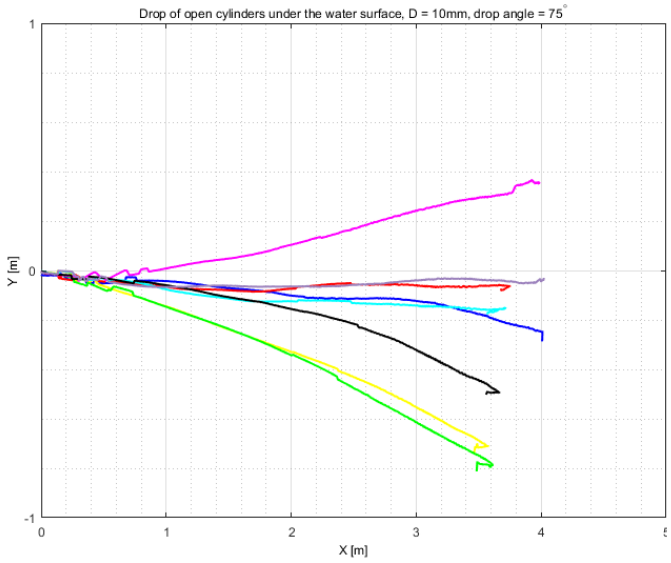

Figure 103: X-Y view: Drop of open 10mm diameter cylinders under the water surface at 75° initial drop angle. Each coloured line represents a drop.

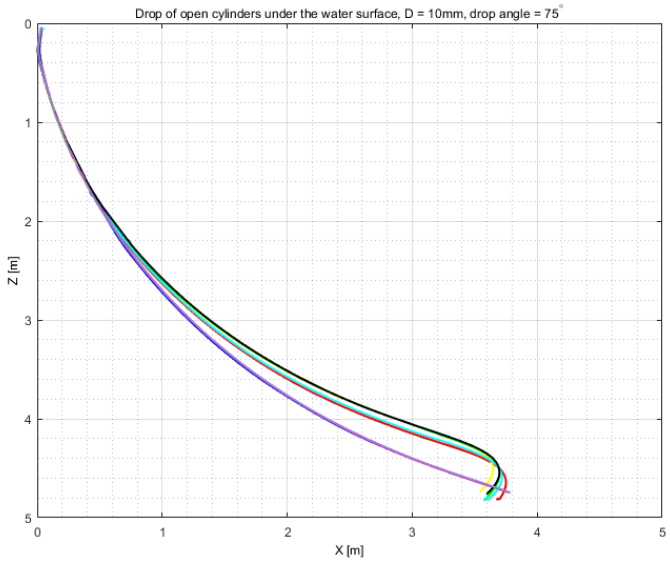

Figure 104: X-Z view: Drop of open 10mm diameter cylinders under the water surface at 75° initial drop angle. The X-coordinates are radial coordinates from the XY plane and each coloured line represents a drop.

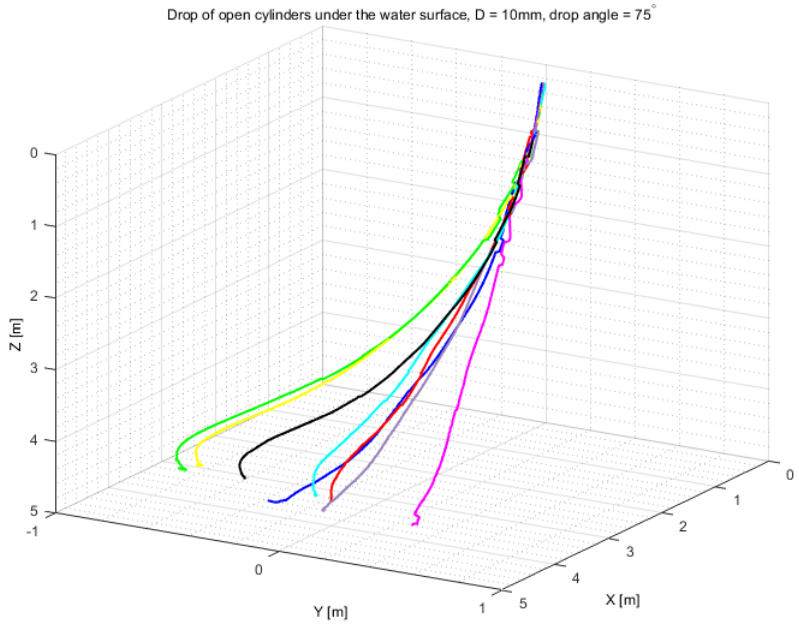

Figure 105: X-Y-Z view: Drop of open 10mm diameter cylinders under the water surface at 75° initial drop angle. Each coloured line represents a drop.

A.8 Drop of open 19 mm cylinders under the water surface

A.8.1 30° initial drop angle

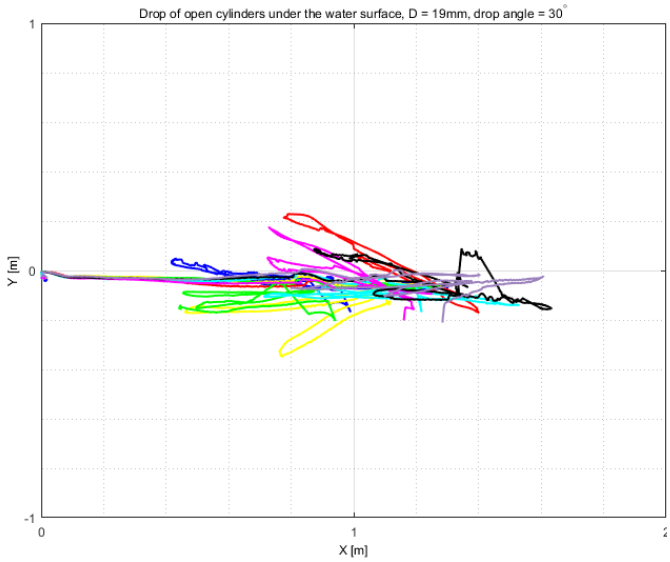

Figure 106: X-Y view: Drop of open 19 mm diameter cylinders under the water surface at 30° initial drop angle. Each coloured line represents a drop.

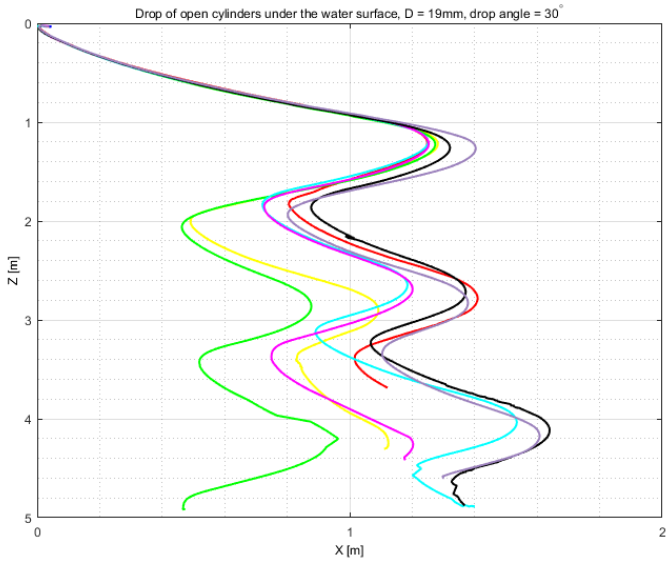

Figure 107: X-Z view: Drop of open 19 mm diameter cylinders under the water surface at 30° initial drop angle. The X-coordinates are radial coordinates from the XY plane and each coloured line represents a drop.

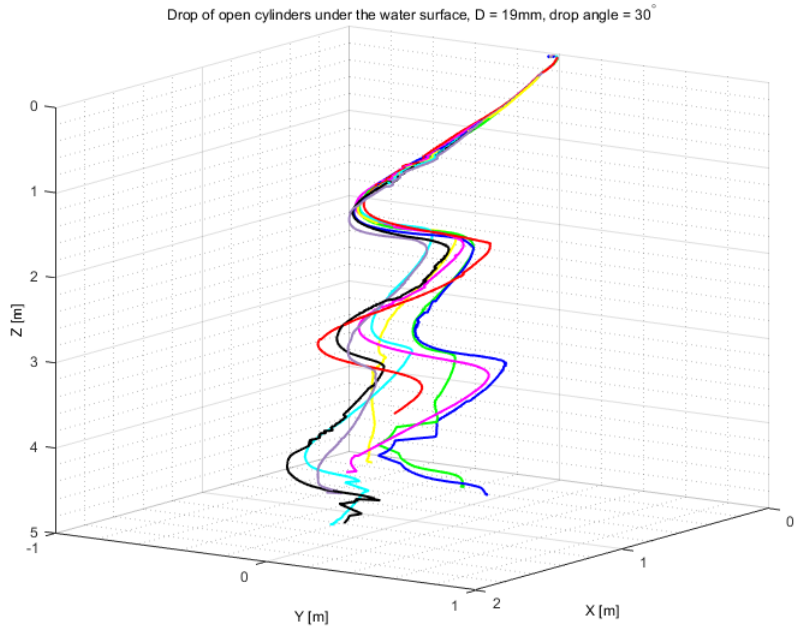

Figure 108: X-Y-Z view: Drop of open 19mm diameter cylinders under the water surface at 30° initial drop angle. Each coloured line represents a drop.

A.8.2 45° initial drop angle

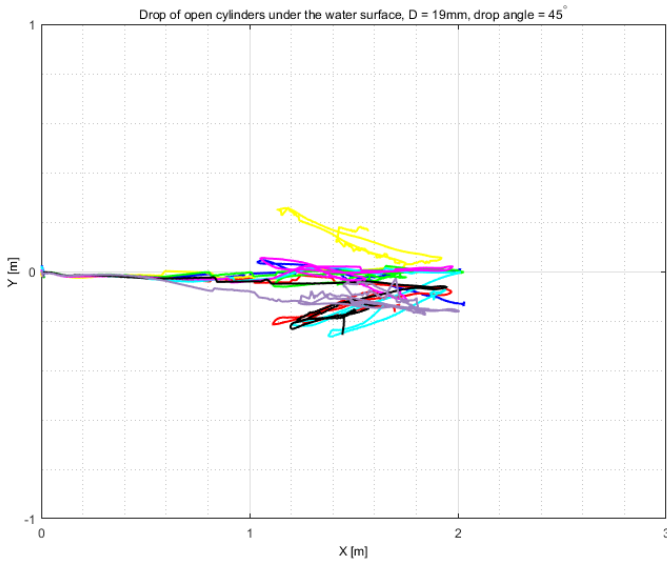

Figure 109: X-Y view: Drop of open 19 mm diameter cylinders under the water surface at 45° initial drop angle. Each coloured line represents a drop.

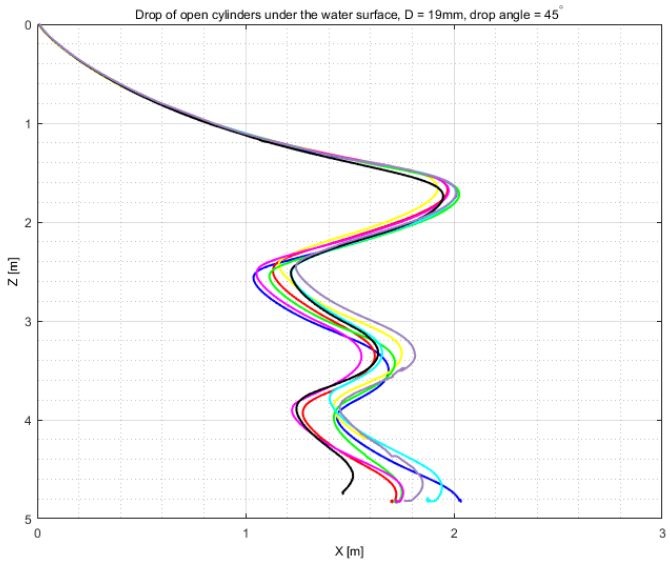

Figure 110: X-Z view: Drop of open 19 mm diameter cylinders under the water surface at 45° initial drop angle. The X-coordinates are radial coordinates from the XY plane and each coloured line represents a drop.

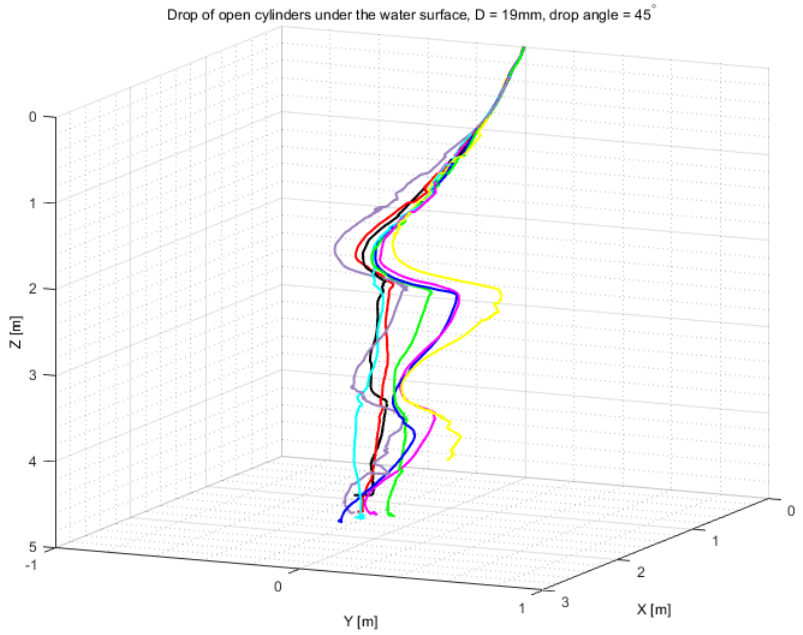

Figure 111: X-Y-Z view: Drop of open 19mm diameter cylinders under the water surface at 45° initial drop angle. Each coloured line represents a drop.

A.8.3 60° initial drop angle

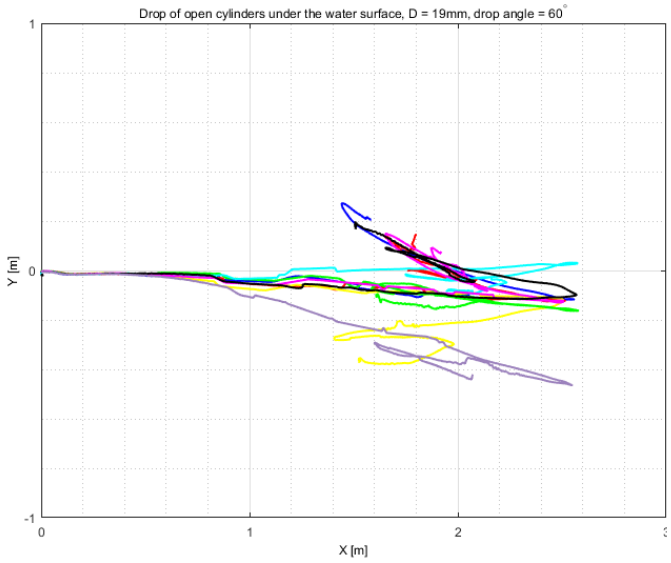

Figure 112: X-Y view: Drop of open 19 mm diameter cylinders under the water surface at 60° initial drop angle. Each coloured line represents a drop.

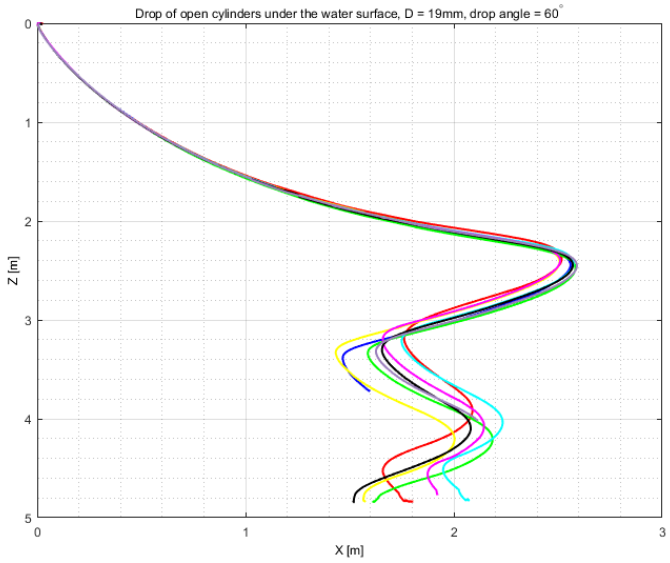

Figure 113: X-Z view: Drop of open 19 mm diameter cylinders under the water surface at 60° initial drop angle. The X-coordinates are radial coordinates from the XY plane and each coloured line represents a drop.

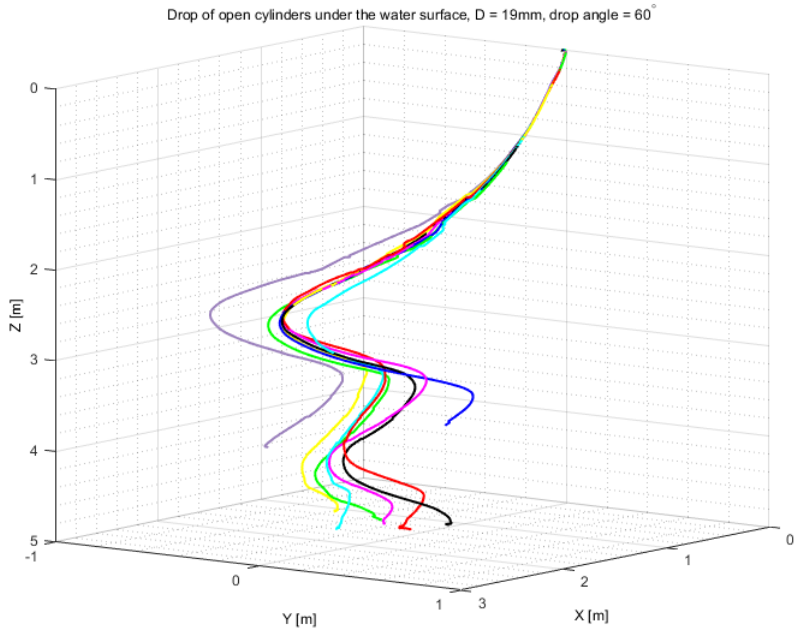

Figure 114: X-Y-Z view: Drop of open 19mm diameter cylinders under the water surface at 60° initial drop angle. Each coloured line represents a drop.

A.8.4 75° initial drop angle

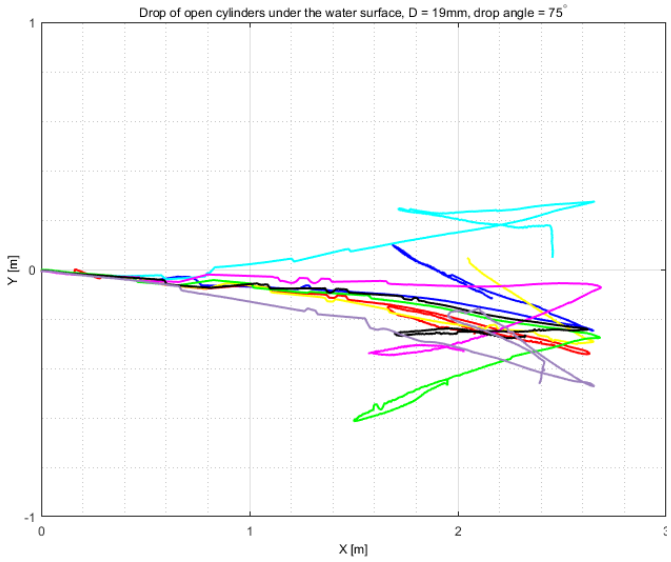

Figure 115: X-Y view: Drop of open 19 mm diameter cylinders under the water surface at 75° initial drop angle. Each coloured line represents a drop.

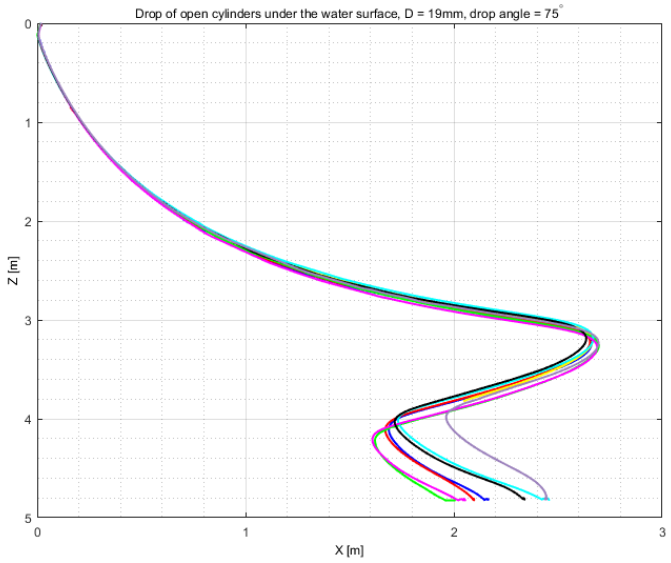

Figure 116: X-Z view: Drop of open 19 mm diameter cylinders under the water surface at 75° initial drop angle. The X-coordinates are radial coordinates from the XY plane and each coloured line represents a drop.

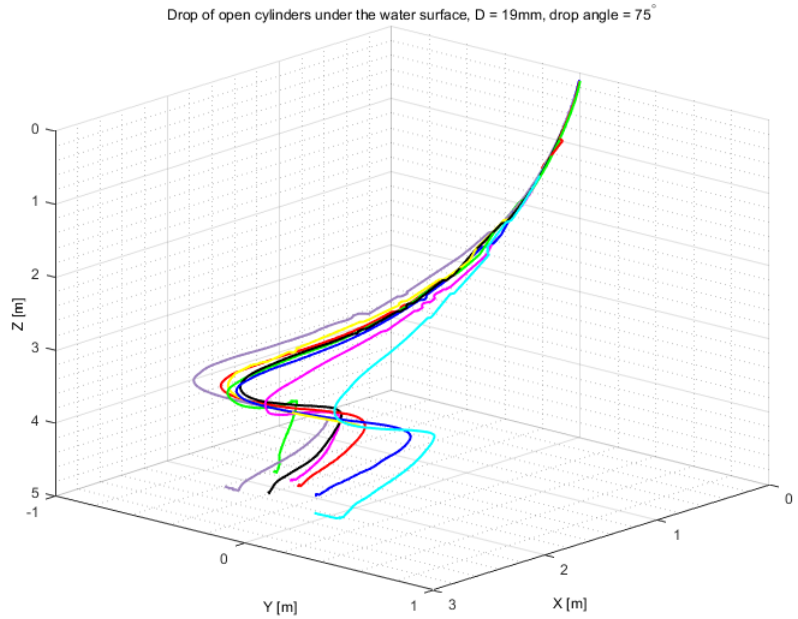

Figure 117: X-Y-Z view: Drop of open 19mm diameter cylinders under the water surface at 75° initial drop angle. Each coloured line represents a drop.

A.9 Drop of 10mm diameter cylinders under the water surface with COG displaced with 1.4cm (COG over COV)

A.9.1 15° initial drop angle

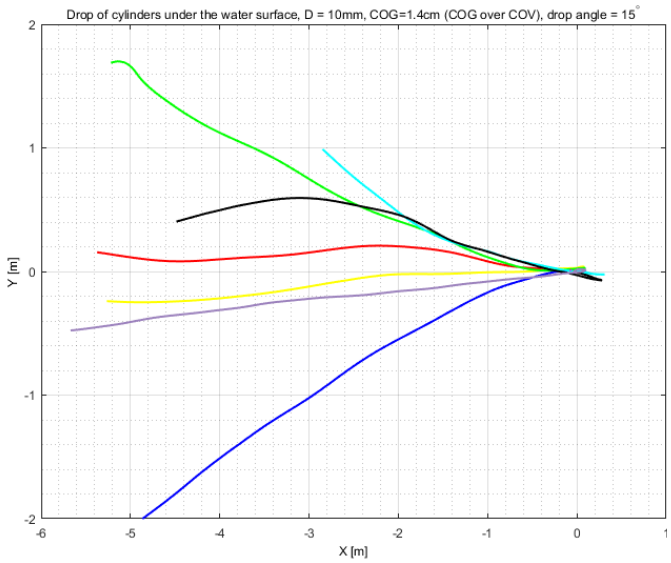

Figure 118: X-Y view: Drop of 10mm diameter cylinders under the water surface at 15° initial angle with COG displaced 1.4cm (Centre of Gravity (COG) over Centre of Volume (COV)). Each coloured line represents a drop. NB! The fore end of the cylinder has been tracked for this drop.

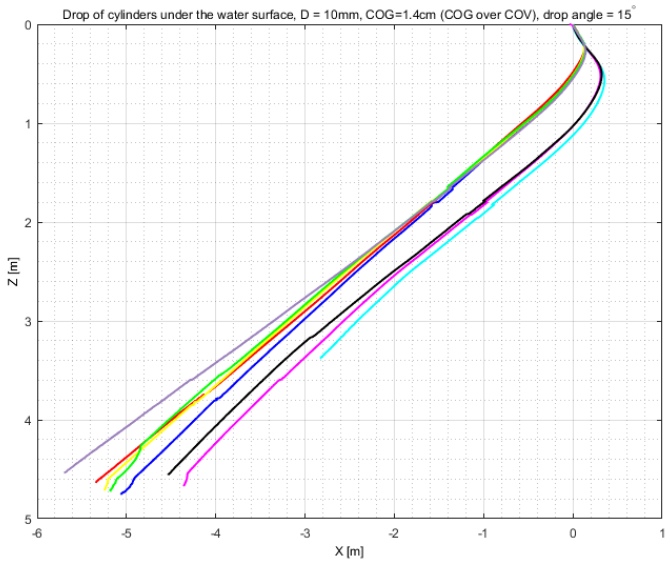

Figure 119: X-Z view: Drop of 10mm diameter cylinders under the water surface at 15° initial angle with COG displaced 1.4cm (Centre of Gravity (COG) over Centre of Volume (COV)). The X-coordinates are radial coordinates from the XY plane and each coloured line represents a drop. NB! The fore end of the cylinder has been tracked for this drop.

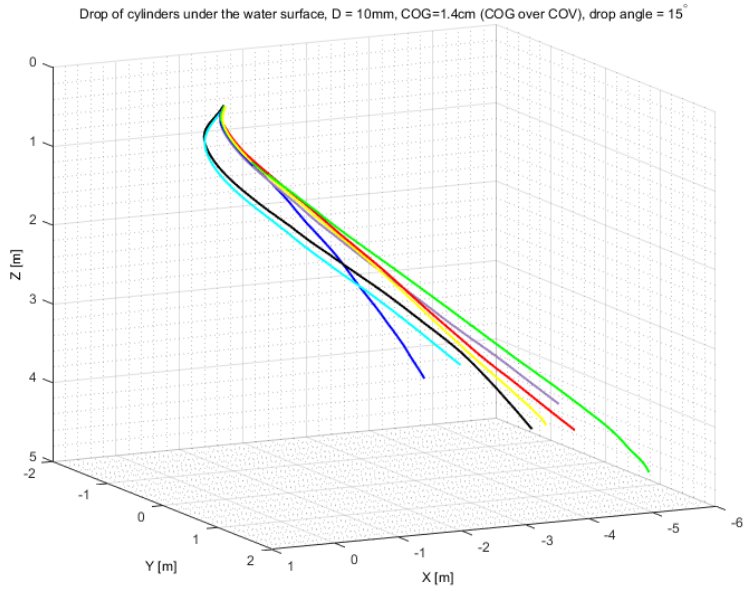

Figure 120: X-Y-Z view: Drop of 10mm diameter cylinders under the water surface at 15° initial angle with COG displaced 1.4cm (Centre of Gravity (COG) over Centre of Volume (COV)). Each coloured line represents a drop. NB! The fore end of the cylinder has been tracked for this drop.

A.9.2 30° initial drop angle

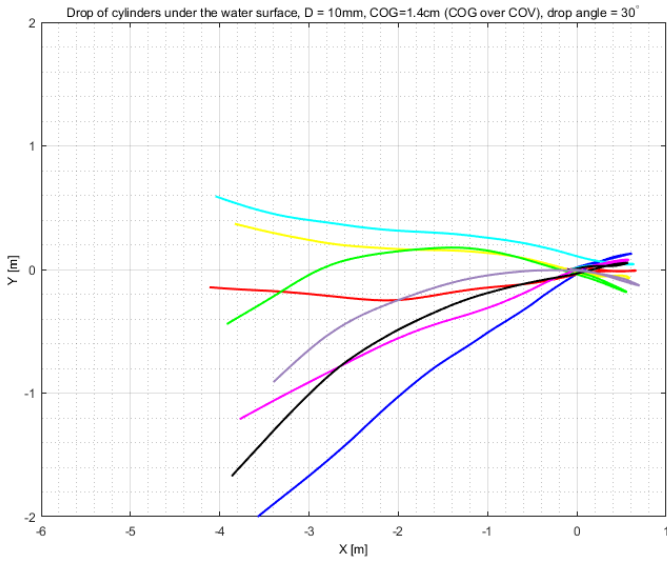

Figure 121: X-Y view: Drop of 10mm diameter cylinders under the water surface at 30° initial angle with COG displaced 1.4cm (Centre of Gravity (COG) over Centre of Volume (COV)). Each coloured line represents a drop. NB! The fore end of the cylinder has been tracked for this drop.

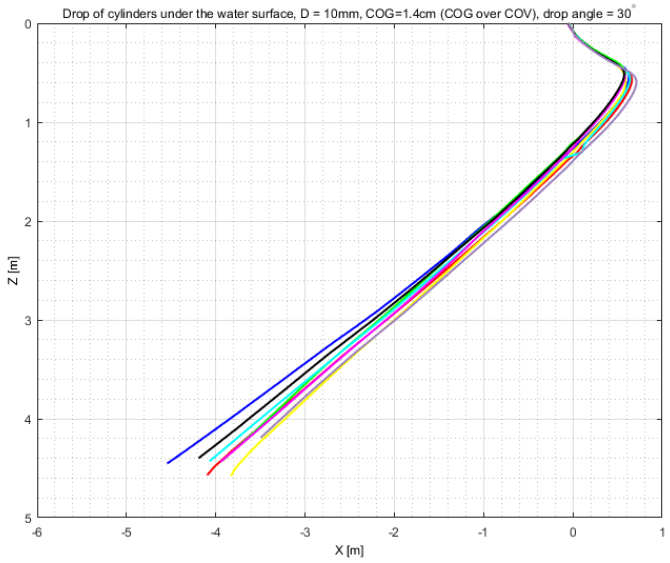

Figure 122: X-Z view: Drop of 10mm diameter cylinders under the water surface at 30° initial angle with COG displaced 1.4cm (Centre of Gravity (COG) over Centre of Volume (COV)). The X-coordinates are radial coordinates from the XY plane and each coloured line represents a drop. NB! The fore end of the cylinder has been tracked for this drop.

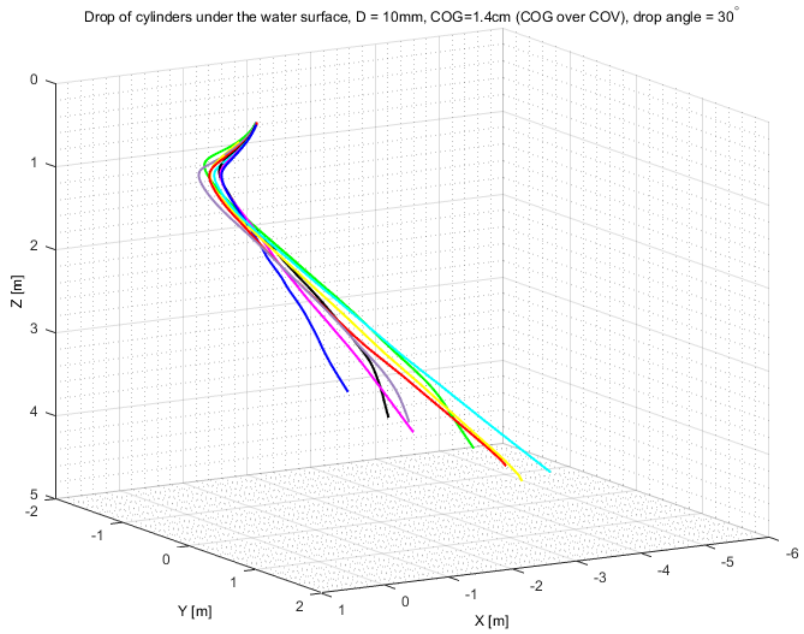

Figure 123: X-Y-Z view: Drop of 10mm diameter cylinders under the water surface at 30° initial angle with COG displaced 1.4cm (Centre of Gravity (COG) over Centre of Volume (COV)). Each coloured line represents a drop. NB! The fore end of the cylinder has been tracked for this drop.

A.9.3 45° initial drop angle

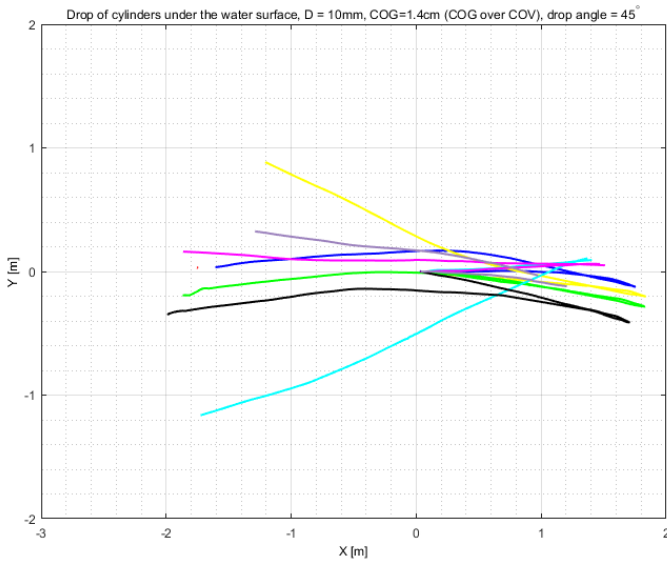

Figure 124: X-Y view: Drop of 10mm diameter cylinders under the water surface at 45° initial angle with COG displaced 1.4cm (Centre of Gravity (COG) over Centre of Volume (COV)). Each coloured line represents a drop. NB! The fore end of the cylinder has been tracked for this drop.

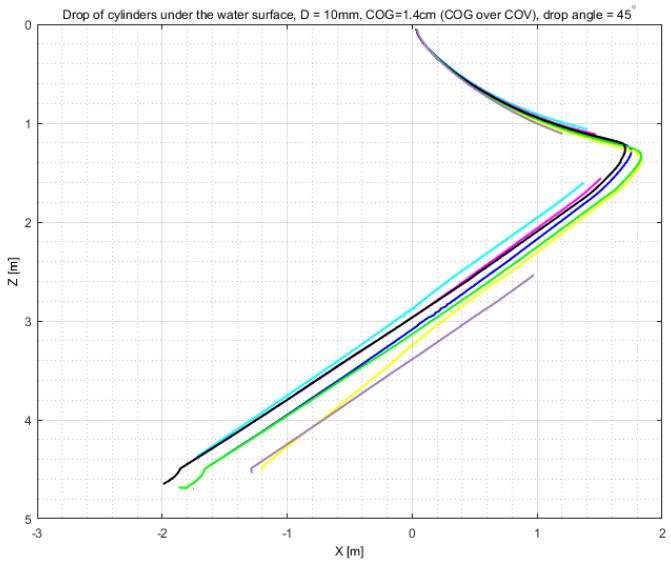

Figure 125: X-Z view: Drop of 10mm diameter cylinders under the water surface at 45° initial angle with COG displaced 1.4cm (Centre of Gravity (COG) over Centre of Volume (COV)). The X-coordinates are radial coordinates from the XY plane and each coloured line represents a drop. NB! The fore end of the cylinder has been tracked for this drop.

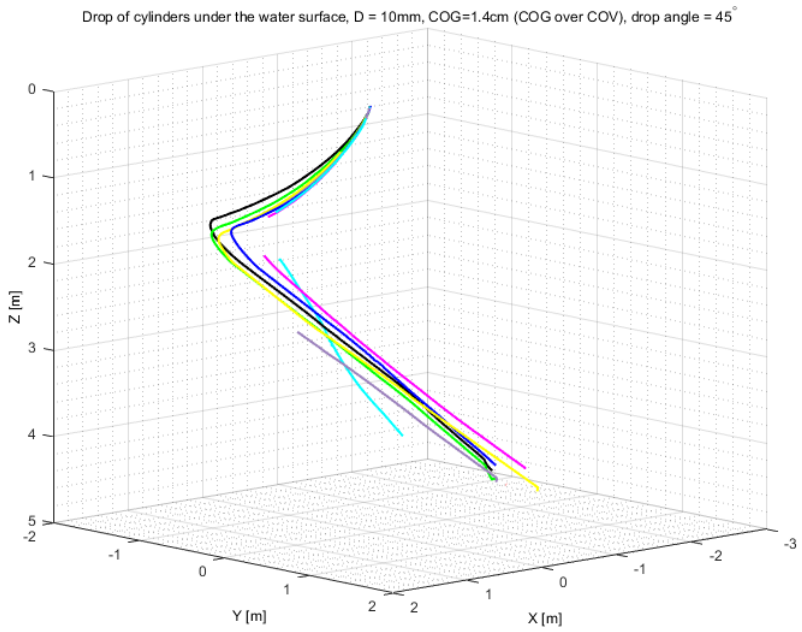

Figure 126: X-Y-Z view: Drop of 10mm diameter cylinders under the water surface at 45° initial angle with COG displaced 1.4cm (Centre of Gravity (COG) over Centre of Volume (COV)). Each coloured line represents a drop. NB! The fore end of the cylinder has been tracked for this drop.

A.9.4 60° initial drop angle

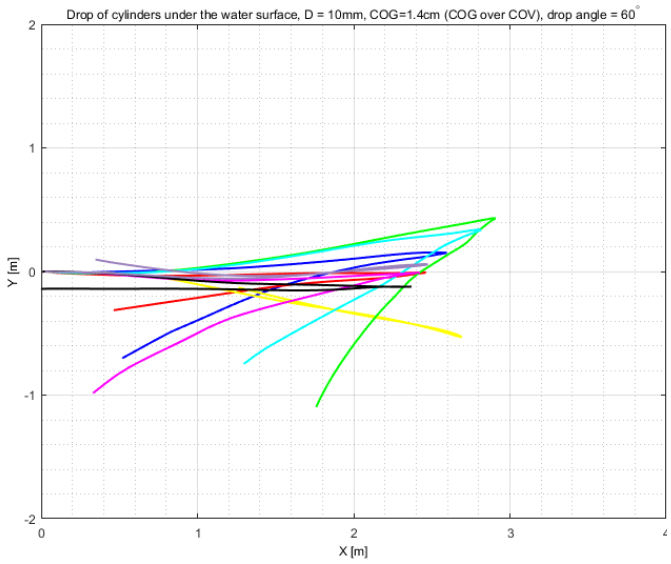

Figure 127: X-Y view: Drop of 10mm diameter cylinders under the water surface at 60° initial angle with COG displaced 1.4cm (Centre of Gravity (COG) over Centre of Volume (COV)). Each coloured line represents a drop.

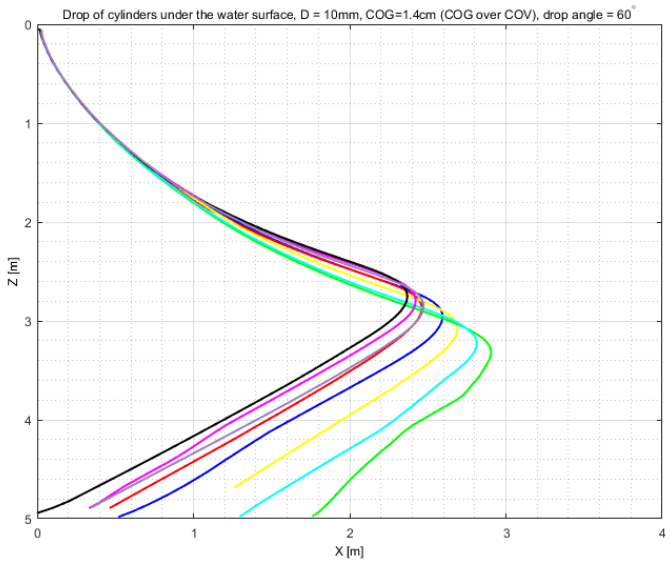

Figure 128: X-Z view: Drop of 10mm diameter cylinders under the water surface at 60° initial angle with COG displaced 1.4cm (Centre of Gravity (COG) over Centre of Volume (COV)). The X-coordinates are radial coordinates from the XY plane and each coloured line represents a drop.

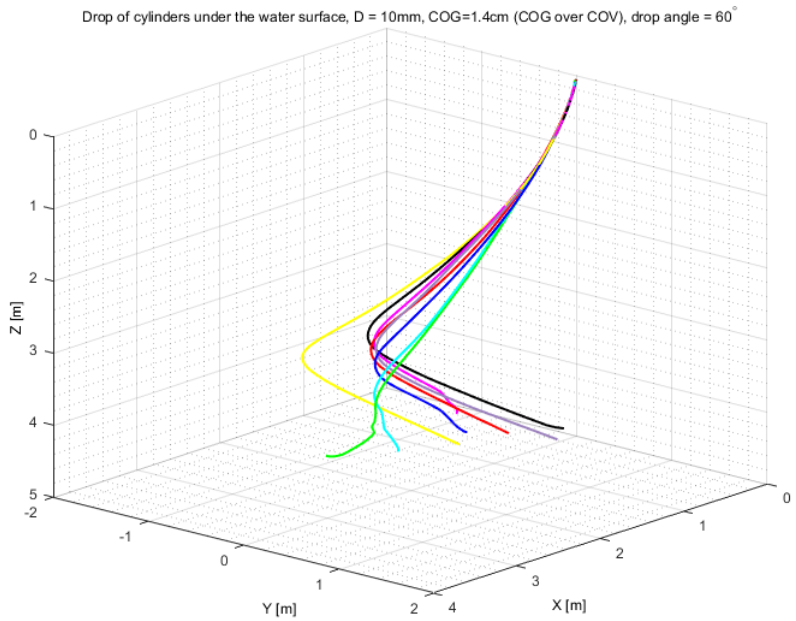

Figure 129: X-Y-Z view: Drop of 10mm diameter cylinders under the water surface at 60° initial angle with COG displaced 1.4cm (Centre of Gravity (COG) over Centre of Volume (COV)). Each coloured line represents a drop.

A.9.5 75° initial drop angle

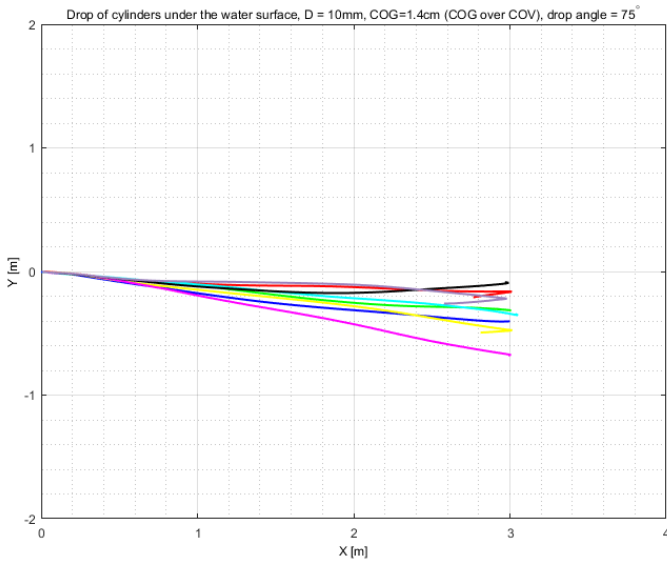

Figure 130: X-Y view: Drop of 10mm diameter cylinders under the water surface at 75° initial angle with COG displaced 1.4cm (Centre of Gravity (COG) over Centre of Volume (COV)). Each coloured line represents a drop.

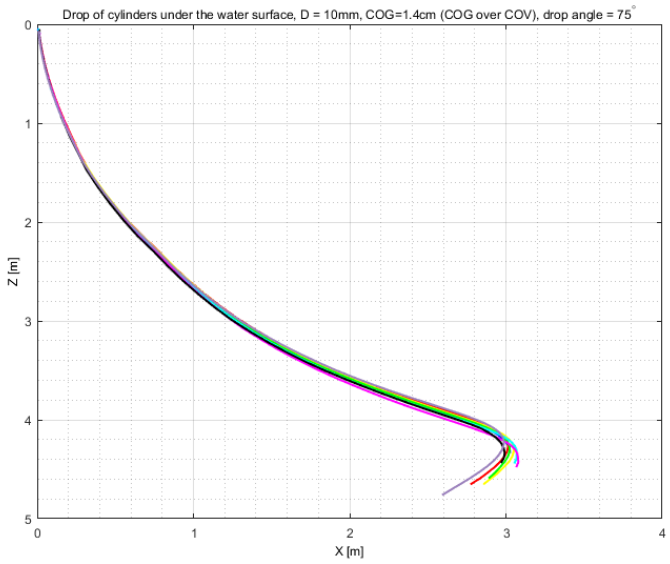

Figure 131: X-Z view: Drop of 10mm diameter cylinders under the water surface at 75° initial angle with COG displaced 1.4cm (Centre of Gravity (COG) over Centre of Volume (COV)). The X-coordinates are radial coordinates from the XY plane and each coloured line represents a drop.

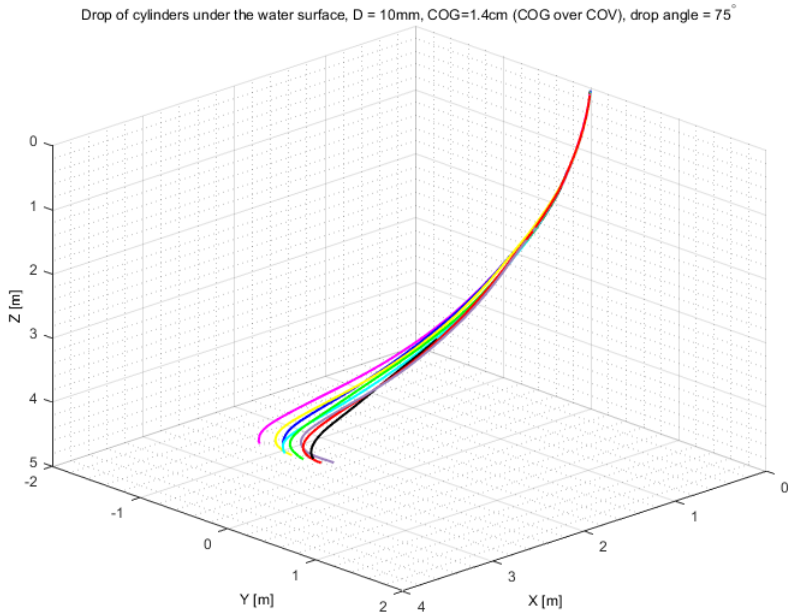

Figure 132: X-Y-Z view: Drop of 10mm diameter cylinders under the water surface at 75° initial angle with COG displaced 1.4cm (Centre of Gravity (COG) over Centre of Volume (COV)). Each coloured line represents a drop.

A.10 Drop of 10mm diameter cylinders under the water surface with COG placed with 1.4 cm (COG under COV)

A.10.1 15° initial drop angle

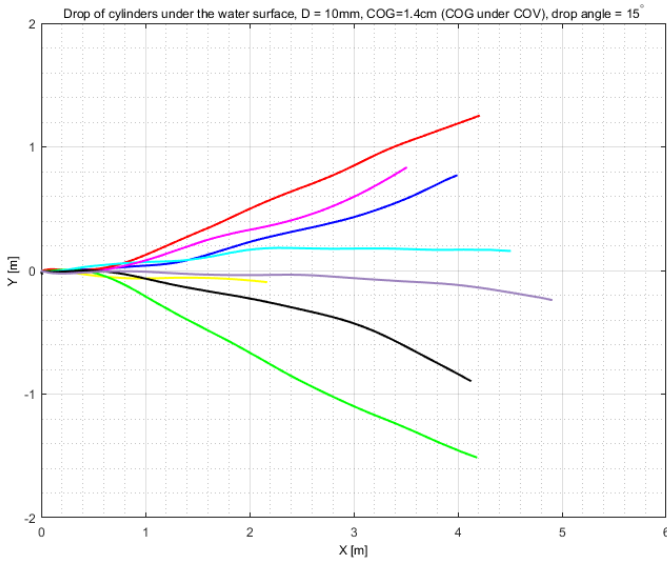

Figure 133: X-Y view: Drop of 10mm diameter cylinders under the water surface at 15° initial angle with COG displaced 1.4 cm (Centre of Gravity (COG) under Centre of Volume (COV)). Each coloured line represents a drop.

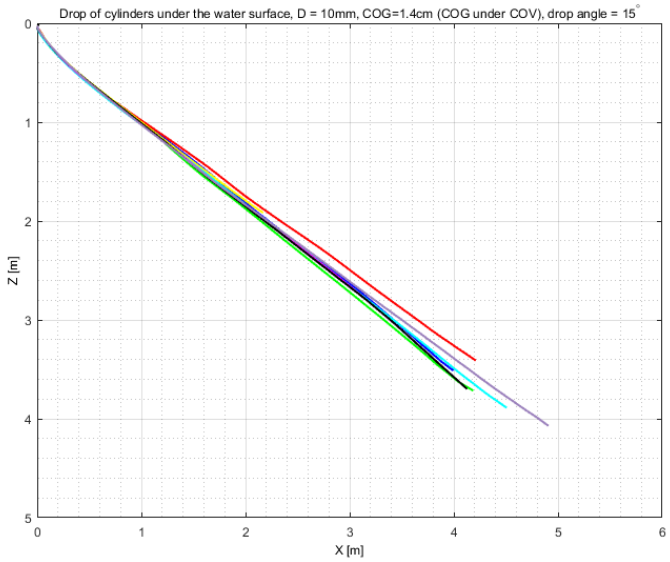

Figure 134: X-Z view: Drop of 10mm diameter cylinders under the water surface at 15° initial angle with COG displaced 1.4 cm (Centre of Gravity (COG) under Centre of Volume (COV)). The X-coordinates are radial coordinates from the XY plane and each coloured line represents a drop.

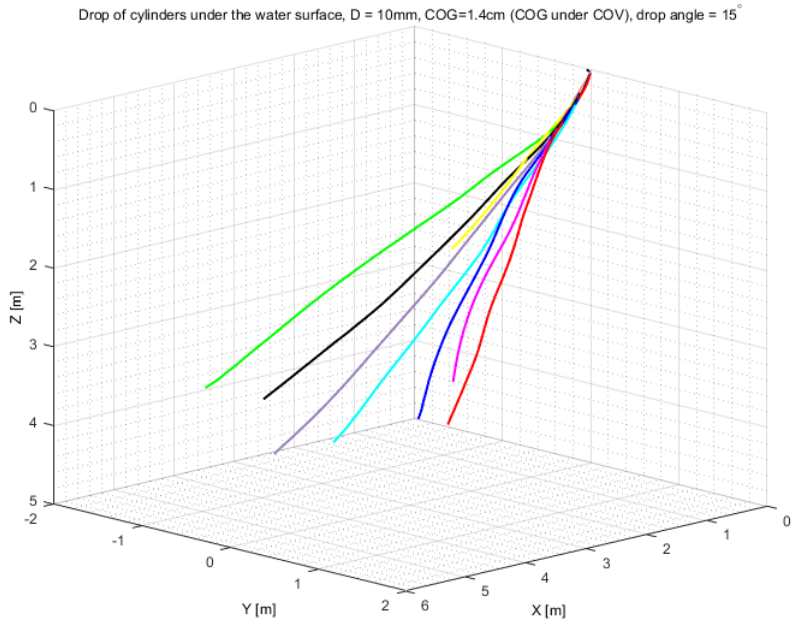

Figure 135: X-Y-Z view: Drop of 10mm diameter cylinders under the water surface at 15° initial angle with COG displaced 1.4 cm (Centre of Gravity (COG) under Centre of Volume (COV)). Each coloured line represents a drop.

A.10.2 30° initial drop angle

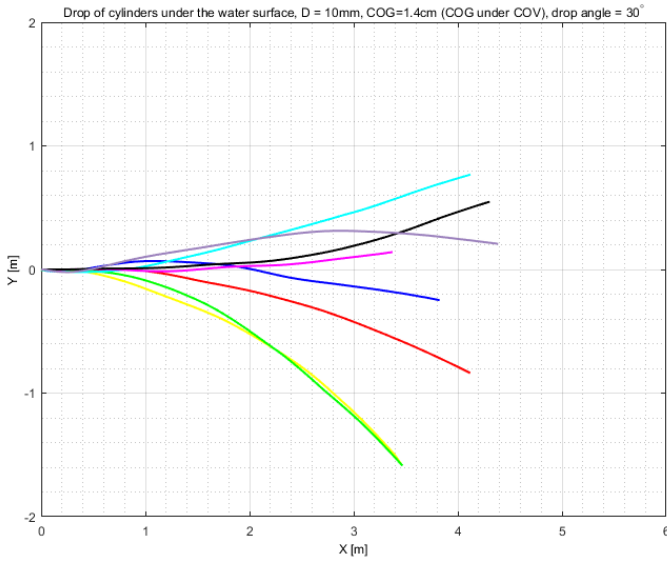

Figure 136: X-Y view: Drop of 10mm diameter cylinders under the water surface at 30° initial angle with COG displaced 1.4 cm (Centre of Gravity (COG) under Centre of Volume (COV)). Each coloured line represents a drop.

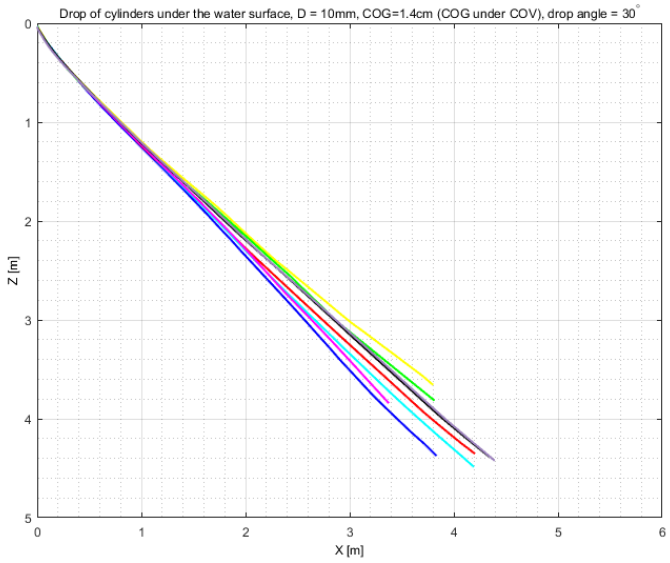

Figure 137: X-Z view: Drop of 10mm diameter cylinders under the water surface at 30° initial angle with COG displaced 1.4 cm (Centre of Gravity (COG) under Centre of Volume (COV)). The X-coordinates are radial coordinates from the XY plane and each coloured line represents a drop.

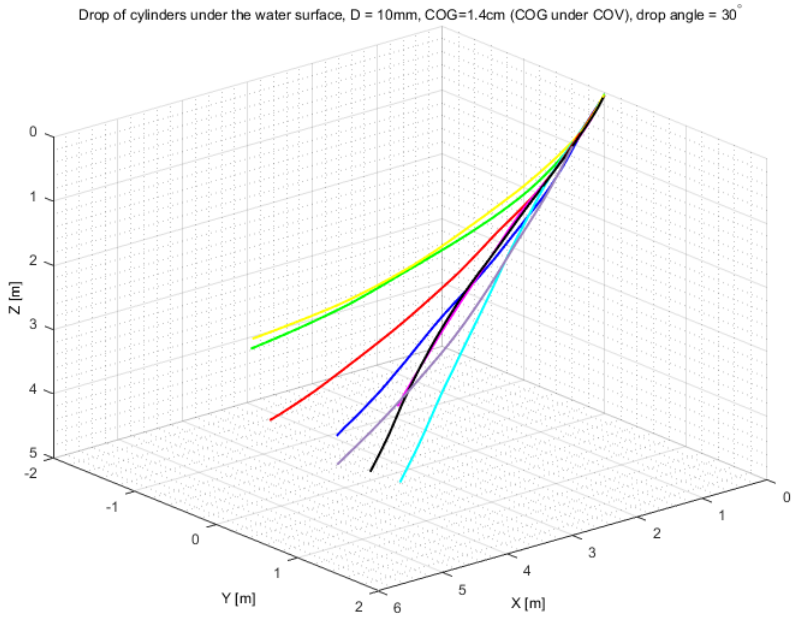

Figure 138: X-Y-Z view: Drop of 10mm diameter cylinders under the water surface at 30° initial angle with COG displaced 1.4 cm (Centre of Gravity (COG) under Centre of Volume (COV)). Each coloured line represents a drop.

A.10.3 45° initial drop angle

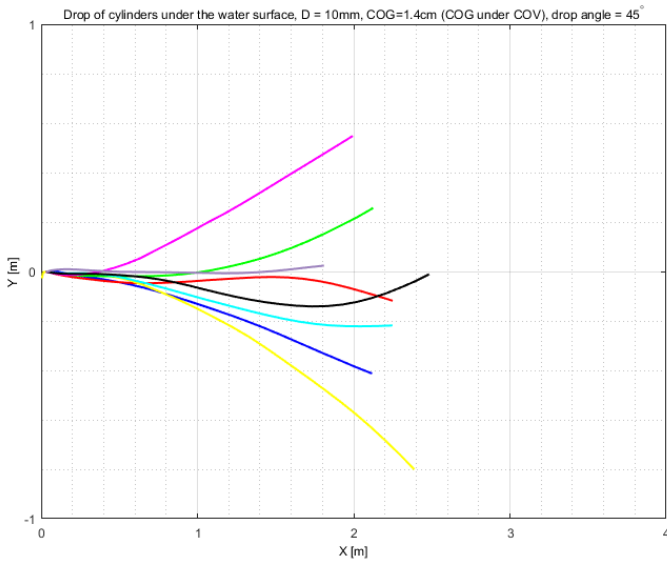

Figure 139: X-Y view: Drop of 10mm diameter cylinders under the water surface at 45° initial angle with COG displaced 1.4 cm (Centre of Gravity (COG) under Centre of Volume (COV)). Each coloured line represents a drop.

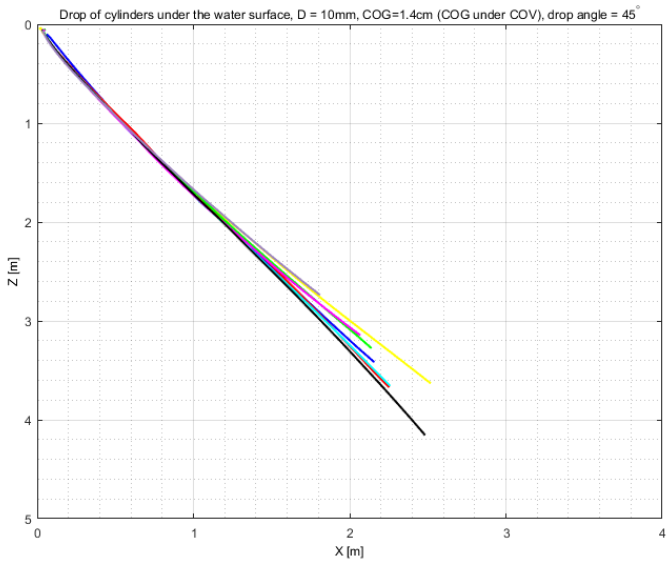

Figure 140: X-Z view: Drop of 10mm diameter cylinders under the water surface at 45° initial angle with COG displaced 1.4 cm (Centre of Gravity (COG) under Centre of Volume (COV)). The X-coordinates are radial coordinates from the XY plane and each coloured line represents a drop.

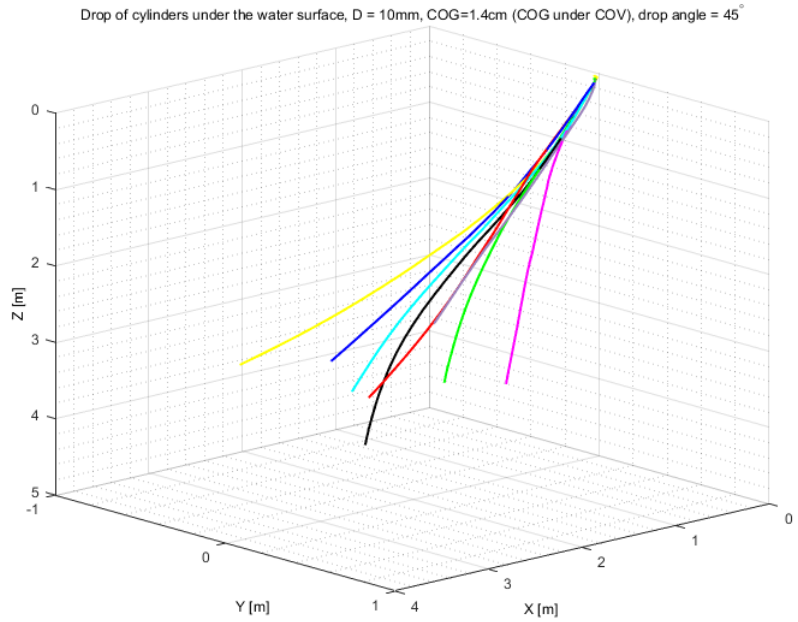

Figure 141: X-Y-Z view: Drop of 10mm diameter cylinders under the water surface at 45° initial angle with COG displaced 1.4 cm (Centre of Gravity (COG) under Centre of Volume (COV)). Each coloured line represents a drop.

A.10.4 60° initial drop angle

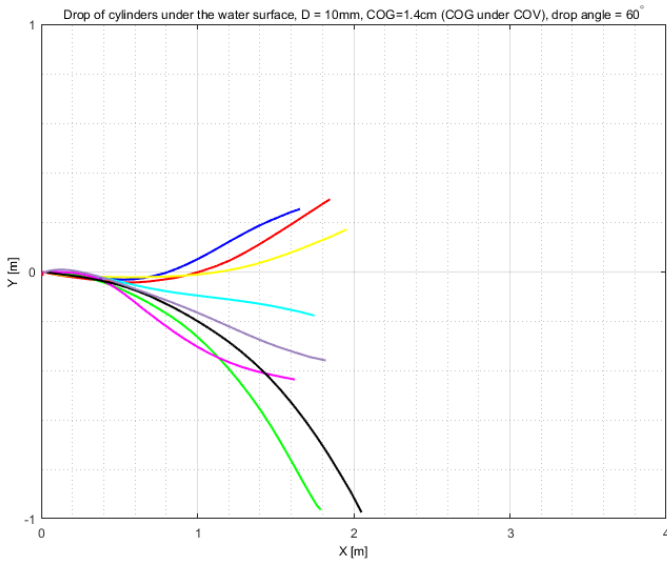

Figure 142: X-Y view: Drop of 10mm diameter cylinders under the water surface at 60° initial angle with COG displaced 1.4cm (Centre of Gravity (COG) under Centre of Volume (COV)). Each coloured line represents a drop.

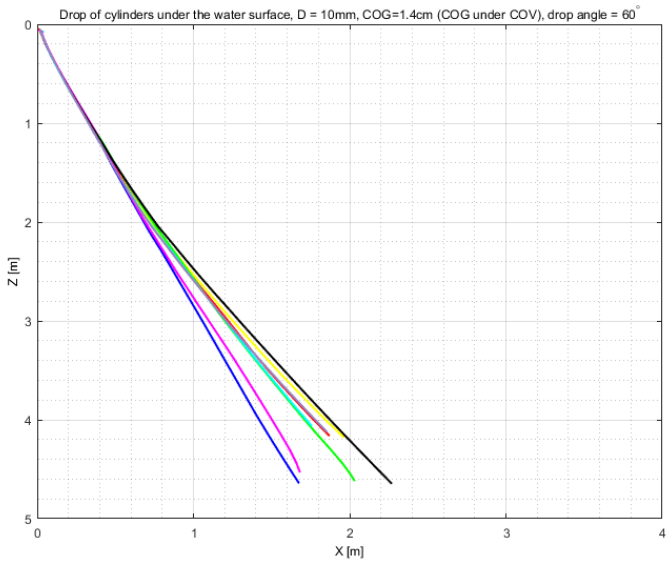

Figure 143: X-Z view: Drop of 10mm diameter cylinders under the water surface at 60° initial angle with COG displaced 1.4cm (Centre of Gravity (COG) under Centre of Volume (COV)). The X-coordinates are radial coordinates from the XY plane and each coloured line represents a drop.

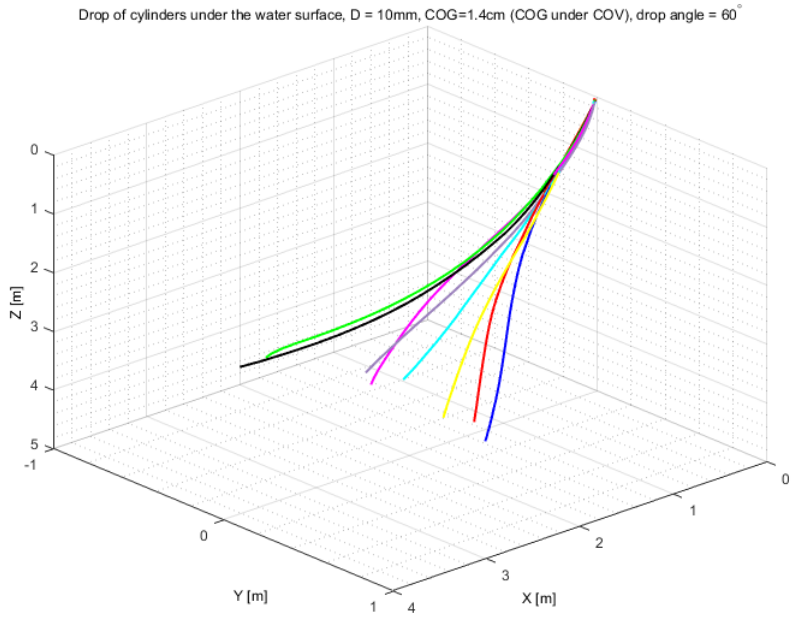

Figure 144: X-Y-Z view: Drop of 10mm diameter cylinders under the water surface at 60° initial angle with COG displaced 1.4cm (Centre of Gravity (COG) under Centre of Volume (COV)). Each coloured line represents a drop.

A.10.5 75° initial drop angle

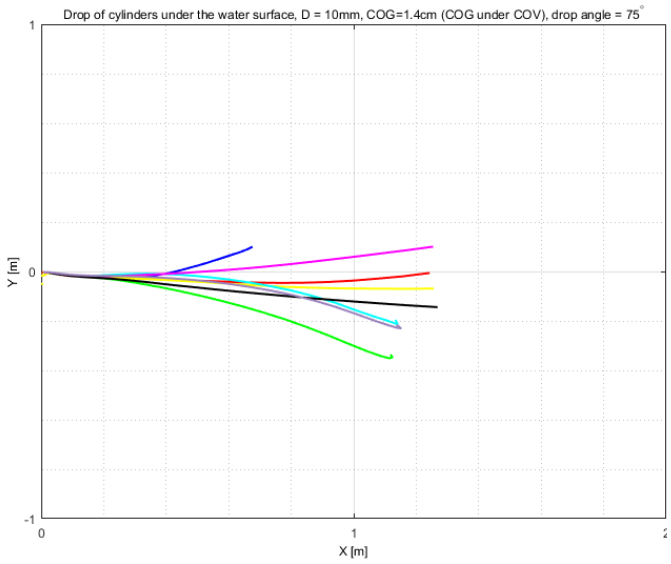

Figure 145: X-Y view: Drop of 10mm diameter cylinders under the water surface at 75° initial angle with COG displaced 1.4cm (Centre of Gravity (COG) under Centre of Volume (COV)). Each coloured line represents a drop.

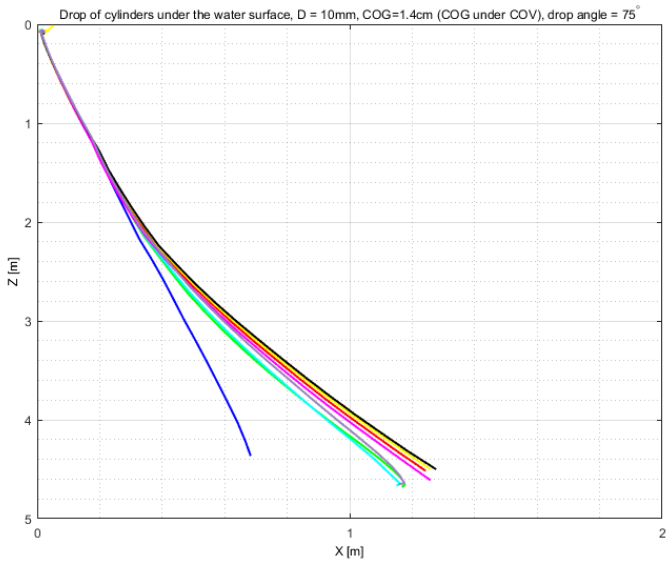

Figure 146: X-Z view: Drop of 10mm diameter cylinders under the water surface at 75° initial angle with COG displaced 1.4cm (Centre of Gravity (COG) under Centre of Volume (COV)). The X-coordinates are radial coordinates from the XY plane and each coloured line represents a drop.

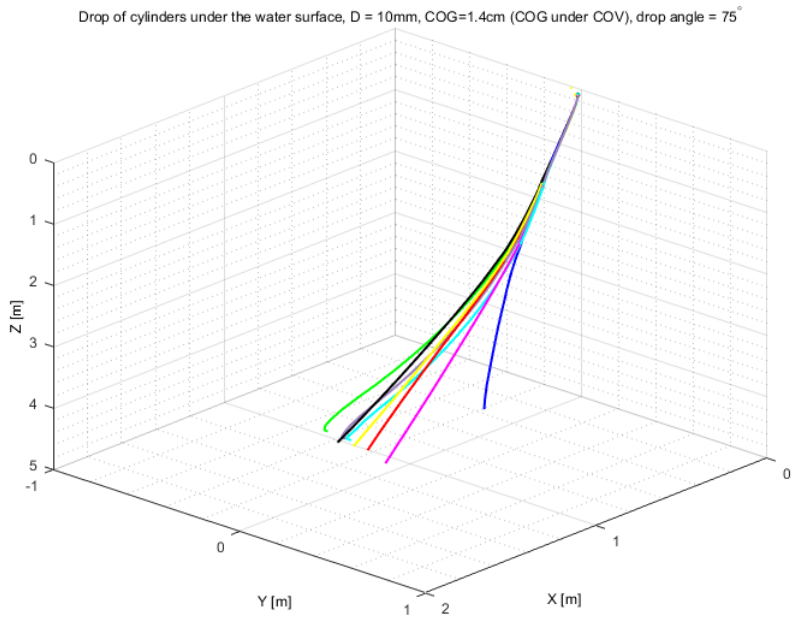

Figure 147: X-Y-Z view: Drop of 10mm diameter cylinders under the water surface at 75° initial angle with COG displaced 1.4cm (Centre of Gravity (COG) under Centre of Volume (COV)). Each coloured line represents a drop.

A.11 Drop of 10mm diameter cylinders under the water surface with COG placed with 3cm (COG over COV)

A.11.1 15° initial drop angle

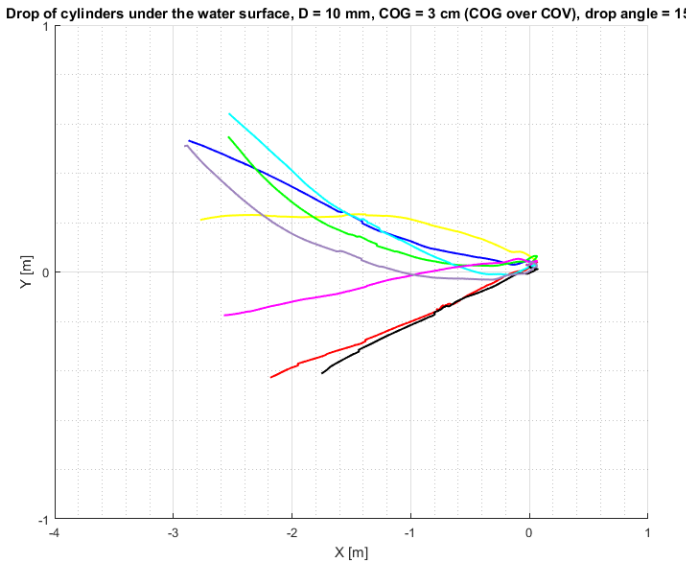

Figure 148: X-Y view: Drop of 10mm diameter cylinders under the water surface at 15° initial angle with COG displaced 3cm (Centre of Gravity (COG) over Centre of Volume (COV)). Each coloured line represents a drop.

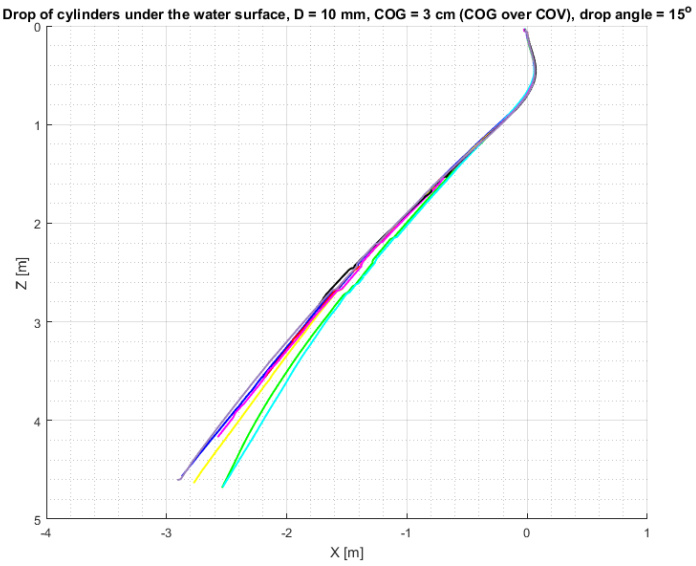

Figure 149: X-Z view: Drop of 10mm diameter cylinders under the water surface at 15° initial angle with COG displaced 3cm (Centre of Gravity (COG) over Centre of Volume (COV)). The X-coordinates are radial coordinates from the XY plane and each coloured line represents a drop.

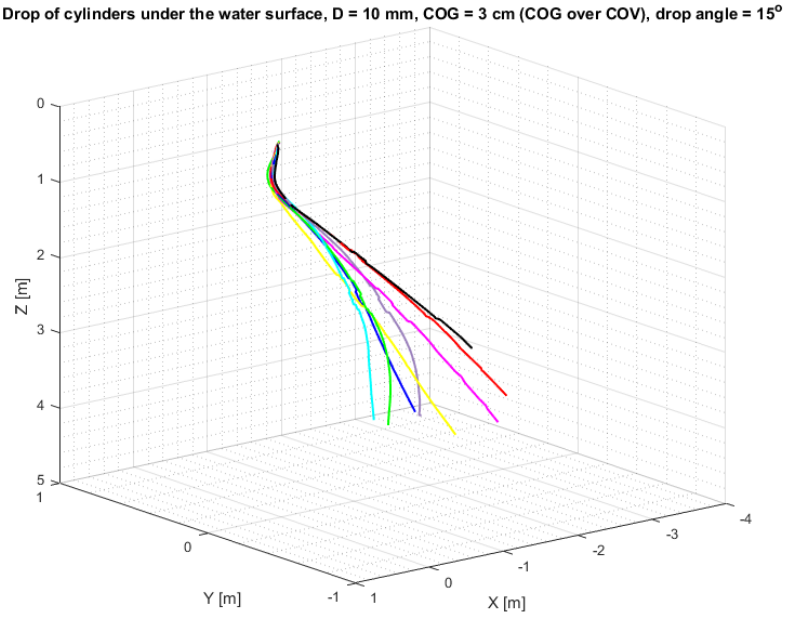

Figure 150: X-Y-Z view: Drop of 10mm diameter cylinders under the water surface at 15° initial angle with COG displaced 3cm (Centre of Gravity (COG) over Centre of Volume (COV)). Each coloured line represents a drop.

A.11.2 30° initial drop angle

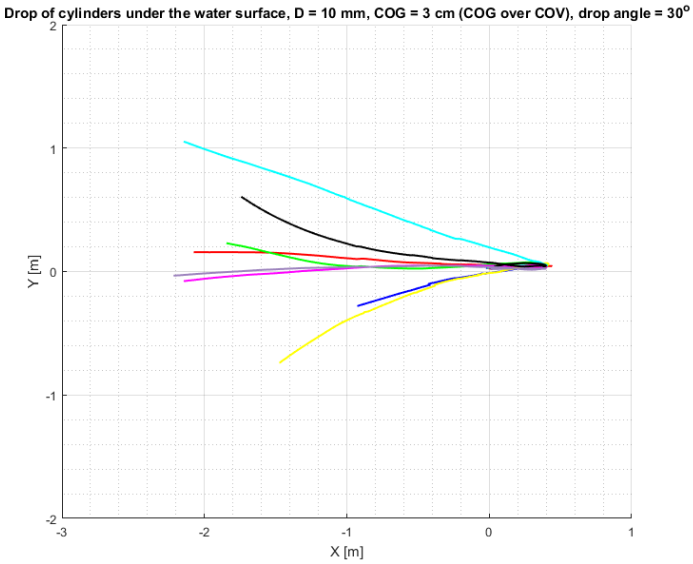

Figure 151: X-Y view: Drop of 10mm diameter cylinders under the water surface at 30° initial angle with COG displaced 3cm (Centre of Gravity (COG) over Centre of Volume (COV)). Each coloured line represents a drop.

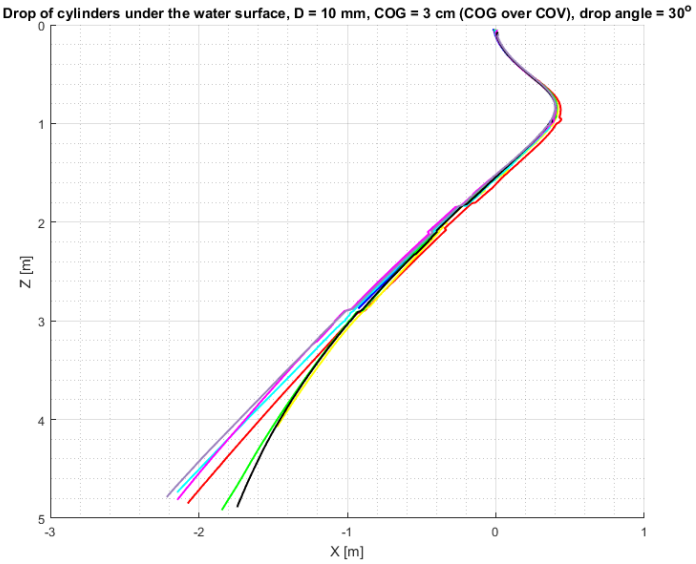

Figure 152: X-Z view: Drop of 10mm diameter cylinders under the water surface at 30° initial angle with COG displaced 3cm (Centre of Gravity (COG) over Centre of Volume (COV)). The X-coordinates are radial coordinates from the XY plane and each coloured line represents a drop.

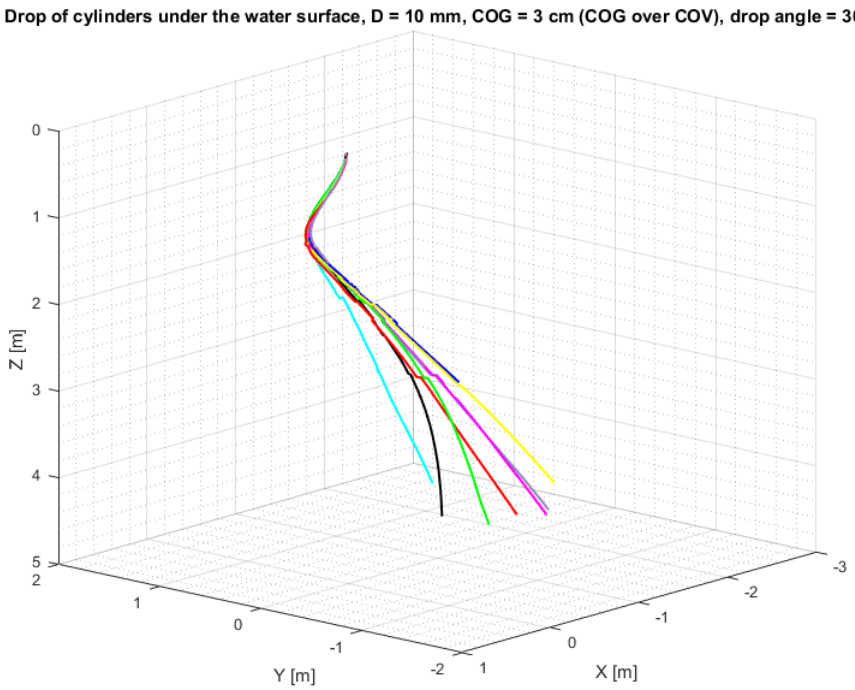

Figure 153: X-Y-Z view: Drop of 10mm diameter cylinders under the water surface at 30° initial angle with COG displaced 3cm (Centre of Gravity (COG) over Centre of Volume (COV)). Each coloured line represents a drop.

A.11.3 45° initial drop angle

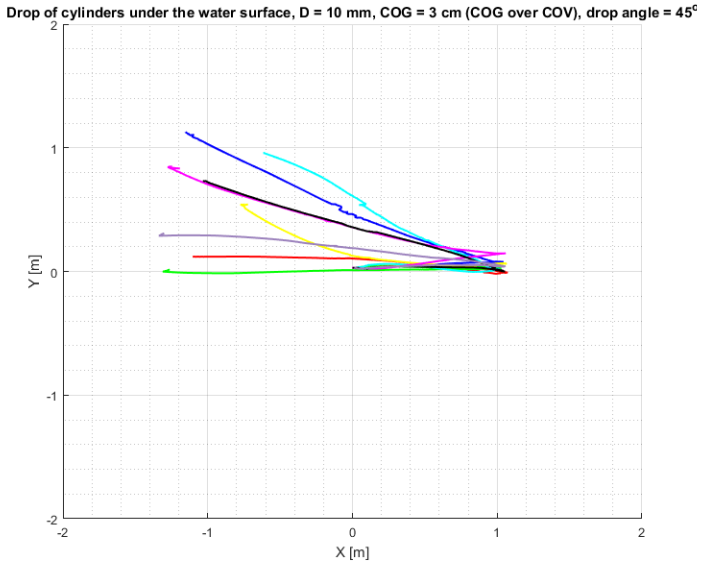

Figure 154: X-Y view: Drop of 10mm diameter cylinders under the water surface at 45° initial angle with COG displaced 3cm (Centre of Gravity (COG) over Centre of Volume (COV)). Each coloured line represents a drop.

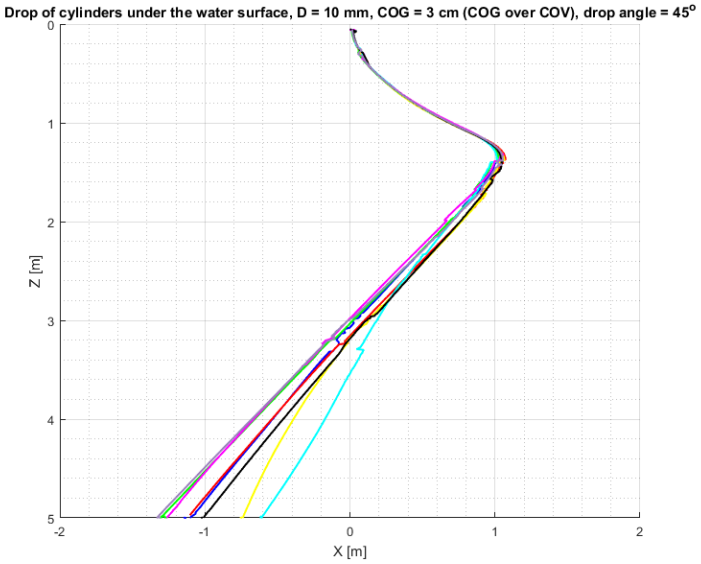

Figure 155: X-Z view: Drop of 10mm diameter cylinders under the water surface at 45° initial angle with COG displaced 3cm (Centre of Gravity (COG) over Centre of Volume (COV)). The X-coordinates are radial coordinates from the XY plane and each coloured line represents a drop.

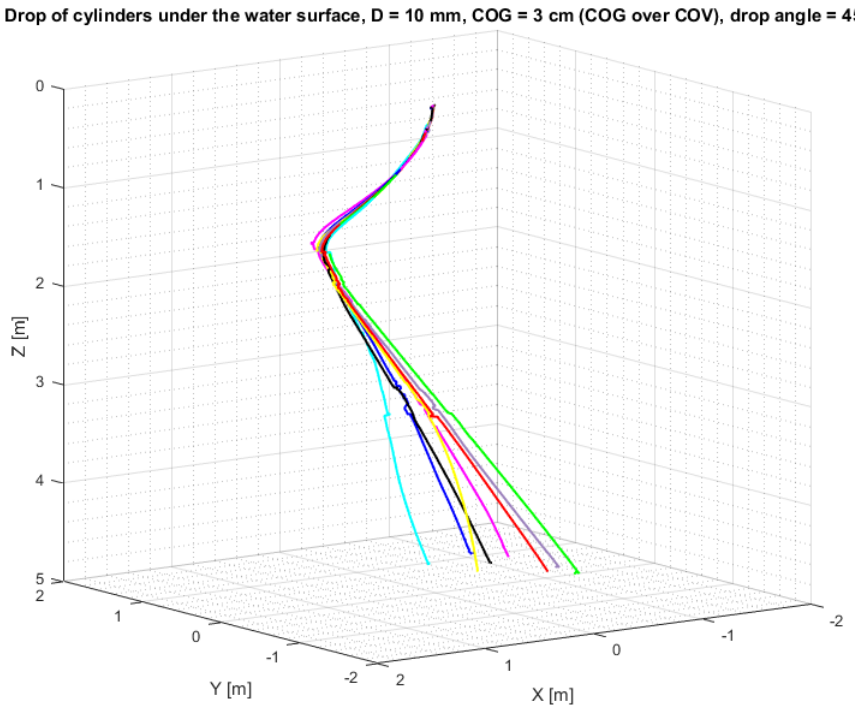

Figure 156: X-Y-Z view: Drop of 10mm diameter cylinders under the water surface at 45° initial angle with COG displaced 3cm (Centre of Gravity (COG) over Centre of Volume (COV)). Each coloured line represents a drop.

A.11.4 60° initial drop angle

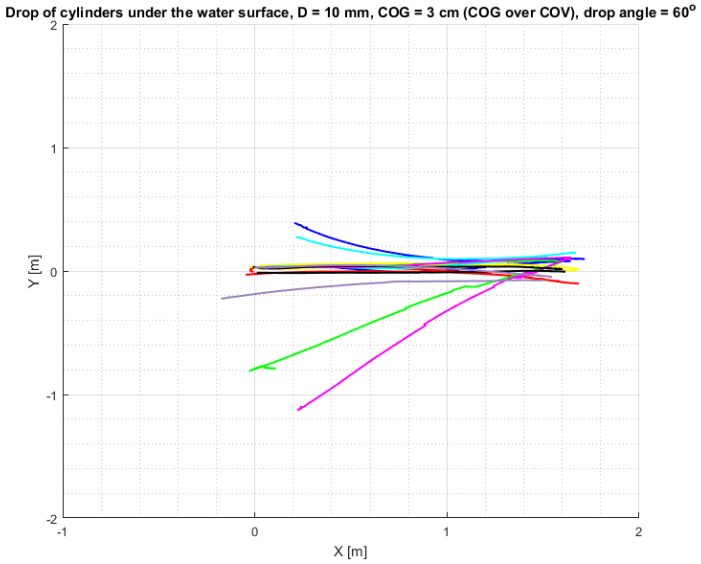

Figure 157: X-Y view: Drop of 10mm diameter cylinders under the water surface at 60° initial angle with COG displaced 3cm (Centre of Gravity (COG) over Centre of Volume (COV)). Each coloured line represents a drop.

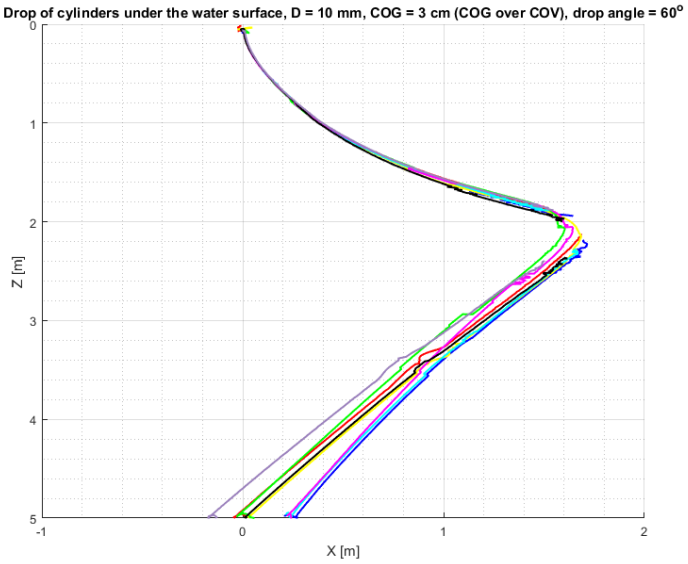

Figure 158: X-Z view: Drop of 10mm diameter cylinders under the water surface at 60° initial angle with COG displaced 3cm (Centre of Gravity (COG) over Centre of Volume (COV)). The X-coordinates are radial coordinates from the XY plane and each coloured line represents a drop.

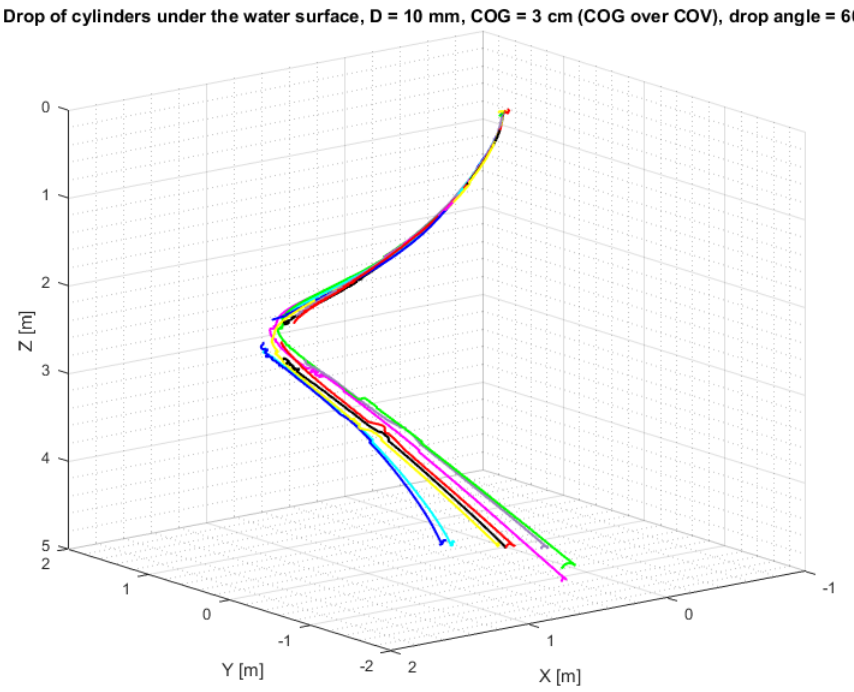

Figure 159: X-Y-Z view: Drop of 10mm diameter cylinders under the water surface at 60° initial angle with COG displaced 3cm (Centre of Gravity (COG) over Centre of Volume (COV)). Each coloured line represents a drop.

A.11.5 75° initial drop angle

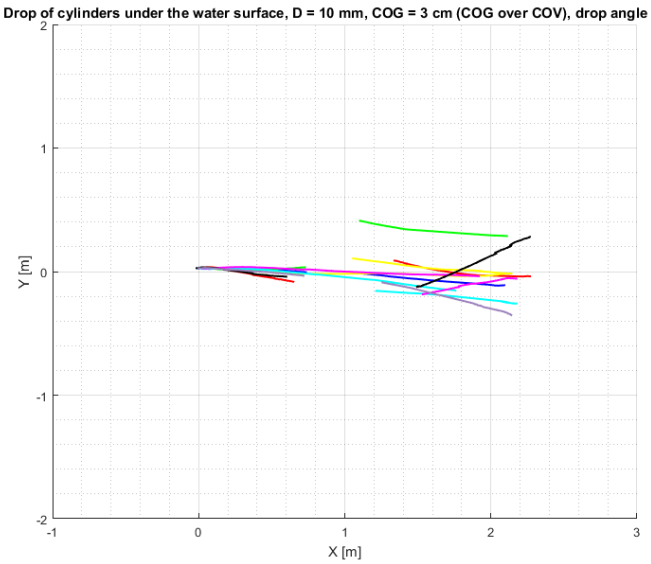

Figure 160: X-Y view: Drop of 10mm diameter cylinders under the water surface at 75° initial angle with COG displaced 3cm (Centre of Gravity (COG) over Centre of Volume (COV)). Each coloured line represents a drop.

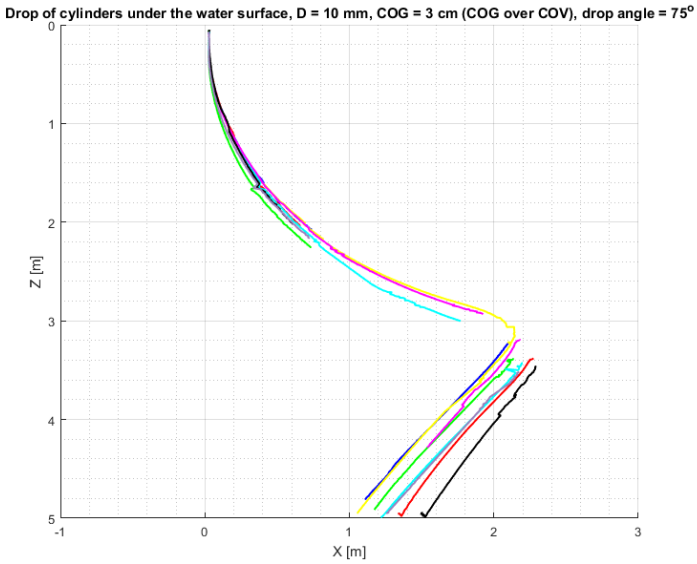

Figure 161: X-Z view: Drop of 10mm diameter cylinders under the water surface at 75° initial angle with COG displaced 3cm (Centre of Gravity (COG) over Centre of Volume (COV)). The X-coordinates are radial coordinates from the XY plane and each coloured line represents a drop.

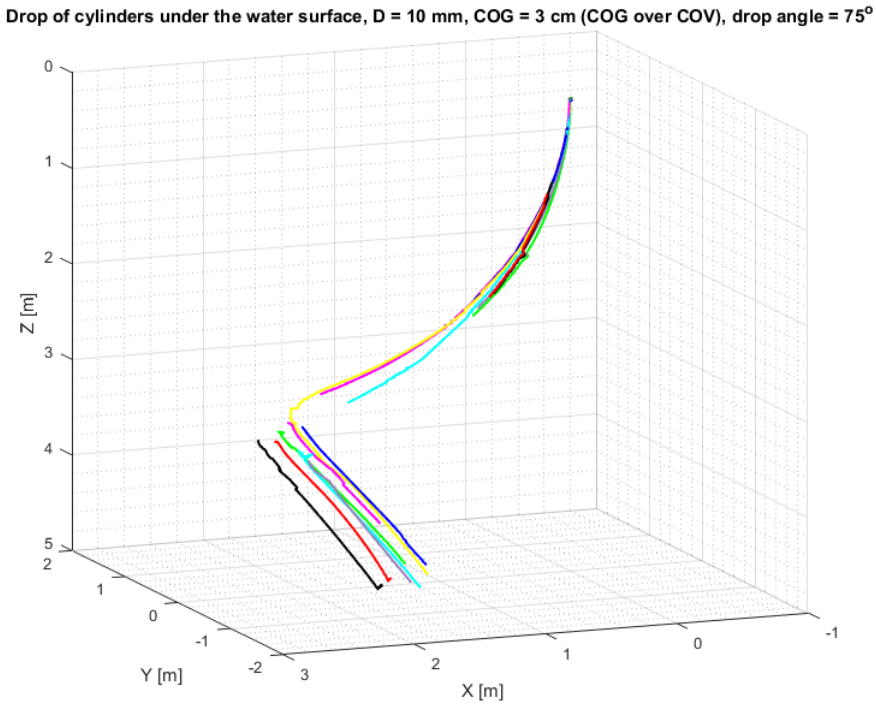

Figure 162: X-Y-Z view: Drop of 10mm diameter cylinders under the water surface at 75° initial angle with COG displaced 3cm (Centre of Gravity (COG) over Centre of Volume (COV)). Each coloured line represents a drop.

A.12 Drop of 10mm diameter cylinders under the water surface with COG placed with 3cm (COG under COV)

A.12.1 15° initial drop angle

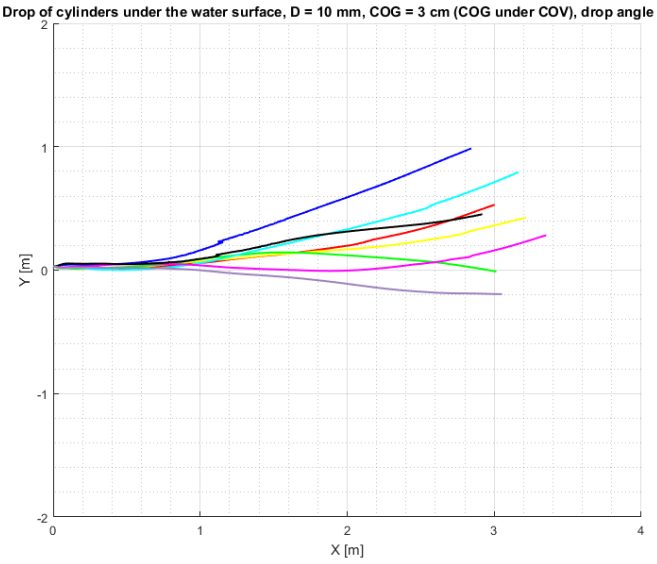

Figure 163: X-Y view: Drop of 10mm diameter cylinders under the water surface at 15° initial angle with COG displaced 3cm (Centre of Gravity (COG) under Centre of Volume (COV)). Each coloured line represents a drop.

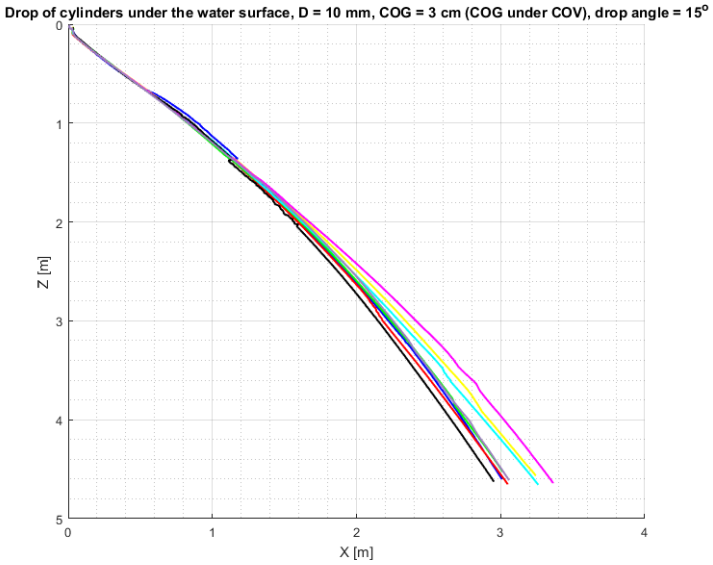

Figure 164: X-Z view: Drop of 10mm diameter cylinders under the water surface at 15° initial angle with COG displaced 3cm (Centre of Gravity (COG) under Centre of Volume (COV)). The X-coordinates are radial coordinates from the XY plane and each coloured line represents a drop.

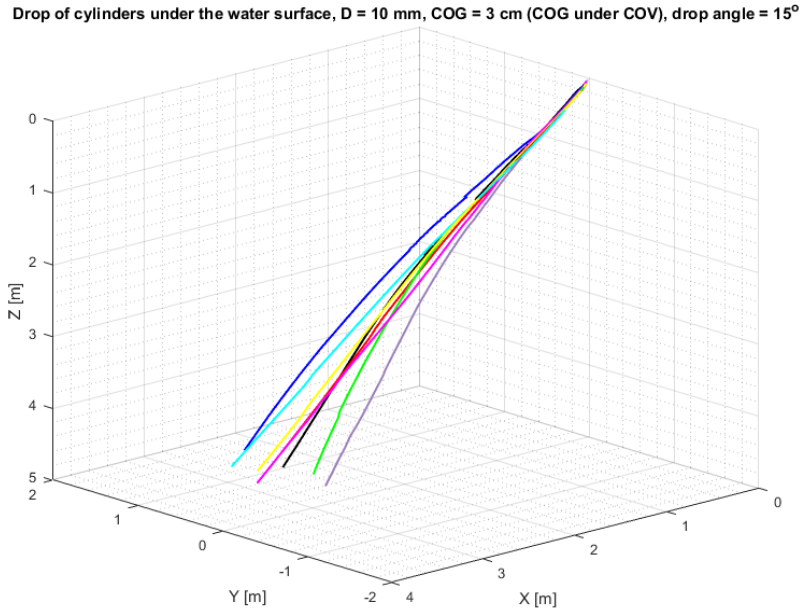

Figure 165: X-Y-Z view: Drop of 10mm diameter cylinders under the water surface at 15° initial angle with COG displaced 3cm (Centre of Gravity (COG) under Centre of Volume (COV)). Each coloured line represents a drop.

A.12.2 30° initial drop angle

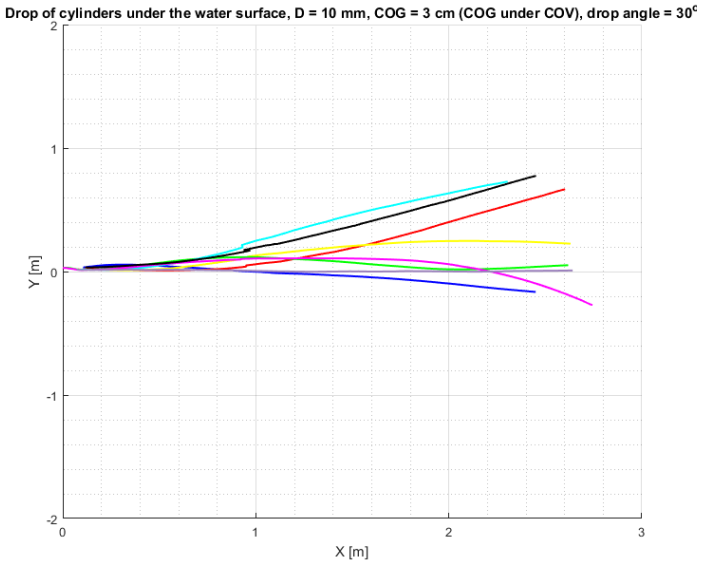

Figure 166: X-Y view: Drop of 10mm diameter cylinders under the water surface at 30° initial angle with COG displaced 3cm (Centre of Gravity (COG) under Centre of Volume (COV)). Each coloured line represents a drop.

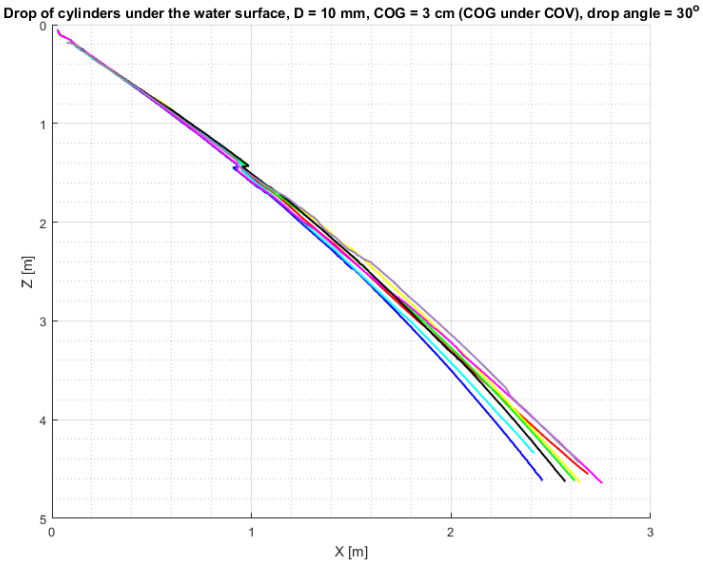

Figure 167: X-Z view: Drop of 10mm diameter cylinders under the water surface at 30° initial angle with COG displaced 3cm (Centre of Gravity (COG) under Centre of Volume (COV)). The X-coordinates are radial coordinates from the XY plane and each coloured line represents a drop.

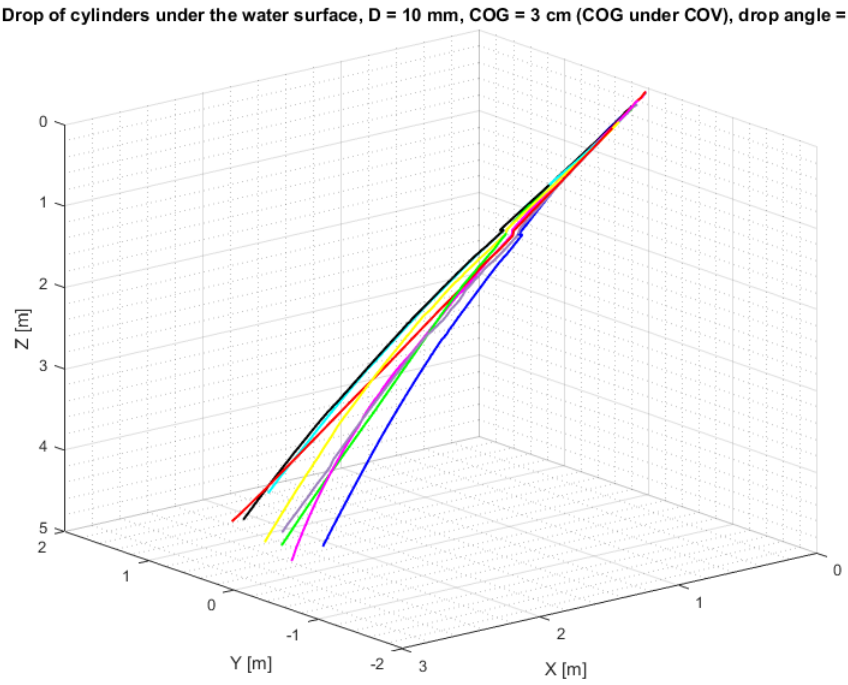

Figure 168: X-Y-Z view: Drop of 10mm diameter cylinders under the water surface at 30° initial angle with COG displaced 3cm (Centre of Gravity (COG) under Centre of Volume (COV)). Each coloured line represents a drop.

A.12.3 45° initial drop angle

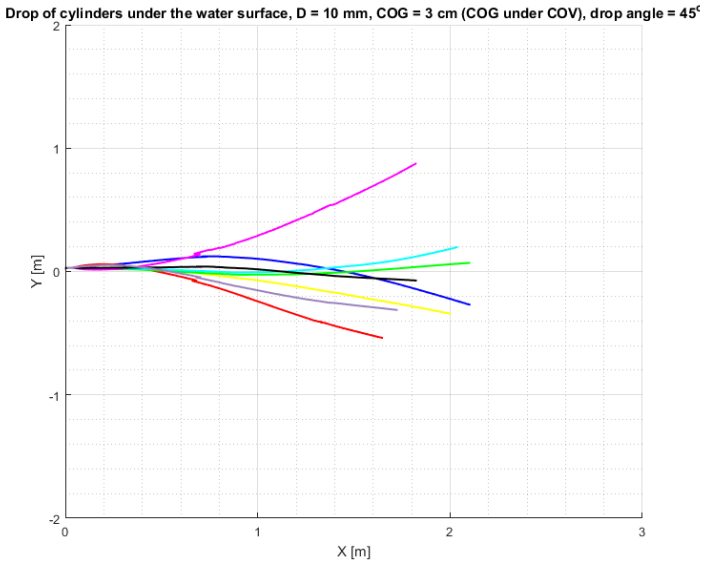

Figure 169: X-Y view: Drop of 10mm diameter cylinders under the water surface at 45° initial angle with COG displaced 3cm (Centre of Gravity (COG) under Centre of Volume (COV)). Each coloured line represents a drop.

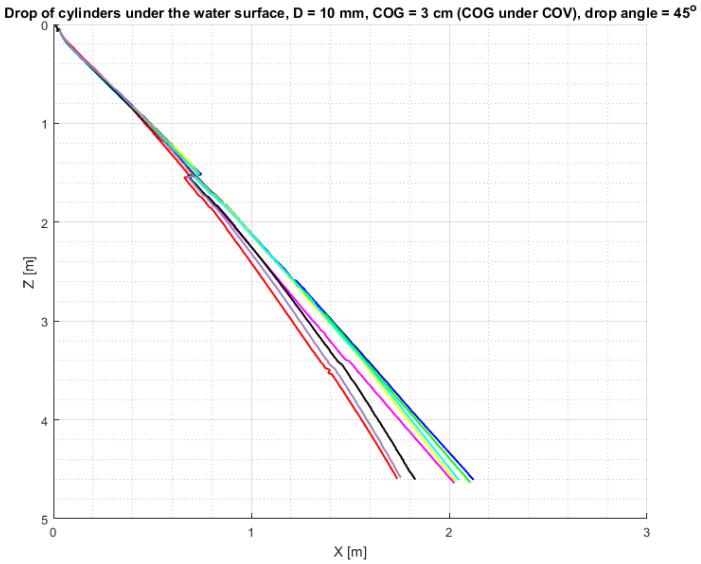

Figure 170: X-Z view: Drop of 10mm diameter cylinders under the water surface at 45° initial angle with COG displaced 3cm (Centre of Gravity (COG) under Centre of Volume (COV)). The X-coordinates are radial coordinates from the XY plane and each coloured line represents a drop.

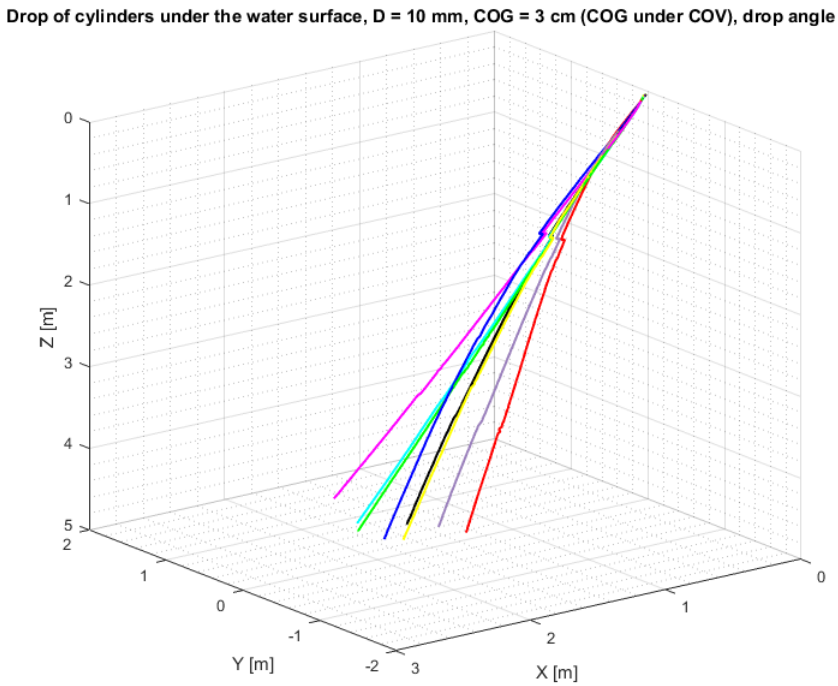

Figure 171: X-Y-Z view: Drop of 10mm diameter cylinders under the water surface at 45° initial angle with COG displaced 3cm (Centre of Gravity (COG) under Centre of Volume (COV)). Each coloured line represents a drop.

A.12.4 60° initial drop angle

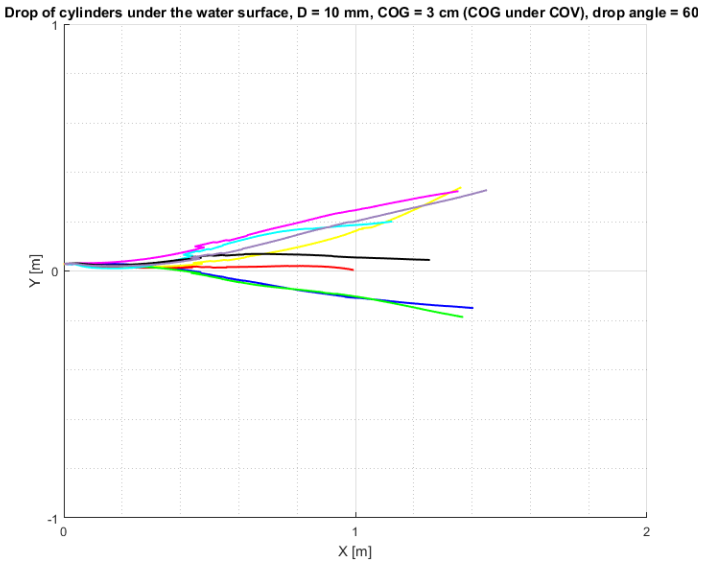

Figure 172: X-Y view: Drop of 10mm diameter cylinders under the water surface at 60° initial angle with COG displaced 3cm (Centre of Gravity (COG) under Centre of Volume (COV)). Each coloured line represents a drop.

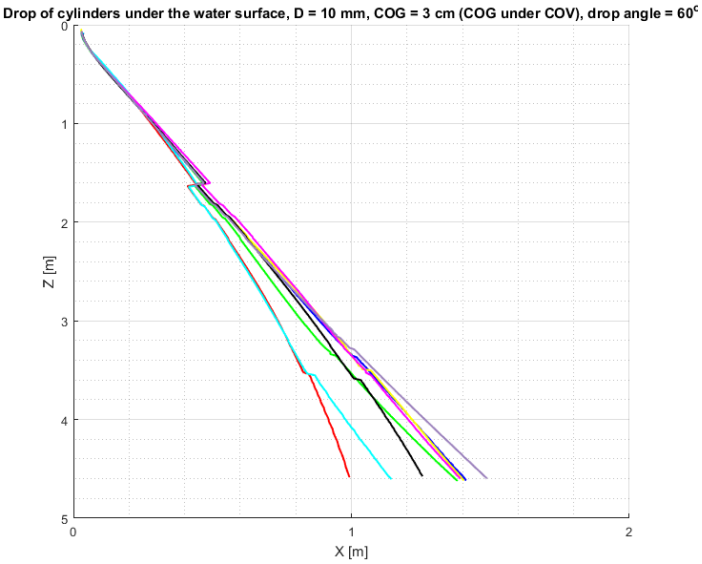

Figure 173: X-Z view: Drop of 10mm diameter cylinders under the water surface at 60° initial angle with COG displaced 3cm (Centre of Gravity (COG) under Centre of Volume (COV)). The X-coordinates are radial coordinates from the XY plane and each coloured line represents a drop.

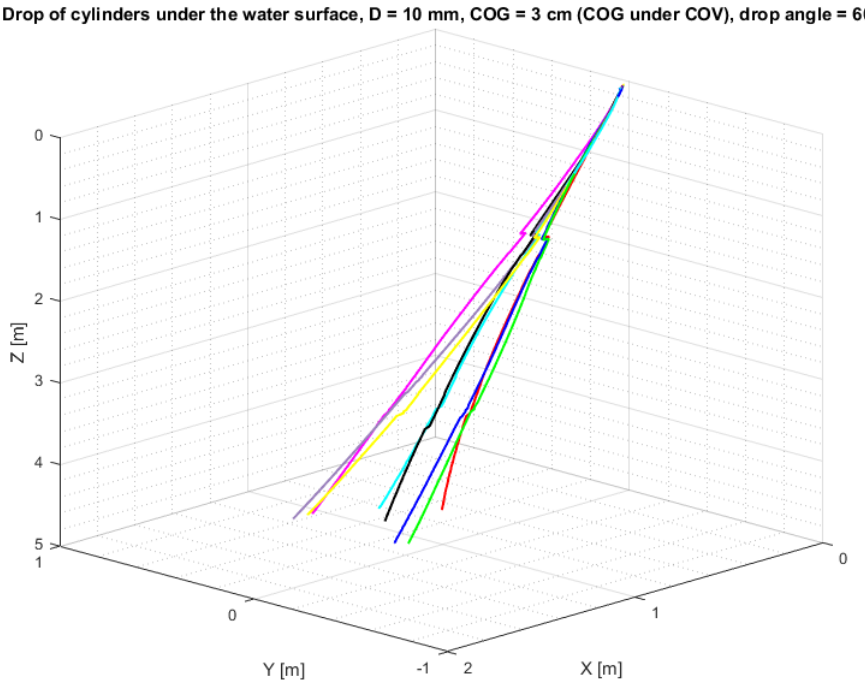

Figure 174: X-Y-Z view: Drop of 10mm diameter cylinders under the water surface at 60° initial angle with COG displaced 3cm (Centre of Gravity (COG) under Centre of Volume (COV)). Each coloured line represents a drop.

A.12.5 75° initial drop angle

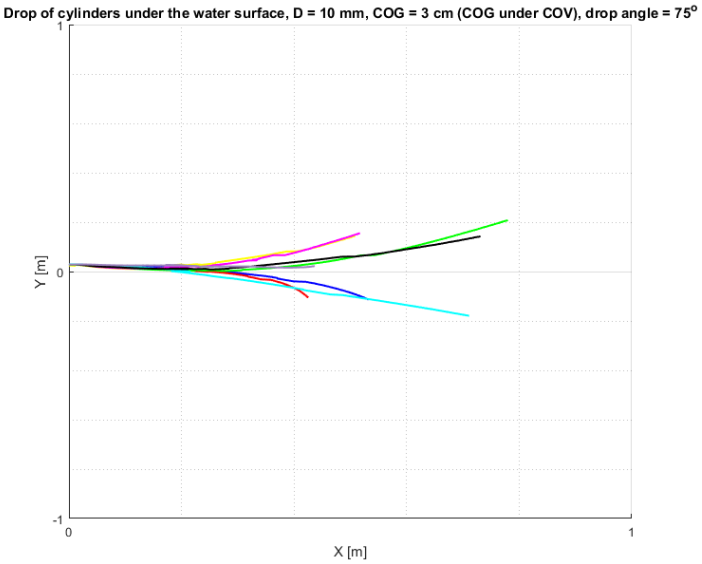

Figure 175: X-Y view: Drop of 10mm diameter cylinders under the water surface at 75° initial angle with COG displaced 3cm (Centre of Gravity (COG) under Centre of Volume (COV)). Each coloured line represents a drop.

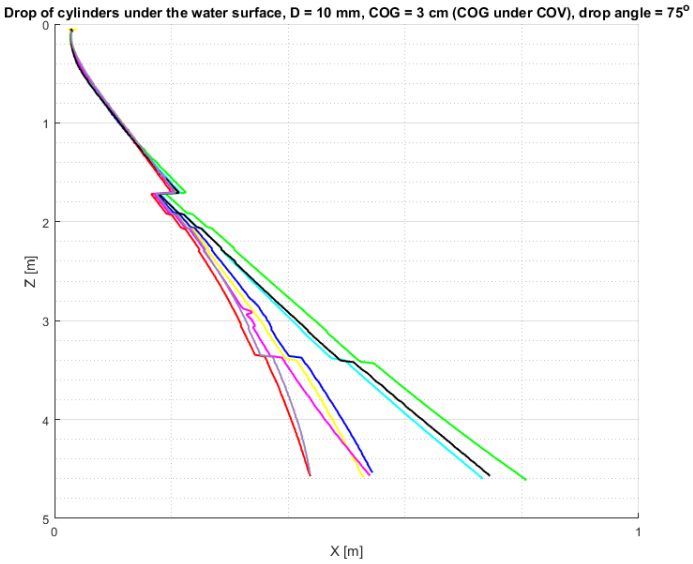

Figure 176: X-Z view: Drop of 10mm diameter cylinders under the water surface at 75° initial angle with COG displaced 3cm (Centre of Gravity (COG) under Centre of Volume (COV)). The X-coordinates are radial coordinates from the XY plane and each coloured line represents a drop.

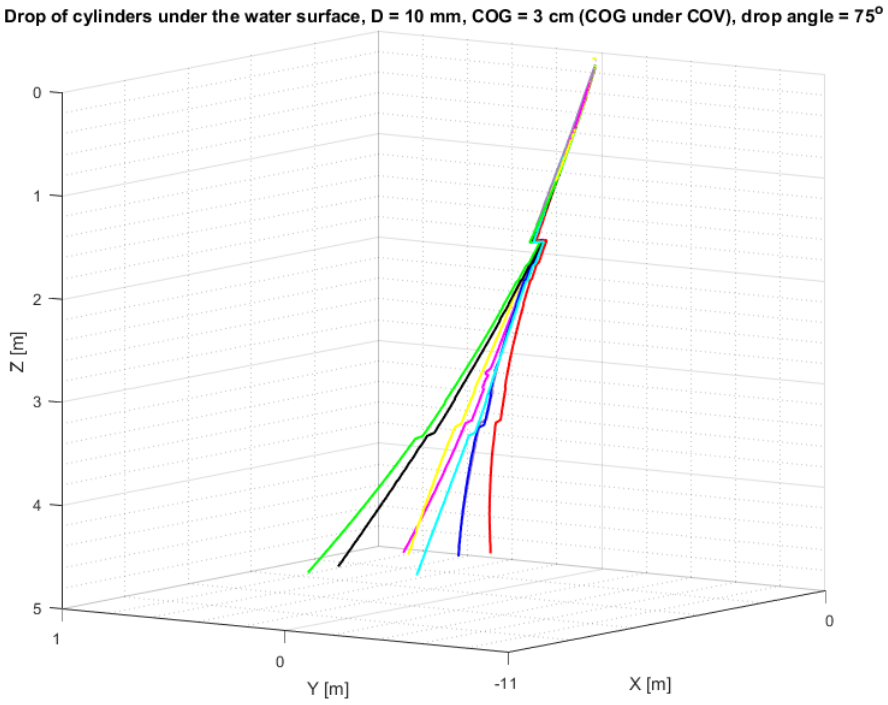

Figure 177: X-Y-Z view: Drop of 10mm diameter cylinders under the water surface at 75° initial angle with COG displaced 3cm (Centre of Gravity (COG) under Centre of Volume (COV)). Each coloured line represents a drop.

B Velocity plots

B.1 Velocity of 10 mm cylinder dropped from under the water surface

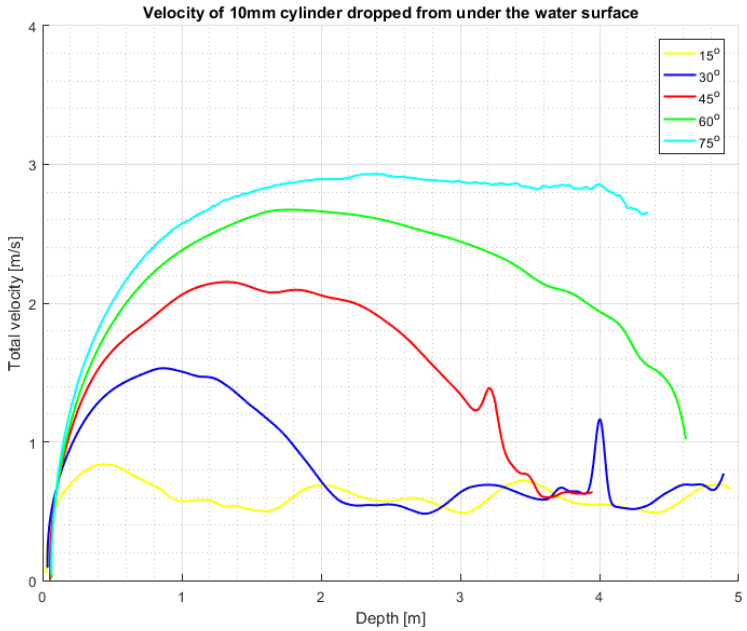

Figure 178: Total velocity compared to depth for closed 10 mm cylinders. The cylinders are dropped under the surface with initial drop angles of 15^o, 30^o, 45^o, 60^o and 75^o. Each plot line represent an example of the total velocity development.

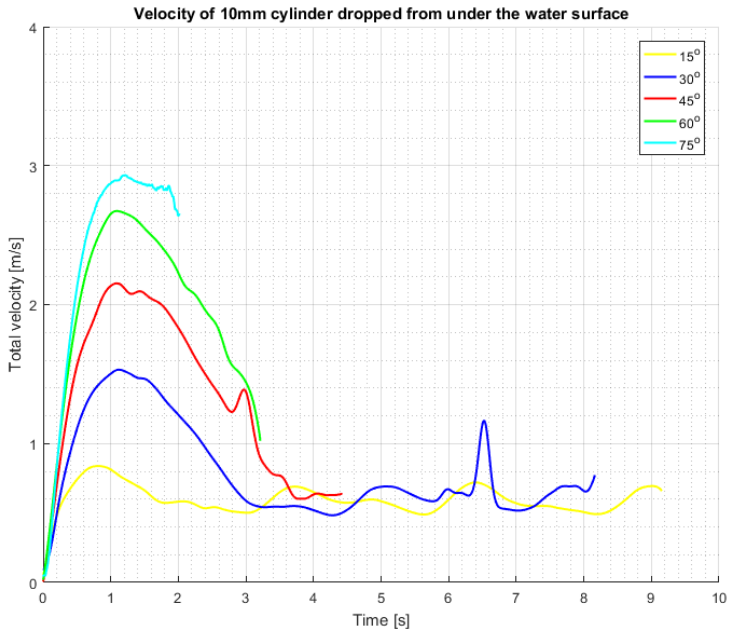

Figure 179: Total velocity compared to time for closed 10 mm cylinders. The cylinders are dropped under the surface with initial drop angles of 15^o, 30^o, 45^o, 60^o and 75^o. Each plot line represent an example of the total velocity development.

B.2 Velocity of 16 mm cylinder dropped from under the water surface

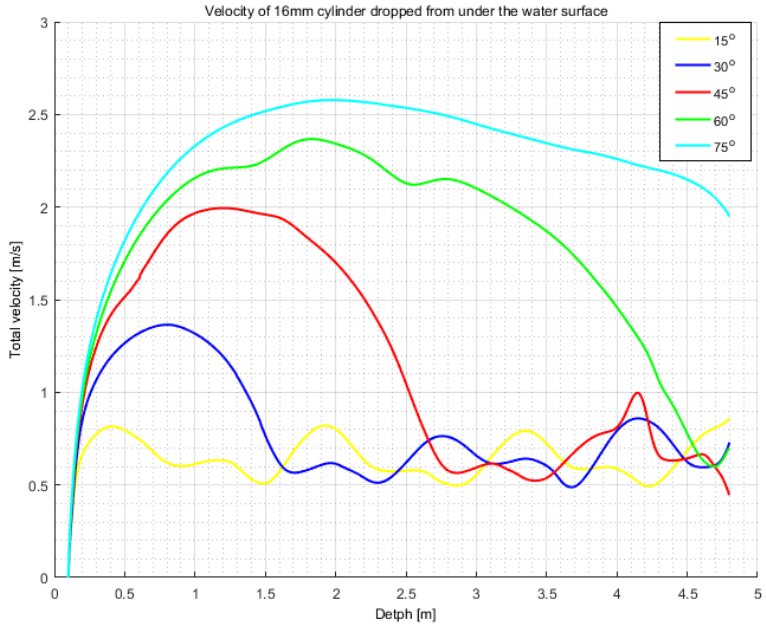

Figure 180: Total velocity compared to depth for closed 16 mm cylinders. The cylinders are dropped under the surface with initial drop angles of 15^o, 30^o, 45^o, 60^o and 75^o. Each plot line represent an example of the total velocity development.

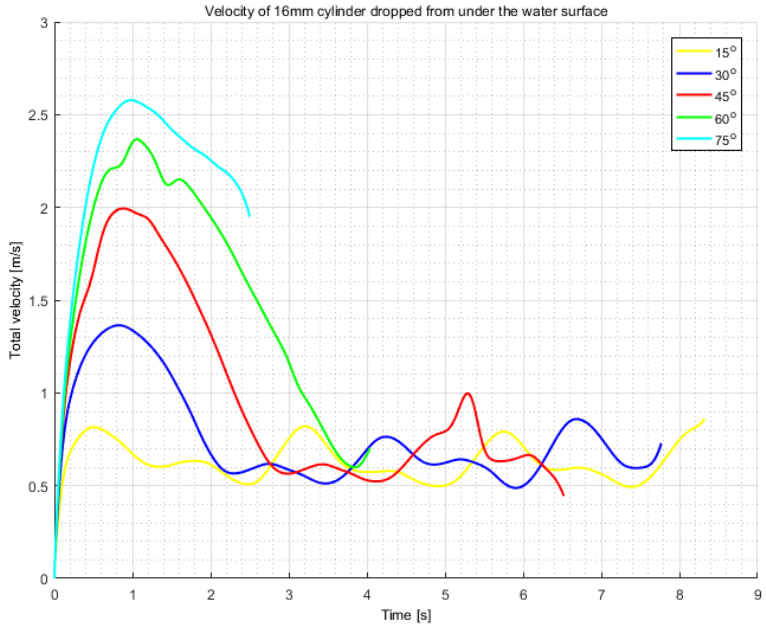

Figure 181: Total velocity compared to time for closed 16 mm cylinders. The cylinders are dropped under the surface with initial drop angles of 15^o, 30^o, 45^o, 60^o and 75^o. Each plot line represent an example of the total velocity development.

B.3 Velocity of 19 mm cylinder dropped from under the water surface

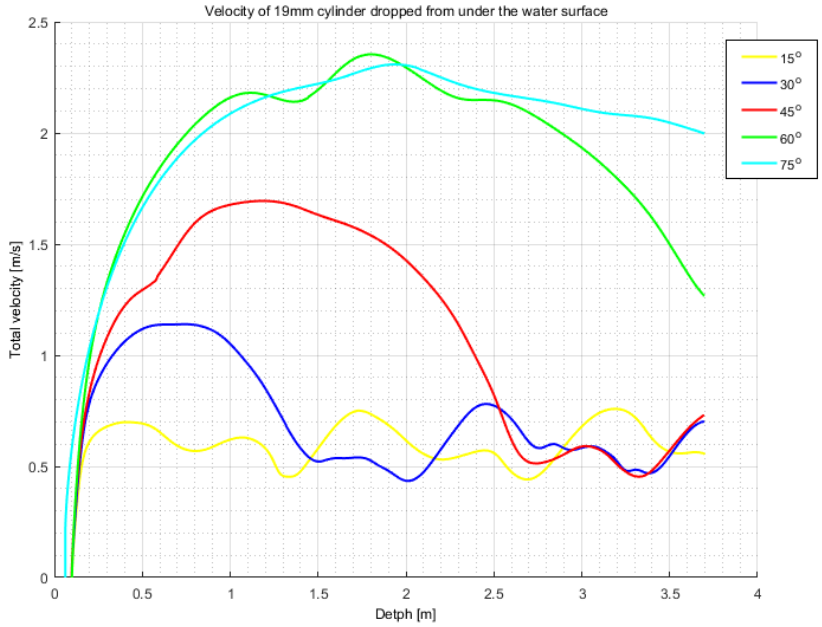

Figure 182: Total velocity compared to depth for closed 19 mm cylinders. The cylinders are dropped under the surface with initial drop angles of 15^o, 30^o, 45^o, 60^o and 75^o. Each plot line represent an example of the total velocity development.

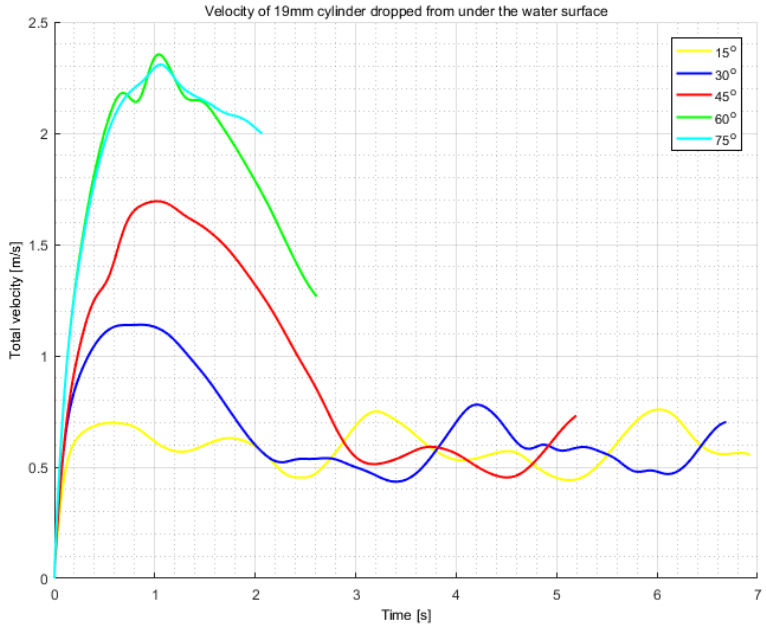

Figure 183: Total velocity compared to time for closed 19 mm cylinders. The cylinders are dropped under the surface with initial drop angles of 15^o, 30^o, 45^o, 60^o and 75^o. Each plot line represent an example of the total velocity development.

B.4 Velocity of 10 mm cylinder dropped from above the water surface

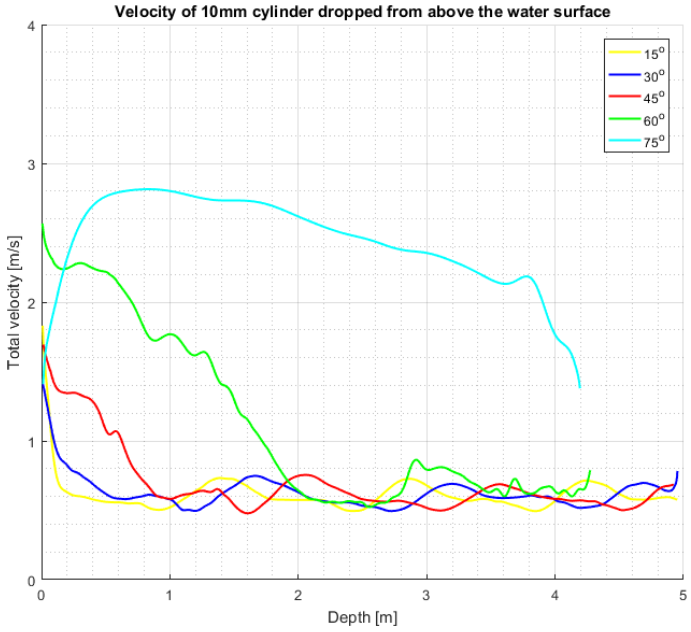

Figure 184: Total velocity compared to depth for closed 10 mm cylinders. The cylinders are dropped above the surface with initial drop angles of 15^o, 30^o, 45^o, 60^o and 75^o. Each plot line represent an example of the total velocity development.

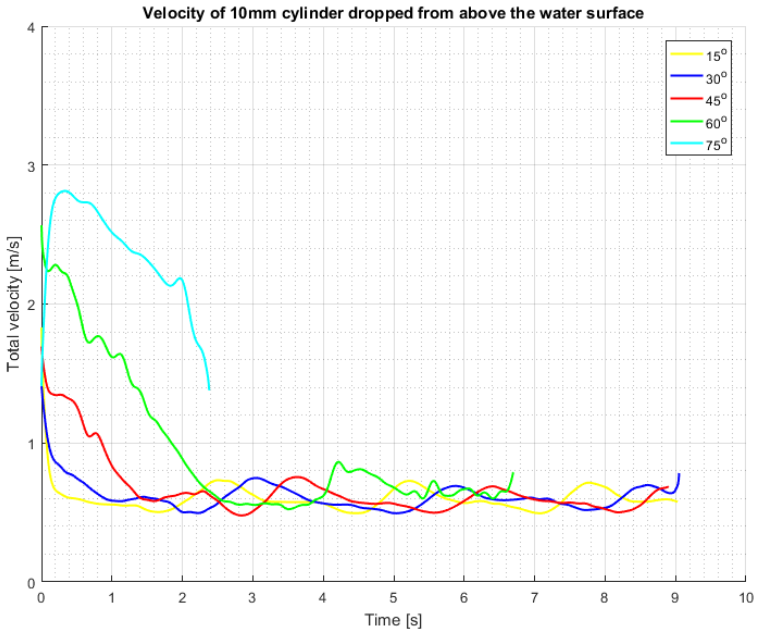

Figure 185: Total velocity compared to time for closed 10 mm cylinders. The cylinders are dropped above the surface with initial drop angles of 15^o, 30^o, 45^o, 60^o and 75^o. Each plot line represent an example of the total velocity development.

B.5 Velocity of 16 mm cylinder dropped from above the water surface

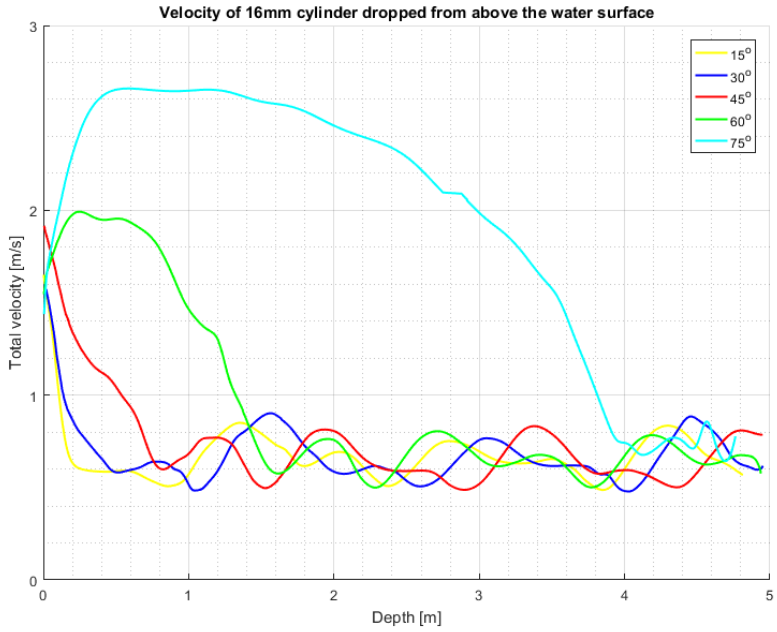

Figure 186: Total velocity compared to depth for closed 16 mm cylinders. The cylinders are dropped above the surface with initial drop angles of 15^o, 30^o, 45^o, 60^o and 75^o. Each plot line represent an example of the total velocity development.

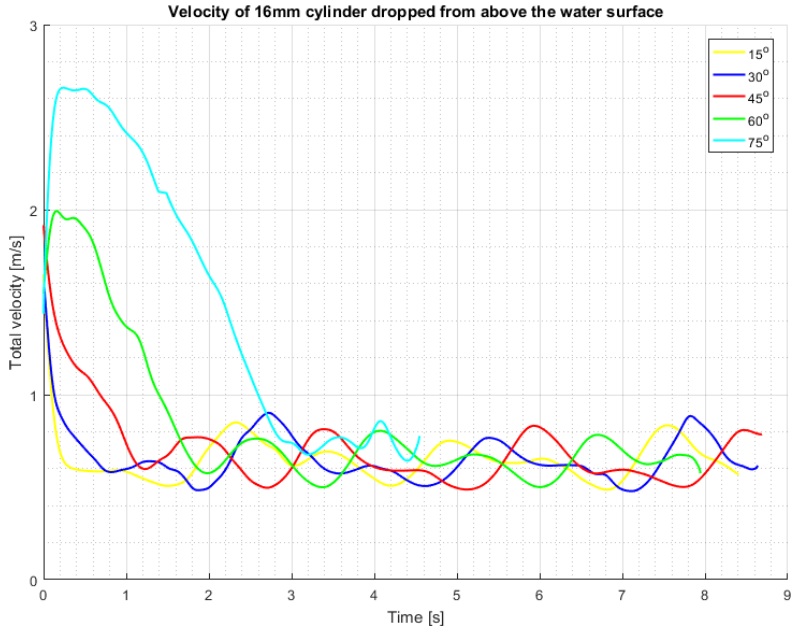

Figure 187: Total velocity compared to time for closed 16 mm cylinders. The cylinders are dropped above the surface with initial drop angles of 15^o, 30^o, 45^o, 60^o and 75^o. Each plot line represent an example of the total velocity development.

B.6 Velocity of 19 mm cylinder dropped from above the water surface

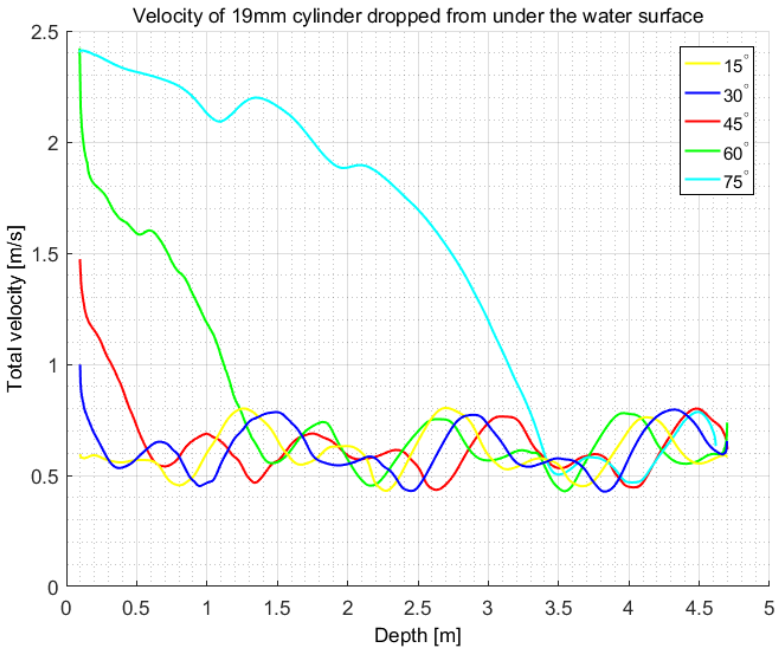

Figure 188: Total velocity compared to depth for closed 19 mm cylinders. The cylinders are dropped above the surface with initial drop angles of 15^o, 30^o, 45^o, 60^o and 75^o. Each plot line represent an example of the total velocity development.

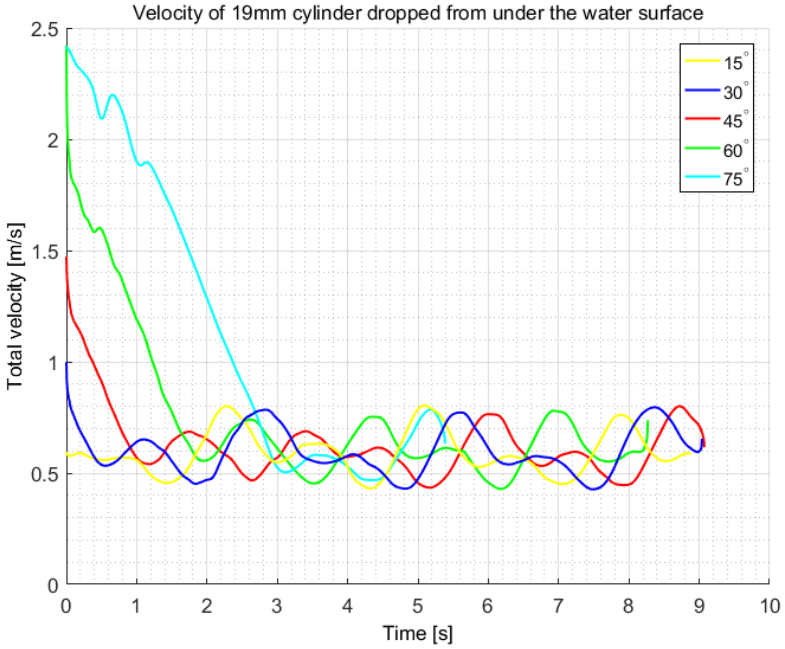

Figure 189: Total velocity compared to time for closed 19 mm cylinders. The cylinders are dropped above the surface with initial drop angles of 15^o, 30^o, 45^o, 60^o and 75^o. Each plot line represent an example of the total velocity development.

B.7 Velocity of open 10 mm cylinders dropped from under the water surface

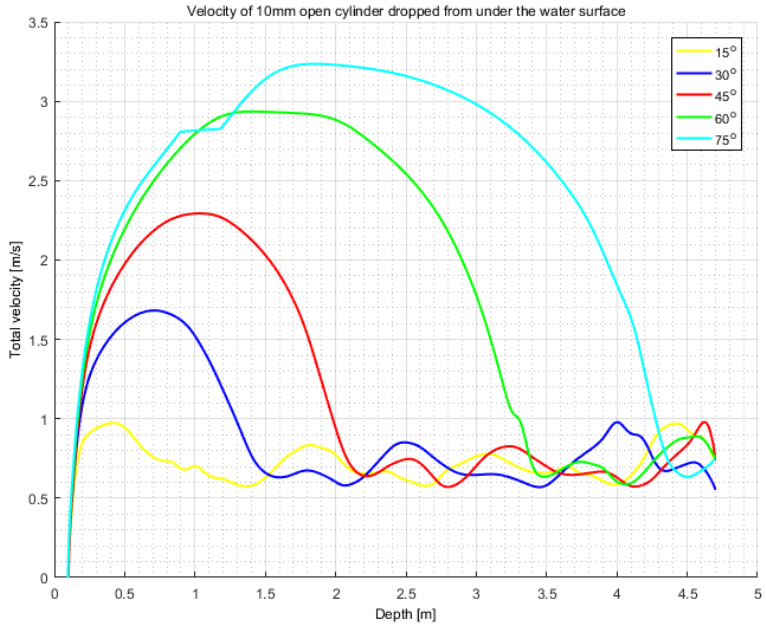

Figure 190: Total velocity compared to depth for open 10 mm cylinders. The cylinders are dropped under the surface with initial drop angles of 15^o, 30^o, 45^o, 60^o and 75^o. Each plot line represent an example of the total velocity development.

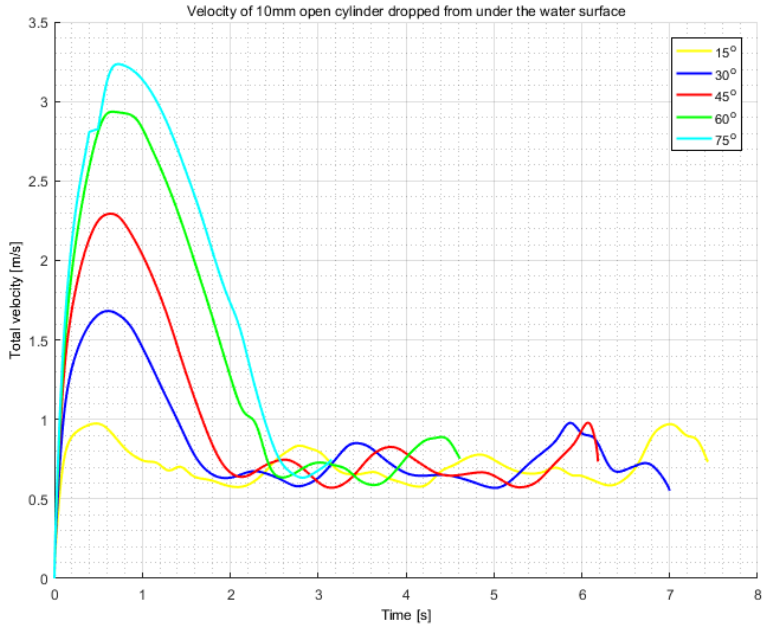

Figure 191: Total velocity compared to time for open 10 mm cylinders. The cylinders are dropped under the surface with initial drop angles of 15^o, 30^o, 45^o, 60^o and 75^o. Each plot line represent an example of the total velocity development.

B.8 Velocity of open 19 mm cylinders dropped from under the water surface

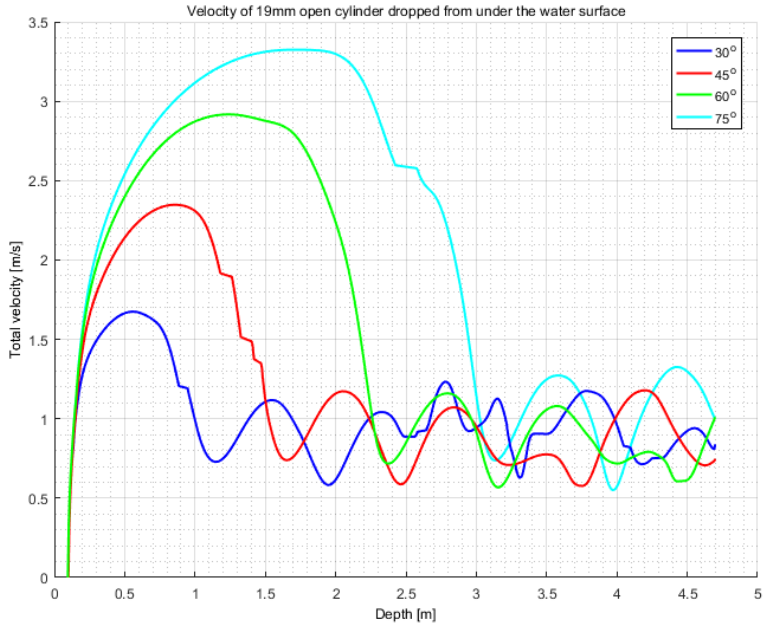

Figure 192: Total velocity compared to depth for open 19 mm cylinders. The cylinders are dropped under the surface with initial drop angles of 30^o, 45^o, 60^o and 75^o. Each plot line represent an example of the total velocity development.

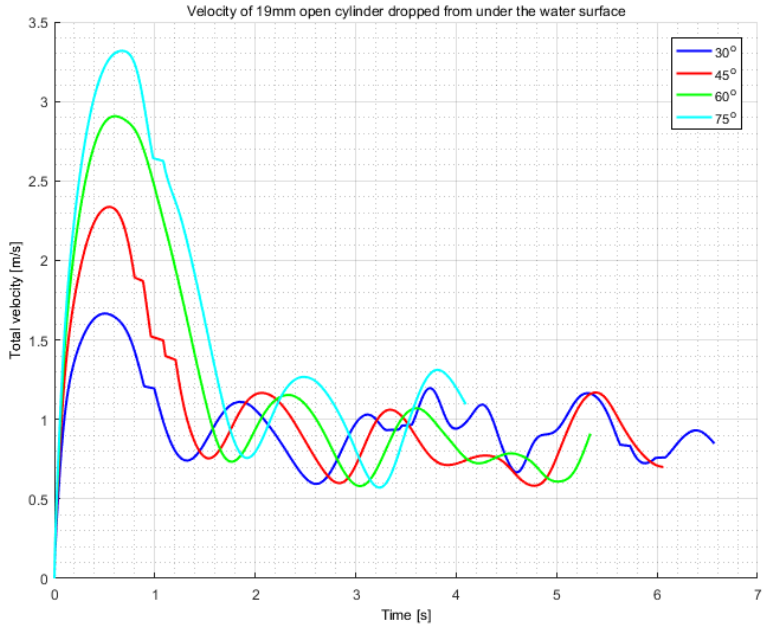

Figure 193: Total velocity compared to time for open 19 mm cylinders. The cylinders are dropped under the surface with initial drop angles of 30^o, 45^o, 60^o and 75^o. Each plot line represent an example of the total velocity development.

B.9 Velocity of 10 mm cylinder dropped from under the water surface with COG displaced 1.4 cm (COG above COV)

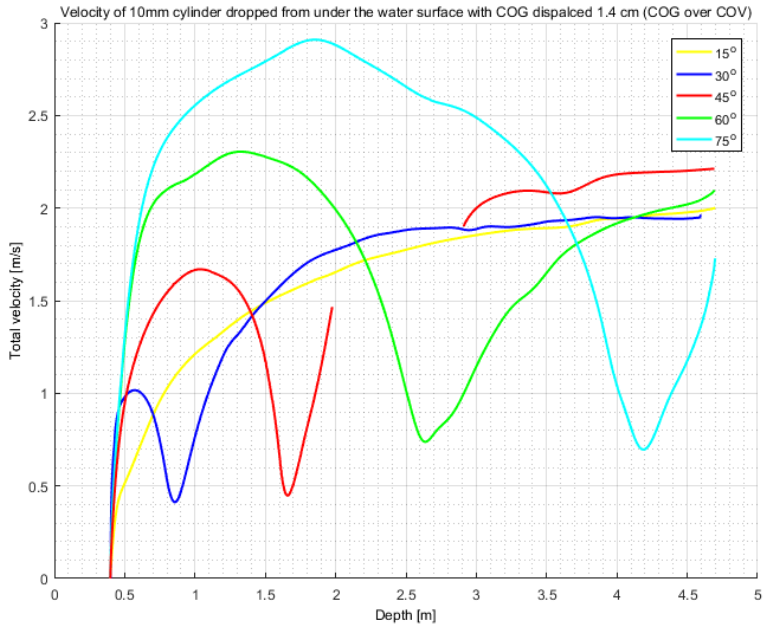

Figure 194: Total velocity compared to depth for cylinders with COG displaced 1.4 cm (Centre of Gravity (COG) over Centre of Volume (COV)). The cylinders are dropped under the surface with initial drop angles of 15^o, 30^o, 45^o, 60^o and 75^o. Each plot line represent an example of the total velocity development.

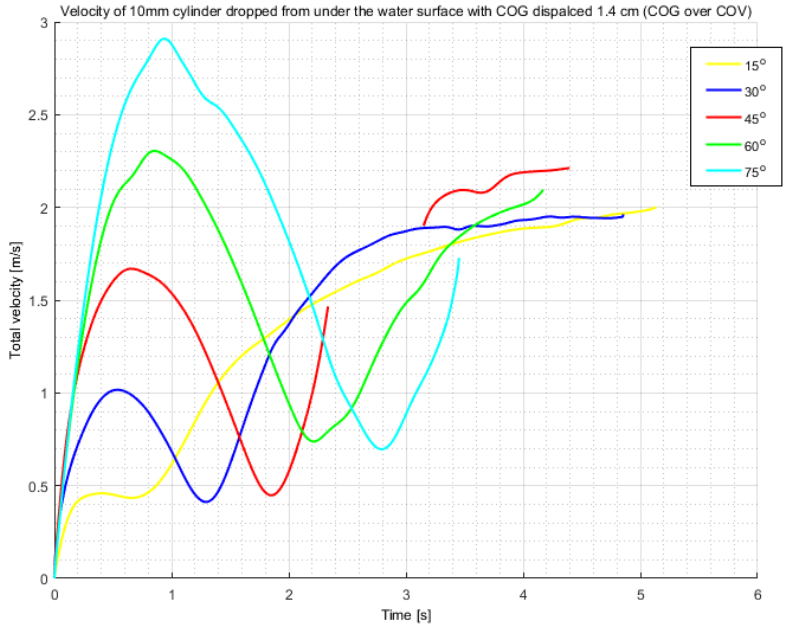

Figure 195: Total velocity compared to time for cylinders with COG 1.4 (Centre of Gravity (COG) over Centre of Volume (COV)). The cylinders are dropped under the surface with initial drop angles of 15^o, 30^o, 45^o, 60^o and 75^o. Each plot line represent an example of the total velocity development.

B.10 Velocity of 10 mm cylinder dropped from under the water surface with COG displaced 1.4 cm (COG under COV)

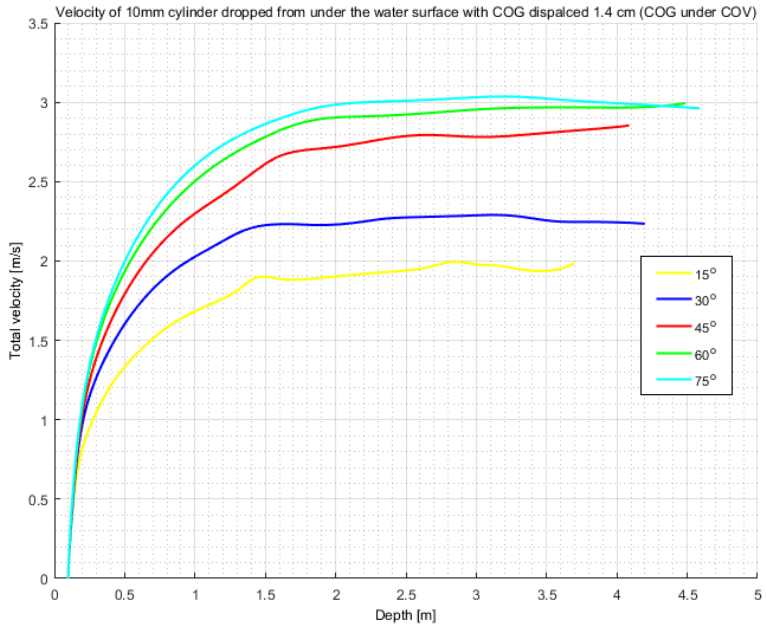

Figure 196: Total velocity compared to depth for cylinders with COG 1.4 cm (Centre of Gravity (COG) under Centre of Volume (COV)). The cylinders are dropped under the surface with initial drop angles of 15^o, 30^o, 45^o, 60^o and 75^o. Each plot line represent an example of the total velocity development.

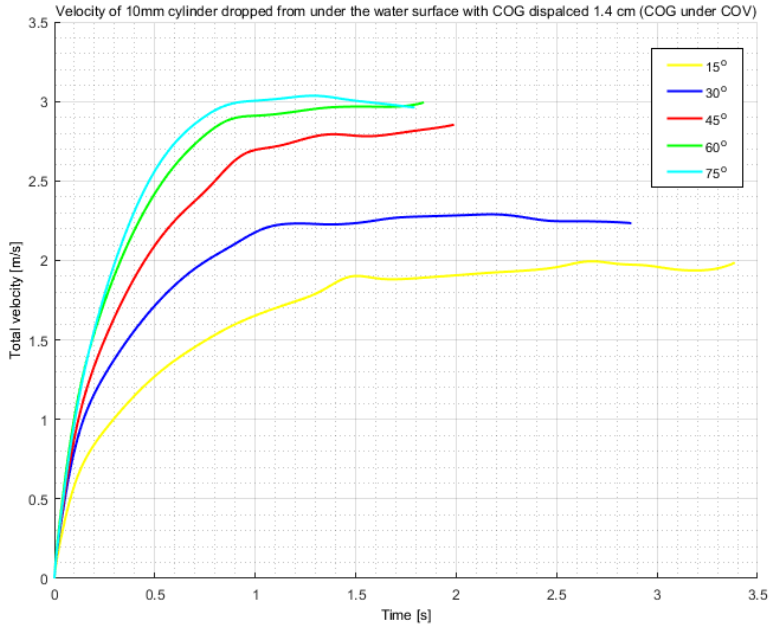

Figure 197: Total velocity compared to time for cylinders with COG 1.4 cm (Centre of Gravity (COG) under Centre of Volume (COV)). The cylinders are dropped under the surface with initial drop angles of 15^o, 30^o, 45^o, 60^o and 75^o. Each plot line represent an example of the total velocity development.

B.11 Velocity of 10 mm cylinder dropped from under the water surface with COG displaced with 3 cm (COG above COV)

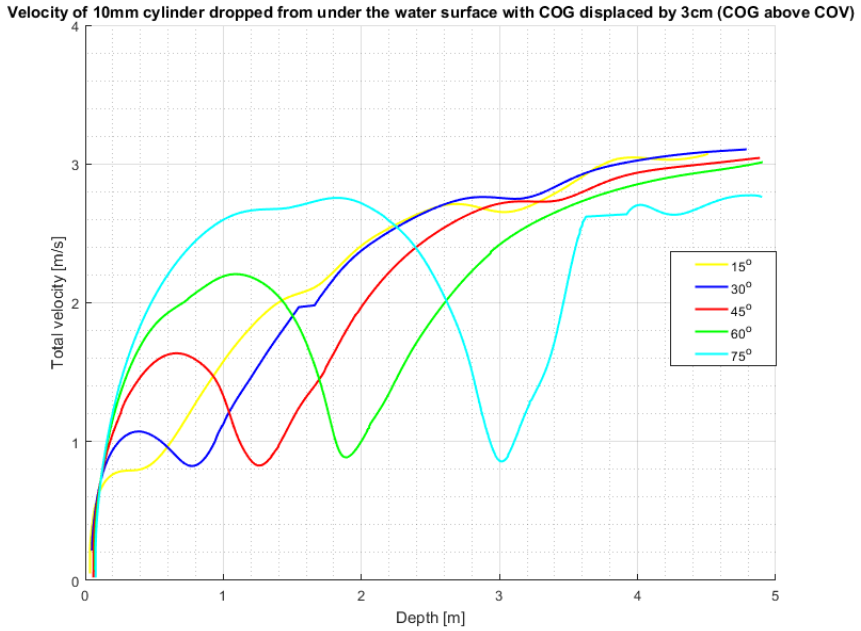

Figure 198: Total velocity compared to depth for cylinders with COG 3 cm (Centre of Gravity (COG) over Centre of Volume (COV)). The cylinders are dropped under the surface with initial drop angles of 15^o, 30^o, 45^o, 60^o and 75^o. Each plot line represent an example of the total velocity development.

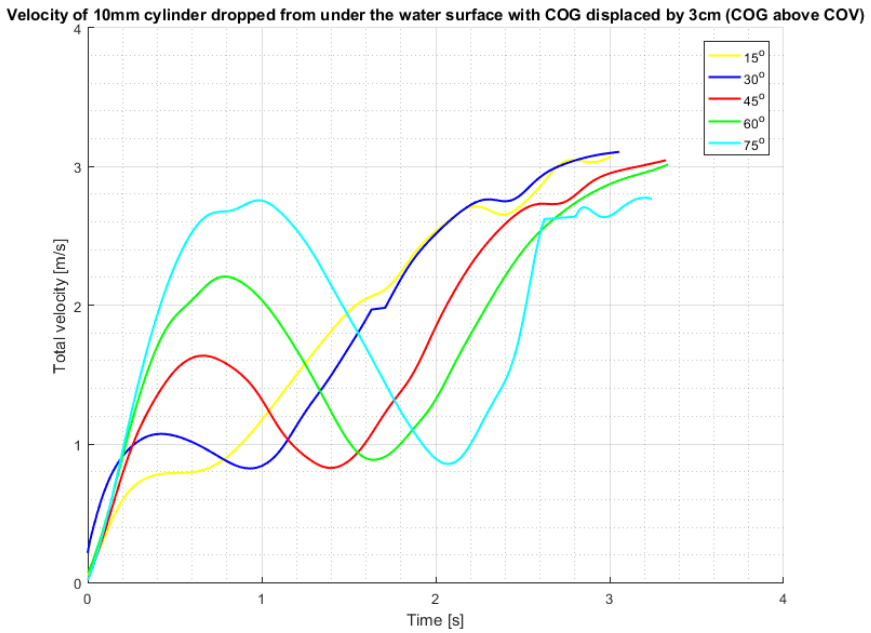

Figure 199: Total velocity compared to time for cylinders with COG 3 cm (Centre of Gravity (COG) over Centre of Volume (COV)). The cylinders are dropped under the surface with initial drop angles of 15^o, 30^o, 45^o, 60^o and 75^o. Each plot line represent an example of the total velocity development.

B.12 Velocity of 10 mm cylinder dropped from under the water surface with COG displaced with 3 cm (COG under COV)

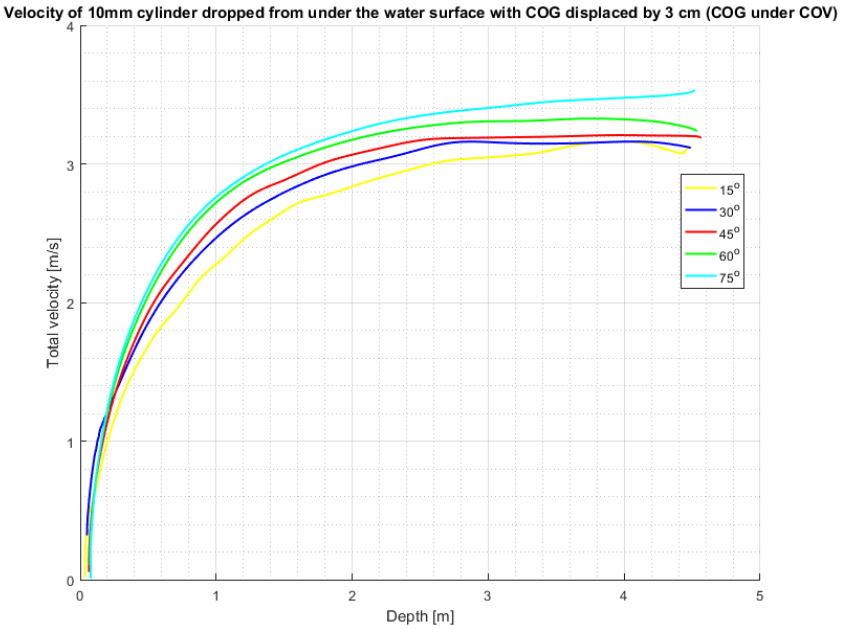

Figure 200: Total velocity compared to depth for cylinders with COG 3 cm (Centre of Gravity (COG) under Centre of Volume (COV)). The cylinders are dropped under the surface with initial drop angles of 15^o, 30^o, 45^o, 60^o and 75^o. Each plot line represent an example of the total velocity development.

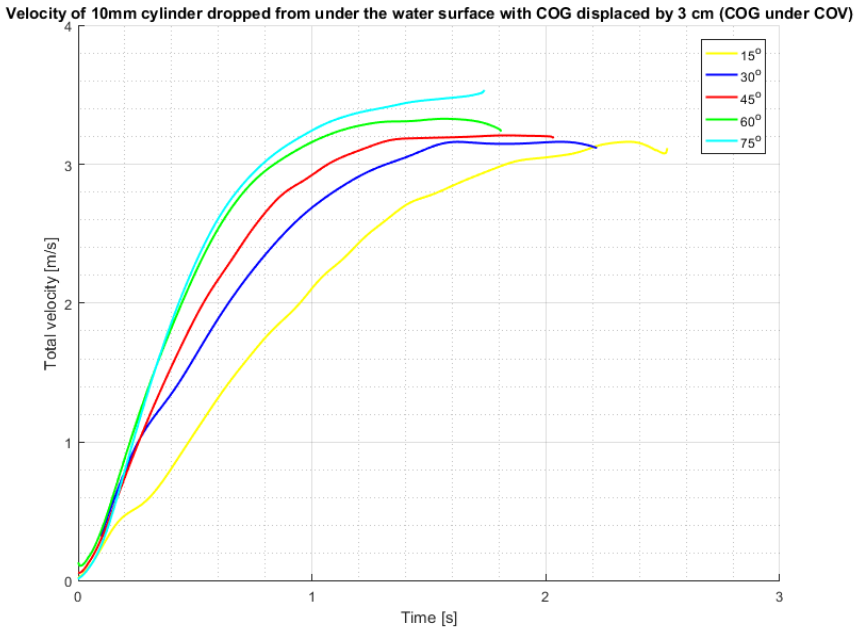

Figure 201: Total velocity compared to time for cylinders with COG 3 cm (Centre of Gravity (COG) under Centre of Volume (COV)). The cylinders are dropped under the surface with initial drop angles of 15^o, 30^o, 45^o, 60^o and 75^o. Each plot line represent an example of the total velocity development.

C Position tables

C.1 Position data for drop of 10, 16 and 19 mm diameter cylinders dropped from under the water surface

Table 1: Position data for closed 10 mm diameter cylinders with closed ends dropped from under the water surface. The table shows radial x-position, y-position and z-position with the corresponding standard deviations at the first and second turn, and at 3 and 4 m depth. Empty cells are due to the fact that the first and second turn does not occur for the drop angles in question.

10 mm cylinder dropped from under the water surface								
Drop angle	**First turn**				**Depth: 3m**			
	rad. x-pos. [m]	**st. dev. [m]**	**z-pos. [m]**	**st. dev. [m]**	**y-pos. [m]**	**st. dev. [m]**	**rad. x-pos. [m]**	**st. dev. [m]**
15°	0.73	0.08	1.13	0.06	-0.02	0.04	0.62	0.18
30°	2.37	0.35	2.20	0.27	-0.13	0.34	2.22	0.37
45°	3.79	0.53	3.63	0.56	-0.14	0.70	3.01	0.30
60°					0.04	0.18	1.71	0.13
75°					-0.01	0.08	0.88	0.09
	Second turn				**Depth: 4m**			
	rad. x-pos. [m]	**st. dev. [m]**	**z-pos. [m]**	**st. dev. [m]**	**y-pos. [m]**	**st. dev. [m]**	**rad. x-pos. [m]**	**st. dev. [m]**
15°	0.46	0.10	1.72	0.08	-0.01	0.05	0.89	0.19
30°	2.14	0.40	2.79	0.24	-0.10	0.36	2.32	0.56
45°	3.17	0.37	3.83	0.19	-0.04	0.81	3.67	0.51
60°					0.06	0.50	2.79	0.39
75°					0.02	0.18	1.49	0.18

Table 2: Position data for 16 mm diameter cylinders with closed ends dropped from under the water surface. The table shows radial x-position, y-position and z-position with the corresponding standard deviations at the first and second turn, and at 3 and 4 m depth.Empty cells are due to the fact that the first and second turn does not occur for the drop angles in question.

16 mm cylinder dropped from under the water surface								
Drop angle	**First turn**				**Depth: 3m**			
	rad. x-pos. [m]	**st. dev. [m]**	**z-pos. [m]**	**st. dev. [m]**	**y-pos. [m]**	**st. dev. [m]**	**rad. x-pos. [m]**	**st. dev. [m]**
15°	0.49	0.05	0.98	0.04	-0.03	0.05	0.41	0.13
30°	1.61	0.23	1.72	0.18	0.05	0.32	1.57	0.30
45°	2.89	0.11	2.93	0.10	-0.05	0.27	2.86	0.09
60°					-0.33	0.26	1.76	0.21
75°					0.05	0.08	0.93	0.03
	Second turn				**Depth: 4m**			
	rad. x-pos. [m]	**st. dev. [m]**	**z-pos. [m]**	**st. dev. [m]**	**y-pos. [m]**	**st. dev. [m]**	**rad. x-pos. [m]**	**st. dev. [m]**
15°	0.26	0.06	1.53	0.04	-0.05	0.04	0.79	0.17
30°	1.33	0.30	2.32	0.12	0.07	0.27	1.51	0.35
45°	2.56	0.10	3.56	0.14	-0.05	0.27	2.79	0.12
60°					-0.73	0.59	2.94	0.45
75°					0.16	0.26	1.68	0.04

Table 3: Position data for 19 mm diameter cylinders with closed ends dropped from under the water surface. The table shows radial x-position, y-position and z-position with the corresponding standard deviations at the first and second turn, and at 3 and 4 m depth. Empty cells are due to the fact that the first and second turn does not occur for the drop angles in question.

19 mm cylinder dropped from under the water surface								
Drop angle	**First turn**				**Depth: 3m**			
	rad. x-pos. [m]	**st. dev. [m]**	**z-pos. [m]**	**st. dev. [m]**	**y-pos. [m]**	**st. dev. [m]**	**rad. x-pos. [m]**	**st. dev. [m]**
15°	0.40	0.07	0.88	0.06	-0.02	0.08	0.22	0.12
30°	1.47	0.09	1.60	0.07	-0.08	0.15	1.40	0.12
45°	2.76	0.16	2.84	0.14	-0.18	0.42	2.68	0.23
60°					-0.47	0.43	1.63	0.33
75°					-0.05	0.15	0.99	0.07
	Second turn				**Depth: 4m**			
	rad. x-pos. [m]	**st. dev. [m]**	**z-pos. [m]**	**st. dev. [m]**	**y-pos. [m]**	**st. dev. [m]**	**rad. x-pos. [m]**	**st. dev. [m]**
15°	0.16	0.12	1.41	0.04	-0.02	0.06	0.35	0.18
30°	1.12	0.11	2.18	0.12	-0.10	0.14	1.35	0.19
45°	2.36	0.16	3.44	0.15	-0.21	0.29	2.58	0.13
60°					-0.73	1.08	2.48	0.67
75°					-0.11	0.46	1.81	0.17

C.2 Position data for drop of 10, 16 and 19 mm diameter cylinders dropped from over the water surface

Table 4: Position data for 10 mm diameter cylinders with closed ends dropped from over the water surface. The table shows radial x-position, y-position and z-position with the corresponding standard deviations at the first and second turn, and at 3 and 4 m depth. Empty cells are due to the fact that the first and second turn does not occur for the drop angle in question.

10 mm cylinder dropped from over the water surface								
Drop angle	**First turn**				**Depth: 3m**			
	rad. x-pos. [m]	**st. dev. [m]**	**z-pos. [m]**	**st. dev. [m]**	**y-pos. [m]**	**st. dev. [m]**	**rad. x-pos. [m]**	**st. dev. [m]**
15°	0.17	0.03	0.44	0.03	0.00	0.03	0.32	0.09
30°	0.50	0.07	0.63	0.07	0.00	0.08	0.51	0.17
45°	1.24	0.11	1.04	0.08	-0.01	0.08	1.14	0.26
60°	2.64	0.20	2.09	0.16	0.22	0.23	2.43	0.34
75°					-0.32	0.42	2.03	0.14
	Second turn				**Depth: 4m**			
	rad. x-pos. [m]	**st. dev. [m]**	**z-pos. [m]**	**st. dev. [m]**	**y-pos. [m]**	**st. dev. [m]**	**rad. x-pos. [m]**	**st. dev. [m]**
15°	0.03	0.04	0.98	0.04	-0.02	0.03	0.22	0.12
30°	0.23	0.18	1.25	0.06	0.01	0.10	0.70	0.25
45°	0.89	0.15	1.64	0.05	-0.04	0.15	1.47	0.28
60°	2.36	0.34	2.74	0.07	0.20	0.31	2.64	0.57
75°					-0.28	0.71	3.21	0.24

Table 5: Position data for 16 mm diameter cylinders with closed ends dropped from over the water surface. The table shows radial x-position, y-position and z-position with the corresponding standard deviations at the first and second turn, and at 3 and 4 m depth.

16 mm cylinder dropped from over the water surface								
Drop angle	**First turn**				**Depth: 3m**			
	rad. x-pos. [m]	**st. dev. [m]**	**z-pos. [m]**	**st. dev. [m]**	**y-pos. [m]**	**st. dev. [m]**	**rad. x-pos. [m]**	**st. dev. [m]**
15°	0.17	0.03	0.38	0.06	0.02	0.04	0.29	0.17
30°	0.44	0.05	0.57	0.05	0.01	0.05	0.32	0.22
45°	0.97	0.08	0.85	0.07	0.09	0.13	0.54	0.19
60°	2.03	0.16	1.64	0.11	-0.13	0.18	1.74	0.15
75°	3.65	0.57	4.13	0.31	0.24	0.55	2.23	0.24
	Second turn				**Depth: 4m**			
	rad. x-pos. [m]	**st. dev. [m]**	**z-pos. [m]**	**st. dev. [m]**	**y-pos. [m]**	**st. dev. [m]**	**rad. x-pos. [m]**	**st. dev. [m]**
15°	0.02	0.08	0.92	0.07	0.05	0.11	0.16	0.29
30°	0.16	0.13	1.16	0.07	0.04	0.05	0.34	0.26
45°	0.44	0.09	1.62	0.09	0.03	0.08	0.90	0.22
60°	1.70	0.57	2.35	0.19	-0.15	0.18	1.66	0.14
75°	3.46	0.20	4.55	0.26	0.39	1.16	3.40	0.49

Table 6: Position data for 19 mm diameter cylinders with closed ends dropped from over the water surface. The table shows radial x-position, y-position and z-position with the corresponding standard deviations at the first and second turn, and at 3 and 4 m depth.

19 mm cylinder dropped from over the water surface								
Drop angle	**First turn**				**Depth: 3m**			
	rad. x-pos. [m]	**st. dev. [m]**	**z-pos. [m]**	**st. dev. [m]**	**y-pos. [m]**	**st. dev. [m]**	**rad. x-pos. [m]**	**st. dev. [m]**
15°	0.15	0.01	0.42	0.01	0.00	0.03	0.22	0.13
30°	0.34	0.04	0.51	0.05	-0.06	0.08	0.14	0.19
45°	0.90	0.06	0.84	0.07	-0.14	0.29	0.48	0.09
60°	1.96	0.35	1.68	0.34	-0.32	0.71	1.58	0.44
75°					-0.37	0.90	2.22	0.27
	Second turn				**Depth: 4m**			
	rad. x-pos. [m]	**st. dev. [m]**	**z-pos. [m]**	**st. dev. [m]**	**y-pos. [m]**	**st. dev. [m]**	**rad. x-pos. [m]**	**st. dev. [m]**
15°	-0.06	0.03	1.04	0.20	-0.03	0.03	0.04	0.15
30°	-0.05	0.09	1.14	0.17	-0.08	0.13	0.05	0.20
45°	0.45	0.07	1.52	0.07	-0.12	0.16	0.64	0.17
60°	1.44	0.46	2.35	0.26	-0.36	0.72	1.54	0.54
75°	3.46	0.20	4.55	0.26	-0.43	1.50	2.83	0.47

C.3 Position data for drop of 10 and 19 mm diameter cylinders with open ends dropped from under the water surface

Table 7: Position data for 10 mm diameter cylinders with open ends dropped from under the water surface. The table shows radial x-position, y-position and z-position with the corresponding standard deviations at the first and second turn, and at 3 and 4 m depth. All empty cells are due to the fact that the cylinder does not have a second turn at 75°.

10 mm cylinder with open ends dropped from under the water surface								
Drop angle	**First turn**				**Depth: 3m**			
	rad. x-pos. [m]	**st. dev. [m]**	**z-pos. [m]**	**st. dev. [m]**	**y-pos. [m]**	**st. dev. [m]**	**rad. x-pos. [m]**	**st. dev. [m]**
15°	0.71	0.08	1.01	0.04	-0.10	0.04	0.72	0.10
30°	1.85	0.09	1.63	0.05	-0.17	0.19	1.90	0.13
45°	2.63	0.10	2.31	0.06	-0.18	0.25	2.35	0.14
60°	3.41	0.13	3.41	0.11	-0.06	0.18	2.89	0.13
75°	3.70	0.04	4.57	0.05	-0.10	0.08	1.30	0.07
	Second turn				**Depth: 4m**			
	rad. x-pos. [m]	**st. dev. [m]**	**z-pos. [m]**	**st. dev. [m]**	**y-pos. [m]**	**st. dev. [m]**	**rad. x-pos. [m]**	**st. dev. [m]**
15°	0.55	0.07	1.51	0.06	-0.15	0.08	0.85	0.13
30°	1.59	0.11	2.21	0.04	-0.19	0.18	1.91	0.14
45°	2.33	0.14	2.90	0.03	-0.22	0.28	2.57	0.17
60°	3.09	0.10	4.01	0.13	-0.10	0.25	3.12	0.12
75°					-0.20	0.24	2.62	0.26

Table 8: Position data for 19 mm diameter cylinders with open ends dropped from under the water surface. The table shows radial x-position, y-position and z-position with the corresponding standard deviations at the first and second turn, and at 3 and 4 m depth. No measurement exist of for drop angle 15°, hence the empty cells.

19 mm cylinder with open ends dropped from under the water surface								
Drop angle	**First turn**				**Depth: 3m**			
	rad. x-pos. [m]	**st. dev. [m]**	**z-pos. [m]**	**st. dev. [m]**	**y-pos. [m]**	**st. dev. [m]**	**rad. x-pos. [m]**	**st. dev. [m]**
15°								
30°	1.29	0.05	1.23	0.02	-0.07	0.04	1.08	0.19
45°	1.98	0.04	1.70	0.03	-0.06	0.10	1.44	0.10
60°	2.55	0.03	2.43	0.03	-0.09	0.14	1.95	0.08
75°	2.67	0.02	3.23	0.03	-0.18	0.19	2.37	0.08
	Second turn				**Depth: 4m**			
	rad. x-pos. [m]	**st. dev. [m]**	**z-pos. [m]**	**st. dev. [m]**	**y-pos. [m]**	**st. dev. [m]**	**rad. x-pos. [m]**	**st. dev. [m]**
15°								
30°	0.68	0.16	1.93	0.10	-0.06	0.09	1.20	0.37
45°	1.15	0.08	2.51	0.05	-0.07	0.14	1.38	0.10
60°	1.62	0.12	3.29	0.07	-0.10	0.19	2.09	0.10
75°	1.71	0.12	4.10	0.09	-0.14	0.24	1.79	0.09

C.4 Position data for drop of 10 mm diameter cylinders with centre of gravity displaced 1.4 cm.

Table 9: Position data for 10 mm diameter cylinders with closed ends and the centre of gravity displaced 1.4 cm. The cylinders is dropped with the initial position of the centre of gravity (COG) over the cylinder volume centre (COV). The table shows radial x-position, y-position and z-position with the corresponding standard deviations at the first and second turn, and at 3 and 4 m depth. The empty cells are due to the fact that a second turn does not occur.

10 mm cylinder with COG displaced 1.4 cm dropped from under the water surface (COG over COV)								
Drop angle	**First turn**				**Depth: 3m**			
	rad. x-pos. [m]	**st. dev. [m]**	**z-pos. [m]**	**st. dev. [m]**	**y-pos. [m]**	**st. dev. [m]**	**rad. x-pos. [m]**	**st. dev. [m]**
15°	0.21	0.10	0.36	0.15	0.04	0.66	-3.01	0.33
30°	0.65	0.05	0.57	0.03	-0.25	0.46	-2.10	0.11
45°	1.74	0.09	1.29	0.08	0.02	0.26	0.09	0.21
60°	2.62	0.21	2.97	0.21	0.03	0.28	2.53	0.17
75°	3.04	0.03	4.31	0.05	-0.16	0.05	1.26	0.02
	Second turn				**Depth: 4m**			
	rad. x-pos. [m]	**st. dev. [m]**	**z-pos. [m]**	**st. dev. [m]**	**y-pos. [m]**	**st. dev. [m]**	**rad. x-pos. [m]**	**st. dev. [m]**
15°					-0.27	0.94	-4.35	0.41
30°					-0.57	0.80	-3.43	0.20
45°					0.01	0.54	-1.04	0.24
60°					-0.13	0.14	1.72	0.46
75°					-0.31	0.15	2.73	0.06

Table 10: Position data for 10 mm diameter cylinders with closed ends and the centre of gravity displaced 1.4 cm. The cylinders is dropped with the initial position of the centre of gravity (COG) under the cylinder volume centre (COG). The table shows radial x-position, y-position and z-position with the corresponding standard deviations at the first and second turn, and at 3 and 4 m depth. The empty cells are due to the lack of turns.

10 mm cylinder with COG displaced 1.4 cm dropped from under the water surface (COG under COV)								
Drop angle	**First turn**				**Depth: 3m**			
	rad. x-pos. [m]	**st. dev. [m]**	**z-pos. [m]**	**st. dev. [m]**	**y-pos. [m]**	**st. dev. [m]**	**rad. x-pos. [m]**	**st. dev. [m]**
15°					0.22	0.81	3.55	0.16
30°					-0.18	0.54	2.77	0.14
45°					-0.07	0.32	1.89	0.06
60°					-0.15	0.17	1.19	0.08
75°					-0.05	0.03	0.60	0.03
	Second turn				**Depth: 4m**			
	rad. x-pos. [m]	**st. dev. [m]**	**z-pos. [m]**	**st. dev. [m]**	**y-pos. [m]**	**st. dev. [m]**	**rad. x-pos. [m]**	**st. dev. [m]**
15°					0.20	1.28	4.65	0.22
30°					-0.43	1.08	3.79	0.27
45°					-0.16	0.57	2.59	0.17
60°					-0.22	0.38	1.70	0.16
75°					-0.09	0.09	0.98	0.04

C.5 Position data for drop of 10 mm diameter cylinders with centre of gravity displaced 3 cm.

Table 11: Position data for 10 mm diameter cylinders with closed ends and the centre of gravity displaced 3 cm. The cylinders is dropped with the initial position of the centre of gravity over the cylinder volume centre. The table shows radial x-position, y-position and z-position with the corresponding standard deviations at the first and second turn, and at 3 and 4 m depth. The empty cells are due to the fact that no second turn occur.

10 mm cylinder with COG displaced 3 cm dropped from under the water surface (COG over COV)								
Drop angle	**First turn**				**Depth: 3m**			
	rad. x-pos. [m]	**st. dev. [m]**	**z-pos. [m]**	**st. dev. [m]**	**y-pos. [m]**	**st. dev. [m]**	**rad. x-pos. [m]**	**st. dev. [m]**
15°	0.07	0.01	0.45	0.01	0.03	0.28	-1.81	0.09
30°	0.41	0.01	0.84	0.01	-0.04	0.47	-1.10	0.15
45°	1.04	0.02	1.35	0.02	0.25	0.17	0.13	0.30
60°	1.66	0.03	2.15	0.05	-0.03	0.11	1.18	0.07
75°	2.14	0.00	3.17	0.07	0.25	0.87	1.96	0.44
	Second turn				**Depth: 4m**			
	rad. x-pos. [m]	**st. dev. [m]**	**z-pos. [m]**	**st. dev. [m]**	**y-pos. [m]**	**st. dev. [m]**	**rad. x-pos. [m]**	**st. dev. [m]**
15°					0.07	0.45	-2.49	0.19
30°					0.04	0.50	-1.66	0.14
45°					0.41	0.29	-0.71	0.15
60°					-0.12	0.30	0.65	0.15
75°					-0.03	0.19	1.80	0.14

Table 12: Position data for 10 mm diameter cylinders with closed ends and the centre of gravity displaced 3 cm. The cylinders is dropped with the initial position of the centre of gravity under the cylinder volume centre. The table shows radial x-position, y-position and z-position with the corresponding standard deviations at the first and second turn, and at 3 and 4 m depth. The empty cells are due to the lack of turns in the trajectory of the cylinders.

10 mm cylinder with COG displaced 3 cm dropped from under the water surface (COG under COV)								
Drop angle	**First turn**				**Depth: 3m**			
	rad. x-pos. [m]	**st. dev. [m]**	**z-pos. [m]**	**st. dev. [m]**	**y-pos. [m]**	**st. dev. [m]**	**rad. x-pos. [m]**	**st. dev. [m]**
15°					0.23	0.24	2.26	0.09
30°					0.20	0.23	1.85	0.05
45°					-0.03	0.23	1.33	0.08
60°					0.07	0.11	0.84	0.07
75°					0.01	0.04	0.37	0.05
	Second turn				**Depth: 4m**			
	rad. x-pos. [m]	**st. dev. [m]**	**z-pos. [m]**	**st. dev. [m]**	**y-pos. [m]**	**st. dev. [m]**	**rad. x-pos. [m]**	**st. dev. [m]**
15°					0.33	0.33	2.81	0.12
30°					0.24	0.34	2.34	0.07
45°					-0.05	0.36	1.73	0.12
60°					0.10	0.17	1.14	0.12
75°					0.02	0.10	0.52	0.10

D Velocity tables

D.1 Velocity tables for drop of 10, 16 and 19 mm diameter cylinders dropped from under the water surface

Table 13: The average maximal velocity and standard deviation for 10, 16 and 19 mm cylinders with closed ends, dropped from under the water surface.

Cylinders dropped from under the water surface						
Drop angle	**10 mm**		**16 mm**		**19 mm**	
	Average max. vel. [m/s]	std. dev. [m/s]	Average max. vel. [m/s]	std. dev. [m/s]	Average max. vel. [m/s]	std. dev. [m/s]
15°	0.85	0.02	0.85	0.03	0.79	0.02
30°	1.53	0.09	1.33	0.09	1.17	0.03
45°	2.17	0.09	1.92	0.07	1.70	0.03
60°	2.68	0.07	2.43	0.10	2.43	0.10
75°	2.96	0.05	2.60	0.02	2.33	0.03

D.2 Velocity tables for drop of 10, 16 and 19 mm diameter cylinders dropped from over the water surface

Table 14: The average maximal velocity and standard deviation for 10, 16 and 19 mm cylinders with closed ends, dropped from over the water surface.

Cylinders dropped from over the water surface						
Drop angle	**10 mm**		**16 mm**		**19 mm**	
	Average max. vel. [m/s]	std. dev. [m/s]	Average max. vel. [m/s]	std. dev. [m/s]	Average max. vel. [m/s]	std. dev. [m/s]
15°	1.91	0.50	1.56	0.19	0.78	0.03
30°	1.51	0.15	1.74	0.35	0.81	0.04
45°	1.76	0.30	1.66	0.20	1.22	0.04
60°	2.13	0.19	2.09	0.20	1.79	0.07
75°	2.88	0.14	2.65	0.09	2.39	0.05

D.3 Velocity tables for drop of 10 and 19 mm diameter cylinders with open ends dropped from under the water surface

Table 15: The average maximal velocity and standard deviation for 10 and 19 mm cylinders with open ends, dropped from under the water surface.

Cylinders with open ends dropped from under the water surface				
Drop angle	**10 mm**		**19 mm**	
	Average max. vel. [m/s]	std. dev. [m/s]	Average max. vel. [m/s]	std. dev. [m/s]
15°	1.05	0.05		
30°	1.68	0.05	1.66	0.03
45°	2.35	0.07	2.32	0.04
60°	2.87	0.06	2.89	0.02
75°	3.29	0.05	3.30	0.02

D.4 Velocity tables for drop of 10 mm diameter cylinders with centre of gravity displaced 1.4 cm

Table 16: The average maximal velocity and standard deviation for 10 mm cylinders with closed ends and the centre of gravity displaced 1.4 cm, dropped from under the water surface. The cylinders is dropped with the initial position of the centre of gravity (COG) over and under the cylinder volume centre (COV).

Cylinders with COG displaced 1.4 cm dropped from under the water surface				
Drop angle	**COG over COV**		**COG under COV**	
	Average max. vel. [m/s]	std. dev. [m/s]	Average max. vel. [m/s]	std. dev. [m/s]
15°	1.88	0.20	2.03	0.10
30°	1.94	0.11	2.33	0.15
45°	2.11	0.05	2.75	0.13
60°	2.39	0.04	2.98	0.04
75°	2.88	0.03	3.08	0.05

D.5 Velocity tables for drop of 10 mm diameter cylinders with centre of gravity displaced 3 cm

Table 17: The average maximal velocity and standard deviation for 10 mm cylinders with closed ends and the centre of gravity (COG) displaced 3 cm, dropped from under the water surface. The cylinders is dropped with the initial position of COG over and under the cylinder volume centre (COV).

Cylinders with COG displaced 3 cm dropped from under the water surface				
Drop angle	**COG over COV**		**COG under COV**	
	Average max. vel. [m/s]	std. dev. [m/s]	Average max. vel. [m/s]	std. dev. [m/s]
15°	2.94	0.18	3.20	0.09
30°	3.04	0.12	3.22	0.05
45°	3.03	0.07	3.27	0.11
60°	3.06	0.13	3.33	0.10
75°	2.82	0.09	3.47	0.09